AD NUMBER

AD489720

LIMITATION CHANGES

TO:

Approved for public release; distribution is unlimited.

FROM:

Distribution authorized to U.S. Gov't. agencies and their contractors; Critical Technology; 20 OCT 1965. Other requests shall be referred to Air Force Weapons Laboratory, Attnt: WLDN, Kirtland AFB, NM 87117. This document contains export-controlled technical data.

AUTHORITY

AFWL ltr, 30 Nov 1971

FZK-263-1
20 OCTOBER 1965

NERVA MATERIALS IRRADIATION PROGRAM

Volume 1

GTR Test 16 — AGC Materials Test

Prepared for
Space Nuclear Propulsion Office
of the
National Aeronautics and Space Administration
Cleveland, Ohio

Contract No. AF 29(601)-6643
Supplement 2

NUCLEAR AEROSPACE RESEARCH FACILITY

operated by

GENERAL DYNAMICS | FORT WORTH

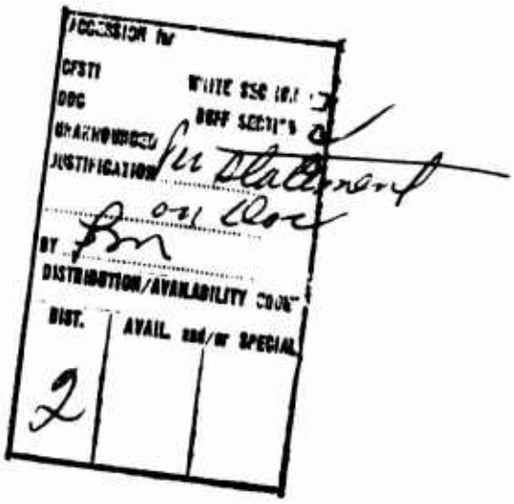

This document is subject to special export controls and each transmittal to foreign governments or foreign nationals may be made only with prior approval of Air Force Weapons Laboratory, Attn: WLDN, Kirtland AFB, New Mexico 87117.

(14) FZK-263-1
(11) 20 OCT [redacted] 65
(12) 400p.

GDDDDDD

NUCLEAR AEROSPACE RESEARCH FACILITY

(6)

NERVA MATERIALS IRRADIATION PROGRAM

Volume 1

GTR Test 16 — AGC Materials Test,

(10) H. G. Thornton

37/A002 Tensile Specimens

37/A003 Shear Specimens

Prepared for
Space Nuclear Propulsion Office
of the
National Aeronautics and Space Administration
Cleveland, Ohio

(15) [redacted] AF 29(601)-6643

GENERAL DYNAMICS | FORT WORTH

(147 720)

FOREWORD

The Nuclear Aerospace Research Facility (NARF) of General Dynamics/Fort Worth is conducting a series of tests on NERVA components and materials for the Space Nuclear Propulsion Office, Cleveland, Ohio (SNPO-C). Previous tests have been performed under Contracts AF33(657)-7201 and AF29(601)-6213 and are reported in GD/FW Reports FZK-170, Vols. 1 through 8, and FZK-184, Vols. 1 through 6, respectively. The test reported in this document (FZK-263-1) was sponsored by Aerojet-General Corporation and involved the irradiation of various metals in liquid hydrogen. A companion test sponsored by Westinghouse Astronuclear Laboratory involved the irradiation of metallic and graphite materials in liquid nitrogen and is reported in FZK-263-2. Both tests were performed in the GTR Radiation Effects Testing Facility of NARF under Supplemental Agreement 2, Contract AF29(601)-6643, and are designated GTR Test 16.

ACKNOWLEDGMENTS

The author wishes to acknowledge the participation of several groups and individuals in the performance of this test and the preparation of the report:

Dr. W. Weleff, C. E. Dixon, and L. E. Krelovich were the Aerojet-General Corporation monitors and are to be commended for their cooperation and assistance in the planning and performance of this test.

Numerous General Dynamics Radiation Effects personnel have contributed to this report in the areas of design, testing, data reduction, and nuclear measurement.

Z. R. Wolanski and M. R. Sargent of the GD/FW Engineering Test Laboratory were primarily responsible for the metallography studies.

J. B. Wattier performed the statistical analysis of the stress-strain data.

E. T. Smith accomplished the calculations for determination of the gage-length correction factor.

D. N. Hurst was responsible for editing of the report.

SUMMARY

The test described in this report was designed to determine the combined effects of nuclear radiation and liquid-hydrogen temperatures on the tensile and shear properties of specific metals considered for structural applications in the NERVA propulsion system. Specimens of the materials were mounted in AGC cryogenic materials pulling assemblies, submerged in liquid hydrogen, and irradiated for close to 200 hr. While still in liquid hydrogen, the specimens were pulled in tension or shear until fracture occurred. After the radioactivity had decayed sufficiently, the specimens were removed and measured for elongation and reduction in cross section. Selected specimens were then subjected to x-ray diffraction and metallographic studies.

Two irradiations were required; both were terminated before the scheduled 200 hr because of suspected hydrogen leaks. Two assemblies were used in the first irradiation (190 hr) and one in the second irradiation (178 hr).

Analysis of the neutron monitoring foils exposed during the irradiations indicates that a typical neutron flux above 1.0 Mev was 2.44×10^4 n/cm^2-sec-watt, or 5×10^{16} n/cm^2 integrated flux. Integrated fast- and thermal-neutron flux profiles giving the exposure at various specimen positions are included in the body of the report.

From a statistical analysis of the stress-strain data, it was found that a radiation-effect threshold was obtained. Definite trends of decreased elongation and increased yield strength were

noted. Some variation in ultimate tensile strength and shear strength was also noted. No significant change was encountered in the analysis of the notched-tensile-specimen data. On the opposite page is a table showing the percentage changes for shear and unnotched tensile specimens.

Summary of Mechanical Property Results

Material	Specimen Type	Percent Change in Mechanical Properties			
		Ultimate Elorgation	Ult. Tensile Strength	Yield Strength	Shear Strength
Al A356-T6	LU	-30.5	+18.0**	+38.1**	
Al A356-T6	S				- 9.5**
Al 6061-T6	LU	+ 4.4	+ 6.0	+18.3**	
Al 6061-T6	LWU	+18.7	- 3.2	- 7.6	
Al 6061-T6	TWU	- 5.1	+ 6.4	+21.5**	
Al 6061-T6	LWU*	-71.8**	-28.3**	+ 0.3	
Al 6061-T6	TWU*	+ 0.4	-16.6**	-11.0	~~+5.0**~~
Al 6061-T6	S				+5.0**
Al 7075-T6	LU	-17.6**	+ 2.7	+ 5.2	
Al 7075-T6	S				-15.7**
SS 347	LWU	+ 6.5	+ 2.4	-35.1**	
SS 347	S				- 1.4
SS 347C	LU	- 7.7	- 2.0	- 3.4	
SS A-286	LU	-14.9**	- 1.0	+ 0.8	
SS A-286	S				- 6.7
Inconel X-750	LU	-11.8**	-10.0	+ 8.1	
Inconel X-750	S				+ 6.0**
Inconel 713C	LU	-16.3	+19.0**	+23.3**	
Ti A-110-AT	TU	+ 4.0	+ 4.0	+ 2.8	
Ti A-110-AT	TWU	-19.7	+ 1.0	+ 2.8	
Ti A-110-AT	S				+ 9.1
Hastelloy C	LU	--	- 0.2	+ 0.5	
Hastelloy C	S				-14.8**
D-979	S				+10.2

L - Tensile specimens pulled longitudinal to the rolling direction

T - Tensile specimens pulled transverse to the rolling direction

U - Unnotched specimens

W - Welded specimens

S - Shear specimens

* - Specimens tested in the "as welded" condition

** - The percent change shown is statistically significant

BLANK PAGE

TABLE OF CONTENTS

TABLE OF CONTENTS (Cont'd)

LIST OF FIGURES

LIST OF FIGURES (Cont'd)

LIST OF TABLES

BLANK PAGE

I. INTRODUCTION

GTR Test 16 is part of a series of tests being conducted at the Nuclear Aerospace Research Facility (NARF) of General Dynamics/Fort Worth for the Space Nuclear Propulsion Office at Cleveland, Ohio (SNPO-C). The purpose of these tests is to determine the effects that a liquid-hydrogen and/or nuclear-radiation environment will have on the components and materials proposed for use in the NERVA engine. The Aerojet-General Corporation (AGC) has prime responsibility for development of the NERVA engine; the nuclear reactor in the engine is being developed by Westinghouse Astronuclear Laboratory (WANL). Previous tests in the series and the results of these tests are given in Reference 1 and 2. GTR Test 16 is documented in two volumes: Volume 1, reporting on the irradiation and testing at LH_2 temperatures of tensile and shear metallic specimens supplied by AGC; and Volume 2, reporting on the irradiation at LN_2 temperatures of materials and components supplied by WANL (Ref. 3).

The AGC test, as set forth in the AGC specifications (Ref. 4), consisted of three parts: 37/A002, 37/A003, and 37/A004. The latter, a thermal-conductivity test of metallic specimens at LH_2 temperatures, was cancelled during preirradiation control testing because of malfunctions in the test apparatus. The other two specified: (1) the irradiation of metallic tensile and shear specimens for approximately 200 hr at LH_2 temperatures, (2) the subsequent testing (pulling in tension or shear until fracture

occurs) of the specimens while still in LH_2, (3) measurement in the laboratory of elongation and percent reduction in cross-section, and (4) x-ray diffraction and metallographic studies.

A list of the materials tested is given at the beginning of Section II. This is followed by a description of the specimen loading arrangement, the irradiation and testing procedures, and the equipment and instrumentation. In Section III is a statistical analysis of the mechanical property data; a discussion of the methods used for correlating and correcting the data; and a description of the dosimetry used, along with curves showing the integrated neutron fluxes and the gamma doses to which the specimens were exposed.

The Radiation Effects Testing Facility is described in Appendix A. The methods used to attain the gage-length correction factor are discussed in Appendix B. Detailed mechanical-property data, stress-strain curves, and the results of the x-ray diffraction and metallographic studies are presented in Appendix C.

II. TEST PROGRAM

The GTR Radiation Effects Testing System at NARF is described briefly in Appendix A and in detail in Section 2 of Reference 5. The GTR is located in a water-filled tank that occupies one-third of a 20- by 30- by 27-ft-deep "swimming pool." The other two-thirds makes up the irradiation test cell. For irradiations, the reactor is traversed into a closet-like structure located midway in the tank wall separating the two areas of the pool. Items to be irradiated may be placed at any or all of the three sides: the north side, with 2 in. of water shielding, or the east and west sides, with 4 in. of water. The AGC specimens were located at the east and west positions, the WANL specimens at the north position (Fig. 2-1).

The tensile and shear specimens, all of which were provided by AGC, were fabricated from the following materials:

Tensile Specimens	Shear Specimens
Aluminum	Aluminum
A356-T6	A356-T6
6061-T6	6061-T6
7075-T6	7075-T6
Stainless Steel	Stainless Steel
347	347
440C	410
A-286	A-286
	D-979
Nickel Alloy	Nickel Alloy
Inconel X-750	Inconel X-750
Inconel 713C	Hastelloy C
Hastelloy C	
Titanium	Titanium
A-110-AT	A-110-AT

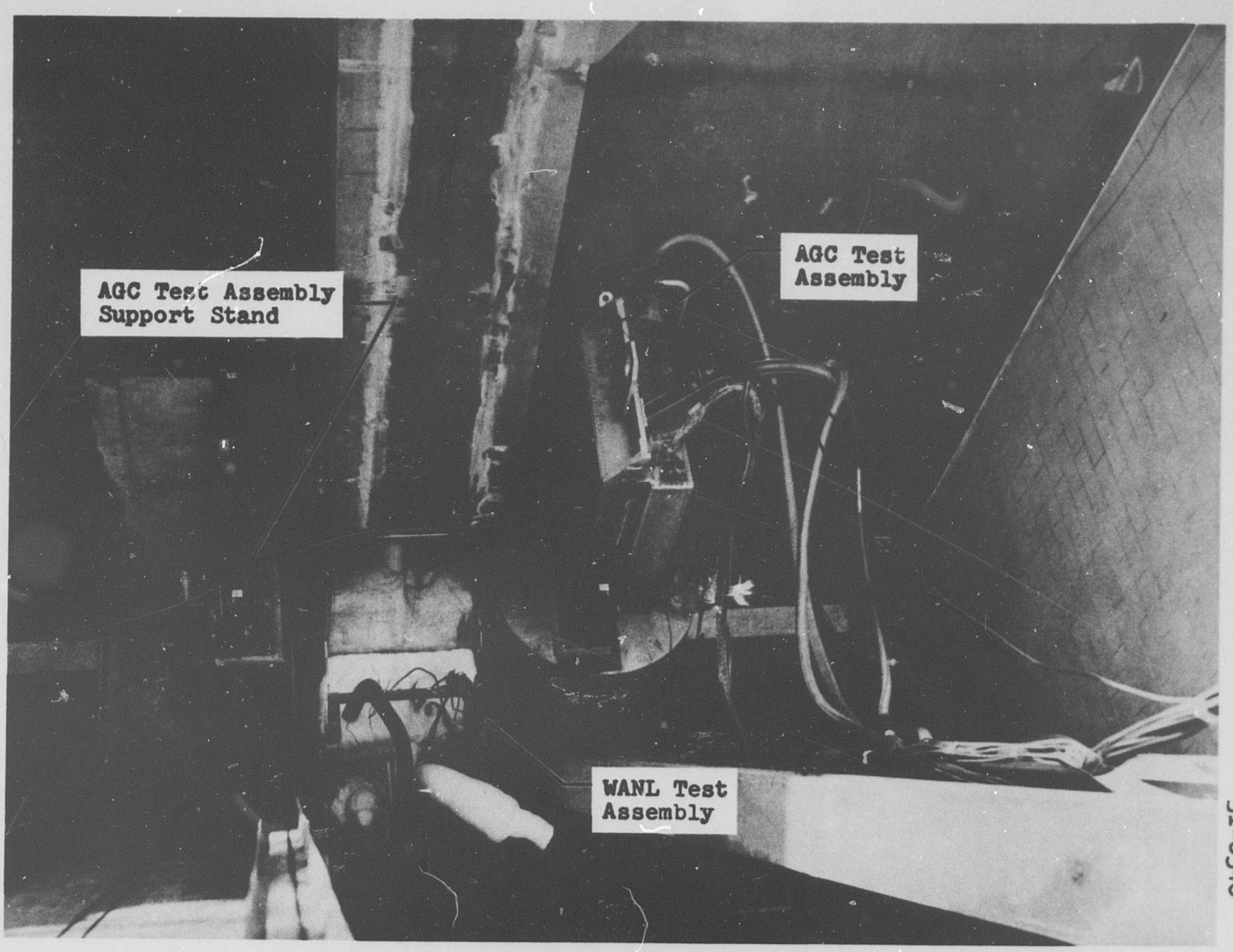

NPC 22,732
31-8348

Figure 2-1 GTR-16 Test Hardware in Irradiation Position

2.1 Test Procedures

To accommodate all the specimens, two 200-hr irradiations were planned, with a testing and re-setup period in between. During the first irradiation, two pulling assemblies were used - one on the east side of the closet and one on the west. The east assembly contained 52 tensile specimens and the west assembly contained 40 tensile and 20 shear specimens. During the second irradiation, only one pulling assembly was used. It was placed in the east position and contained 44 tensile and 20 shear specimens. The first irradiation was terminated after 190 hr and the second after 178 hr because of suspected hydrogen leaks.

2.1.1 Specimen Loading Arrangement

All specimens were cataloged and measured at NARF, then loaded in the pulling assemblies according to the schedule provided by AGC. Figure 2-2 of the east assembly, second irradiation, shows a typical loading of tensile and shear specimens before irradiation. Figure 2-3 of the east assembly, first irradiation, shows specimens after being pulled to fracture in tension. As indicated in these photographs, the specimens at any one of the four pull-rod positions can be pulled sequentially by a continuous upward stroke of the pull rods. The length of the slot in the upper, reinforced section of each specimen is designed to vary in such a way that only one specimen will be pulled at a time. Figure 2-4, a drawing of the general specimen design, illustrates how the slot length determines the distance B, which is equivalent to the distance between the clevis

NPC 23,538
31-8355

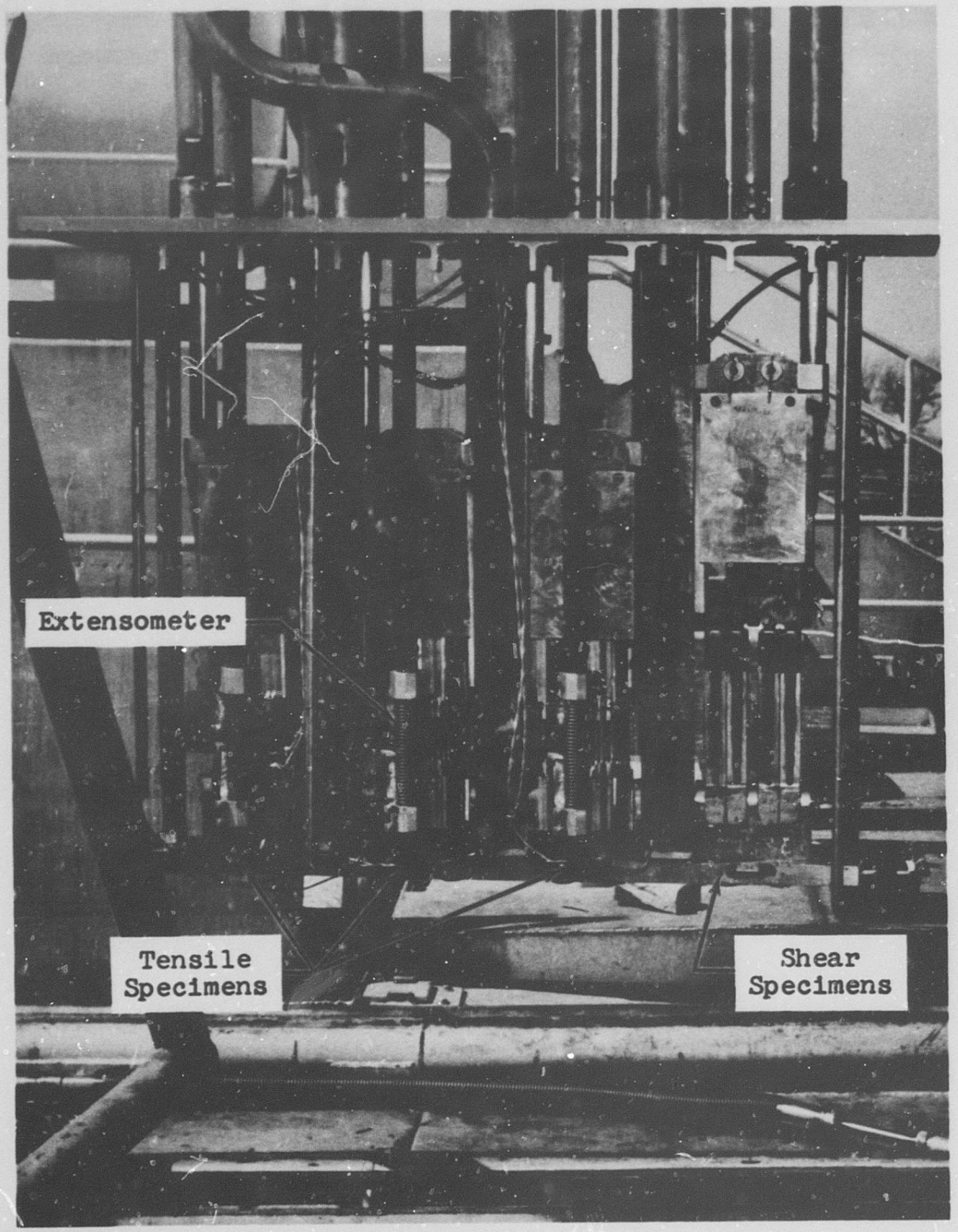

Figure 2-2 Typical Specimen Loading for AGC Cryogenic Materials Test Assembly

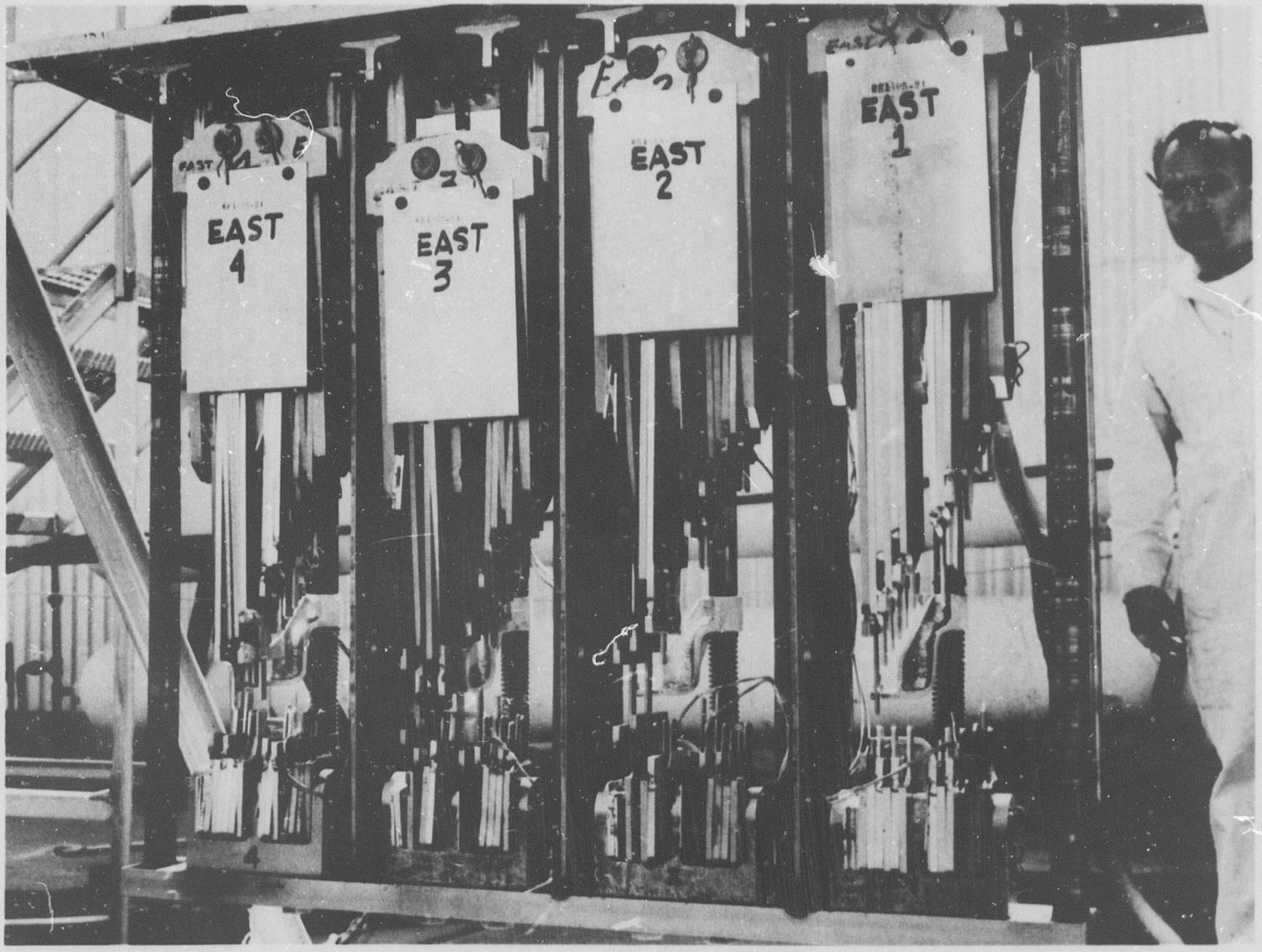

NPC 23,537
31-8381

Figure 2-3 AGC Tensile Specimens in Test Assembly after Fracture

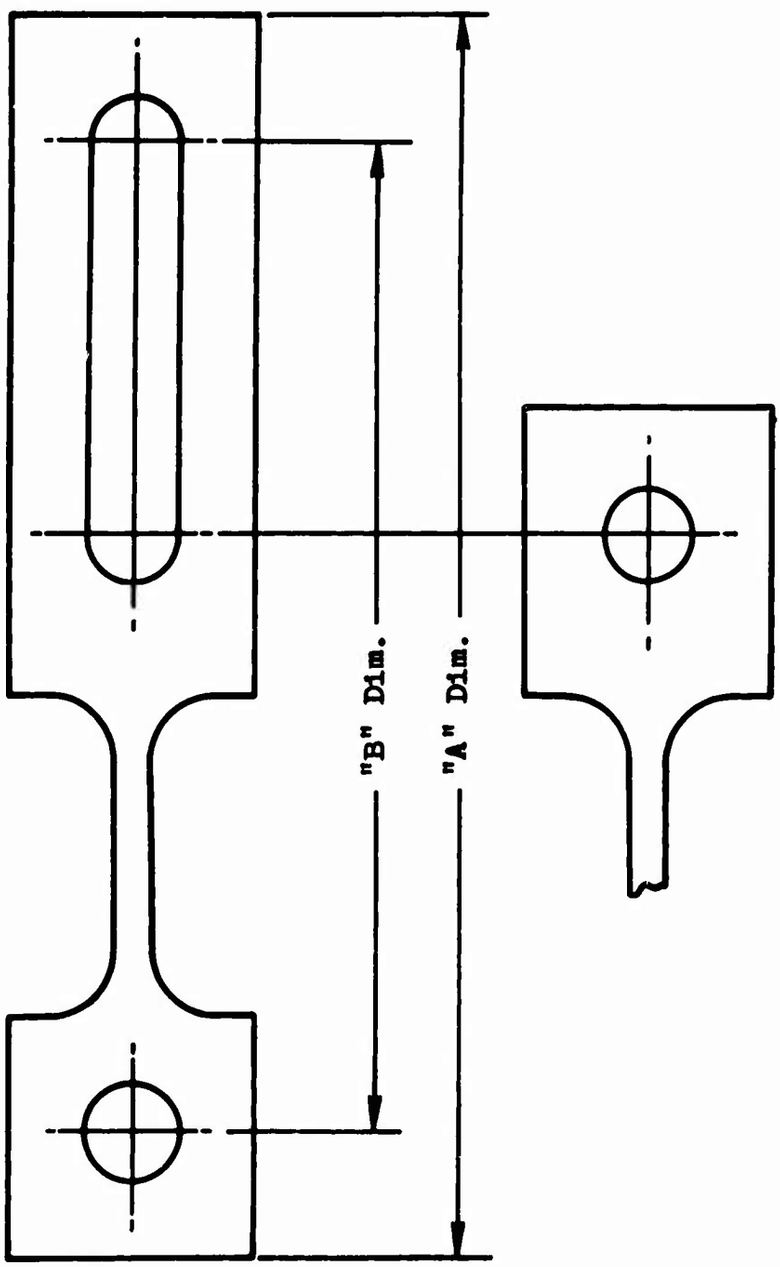

Figure 2-4 Representative Sketch of Specimen Showing Variation in Slot Length

pins at the time a tensile force is applied to the specimens. Figure 2-5 shows a typical notched and an unnotched specimen. The pulling assembly is described in more detail in Section 2.2.1.

The loading schedules for the three pulling assemblies are given in Tables 2-1, 2-2, and 2-3. Each table lists the specimen material, condition, identification number, and the distance B. The notation in the "condition" column is used throughout the report and is to be interpreted as follows:

L - specimens pulled longitudinal to the direction in which the material was rolled

T - specimens pulled transverse to the direction in which the material was rolled

N - notched specimens

U - unnotched specimens

W - welded specimens

W (as welded) - specimens that have not been subjected to heat treatment after welding

2.1.2 Irradiation Procedure

The main steps followed in preparing for the irradiations are described below:

1. Identify all specimens and record all pertinent data. Apply a Microdot weldable strain gage to one specimen in each pull position (see Tables 2-1, 2-2, and 2-3).

2. Charge and bleed the pulling and indexing hydraulic systems. (These systems have identical plumbing.)

3. Check all specimens and load in accordance with the AGC loading schedule described in Section 2.1.1. Check out each extensometer mechanism and make necessary adjustments.

4. Mate each AGC Cryogenic Materials Test Assembly to an AGC dewar; hook up and check all associated cryogenic plumbing. Hook up and check all purge equipment and instrumentation.

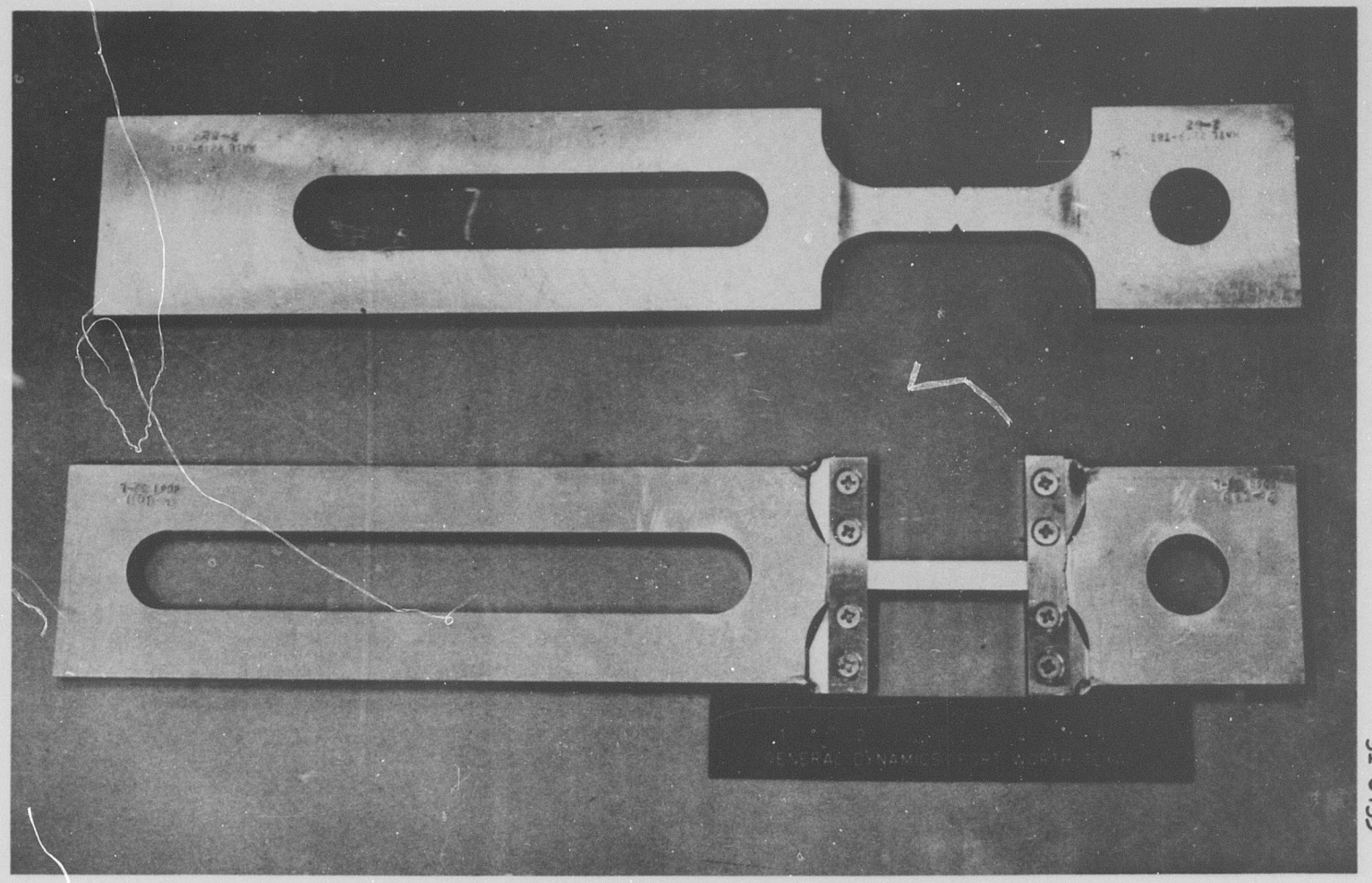

NPC 23,536
31-8435

Figure 2-5 Typical AGC Notched and Unnotched Tensile Specimens

Table 2-1

Specimen Locations in East Pulling Assembly
First Irradiation

Pull Rod 1 (South Position)				Pull Rod 2			
Material	Condition	No.	B (in.)	Material	Condition	No.	B (in.)
347	LU	701	13.00	440C	LU	201	13.00
7075-T6	LN	117	12.625	440C	LU	197	12.625
7075-T6	LU	105	12.125	6061-T6	LWU[a]	724	12.00
7075-T6	LN	113	11.75	347	LN	707	11.50
7075-T6	LU	101	11.25	347	LN	705	11.00
6061-T6	LN	2-93	10.75	A-286	LN	225	10.50
6061-T6	LU	R-83	9.875	A-286	LU	213	9.375
6061-T6	LN	2-89	9.375	A-286	LN	221	8.875
6061-T6	LU[b]	2-77	8.50	A-286	LU[b]	210	7.75
A-110-AT	TN	333	8.00	A-110-AT	TWN	345	7.375
A-110-AT	TU	285	7.25	A-110-AT	TWU	297	6.875
A-110-AT	TN	329	5.75	A-110-AT	TWN	341	6.50
A-110-AT	TU	281	5.99	A-110-AT	TWU	293	5.99

Pull Rod 3				Pull Rod 4			
Material	Condition	No.	B (in.)	Material	Condition	No.	B (in.)
440C	LU	202	13.00	347	LU	702	13.00
440C	LU	198	12.625	7075-T6	LN	118	12.625
6061-T6	LWU[a]	725	12.00	7075-T6	LU	106	12.125
347	LN	708	11.50	7075-T6	LN	114	11.75
347	LN	706	11.00	7075-T6	LU	102	11.25
A-286	LN	226	10.50	6061-T6	LN	2-94	10.75
A-286	LU	214	9.375	6061-T6	LU	R-82	9.875
A-286	LN	222	8.875	6061-T6	LN	2-90	9.375
A-286	LU[b]	211	7.75	6061-T6	LU[b]	2-78	8.50
A-110-AT	TWN	346	7.375	A-110-AT	TN	334	8.00
A-110-AT	TWU	298	6.875	A-110-AT	TU	286	7.25
A-110-AT	TWN	342	6.50	A-110-AT	TN	330	6.75
A-110-AT	TWU	294	5.99	A-110-AT	TU	282	5.99

[a]Specimens tested in the "as welded" condition (without heat treatment).

[b]Strain gage welded to specimen to measure strain in reduced cross section.

Table 2-2

Specimen Locations in West Pulling Assembly
First Irradiation

Pull Rod 4 (South Position)				Pull Rod 2			
Material	Condition	No.	B (in.)	Material	Condition	No.	B (in.)
347	LU	703	13.25	6061-T6	TWU	3-31	13.00
347	LU[a]	704	12.125	6061-T6	TWU[a]	3-35	12.50
A356-T6	LN	22	11.75	6061-T6	TWN	3-42	12.125
A356-T6	LU	10	11.25	6061-T6	TWN	3-44	11.75
A356-T6	LN	18	10.875	6061-T6	TWN	3-46	11.375
A356-T6	LU	6	10.375	6061-T6	TWN	3-48	11.00
347C	LU	177	9.937	347	LWN	216	10.75
347C	LN	185	9.562	347	LWU	204	9.75
347C	LU	173	9.125	347	LWN	214	9.50
Hastelloy C	LN	369	8.625	347	LWU	202	8.50
Hastelloy C	LU	357	7.50	347	LWN	212	8.25
Hastelloy C	LN	365	7.00	347	LWU	200	7.25
Hastelloy C	LU	353	5.99	347	LWN	210	6.875
				347	LWU[a]	198	5.99

Pull Rod 3				Pull Rod 1	
Material	Condition	No.	B (in.)	Material[b]	No.
6061-T6	TWU	3-32	13.00		
6061-T6	TWU	3-36	12.50	6061-T6	1
A356-T6	LN	21	11.75	6061-T6	2
A356-T6	LU	9	11.25	6061-T6	3
A356-T6	LN	17	10.875	6061-T6	4
A356-T6	LU[a]	5	10.375	A-286	5
347C	LU	178	9.937	Hastelloy C	6
347C	LN	186	9.562	Hastelloy C	7
347C	LU	174	9.125	Hastelloy C	8
Hastelloy C	LN	370	8.65	Hastelloy C	9
Hastelloy C	LU	358	7.50	A-286	10
Hastelloy C	LN	366	7.00	A356-T6	11
Hastelloy C	LU	354	5.99	A356-T6	12
				A356-T6	13
				A356-T6	14
				A-286	15
				7075-T6	16
				7075-T6	17
				7075-T6	18
				7075-T6	19
				A-286	20

[a]Strain gage welded to specimen to measure strain in reduced cross section.

[b]Shear specimens

Table 2-3

Specimen Locations in East Pulling Assembly
Second Irradiation

Pull Rod 4 (South Position)			
Material	Condition	No.	B (in.)
Inconel X-750	LU	381	13.00
Inconel X-750	LN	389	12.50
Inconel X-750	LU[b]	377	11.375
6061-T6	LWN[a]	3-114	11.00
6061-T6	LWN[a]	727	10.75
6061-T6	TWU[a]	720	10.25
6061-T6	TWN[a]	723	9.875
6061-T6	TWU[a]	719	9.375
6061-T6	TWN[a]	722	9.00
6061-T6	TWU[a]	718	8.50
6061-T6	TWN[a]	721	8.125
6061-T6	TWU[ab]	717	7.625
Inconel 713C	LN	417	7.25
Inconel 713C	LU	405	6.812
Inconel 713C	LN	413	6.437
Inconel 713C	LU	401	5.99

Pull Rod 2			
Material	Condition	No.	B (in.)
Inconel X-750	LU	382	13.00
Inconel X-750	LN	390	12.50
Inconel X-750	LU	378	11.375
6061-T6	TWN	288	11.00
6061-T6	LU	761	10.25
6061-T6	LWU[a]	760	9.875
6061-T6	LWN	3-92	9.00
6061-T6	LWU	3-80	8.50
6061-T6	LWN	3-90	8.125
6061-T6	LWU[b]	3-78	7.625
Inconel 713C	LN	418	7.25
Inconel 713C	LU	406	6.812
Inconel 713C	LN	414	6.437
Inconel 713C	LU	402	5.99

Pull Rod 3			
Material	Condition	No.	B (in.)
Inconel X-750	LN	392	13.00
Inconel X-750	LN	391	12.50
6061-T6	LWU[a]	726	12.00
347C	LN	190	11.50
347C	LN	189	11.00
6061-T6	LWN	3-96	10.625
6061-T6	LWU	R-84	9.75
6061-T6	LWN	3-94	9.375
6061-T6	LWU[b]	3-82	8.50
440C	LN	610	8.00
440C	LN	608	7.50
440C	LN	606	7.00
440C	LN	604	6.50
6061-T6	LWN[a]	728	5.99

Pull Rod 4	
Material[c]	No.
A-110-AT	1
A-110-AT	2
A-110-AT	3
A-110-AT	4
D-979	5
Inconel X	6
Inconel X	7
Inconel X	8
Inconel X	9
D-979	10
347	11
347	12
347	13
347	14
D-979	15
410	16
410	17
410	18
410	19
D-979	20

[a]Specimens tested in the "as welded" condition (without heat treatment).

[b]Strain gage welded to specimen to measure strain in reduced cross section.

[c]Shear specimens

5. Attach each test-assembly support stand to a pallet on the shuttle system (see Appendix A) and lower into position adjacent to the reactor closet (Fig. 2-1). By means of the overhead crane, lower each test assembly into position (Fig. 2-6).

6. Fill each dewar with LH_2 and stabilize the level. Bring the reactor to 3 Mw power and slowly traverse it into position in the closet.

The first irradiation was terminated after 190 hr because of a hydrogen leak indicated by a General Monitor sensor located at the top of the dewar shroud on the west assembly. No other sensor on either assembly indicated a leak. Since 95% of the scheduled amount of radiation was obtained, it was decided to terminate the irradiation and test the specimens.

The second irradiation was terminated after 178 hr, also because of a suspected hydrogen leak which was indicated by two General Monitors sensors located in the same general area as the one in the first irradiation. It was again decided to consider this amount of radiation adequate and test the samples.

2.1.3 Postirradiation Tests

At the conclusion of the irradiation, the reactor was shut down and the specimens pulled in tension or shear until fracture. The sequence of operations was as follows:

1. Wait 1 hr after reactor shutdown for the assemblies to reach an equilibrium condition.

2. Position the hydraulic valves on the interconnect panel to the desired assembly.

3. Assure that the hydraulic and instrumentation systems are zeroed.

4. Set Instron crosshead travel at 0.050 in./min.

5. Start recording systems and then Instron crosshead travel.

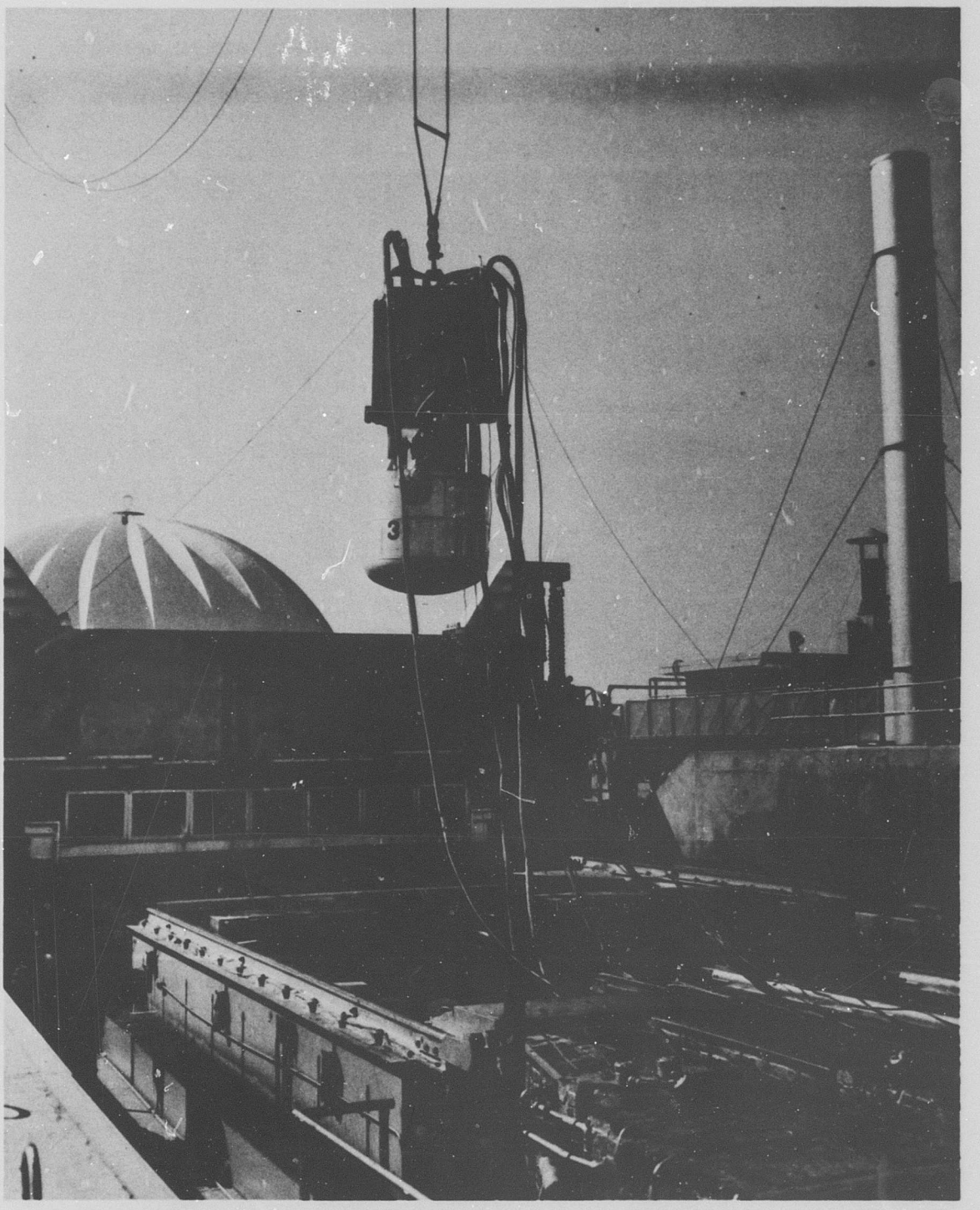

Figure 2-6 Installation of AGC Cryogenic Materials Test Assembly in the Irradiation Cell

6. Continue crosshead travel until fracture of the specimen is noted.

7. Stop Instron crosshead travel immediately after tensile specimen fracture and index extensometer mechanism to next specimen. (No indexing is required for the shear specimens.)

8. Advance Instron crosshead to pickup point for next specimen and stop to assure readiness of hydraulic and recording systems for pulling operation.

All specimens in both irradiations were tested satisfactorily, but some minor irregularities occurred during the first irradiation. These are described below:

1. A load-cell strain gage on pull rod No. 3 in the west assembly came loose while pulling the third specimen. Instron data were correlated to the strain data, as explained in Section 3.3, to present the stress-strain relationship.

2. Because of inadequate specimen spacing, the No. 2 specimen on pull rod No. 4 in the west assembly was picked up prior to failure of the No. 1 specimen. In order to test the remaining specimens on this rod, it was necessary to fracture these two specimens together, thus producing an overload condition and a resulting null shift of the load cell. Instron data were correlated as stated above.

3. The load cell for pull rod No. 3 in the east assembly was erratic and unreliable. Instron data were correlated to the strain data as previously described.

4. Extensometer data were lost on several specimens because of specimen irregularities. The rod-movement data were used to present the stress-strain relationship for determination of the yield points.

5. Considerable difficulty was encountered with the indexing hydraulic system due to gas evolution. This was corrected before the second irradiation by providing a circuit for bleeding each indexing hydraulic ram after irradiation.

After completion of the tests, cryogen flow was terminated and each assembly was purged according to established procedures detailed in the approved planning document. When the purge was

completed, the assemblies were left in the test cell for one week to allow for radioactivity decay. The systems were then removed from the test cell and stored in an isolation area.

Specimens and dosimetry from the east assembly used during the first irradiation were removed after about two weeks in the isolation area. The other two assemblies were first leak-checked, as described in Section 2.1.4, then demated for specimen and dosimetry removal. All specimens were taken to the Irradiated Materials Laboratory and measured for final gage length and cross section. Selected specimens were then sectioned and sent to the appropriate laboratories for the x-ray diffraction and metallographic studies.

2.1.4 Postirradiation Hydrogen Leak Check

The two systems with suspected leaks were positioned on the ramp and prepared for checkout to attempt to determine if a leak actually existed.

The west system was pressurized with helium gas to 7 psig. A significant leak was detected in the 1.5-in. flexible exhaust line approximately 12 ft from the top of the dewar shroud. A section of the bellows appeared to have been damaged and was dented and cracked. It is not possible to say if this happened during the test setup or upon removal of the equipment from the test cell. The leak in the exhaust line was repaired and the system was prepared for an LH_2 leak-check. The dewar was filled with LH_2 and stabilized at the normal level for 2 hr. The system was continuously checked during this 2-hr period, but no leaks were detected.

The east system (second irradiation) was pressurized with helium gas to 7 psig with no detectable leaks; a pressure decay of approximately 0.1 psi/hr was noted. The dewar was then filled with LH_2 and stabilized for 2 hr. No leaks were detected. M.S.A. portable detectors were utilized for leak-checking. The General Monitor gas-analyzing system is being examined and tested for possible inadequacies and/or radiation damage.

2.2 Test Hardware and Instrumentation

2.2.1 Cryogenic Materials Test Assembly

The test assemblies are rated for a load application of 12,000 lb. An allowable overload of 25% permits a resultant maximum load of 15,000 lb. The hydraulic rams and load cells are the limiting factors. The complete pulling assembly is shown in Figure 2-7.

Each assembly has four pull positions. The tensile specimens are secured between a stationary clevis and a movable clevis at each pull position. The movable clevis is connected to two pull rods extending through the flange plate. The pull rods extend through two guide bushings and an asbestos sealing gland. Above the flange plate the pull rods are connected to a pull-bar actuator. The hydraulic ram at each position is connected to the respective pull-bar actuator through a load-cell coupling. The stationary clevis is secured to the base plate with 0.75-in. stainless-steel (NAS1012-15) bolts. The base plate is, in turn, secured to compression members to transmit loading to the ram mounting structure. Mounting fixtures are provided for shear specimens and secured between the clevises for load application. Each clevis contains

NPC 22,739
31-8207

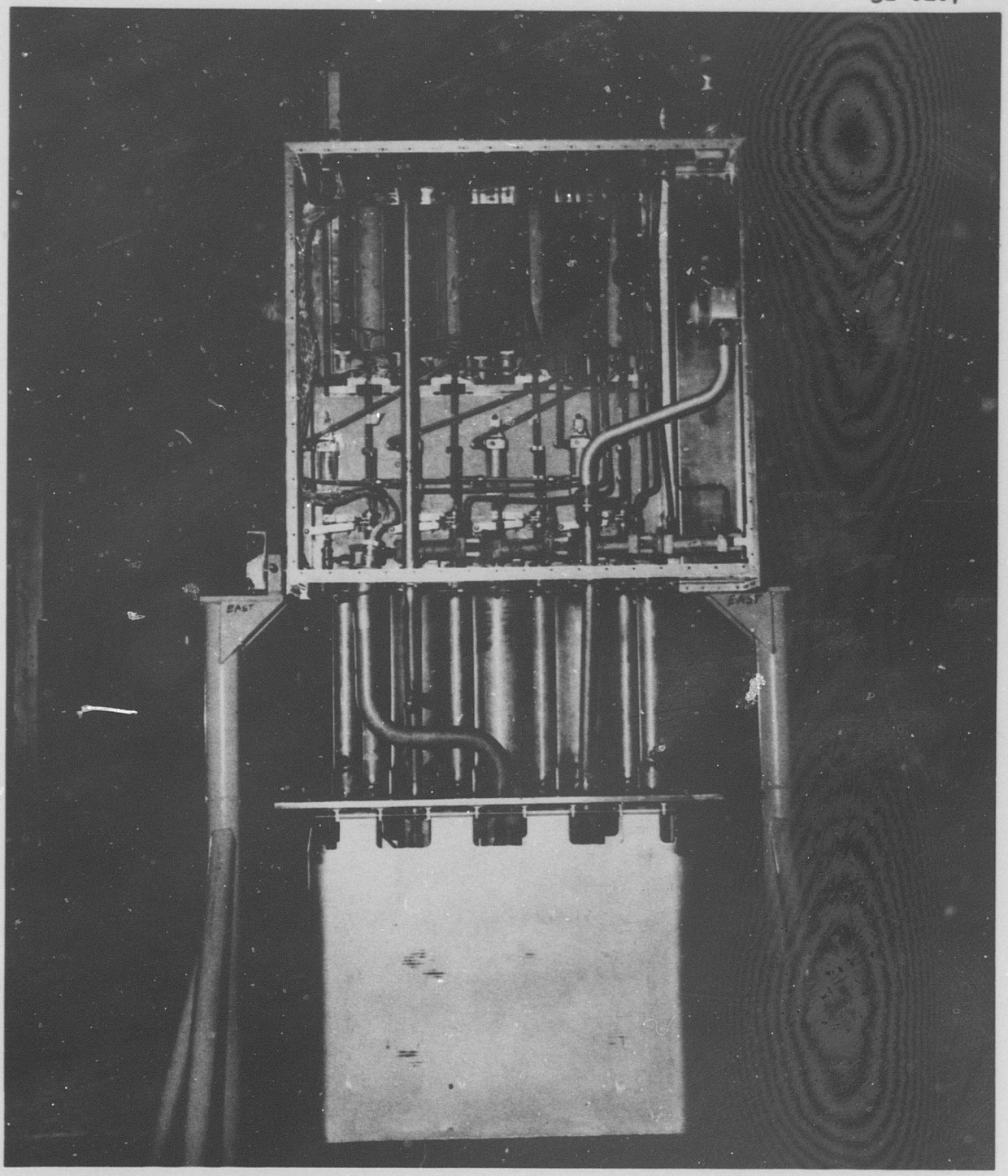

Figure 2-7 AGC Cryogenic Materials Test Assembly with Cryogen Can Installed

four progressive shear fixtures.

Each clevis is divided into two sections, each section being 2.06 in. wide. This permits a possible sample loading as follows:

Tensile	14 specimens, of 0.25-in. grip thickness, per pull position for a total of 56 specimens per pulling assembly.
Shear	5 specimens per shear fixture for a total of 20 specimens per pull position and 80 per assembly.

Various combinations of tensile and shear samples may be tested in any given assembly.

2.2.2 Liquid-Hydrogen Dewar

The cylindrical dewar is composed of two concentric cylinders, with similar 2:1 elliptical closures on the bottom connected to a common circular plate on the top (Fig. 2-8). A vacuum is maintained between the cylindrical vessels for insulation. The inner vessel contains the cryogen can, which is secured to the underside of the pulling assembly flange plate (see Fig. 2-7). The evaporated cryogen is discharged from the bottom of the dewar through a 1.25-in. exhaust line.

The dewar is secured to the test assembly flange plate with twenty 0.5-in. bolts and sealed with a 0.0625-in.-thick asbestos gasket. The bolts, of A-286 specification, are external wrenching with allowables in tension of 140,000 psi minimum at room temperature. When the system is assembled, the test assembly is eccentric to the dewar centerline by approximately 5 in.

Specifications and structural analyses of the dewars are available in References 6 and 7, respectively.

NPC 22,740
31-8210

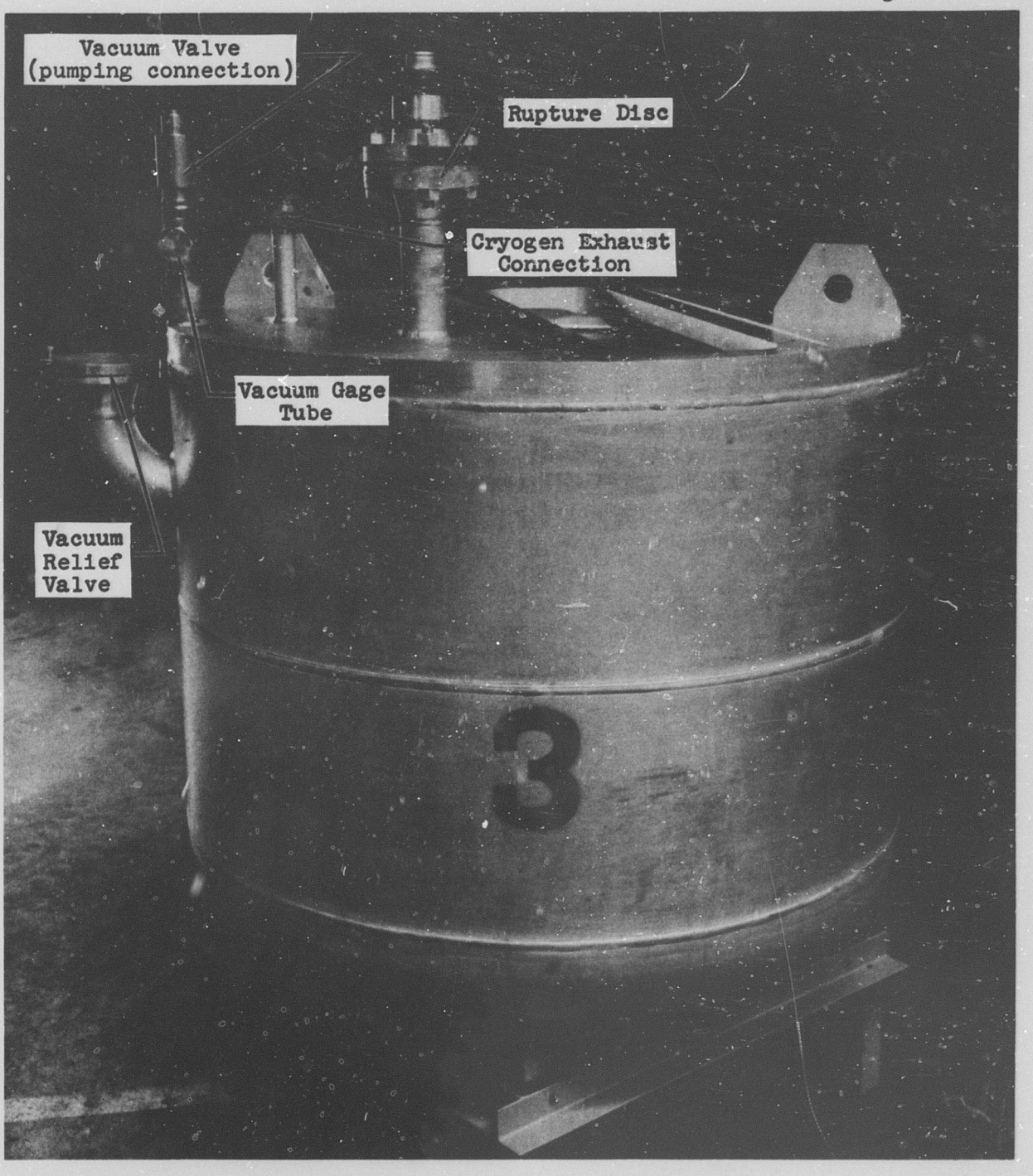

Figure 2-8 Dewar for AGC Cryogenic Materials Test Assembly

2.2.3 Equipment Safety Provisions

Safety provisions for all test equipment are described below:

1. The entire upper portion of each test assembly is enclosed in a shroud. All access fittings or lines are routed into or through the shroud for termination of connections. The shroud is continuously purged with helium gas at approximately 2 cfm to maintain an inert atmosphere. The shroud exhaust is routed through a 1.25-in. swing check valve at the top of the shroud and vented out of the pool to a vent stack at the north end of the facility. The shroud vent lines are 1.50-in. stainless-steel flex lines and are paralleled into the 3-in. vent system.

2. A pop safety valve is incorporated as overpressure protection for each test assembly and is set at 7.5 psi. The valve is positioned in and vented into the shroud. When the valve is actuated, a hermetic microswitch sets off both a visual and an audible alarm in the control room. The valve is connected to the dewar by a 1.25-in. stainless-steel tube flanged at the shroud and welded at the assembly mounting flange. In case the valve should be actuated, the shroud exhaust is sized sufficiently to handle the normal boil-off.

3. A 2.00-in., 22-psi rupture disc is incorporated in the upper closure of the dewar. The rupture disc is ported to the shroud exhaust system for venting out of the pool.

4. The normal exhaust is vented from the dewar to the burn stack. The exhaust fitting at the dewar and the rupture disc are enclosed in an inert shroud. The shroud is purged continuously with helium gas at approximately 2 cfm. The dewar shroud exhaust is vented into the pull-assembly shroud system.

5. Liquid hydrogen is supplied to each dewar through a 0.75-in. vacuum-insulated flexible supply line. The termination at the test assembly is made inside the shroud. A rigid vacuum-insulated stainless-steel line is routed from the shroud to the dewar and welded into the pull-assembly mounting flange.

6. The electrical wiring required for liquid-level indication, temperature monitoring, and strain gages is routed out of the dewar through a 2-in. stainless-steel tube. The tube is welded at the mounting flange and bolted with an asbestos seal at the shroud. At the shroud, the

wiring is terminated in a hermetic connector. This wiring, plus additional instrumentation and control parameter wiring, is routed out of the shroud through hermetic connectors.

7. Dewar pressure and shroud pressure are monitored continuously throughout the test. IRC 0-15 psig transducers are utilized as pressure transmitters. The output signal of each transducer is continuously recorded on a strip recorder in the control room (see Fig. 2-9). The transducers are mounted in the handling area and connected to the dewar and shroud with 50 ft of 0.25-in. copper tubing. The line to the dewar is routed through the shroud with a connection made inside the shroud.

2.2.4 Hydraulic System

Loads are applied to the tensile and shear specimens by means of hydraulic rams. Each basic system has the following components:

1. A master cylinder, which is secured between the movable crosshead and the load cell of the Instron tensile testing machine (see Fig. 2-10).
2. Four slave (or pulling) cylinders located on each assembly.
3. Pressure and return manifold gages.
4. Make-up and bleed reservoir.
5. Supply reservoir and pressure pump.
6. Interconnecting lines, valves, and fittings.

Each cylinder has a bore of 3.25 in., a stroke of 14 in., and a rod diameter of 1.375 in. This gives an effective rod-end piston area of 6.8 sq. in. The lines are connected to the cylinders to permit pressure application to the rod end.

2.2.5 Cryogenic Transfer System

Liquid hydrogen is supplied to each test assembly from an LH_2 transfer trailer located adjacent to the reactor pool. An LH_2 supply manifold, equipped with remotely operated supply

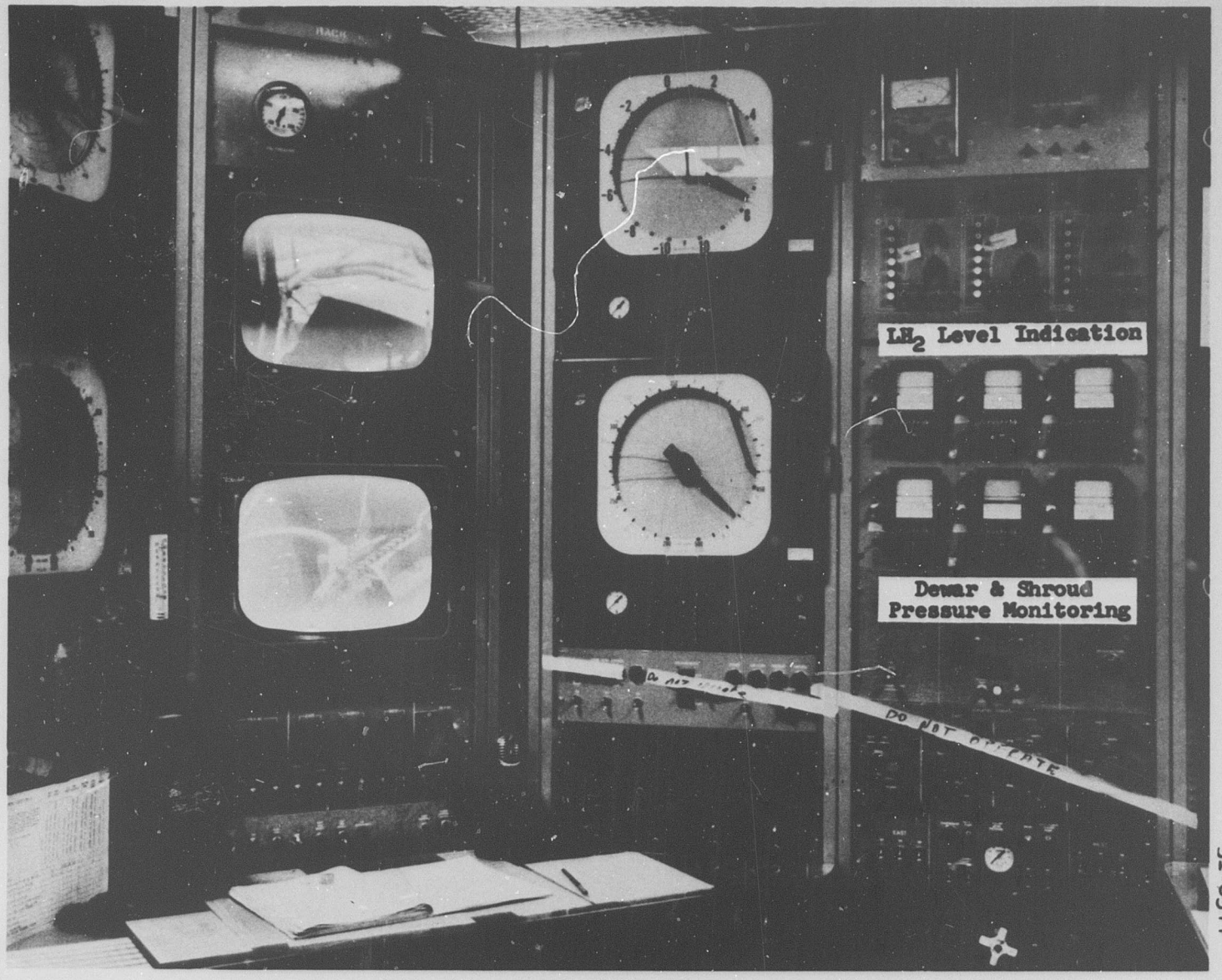

NPC 22,741
31-8344

Figure 2-9 Radiation Effects Console in Reactor Control Room: Right Side

NPC 22,742
31-8339

Figure 2-10 Instron Machine with Master Cylinder Installed

valves, is located outside the facility shield. Each supply valve is equipped with a pneumatically controlled positioner to permit proportional control of the cryogen flow. Each test assembly is connected to the manifold with 90 ft (two sections) of nominal 0.75-in.-ID, vacuum-insulated flexible lines. The manifold is equipped with two inlet valves to permit change-over of LH_2 trailers without interrupting flow to the test assemblies.

2.2.6 Cryogenic Exhaust System

Liquid hydrogen is contained in a can inside of and open to the dewar. The evaporated cryogen is exhausted through a 1.5-in. line connected at the top of the dewar. The exhaust is ported through a combination of flexible and rigid 1.5-in. lines to a point outside the facility shield. Each 1.5-in. line is routed through a gate valve and check valve into a common 5-in. line. The 5-in. line ties into the burn stack. The exhaust system is equipped to vacuum purge the test assemblies.

The vacuum purge system is composed of a valve network, a mechanical vacuum gage, a compound pressure-vacuum gage, and a vacuum pump. The valves are 1.5-in. unrestricted gate valves for vacuum and/or cryogenic service. The vacuum pump is a Kinney KD-30 pump rated at 30-cfm pumping speed, with an optimum capability of 10 microns. The pump and motor are class "B" explosion-proof and are equipped with Lox-Safe oil. The system is designed to purge an individual segment or all segments in parallel.

2.2.7 Cryogenic Level Indication and Control Systems

A liquid-level indication system continuously monitors the cryogen level in the test assemblies. The system consists of a sensor probe and an indication panel. The panel is shown in Figure 2-9 and the probe in Figure 2-11. The probe consists of seven 0.25-watt carbon resistors mounted in a rake and spaced 29.50, 21.75, 19.00, 11.00, 9.00, 6.25, and 4.12 in. below the dewar flange. The optimum control level will be between 9 and 11 in. (10 in.) below the dewar flange.

Each resistor in the probe is excited to dissipate its rated power for maximum sensitivity and response. The large difference in the heat-transfer rate of the sensor when it is in liquid and when it is in vapor produces a temperature and corresponding resistance change in the sensing element. As this resistance reaches a threshold value, t activates an output signal in the transistorized control panel. This signal triggers an indication light and/or alarm system.

A liquid-level control system is utilized to maintain a near constant level in each test assembly. A Bristol control unit, with a +100° to -430°F range kit, is used as the controlling device (see Fig. 2-12). A copper-constantan thermocouple is positioned in the dewar relative to the desired control level. The thermocouple EMF is converted to a proportional pneumatic signal in the Bristol controller. This pneumatic signal is fed to a Fisher proportional positioner, which is an integral part of the cryogen manifold and is connected in such a way as to control the outlet valve.

NPC 22,743
31-8205

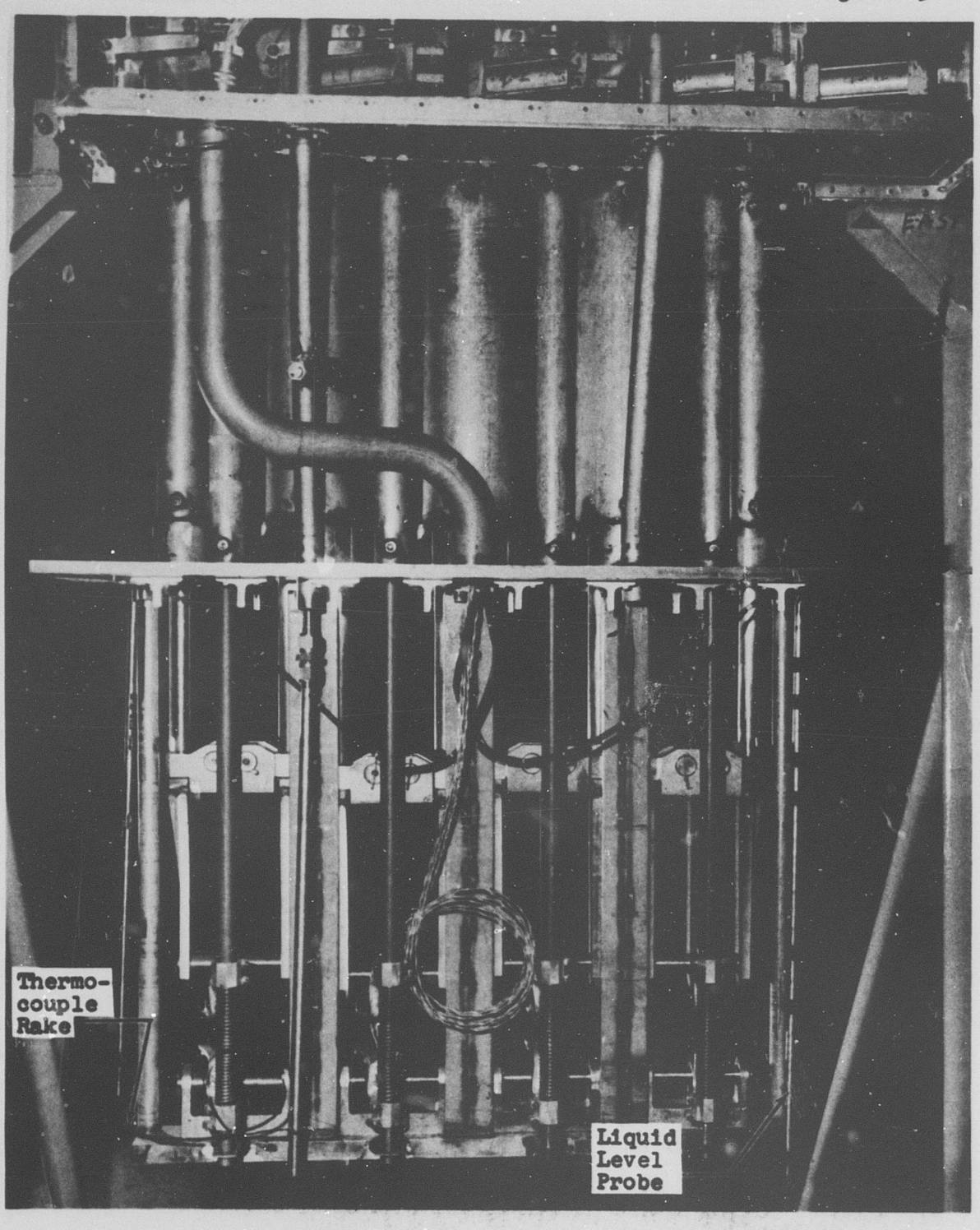

Figure 2-11 Lower Section of AGC Cryogenic Materials Test Assembly

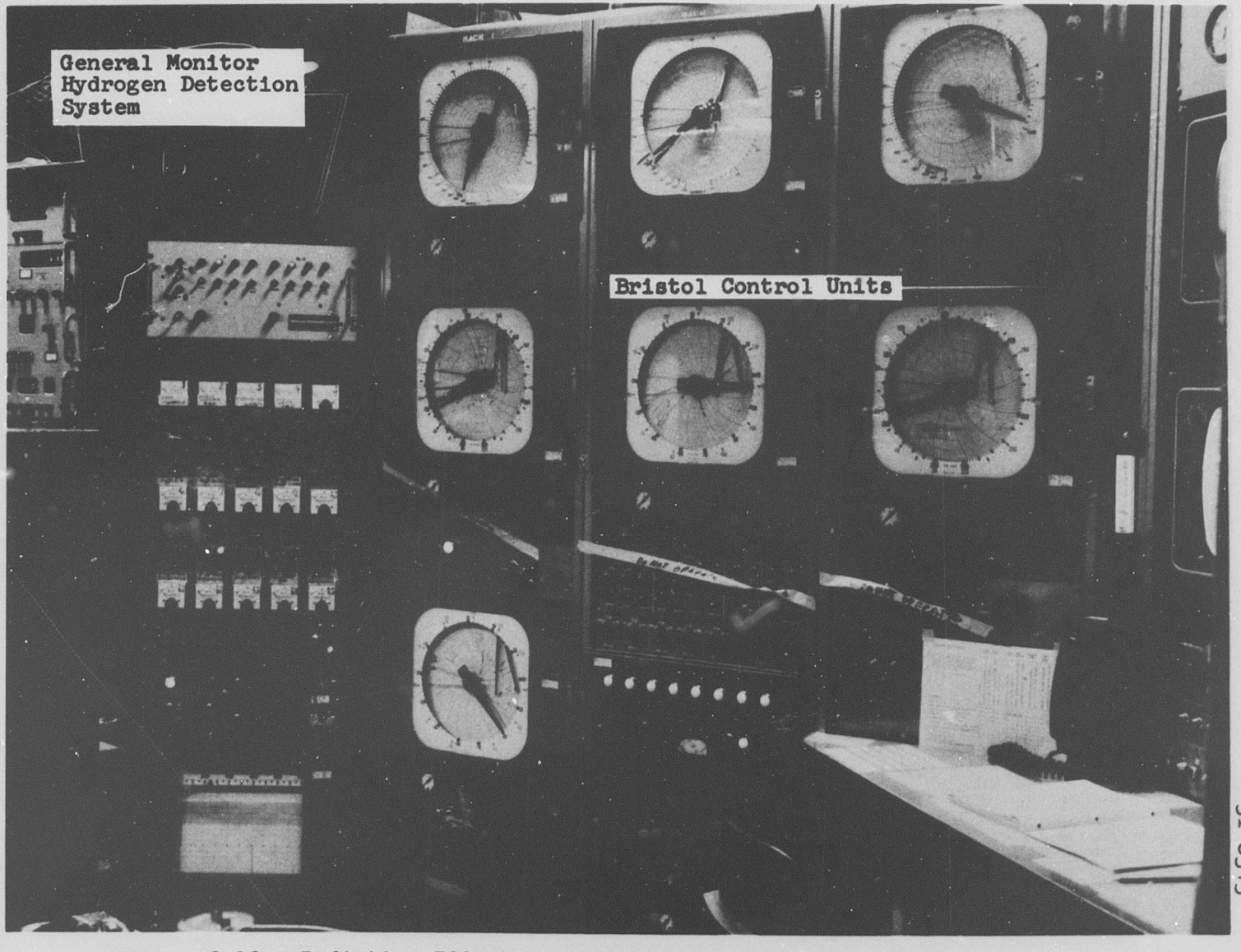

NPC 22,744
31-8343

Figure 2-12 Radiation Effects Console in Reactor Control Room: Left Side

2.2.8 Instrumentation

2.2.8.1 Applied Load Measurement

The applied load to each specimen is measured by a four-arm strain-gage load cell and recorded on an Offner dynagraph recorder. (The load cells can be seen in Figure 2-13.) The strain gages used are BLH weldable gages with ceramic bonding for optimum radiation resistance. Each load cell was calibrated utilizing the Instron tensile testing machine for load application and the Offner dynagraph recorder for data acquisition. Calibration data, shown in Figure 2-14, were obtained in representative increments up to 15,000 lb.

2.2.8.2 Strain Measurement

Representative strain is measured by three methods. These are described as follows:

Gage Length Extensometer. An extensometer mechanism is provided to measure the strain within the specimen gage length. Tabs are clamped and tack-welded to the unnotched tensile specimens to provide a 2-in. gage length. Fingers (or arms) are positioned relative to the tabs and connected to concentric tubes which are in turn connected to a displacement transducer. The fingers can be seen positioned on the specimen tabs in Figures 2-2 and 2-3. The transducer used is a Physical Sciences variable permeance-type, with a $\pm$1.000-in. range. The cryogen gas seal around the concentric tubes is effected by a cylinder-and-piston arrangement utilizing Teflon "bal seals." The extensometer mechanism is indexed from one specimen to another by means of a combination hydraulic and pneumatic indexing system (see Fig. 2-15).

NPC 22,745
31-7818

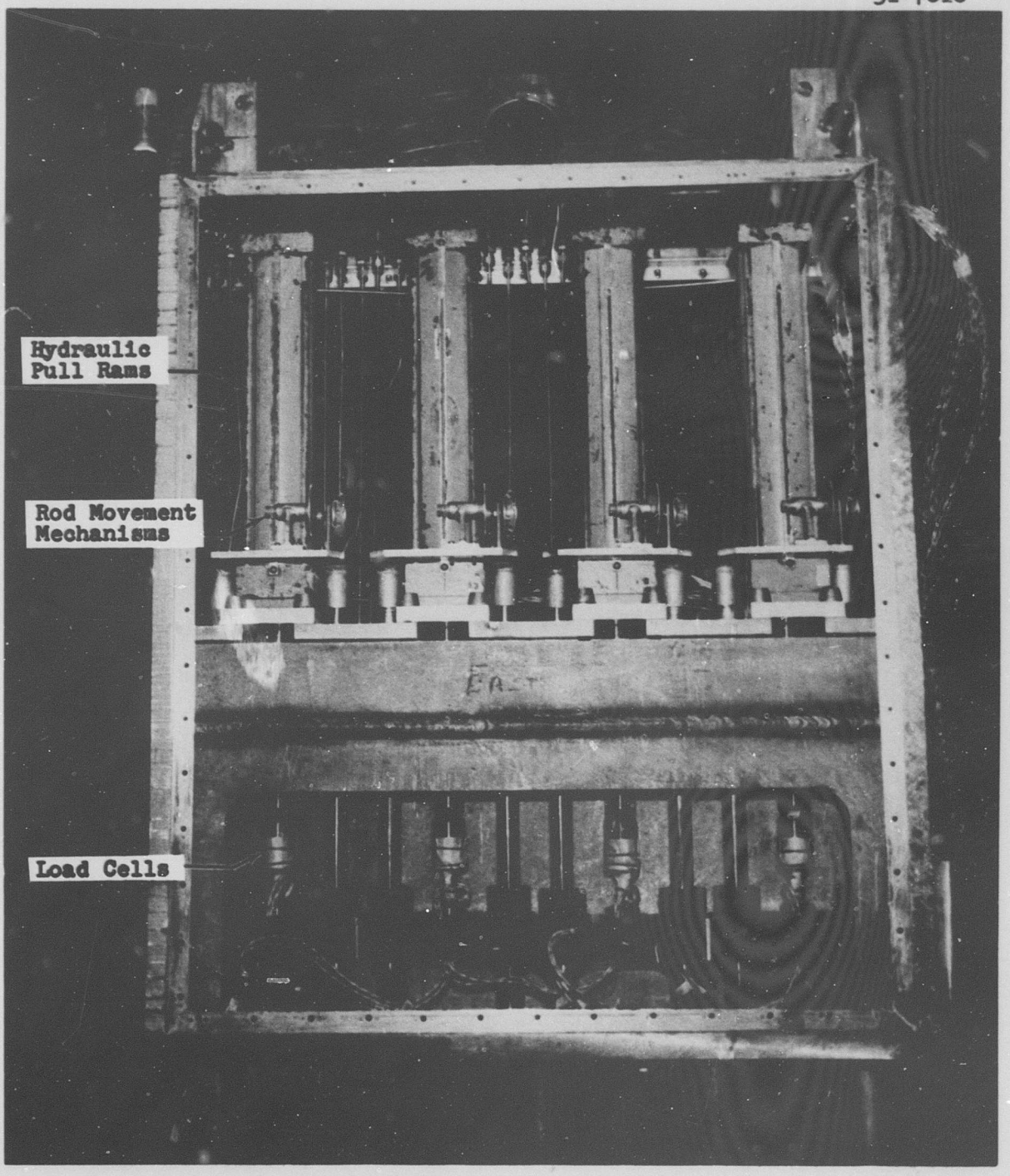

Figure 2-13 Upper Section of AGC Cryogenic Materials Test Assembly: Front Side

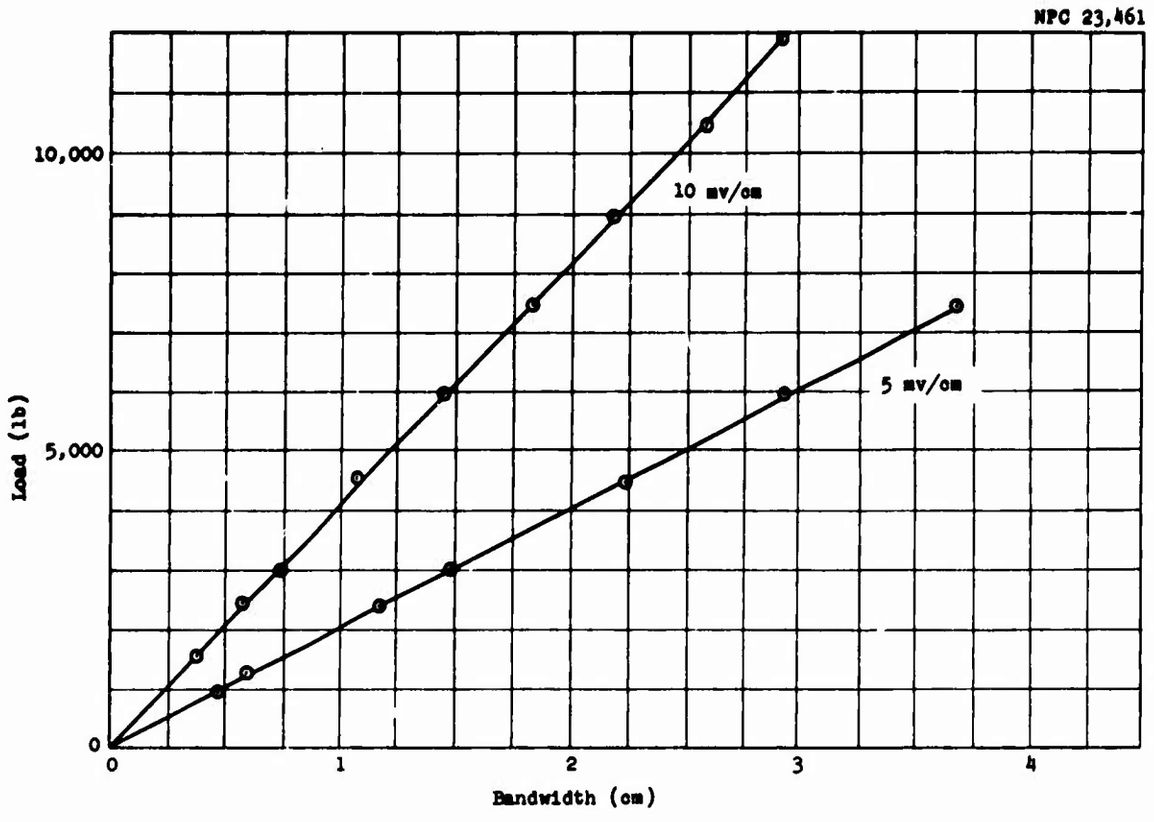

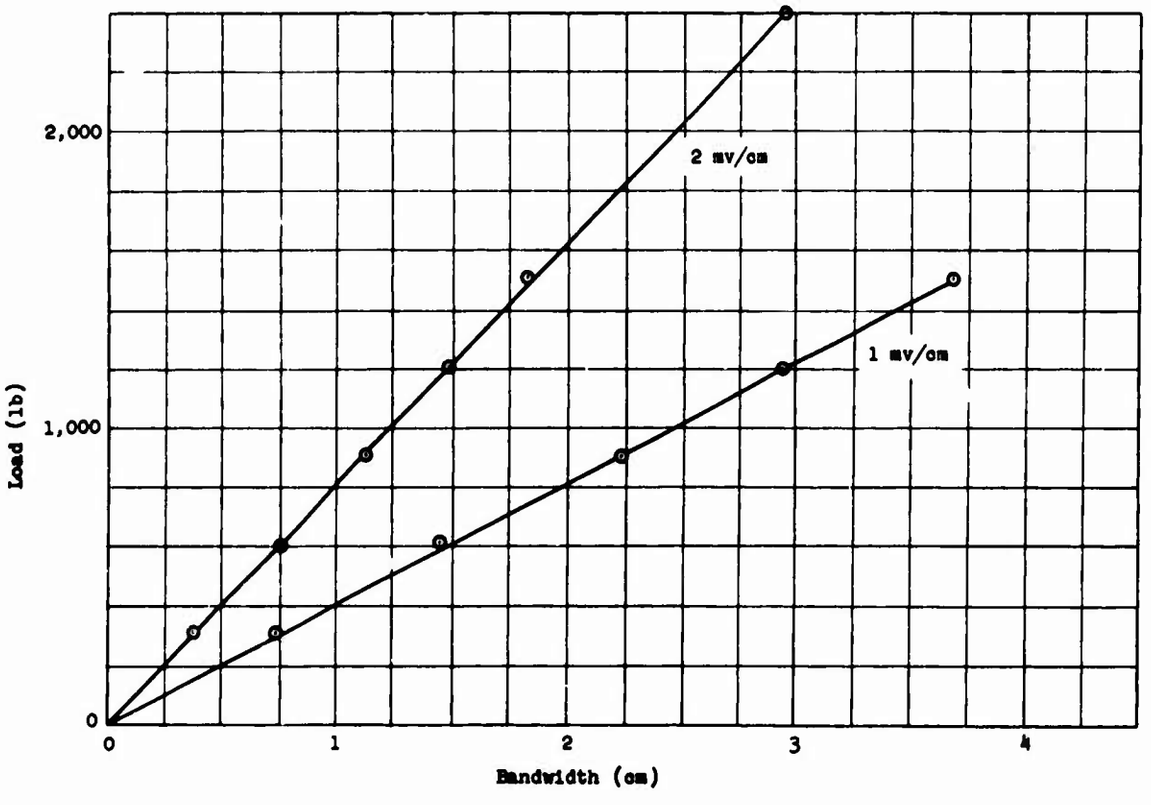

Figure 2-14 Typical Load Cell Calibration Curves

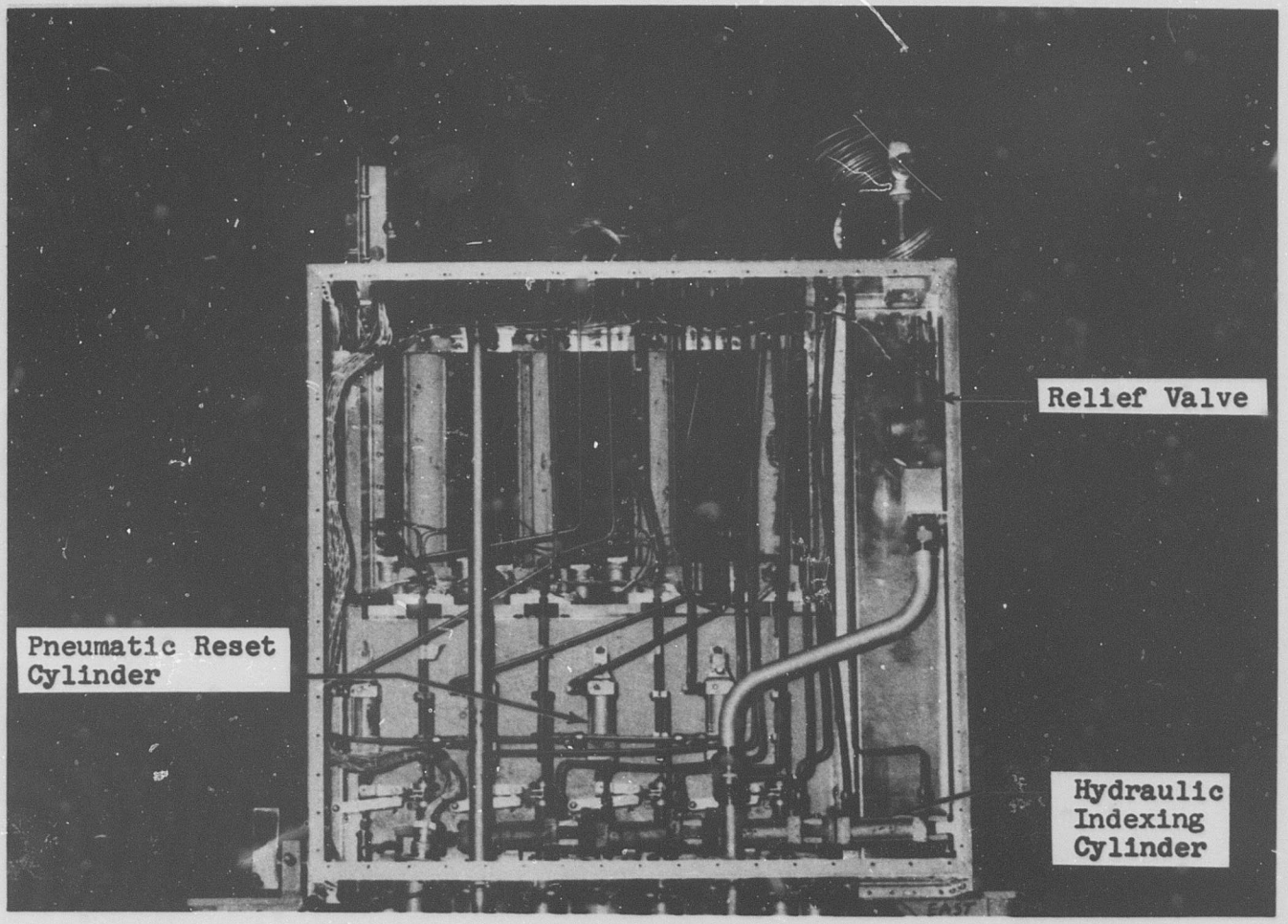

Figure 2-15 Upper Section of AGC Cryogenic Materials Test Assembly: Back Side

NPC 23,496
31-8207

Each extensometer mechanism is calibrated to 0.800 in. in representative progressive increments. Typical calibration curves are shown in Figure 2-16.

Rod Movement Mechanism. A mechanism is provided at each pull position to measure the specimen pull-rod displacement. This measurement is continuous for the total rod movement. A Helipot potentiometer (50,000 ohm, 360° rotation) is geared through a rack and pinion to the specimen pull rods (see Fig. 2-13). The potentiometers have nine equally spaced taps. Selection of the gear ratio and potentiometer tap spacing was made to give 360° of pot rotation per 0.5-in. of rod movement. This gives a resolution of from 0.5 . 1.0 mil with the use of the Offner dynagraph recorder. Each position is calibrated in 0.025-in. increments for 2 in. of rod movement. A typical calibration curve is given in Figure 2-17.

Specimen Strain Gage. A weldable strain gage is attached to one specimen in each pull position to measure the strain in the reduced cross section. Microdot type SS-E-6B strain gages were attached to the stainless-steel specimens and AL-E-6B gages to the aluminum specimens. The active length of all specimen gages is 1.00 in. A compensating gage is provided in each assembly and the signal output of the gages is recorded on the Offner dynagraph recorder

2.2.8.3 Temperature Monitoring

Seven copper-constantan thermocouples are provided in each dewar for monitoring the liquid, vapor, and specimen temperatures (Fig. 2-11). Three of the thermocouples are provided to measure

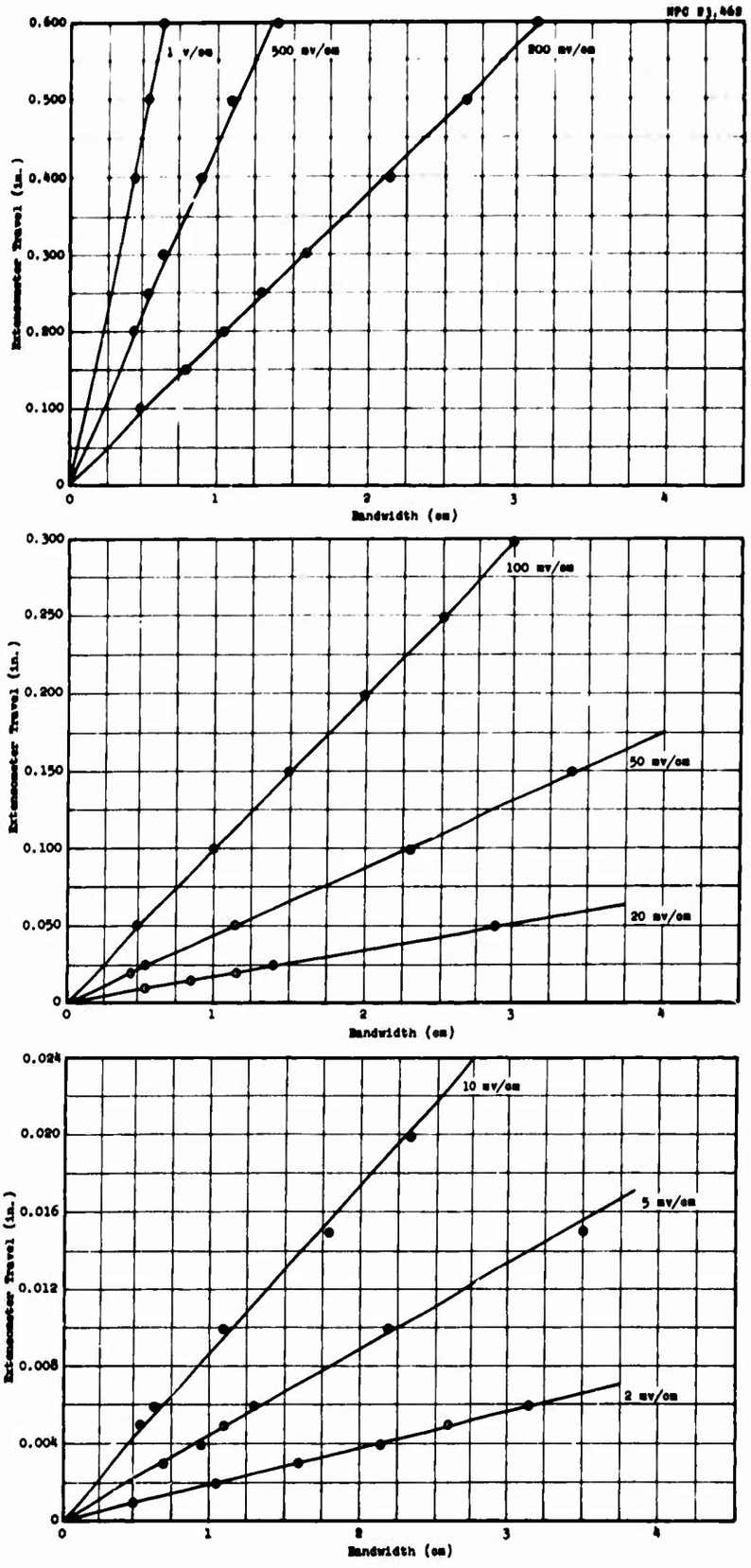

Figure 2-16 Typical Extensometer Calibration Curves

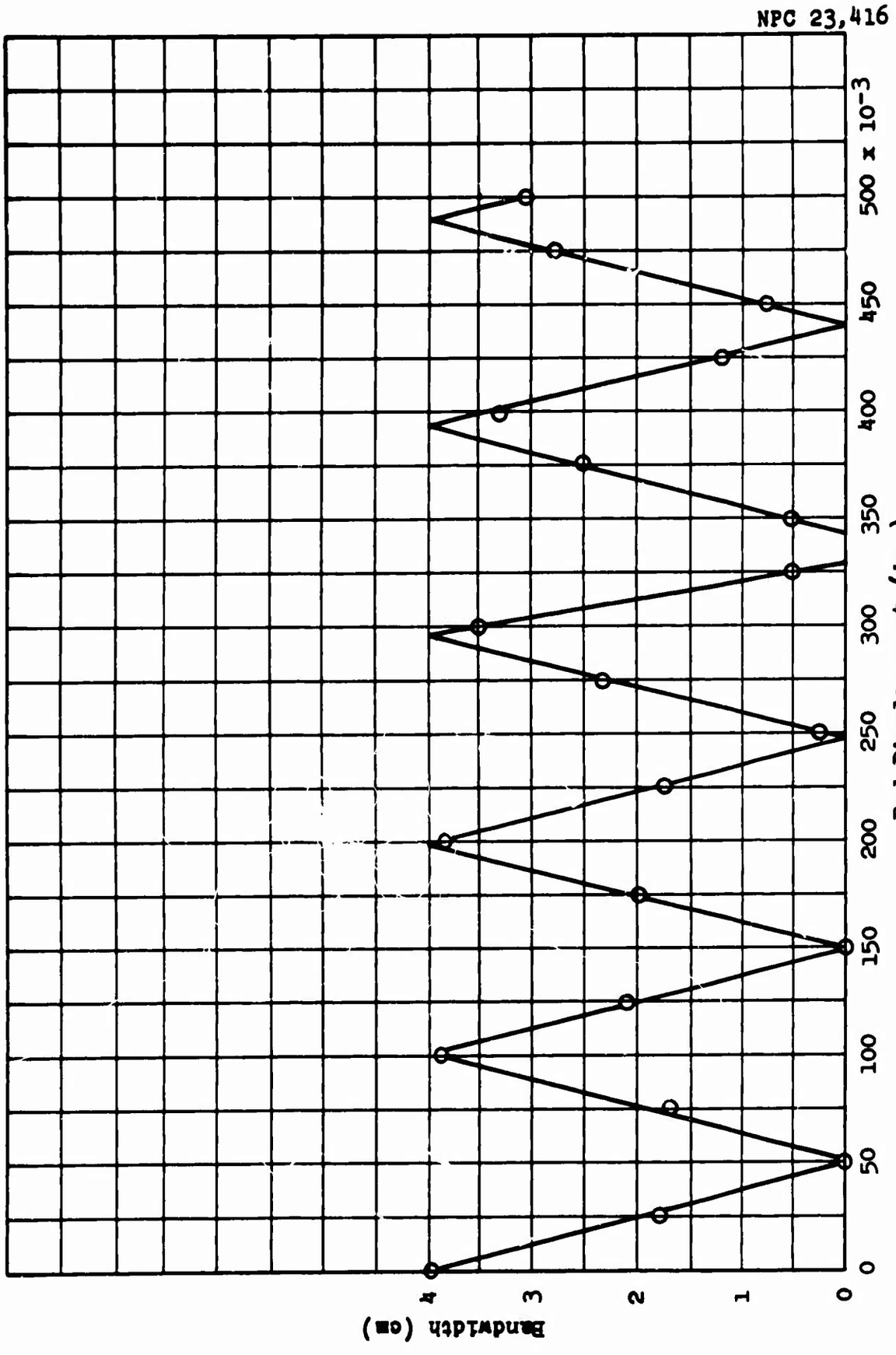

Figure 2-17 Typical Rod-Movement Calibration Curve

the temperature of the hydrogen vapor and supply the signal for the liquid-level control system. The remaining four thermocouples are provided to measure liquid temperature and specimen surface temperature. These thermocouples are located as follows:

1. 12 in. below the dewar flange
2. 24 in. below the dewar flange
3. On a specimen in the No. 1 pull position
4. On a specimen in the No. 2 pull position

These four thermocouples are referenced to liquid nitrogen and the output signal recorded on the Dymec Digital Data Acquisition System.

BLANK PAGE

III. ANALYSIS AND DISCUSSION OF RESULTS

A statistical test of significance was used to evaluate the observed differences between the average values of the pre- and postirradiation mechanical-property data. The preirradiation (control) values are given in Reference 8. The results and interpretation of the results of this analysis are presented in Section 3.1. The tensile and shear test data for individual specimens of each material are reported in tables in Appendix C. Stress-strain curves, x-ray diffraction data, and the results of a metallographic study are also presented in Appendix C.

The extensometer devices used to measure remotely the elongation of the specimens required that a correction factor be applied to the measured values in order to determine the actual elongation of the 2-in. gage length. This correction factor is discussed briefly in Section 3.2 and in detail in Appendix B.

In those cases where the ram load cell was inoperative (see Section 2.1.3), it was necessary to determine the load applied to the specimens from Instron data instead of from the ram load-cell data. The method used to do this is discussed in Section 3.3.

The integrated neutron fluxes to which the specimens in all three assemblies were exposed are given in Section 3.4.

3.1 Statistical Analysis of Mechanical Properties

The averages and standard deviations of the data for the various material conditions are tabulated in Tables 3-1 through 3-5. The last column of each table indicates the significant differences between the preirradiation and postirradiation averages that cannot be accounted for by the specimen variations.

Table 3-1

Comparison of Pre- and Postirradiation Ultimate Elongation of Unnotched Specimens at LH_2 Temperature

Material	Specimen Type*	Average Total Elongation (mils)				% Change in Ultimate Elongation	Statistically Significant Changes (x)
		Preirradiation		Postirradiation			
		Avg	σ	Avg	σ		
Al A356-T6	LU	75.8	21.4	52.7	10.7	-30.5	
Al 6061-T6	LU	577.2	122.1	602.8	47.3	+ 4.4	
Al 6061-T6	LWU	177.5	55.4	210.7	131.1	+18.7	
Al 6061-T6	TWU	257.5	62.2	244.4	10.2	- 5.1	
Al 6061-T6	LWU (as welded)	370.0	58.3	104.5	54.5	-71.8	x
Al 6061-T6	TWU (as welded)	214.3	65.1	215.2	47.2	+ 0.4	
Al 7075-T6	LU	274.0	33.0	225.7	8.9	-17.6	x
SS 347C	LU	225.0	58.3	207.6	68.9	- 7.7	
SS 347	LWU	800.0	147.7	852.3	157.4	+ 6.5	
SS A-286	LU	982.5	106.8	835.6	61.7	-14.9	x
Inconel X-750	LU	972.5	58.3	857.5	31.1	-11.8	x
Inconel 713C	LU	93.5	9.7	76.4	24.7	-18.3	
Ti A-110-AT	TU	505.0	68.0	525.5	18.3	+ 4.0	
Ti A-110-AT	TWU	269.3	106.8	216.2	4.7	-19.7	

*L(T) - Specimens pulled longitudinal (transverse) to rolling direction

U - Unnotched W - Welded σ - Standard Deviation

Table 3-2

Comparison of Pre- and Postirradiation Yield Strengths of Unnotched Specimens at LH_2 Temperature

Material	Specimen Type*	Average Yield Strength (ksi)				% Change in Yield Strength	Statistically Significant Changes (x)
		Preirradiation		Postirradiation			
		Avg	σ	Avg	σ		
Al A356-T6	LU	31.0	0.9	42.8	2.4	+38.1	x
Al 6061-T6	LU	46.5	2.6	55.0	4.4	+18.3	x
Al 6061-T6	LWU	56.9	3.7	52.6	5.6	- 7.6	
Al 6061-T6	TWU	47.4	2.6	57.6	1.2	+21.5	x
Al 6061-T6	LWU (as welded)	34.3	4.8	34.4	2.3	+ 0.3	
Al 6061-T6	TWU (as welded)	34.4	4.7	30.6	2.9	-11.0	
Al 7075-T6	LU	99.1	6.7	104.3	2.2	+ 5.2	
SS 347C	LU	83.0	22.2	80.2	12.6	- 3.4	
SS 347	LWU	97.0	8.8	63.0	10.2	-35.1	x
SS A-286	LU	135.9	6.3	137.0	6.3	+ 0.8	
Inconel X-750	LU	135.8	15.6	146.8	0.7	+ 8.1	
Inconel 713C	LU	108.0	9.4	133.2	4.4	+23.3	x
Hastelloy C	LU	111.0	0.8	111.5	2.9	+ 0.5	
Ti A-110-AT	TU	199.5	8.8	205.1	2.9	+ 2.8	
Ti A-110-AT	TWU	198.6	5.7	204.2	9.2	+ 2.8	

*L(T) - Specimens pulled longitudinal (transverse) to rolling direction

U - Unnotched W - Welded σ - Standard Deviation

Table 3-3

Comparison of Pre- and Postirradiation Ultimate Tensile Strengths of Unnotched Specimens at LH_2 Temperature

Material	Specimen Type*	Average Ult. Tensile Strength (ksi)				% Change in Ult. Tensile Strength	Statistically Significant Changes (x)
		Preirradiation		Postirradiation			
		Avg	σ	Avg	σ		
Al A356-T6	LU	44.7	1.7	52.8	2.3	+18.0	x
Al 6061-T6	LU	64.7	4.6	69.0	3.9	+ 6.0	
Al 6061-T6	LWU	68.9	1.8	66.7	9.3	- 3.2	
Al 6061-T6	TWU	67.3	3.5	71.6	4.6	+ 6.4	
Al 6061-T6	LWU (as welded)	61.5	6.0	44.1	4.7	-28.3	x
Al 6061-T6	TWU (as welded)	54.9	6.0	45.8	2.2	-16.6	x
Al 7075-T6	LU	110.4	8.1	113.4	2.1	+ 2.7	
SS 347C	LU	117.3	5.3	115.4	4.6	- 2.0	
SS 347	LWU	224.2	21.4	229.5	7.7	+ 2.4	
SS A-286	LU	223.6	5.1	219.7	3.7	- 1.0	
Inconel X-750	LU	253.3	29.0	227.6	12.6	-10.0	
Inconel 713C	LU	111.6	9.7	133.4	6.4	+19.0	x
Hastelloy C	LU	185.7	one specimen only	185.4	4.4	- 0.2	
Ti A-110-AT	TU	216.4	7.1	226.5	5.3	+ 4.0	
Ti A-110-AT	TWU	214.6	5.3	217.1	7.9	+ 1.0	

*L(T) - Specimens pulled longitudinal (transverse) to rolling direction

U - Unnotched W - Welded σ - Standard Deviation

Table 3-4

Comparison of Pre- and Postirradiation Ultimate Tensile Strength of Notched Specimens at LH_2 Temperature

Material	Specimen Type*	Average Ult. Tensile Strength (ksi)				% Change in Ult. Tensile Strength	Statistically Significant Changes (x)
		Preirradiation		Postirradiation			
		Avg	σ	Avg	σ		
Al A356-T6	LN	39.7	3.8	43.2	2.6	+ 8.8	
Al 6061-T6	LN	61.4	5.3	65.8	5.5	+ 7.2	
Al 6061-T6	LWN	57.3	9.2	69.8	2.7	+18.3	
Al 6061-T6	TWN	56.5	6.0	65.2	2.8	+15.4	
Al 6061-T6	LWN (as welded)	42.1	one specimen only	41.1	6.1	- 2.4	
Al 6061-T6	TWN (as welded)	31.8	one specimen only	37.9	7.4	+19.2	
Al 7075-T6	LN	70.5	8.8	75.5	4.7	+ 7.0	
SS 347C	LN	99.2	5.4	102.3	4.5	+ 3.0	
SS 347	LWN	136.5	9.4	126.9	3.4	- 7.0	
SS A-286	LN	185.8	4.5	188.6	2.4	+ 2.0	
Inconel X-750	LN	191.6	5.4	197.2	5.1	+ 2.0	
Inconel 713C	LN	127.6	9.3	135.4	10.2	+ 6.0	
Ti A-110-AT	TN	171.0	6.1	153.7	13.9	-10.0	
Ti A-110-AT	TWN	118.1	12.6	121.2	12.1	+ 2.0	

*L(T) - Specimens pulled longitudinal (transverse) to rolling direction

N - Notched W - Welded σ - Standard Deviation

Table 3-5

Comparison of Pre- and Postirradiation Shear Strengths of Specimens at LH_2 Temperature

Material	Average Ultimate Shear Strength (ksi)				% Change in Shear Strength	Statistically Significant Changes (x)
	Preirradiation		Postirradiation			
	Avg	σ	Avg	σ		
Al A356-T6	50.4	2.3	45.6	0.63	- 9.5	x
Al 6061-T6	49.8	1.1	52.3	1.6	+ 5.0	x
Al 7075-T6	95.2	4.8	80.3	3.5	-15.7	x
SS 347	152.4	5.3	150.2	4.0	- 1.4	
SS 410	149.3	4.2	160.7	8.5	+ 5.5	
SS A-286	168.2	12.0	157.0	5.1	- 6.7	
SS D-979	152.5	5.9	168.0	18.1	+10.2	
Inconel X-750	152.8	1.4	162.0	4.9	+ 6.0	x
Hastelloy C*	170.8	3.4	145.6	1.7	-14.8	x
Ti A-110-AT	130.6	4.8	142.5	8.8	+ 9.1	

*Instron data only σ - Standard Deviation

It must be noted that statistical methods determine only the statistical significance of an observed difference in the data. A difference may be statistically significant and yet so small as to be of little engineering importance. On the other hand, when a difference is termed not significant, it does not necessarily imply that there is no difference. In some instances, only a small number of specimens are tested, and the variability in the data is too large for the radiation effects to be detected. When large numbers of specimens are tested, the sensitivity of the experiment is usually increased enough to detect a difference.

In general it can be noted that a radiation-effect threshold was obtained. Definite trends of decreased elongation and increased yield strength are apparent. Some variation in ultimate tensile and shear strength is also indicated.

Table 3-1 indicates a decreased elongation of 71.8% in 6061-T6-LWU (as welded) from the preirradiation to the postirradiation state. This is not considered to be a result of radiation damage; the macrophotograph of this material condition indicates poor weld penetration. It is difficult to say what degree of indicated damage is due to radiation and what degree is due to the poor weld penetration.

3.2 Gage-Length Correction Factor

The AGC test specifications required that the tensile specimens remain submerged in liquid hydrogen during the postirradiation testing. Since all tests were performed remotely through the use of various hydraulic and electrical apparatus, and since a large number of specimens had to be tested, conventional extensometer

devices could not be utilized. It was therefore necessary to design and build extensometer devices for these conditions. A description of their design and operation is contained in Section 2.2.8 of this report.

Metal tabs were tack-welded to the upper and lower grips of each unnotched specimen, with the inside surface of the tabs coinciding with the 2-in. gage length of the specimen. As each specimen was pulled in tension, the extensometer mechanism tracked, or followed, the separation of the tabs. For all practical purposes, the strain, as recorded by the extensometer device, occurred between the grips of the specimen and not entirely within the 2-in. gage length. For this reason it was desirable to calculate a factor which, when applied to the measured elongation, would give the elongation within the 2-in. gage length.

The approach taken applies only within the elastic range of the material. A complete analysis and the associated calculations are presented in Appendix B. The value of the constant was found to be 0.7075. All relevant data appearing in this report have been multiplied by this factor.

3.3 Correlation of Instron Load Data

As described in Section 2.1.3 , three of the twelve ram load cells were lost. The ram load cell is a transducer element that is coupled between the hydraulic ram and the movable clevis to measure the load being applied to the specimens. The load recorded by the master loading device (Instron tensile testing machine)

contains a variable tare load not recorded by the ram load cell. It was therefore necessary to correlate the data recorded by the Instron with that from the ram load cell in order to obtain the load on the specimens at the three pull positions mentioned.

This correlation was accomplished by utilizing the nine remaining load cells that functioned satisfactorily. Each of the nine load cells was considered individually. The load data recorded during the test were plotted (Instron vs ram) to obtain a correlation curve for each cell. The curves obtained were all linear and closely related. The slopes varied from 0.927 to 0.956, with an average of 0.942. A typical correlation curve of one load cell is presented in Figure 3-1.

The 0.942 value was then applied to the recorded Instron loads for the three pull positions in question to obtain equivalent ram loads.

3.4 Dosimetry

Extensive nuclear measurements, made prior to and during GTR-16, were required to provide the data needed to reliably characterize the radiation fields inside the test volumes. Following is a brief analysis of the procedures used for determining the fast-neutron flux ($E > 1$ Mev), the thermal-neutron flux ($E < 0.48$ ev), and the gamma dose rates. All gamma dose values reported are based on the results obtained during two mapping runs made prior to the material tests.

Measurements of the neutron flux were made with standard dosimetry packets attached to the pulling assembly directly in

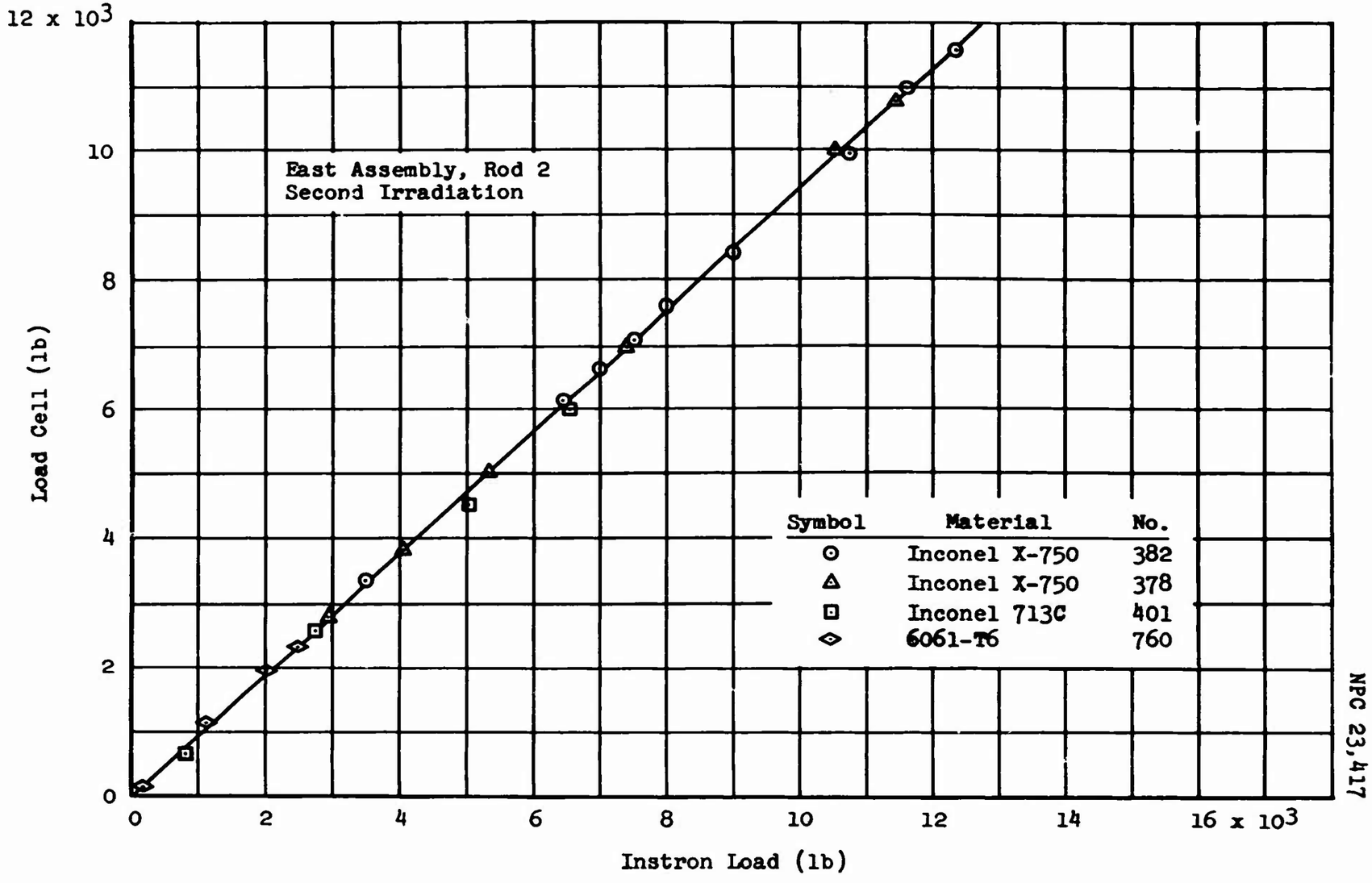

Figure 3-1 Typical Correlation Curve of Instron Load vs Load Cell

front of the material specimens (Fig. 3-2) and in front of and behind the cryogen-fluid can.

Figures 3-3 and 3-4 show the integrated thermal- and fast-neutron flux inside the east and west assemblies during the first irradiation. Figure 3-5 shows the flux inside the east assembly during the second irradiation. A bare and a cadmium-shielded phosphorous pellet were used to measure the thermal-neutron flux, and a cadmium-shielded nickel foil was used to measure the fast neutron flux above 2.9 Mev. Other fast-neutron detectors with lower thresholds could not be used because the exposure exceeded their measuring capacity. The activated foils were processed in the detector counting room and all data reduced using an IBM 7090 computer program.

Neutron spectral measurements (Fig. 2.22 of Ref. 5) made previously in the east and west positions of the GTR irradiation facility show that the ratio of the neutron fluxes, $E > 1$ Mev/ $E > 2.9$ Mev, is 2.82. A preliminary analysis of the mapping experiments made prior to GTR-16 indicates no significant variation in the shape of the neutron spectrum, regardless of position inside the dewar. Further, a comparison of the neutron flux ($E > 2.9$ Mev) measurements made with sulfur during the mapping experiments with those made with nickel foils during the GTR-16 irradiations show them to be virtually identical. The neutron flux for $E > 1$ Mev, therefore, as shown in Figures 3-3, 3-4, and 3-5, is obtained by multiplying the neutron flux for $E > 2.9$ Mev (as measured with the nickel foils) by the factor 2.82.

Figure 3-6 depicts gamma-dose profiles inside the three dewars. Since the gamma doses during this series of tests exceeded the

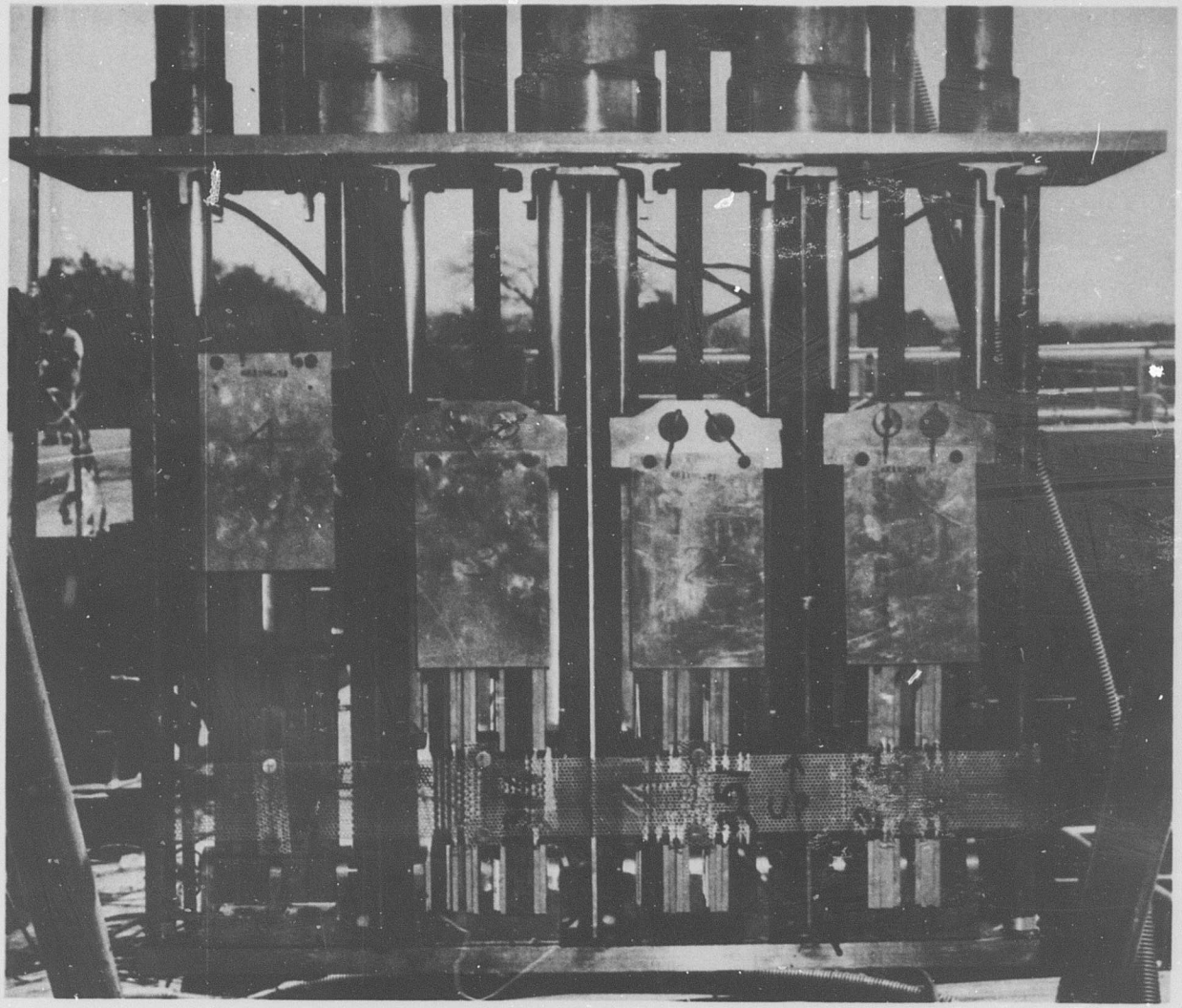

NPC 23,539
31-8354

Figure 3-2 Dosimetry Mounted on AGC Cryogenic Materials Test Assembly

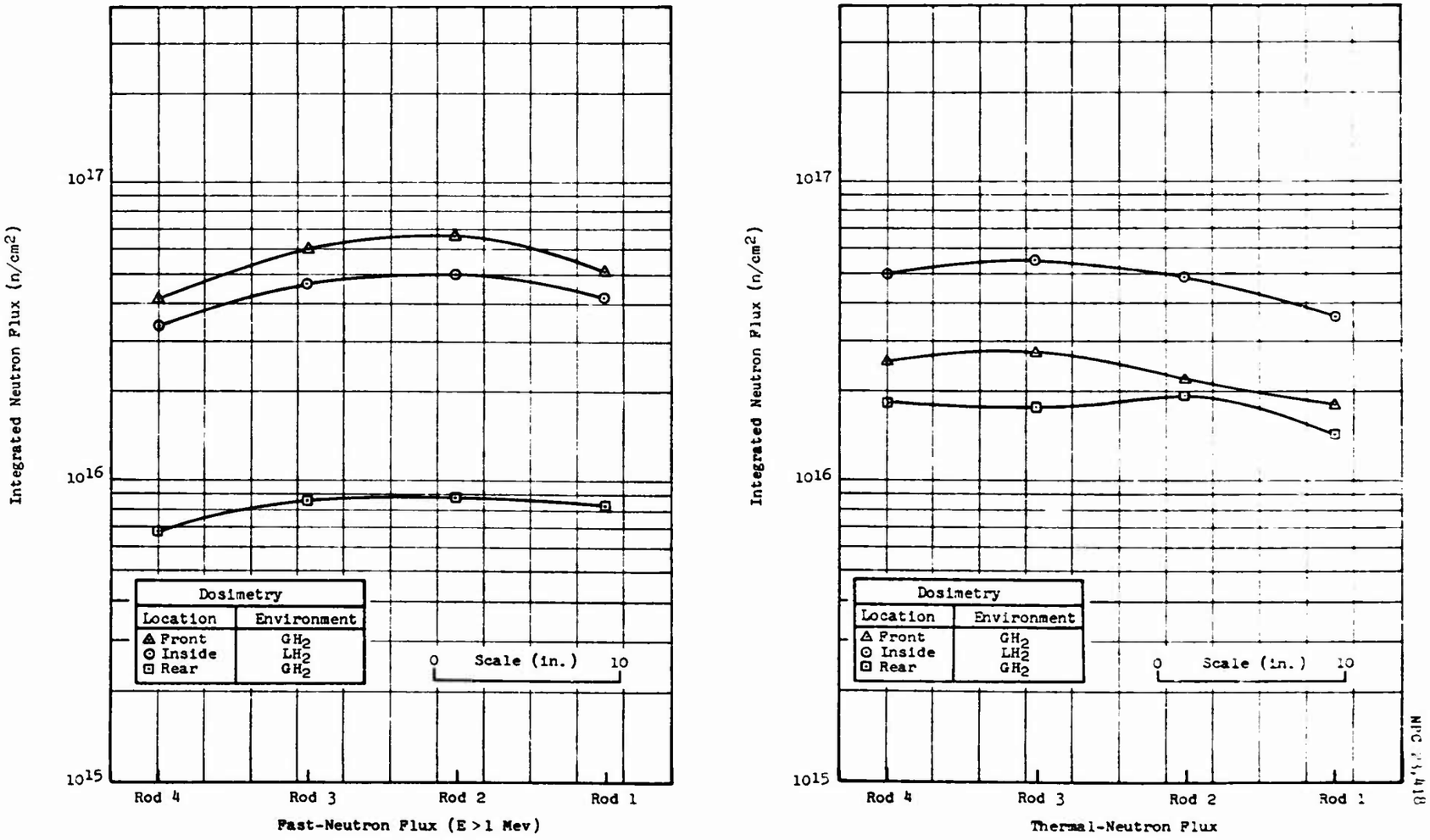

Figure 3-3 Measured Integrated Neutron Flux: First Irradiation, East Assembly

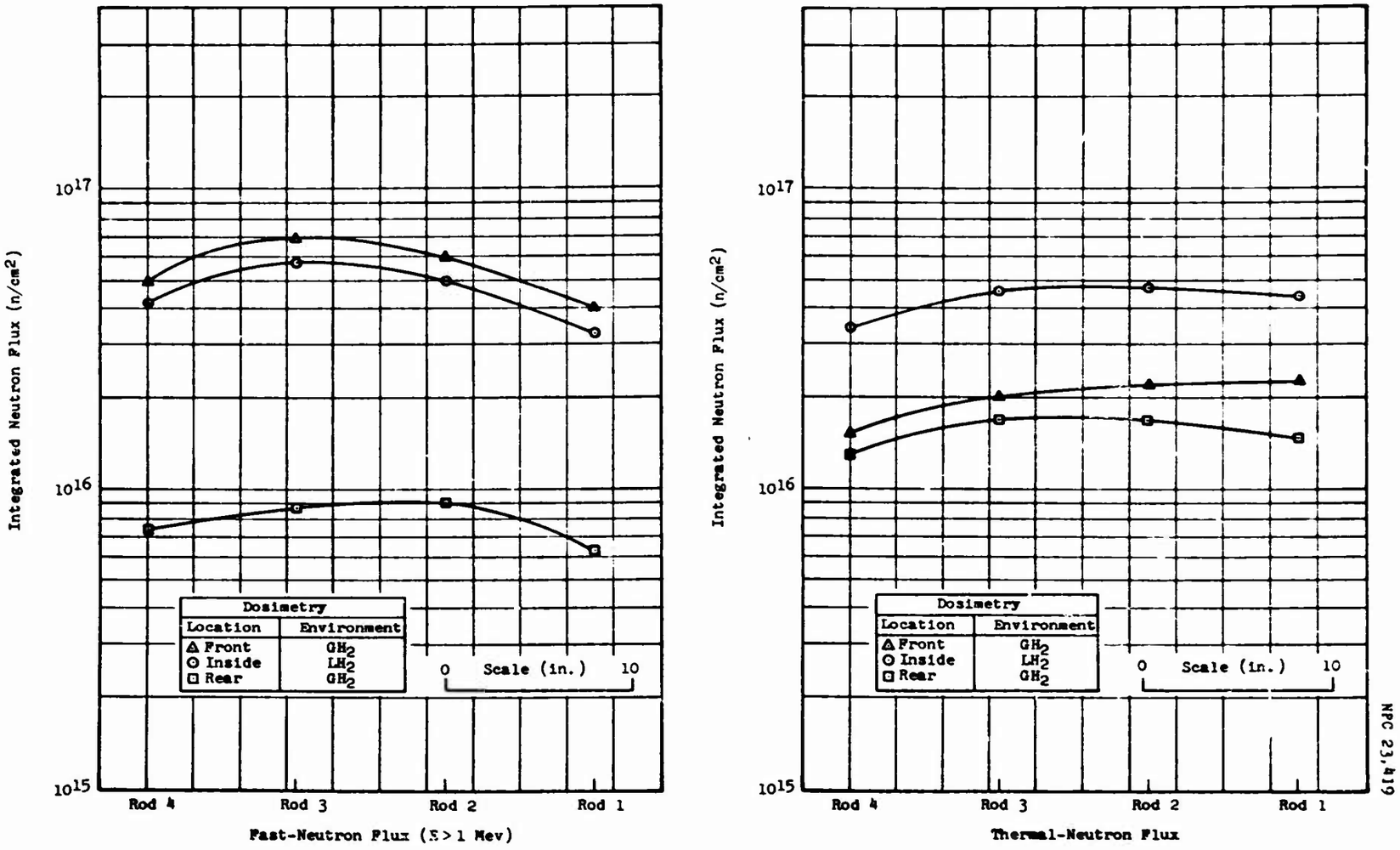

Figure 3-4 Measured Integrated Neutron Flux: First Irradiation, West Assembly

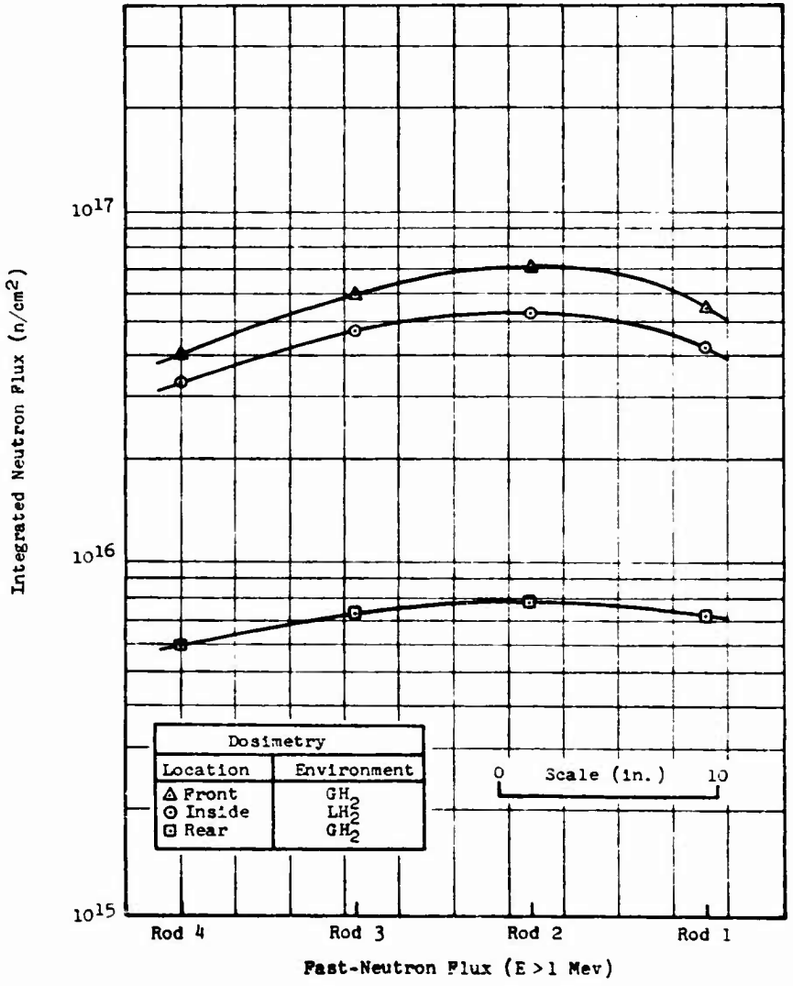

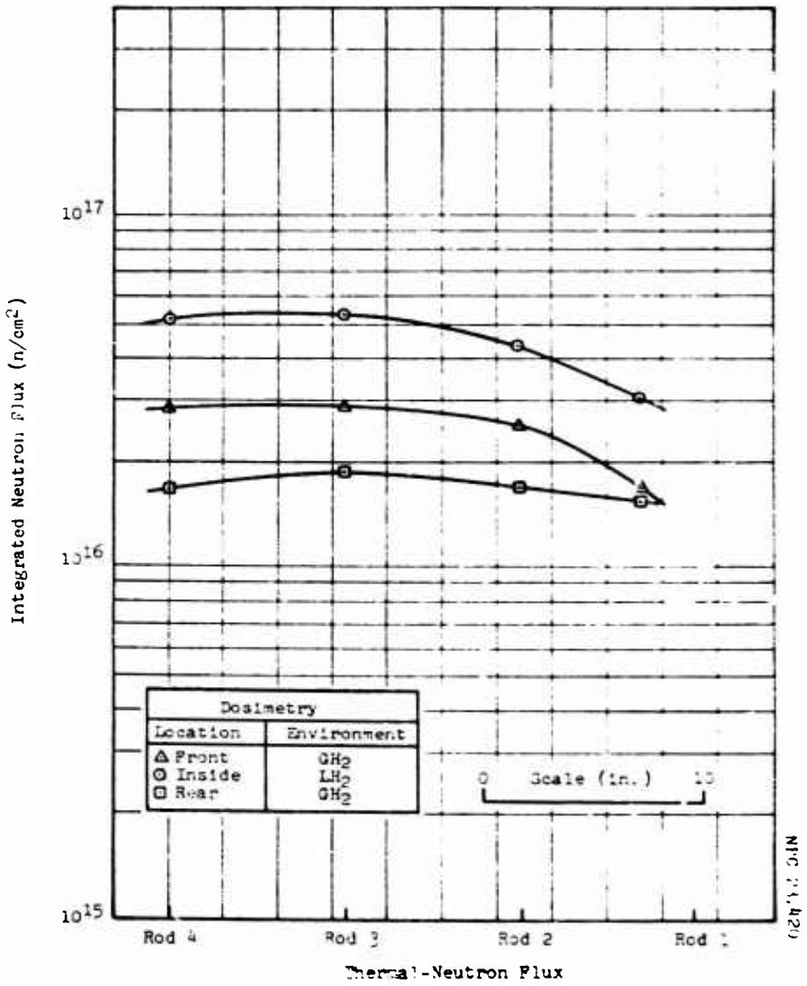

Figure 3-5 Measured Integrated Neutron Flux: Second Irradiation, East Assembly

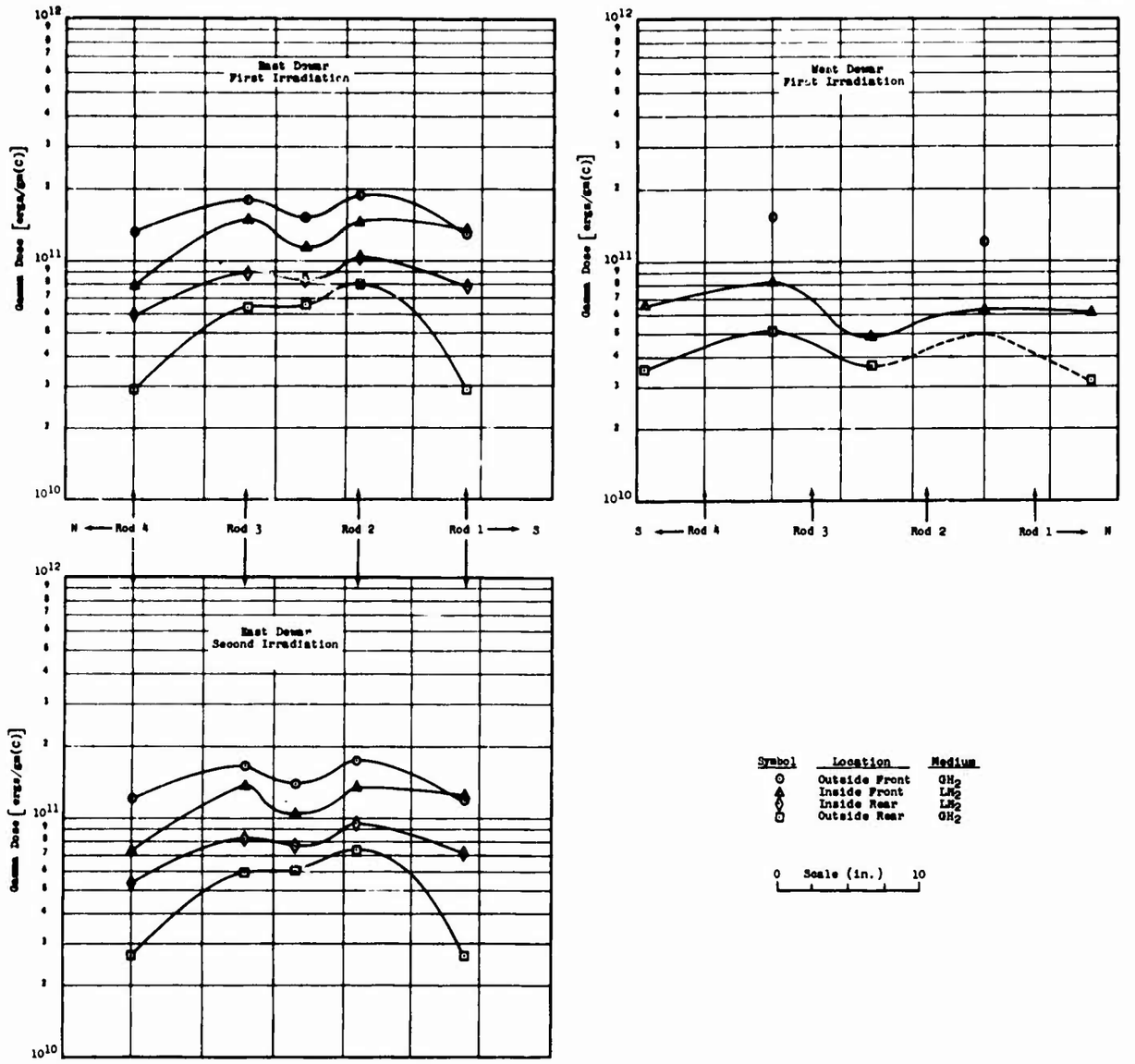

Figure 3-6 Gamma Dose Mapping Profile for AGC Cryogenic Materials Test Assembly

maximum response range of all gamma dose measuring devices, the data shown here were obtained empirically from the mapping experiments.

APPENDIX A

GTR RADIATION EFFECTS TESTING SYSTEM

APPENDIX A

GTR RADIATION EFFECTS TESTING SYSTEM

The GTR Radiation Effects Testing System is located in the Reactor Operations Area at the north end of the NARF complex. Figure A-1 is a plan view and Figure A-2 is a cutaway view of the system. A closeup of the irradiation test cell and the reactor tank is pictured in Figure A-3. During operation, the reactor is moved into the closet-like structure built into the north wall of the GTR tank. Items to be irradiated can be located on the north, east, or west sides of the closet, as indicated in the figures.

The reactor closet is constructed of 1-in. aluminum plate and is partially covered by 1/4-in.-thick boral to attenuate thermal neutrons. The boral extends 36 in. east and west from the closet along the tank wall and 36 in. up and down from the horizontal centerline of the reactor core. The centerline is 57 in. above the test-cell floor.

The Ground Test Reactor (GTR) is a heterogeneous, highly enriched, thermal reactor that utilizes water as neutron moderator and reflector, as radiation shielding, and as coolant. Maximum power generation is 3 Mw. The GTR, in an aluminum enclosure to facilitate cooling-water flow, is suspended by an open framework that is carried on a horizontal positioning mechanism at the top of the reactor tank. This mechanism permits the reactor to be positioned at distances ranging from

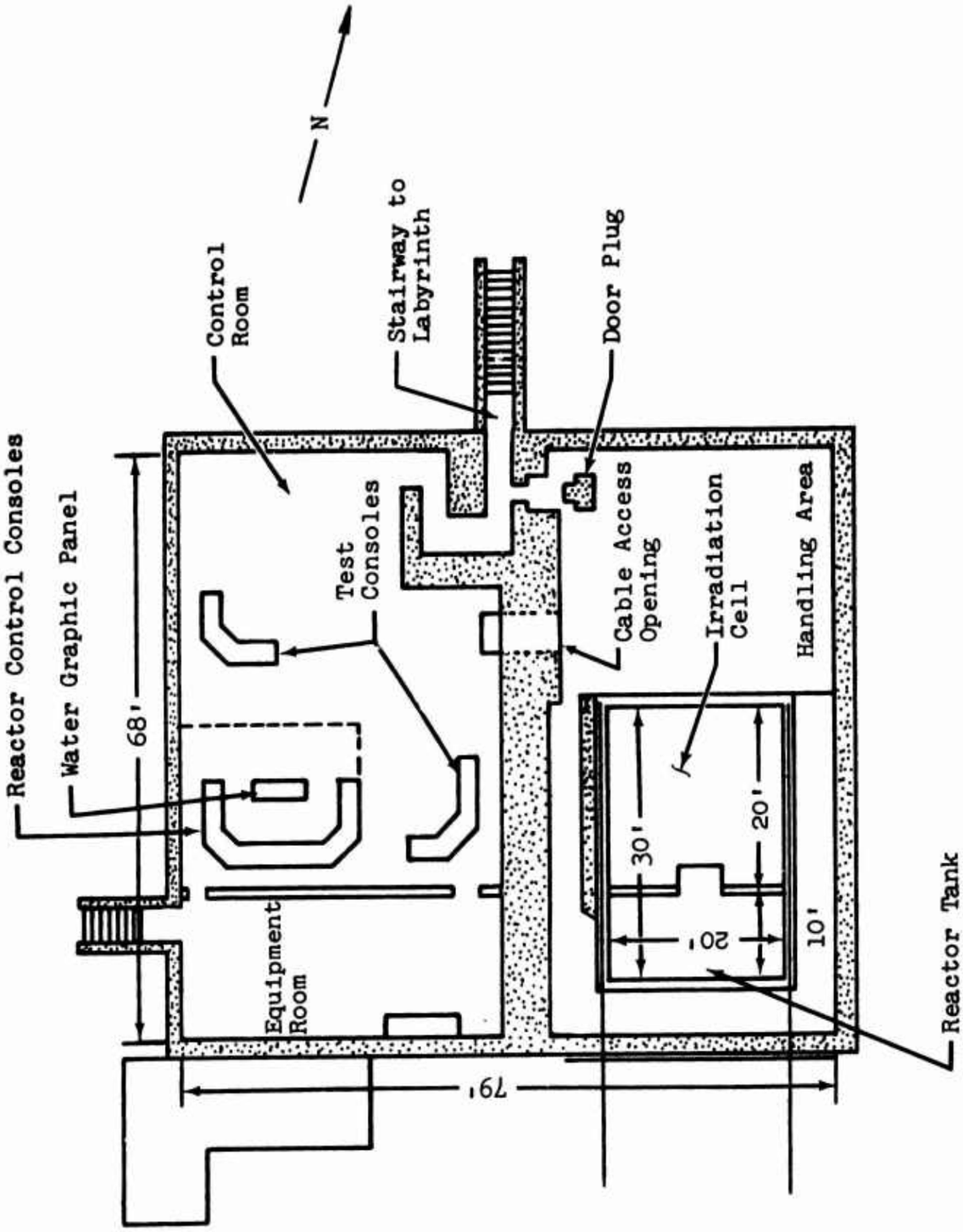

Figure A-1 Operations Building and GTR Facility

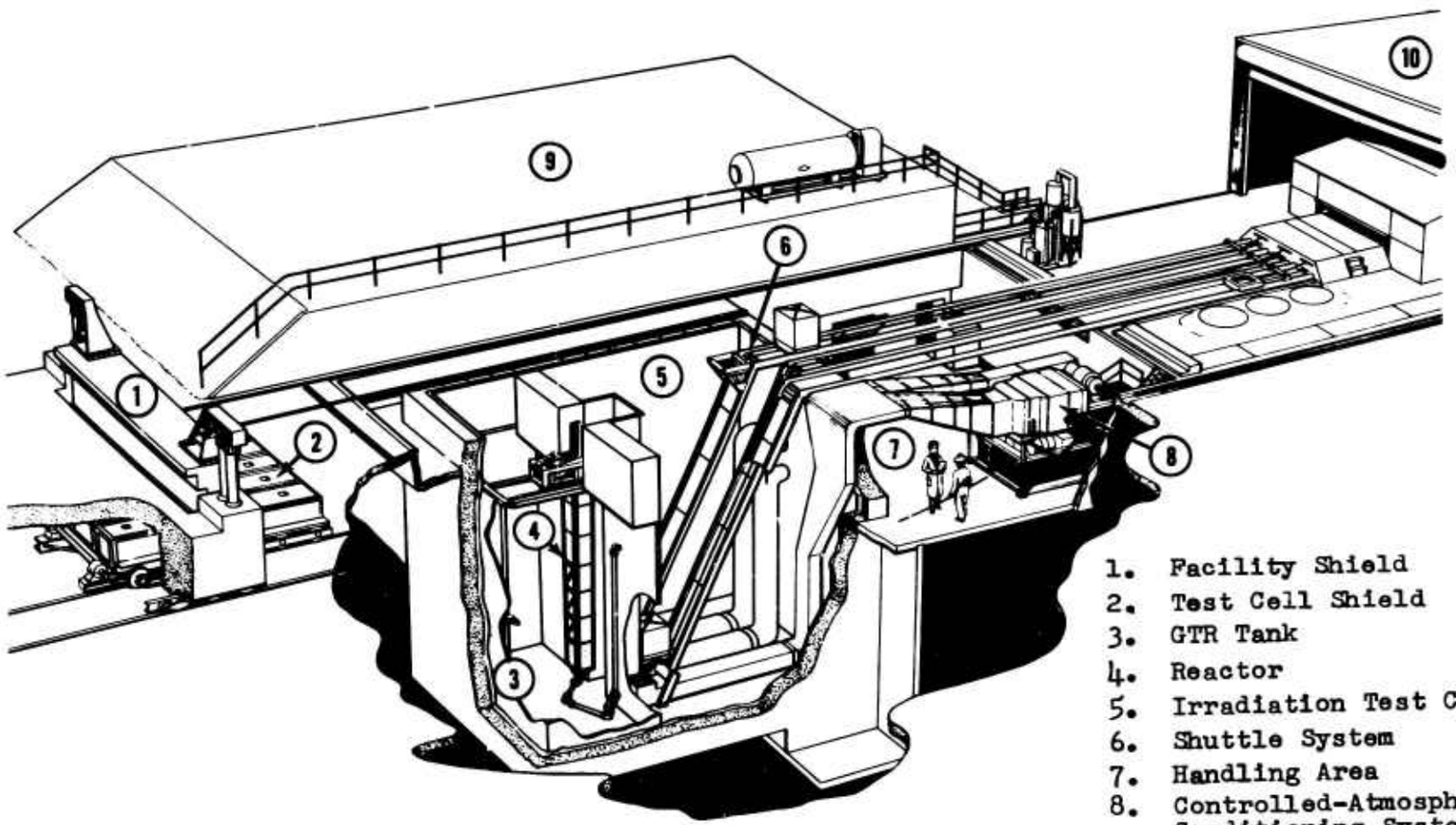

NPC 20,683

Figure A-2 Cutaway View of GTR Radiation Effects System

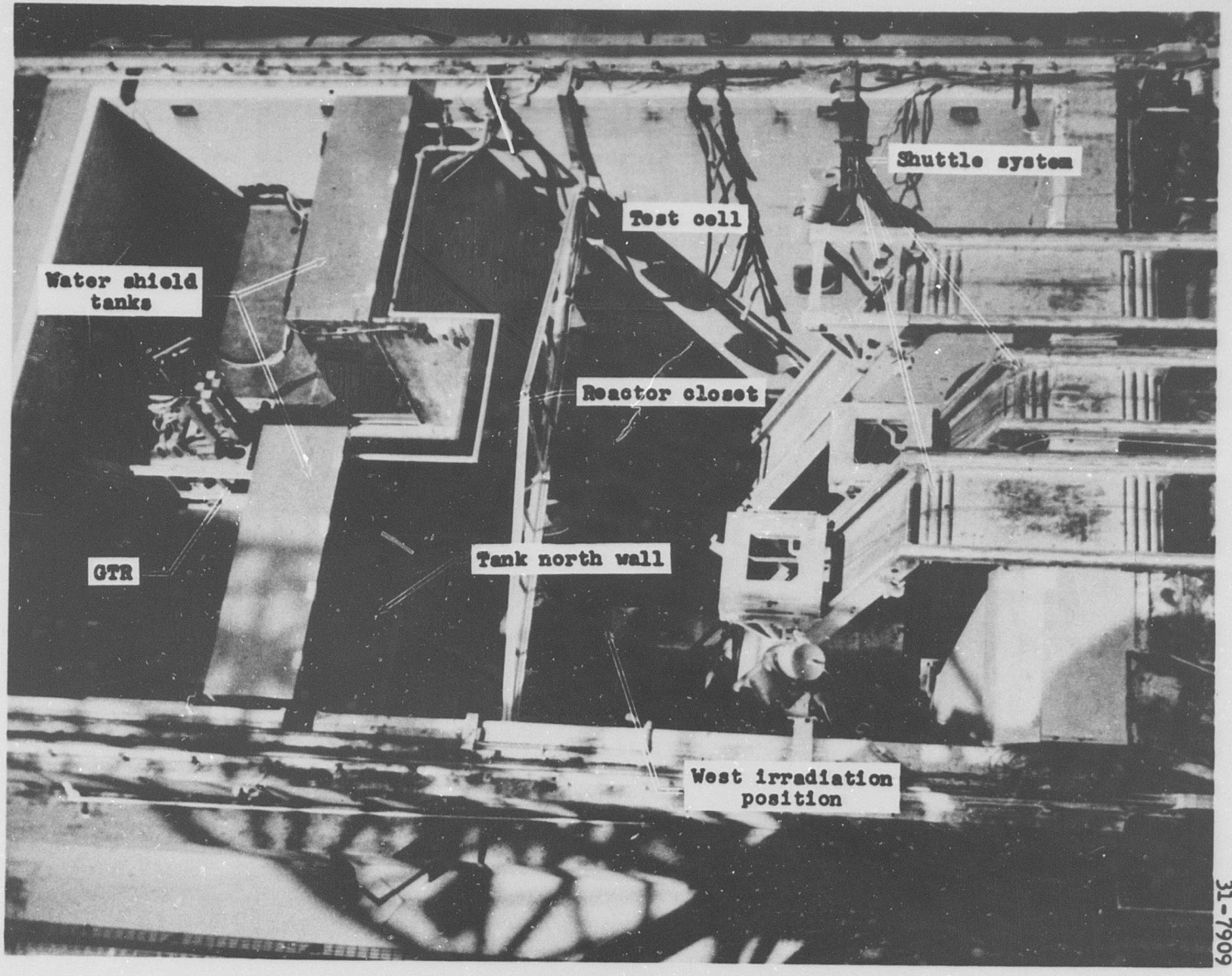

NPC 20,669
31-7909

Figure A-3 Irradiation Test Cell and Reactor Tank

2 to 87 in. from the north face of the closet.

Adjacent to the north wall of the irradiation cell is the handling area. In this area, various connections are made for cryogenic, hydraulic, and pneumatic equipment.

An integral part of the GTR testing facility is the shuttle system, which is used to move test assemblies into irradiation position. This system consists of cable-driven dollies mounted on three sets of parallel tracks. The tracks extend from the irradiation positions adjacent to the reactor closet, up an incline to the north wall of the irradiation cell, and to a loading area on the ramp just north of the handling area. The system can be operated from either the control room or the dolly motor-drive shed on the north ramp. Full-coverage televiewing of the entire shuttle system is provided by means of a closed-circuit television in the control room.

The control room (Fig. A-1) is a below-grade, reinforced concrete structure adjacent to the GTR system. The control room provides a shielded area for reactor instrumentation, control consoles, and test systems as well as special test equipment needed to conduct radiation experiments.

APPENDIX B

CALCULATION OF GAGE-LENGTH CORRECTION FACTOR

APPENDIX B

CALCULATION OF GAGE-LENGTH CORRECTION FACTOR

Standard ASTM procedures for determining stress-strain characteristics of dumbbell-type tensile specimens require that, for elongation measurement, extensometers be used and that they be installed directly to the gage-length section of each individual specimen. Following this procedure is impossible, however, when large numbers of specimens are tested automatically and remotely while submerged in liquid hydrogen. An alternate approach was therefore devised that utilizes the remotely operated extensometer described in Sections 2.2.8.2 and 3.2 and that obtains data in a manner closely approximating that required by ASTM standards. Since use of this approach results in a measurement of the elongation that occurs over the <u>total</u> reduced cross-section portion of the specimens, including the curved portions at each end of the gage-length section, a multiplying factor was derived for use in determining the actual gage-length elongation from the total measured elongation.

From the specimen configuration in Figure B-1, it can be seen that, as the specimen is pulled in tension to fracture, elongation takes place between J and J', and this is the elongation that is seen by the extensometer device. It is, therefore, desired to calculate a factor Q which, when applied to the measured elongation, will give the elongation within the specified gage length, or between points K and K'. To do this it is necessary to derive

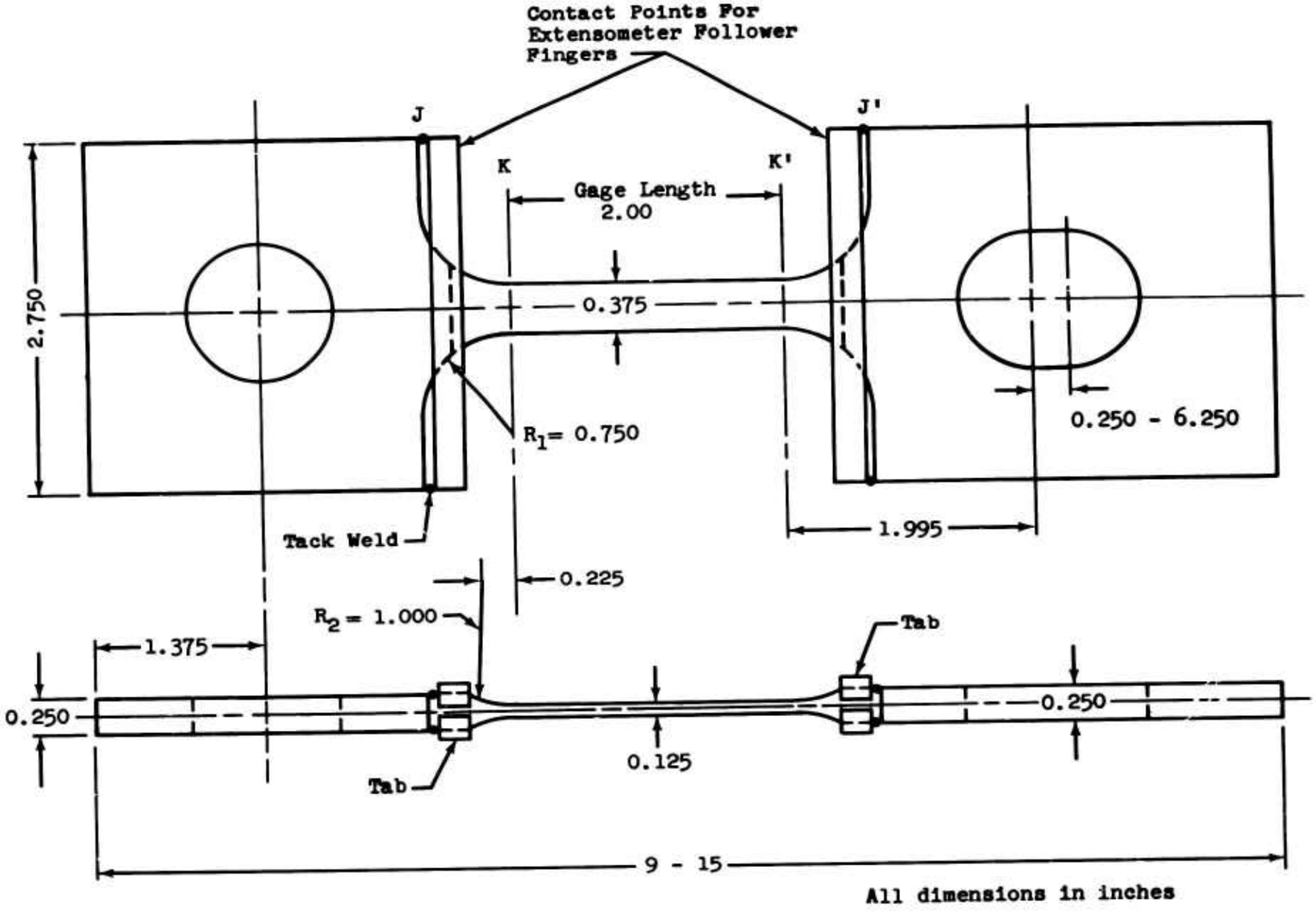

Figure B-1 Typical Dumbbell-Type Flat Tensile Specimen

mathematical expressions for the elongation that occurs between points K and K' and between points J and J'.

B-1 Elongation of Gage-Length Section, K-K'

The elongation of Section K-K' (within the elastic limit of the material) will be the same as that of a uniform straight bar when subjected to an axial load, i.e.,

$$\delta = \frac{Px}{AE} \tag{1}$$

where δ = the elongation

P = the axial load

x = the length of the bar

E = the modulus of elasticity

A = the uniform cross-sectional area of the bar

B-2 Elongation of Curved Sections, J-K and J'-K'

In determining the elongation that occurs within Section J-K (and the identical section, J'-K'), it is important to note that not only is the cross-sectional area variable, but that the variation itself is not uniform. This section may be divided into three smaller sections - A, B, and C - each of which has a different type of cross-sectional area variation (see Fig. B-2). Thus, the elongation between J and K will be the sum of elongations that occur within Sections A, B, and C. The derivation of an expression for the elongation within each of these smaller sections is shown below.

B-2.1 Elongation of Section A

To determine the elongation in a member of nonuniform cross-sectional area, Equation 1 must be put in differential form. In

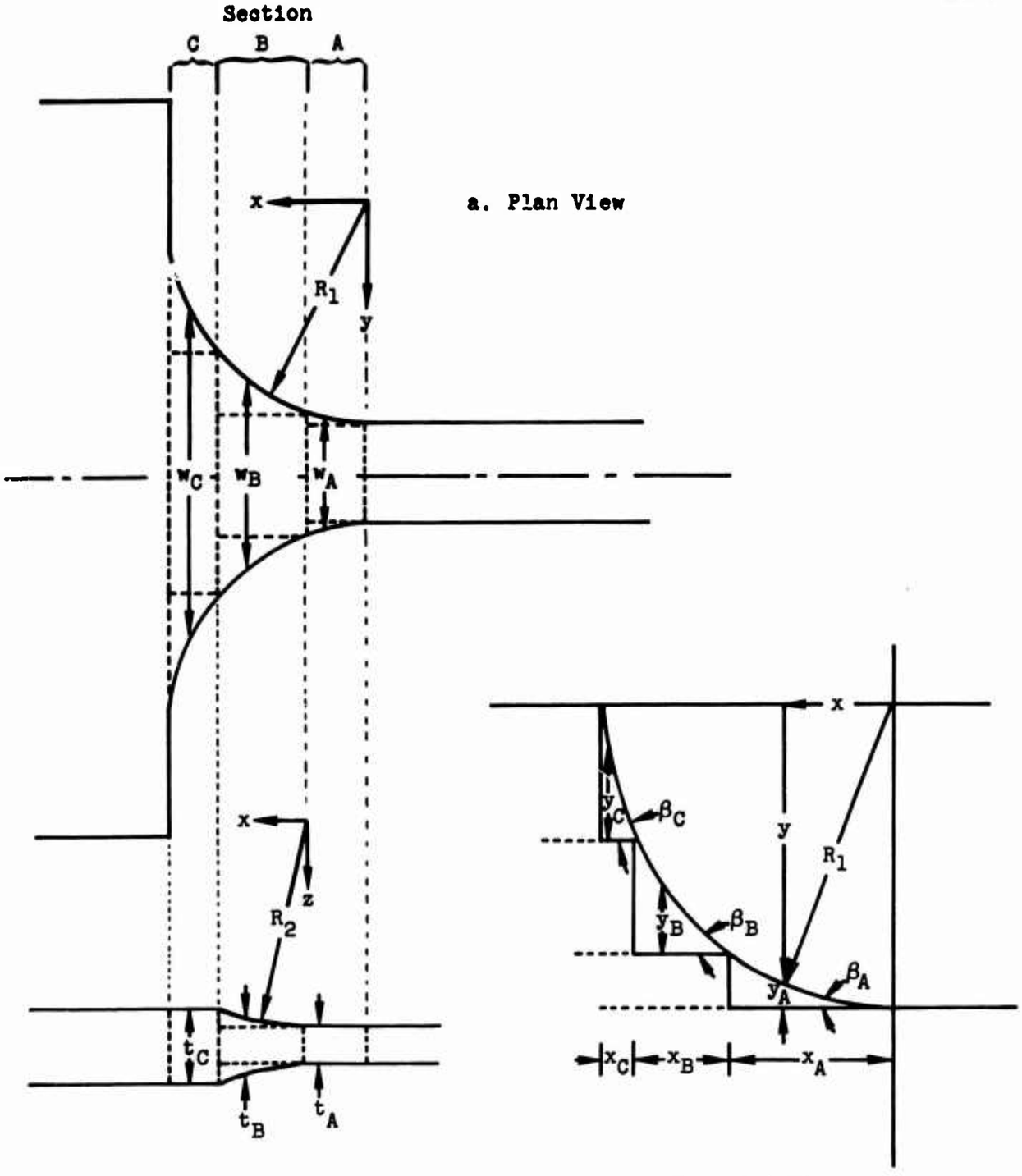

Figure B-2 Geometry of Curved Section

other words, the cross-sectional area may be considered uniform (or constant) only for elemental (dx) values of x, with there being, of course, corresponding elemental (dδ) values for elongation. Therefore, the resulting differential equation is

$$d\delta = \frac{P\,dx}{AE} \tag{2}$$

In Figure B-2 it is obvious that the cross-sectional area of Section A is, at any point, equal to

$$A_A = w_A\, t_A = \left(w_{A_{min}} + 2\, y_A\right) t_A \tag{3}$$

where w_A = the width of Section A at any point

t_A = the thickness (constant) of Section A

$w_{A_{min}}$ = the minimum width of Section A

y_A = one-half the difference between the width at a particular point and the minimum width of Section A

From the geometry of Figure B-2c,

$$y_A = R_1 - |y| = R_1 - \sqrt{R_1^2 - x_A^2} \tag{4}$$

where R_1 is the radius of curvature. The cross-sectional area of Section A therefore becomes

$$A_A = \left(w_{A_{min}} + 2\, R_1 - 2\sqrt{R_1^2 - x_A^2} \right) t_A \tag{5}$$

Substituting into the Equation ?, the elemental elongation of Section A is

$$d\delta_A = \frac{P\, dx_A}{Et_A \left(w_{A_{min}} + 2R_1 - 2\sqrt{R_1^2 - x_A^2} \right)} \tag{6}$$

An expression for δ_A is obtained by integrating this equation. Thus,

$$\delta_A = \frac{P}{Et_A} \int_c^{x_{A_{max}}} \frac{dx_A}{w_{A_{min}} + 2R_1 - 2\sqrt{R_1^2 - x_A^2}} \tag{7}$$

where $w_{A_{min}}$, R_1, P, E, and t_A are all constants.

This equation is not directly integrable. Therefore, to simplify the mathematics it is assumed that the edge surfaces of Section A are not curvilinear but straight, and that the cross-sectional area for this modified section is

$$A'_A = \left(w_{A_{min}} + 2y'_A \right) t_A \tag{8}$$

where y'_A is defined in Figure B-3.

The value of y'_A is larger than y_A by the vertical distance from the actual curved edge of the specimen to the straight edge (or chord) shown by the dotted line. The perpendicular distance between the curved edge and its chord is variable, but one-half the maximum can be used as a very close average. This is equal to one-half the difference between the radius of curvature R_1 and

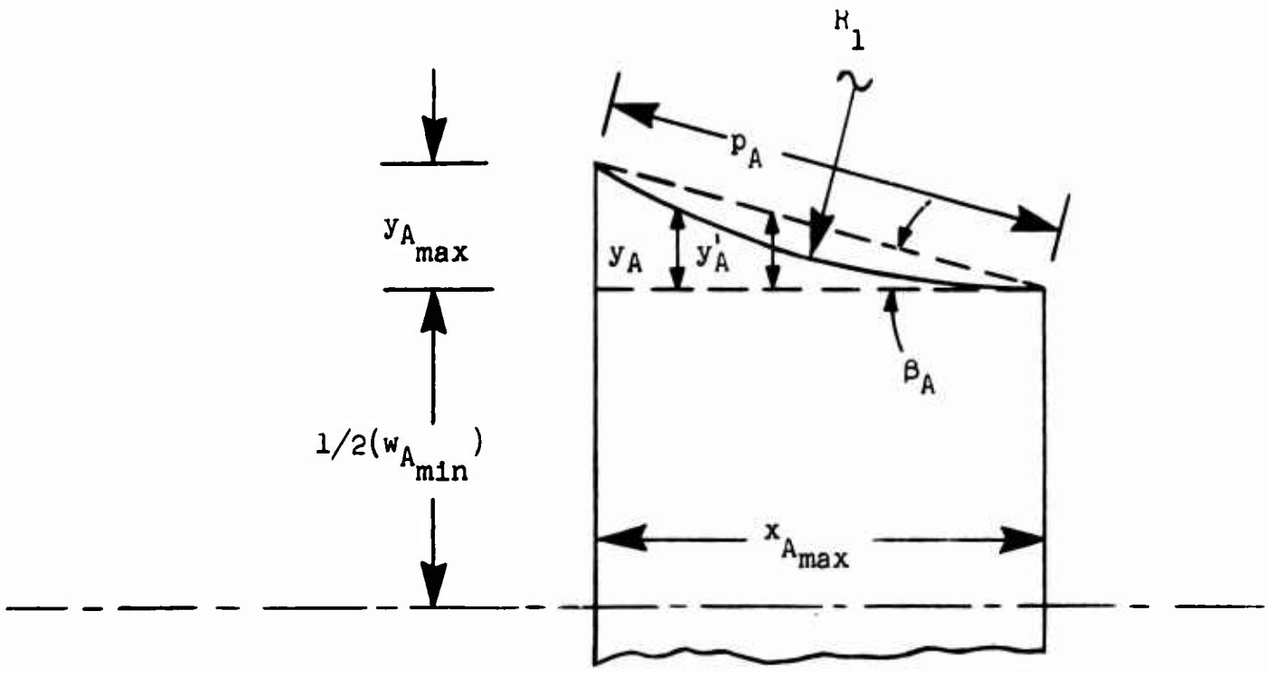

Figure B-3 Expanded View of Section A

the distance from the origin of R_1 to the chord:

$$1/2 \left(R_1 - 1/2\sqrt{4 R_1^2 - p_A^2} \right) \tag{9}$$

where p_A is the length of the chord. So, subtracting this segment out of the value of y_A', the actual area (within a small fraction of a percent) becomes

$$A_A = \left\{ w_{A_{min}} + 2 \left[y_A' - 1/2 \left(R_1 - 1/2\sqrt{4 R_1^2 - p_A^2} \right) \right] \right\} t_A \tag{10a}$$

$$= \left[w_{A_{min}} - \left(R_1 - 1/2\sqrt{4 R_1^2 - p_A^2} \right) + 2 y_A' \right] t_A \tag{10b}$$

$$= w_{A_{min}} t_A - \left(R_1 - 1/2\sqrt{4 R_1^2 - p_A^2} \right) t_A + 2 y_A' t_A \tag{10c}$$

where p_A can be evaluated from known specimen dimensions. Now

$$y'_A = x_A \tan \beta_A = x_A \left(\frac{y_{A_{max}}}{x_{A_{max}}} \right) \tag{11}$$

where $x_{A_{max}}$ is given in the specimen dimensions and $y_{A_{max}}$ can be determined from $x_{A_{max}}$ and the known value of R_1. Therefore, let

$$w_{A_{min}} t_A - \left(R_1 - 1/2 \sqrt{4 R_1^2 - p_A^2} \right) t_A = j_A \tag{12}$$

and

$$2t_A \tan \beta_A = k_A \tag{13}$$

The cross-sectional area of Section A then becomes

$$A_A = j_A + k_A x_A \tag{14}$$

so that the elongation is

$$\delta_A = \frac{P}{E} \int_0^{x_{A_{max}}} \frac{dx_A}{j_A + k_A x_A} \tag{15a}$$

$$= \frac{P}{E} \left[\frac{1}{k_A} \ln (k_A x_A + j_A) \right]_0^{x_{A_{max}}} \tag{15b}$$

B-2.2 Elongation of Section B

The cross-sectional area of Section B in Figure B-2 is,

similarly,

$$A_B = w_B t_B \tag{16}$$

In this case, however, both w_B and t_B are functions of x; the cross-sectional area of the specimen increases in the positive x direction, with both the side (and top and bottom) dimensions increasing circumferentially with x. Therefore, the equation for the cross-sectional area of Section B becomes

$$A_B = \left(w_{B_{min}} + 2y_B \right) \left(t_{B_{min}} + 2z_B \right) \tag{17}$$

The term y_B can be expressed as

$$y_B = R_1 - \sqrt{R_1^2 - \left(x_{A_{max}} + x_B \right)^2} - y_{A_{max}} \tag{18}$$

and the term z_B can be expressed as

$$z_B = R_2 - \sqrt{R_2^2 - x_B^2} \tag{19}$$

The cross-sectional area of Section B thus becomes, in terms of x_B,

$$A_B = \left[w_{B_{min}} + 2R_1 - 2\sqrt{R_1^2 - \left(x_{A_{max}} + x_B \right)^2} - 2y_{A_{max}} \right] \cdot \left[t_{B_{min}} + 2R_2 - 2\sqrt{R_2^2 - x_B^2} \right] \tag{20}$$

However, since

$$w_{B_{min}} = w_{A_{min}} + 2y_{A_{max}} \tag{21}$$

Equation 20 becomes

$$A_B = \left[w_{A_{min}} + 2R_1 - 2\sqrt{R_1^2 - \left(x_{A_{max}} + x_B\right)^2} \right] \cdot \left[t_{B_{min}} + 2R_2 - 2\sqrt{R_2^2 - x_B^2} \right] \tag{22}$$

Substituting Equation 22 into Equation 2, the elemental elongation for Section B is

$$d\delta_B = \frac{P}{E} \left[w_{A_{min}} + 2R_1 - 2\sqrt{R_1^2 - \left(x_{A_{max}} + x_B\right)^2} \right]^{-1} \cdot \left[t_{B_{min}} + 2R_2 - 2\sqrt{R_2^2 - x_B^2} \right]^{-1} dx_B \tag{23}$$

and the elongation is

$$\delta_B = \frac{P}{E} \int_0^{x_{B_{max}}} \left[w_{A_{min}} + 2R_1 - 2\sqrt{R_1^2 - \left(x_{A_{max}} + x_B\right)^2} \right]^{-1} \cdot \left[t_{B_{min}} + 2R_2 - 2\sqrt{R_2^2 - x_B^2} \right]^{-1} dx_B \tag{24}$$

This equation is extremely cumbersome and is not directly integrable. Therefore, the geometry is simplified as shown in Figure B-4 and the new equation for the cross-sectional area takes the form of Equation 10b, except that the term representing the thickness is similar to the term representing the width:

$$A_B = \left[w_{B_{min}} - \left(R_1 - 1/2\sqrt{4R_1^2 - p_B^2} \right) + 2y_B' \right] \left[t_{B_{min}} - \left(R_2 - 1/2\sqrt{4R_2^2 - q^2} \right) + 2z_B' \right] \quad (25)$$

Now, from the geometry of Figures B-2 and B-4,

$$y_B' = x_B \tan \beta_B = x_B \left(\frac{y_{B_{max}}}{x_{B_{max}}} \right) \quad (26a)$$

$$= x_B \frac{R_1 - \sqrt{R_1^2 - \left(x_{A_{max}} + x_{B_{max}} \right)^2} - y_{A_{max}}}{\sqrt{R_2^2 - \left(R_2 - z_{B_{max}} \right)^2}} \quad (26b)$$

$$= x_B \frac{R_1 - \sqrt{R_1^2 - \left[x_{A_{max}} + \sqrt{R_2^2 - \left(R_2 - z_{B_{max}} \right)^2} \right]^2} - y_{A_{max}}}{\sqrt{R_2^2 - \left(R_2 - z_{B_{max}} \right)^2}} \quad (26c)$$

and

$$z_B' = x_B \tan \gamma = x_B \left(\frac{z_{B_{max}}}{x_{B_{max}}} \right) \quad (27a)$$

$$= x_B \frac{z_{B_{max}}}{\sqrt{R_2^2 - \left(R_2 - z_{B_{max}} \right)^2}} \quad (27b)$$

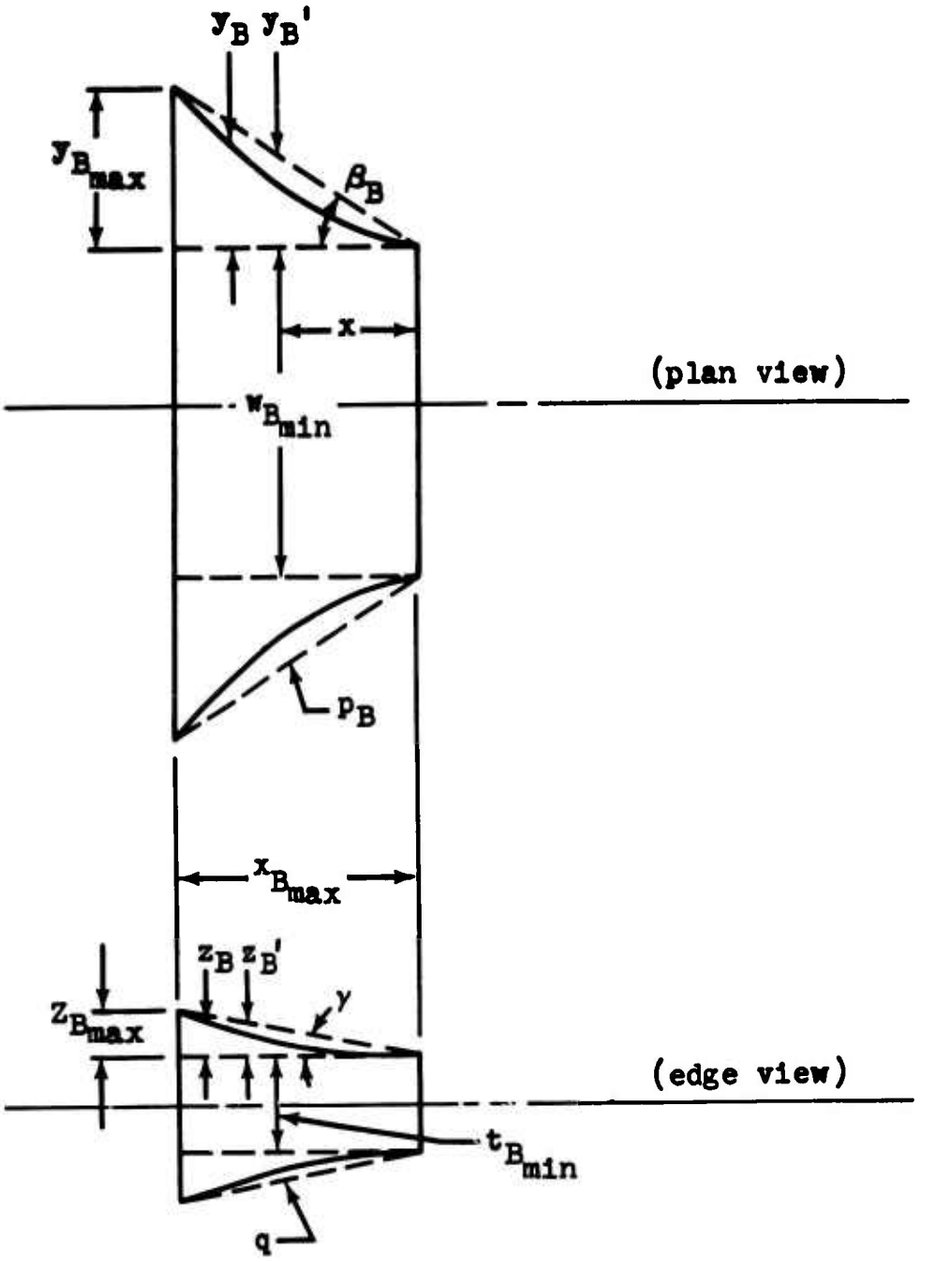

Figure B-4 Geometry of Section B

In the above forms, the terms tan β_B and tan γ can be readily evaluated. We therefore show the cross-sectional area of Section B as

$$A'_B = \left[w_{B_{min}} - \left(R_1 - 1/2\sqrt{4R_1^2 - p_B^2} \right) + 2x_B \tan \beta_B \right] \cdot$$

$$\left[t_{B_{min}} - \left(R_2 - 1/2\sqrt{4R_2^2 - q^2} \right) + 2x_B \tan \gamma \right] \qquad (28)$$

where p_B and q (see Fig. B-4) can also be evaluated from known specimen dimensions. If we now let

$$2 \tan \beta_B = m$$

$$2 \tan \gamma = n$$

$$w_{B_{min}} - \left(R_1 - 1/2\sqrt{4R_1^2 - p_B^2} \right) = r$$

$$t_{B_{min}} - \left(R_2 - 1/2\sqrt{4R_2^2 - q^2} \right) = s \qquad (29)$$

then

$$A_B = (r + mx_B)(s + nx_B) \qquad (30)$$

and

$$B = \frac{P}{E} \int_0^{x_{B_{max}}} \frac{dx_B}{(r + mx_B)(s + nx_B)}$$

$$= \frac{P}{E} \left[\frac{1}{rn - ms} \ln \left(\frac{s + nx_B}{r + mx_B} \right) \right]_0^{x_{B_{max}}} \qquad (31)$$

for

$$(rn - ms \neq 0)$$

B-2.3 Elongation of Section C

From Figure B-2 it is apparent that the cross-sectional area of Section C is equal to

$$A_C = w_C t_C = \left(w_{C_{min}} + 2y_C \right) t_C \tag{32}$$

and that

$$y_C = R_1 - \sqrt{R_1^2 - \left(x_{A_{max}} + x_{B_{max}} + x_C \right)^2} - \left(y_{A_{max}} + y_{B_{max}} \right) \tag{33}$$

Therefore, the cross-sectional area of Section C becomes

$$A_C = \left[w_{C_{min}} + 2R_1 - 2\sqrt{R_1^2 - \left(x_{A_{max}} + x_{B_{max}} + x_C \right)^2} - 2\left(y_{A_{max}} + y_{C_{max}} \right) \right] t_C \tag{34}$$

Substituting into Equation 2, the elemental elongation is

$$d\delta_C = \frac{P\, dx_C}{Et_C \left[w_{C_{min}} + 2R_1 - 2\sqrt{R_1^2 - \left(x_{A_{max}} + x_{B_{max}} + x_C \right)^2} - 2\left(y_{A_{max}} + y_{B_{max}} \right) \right]} \tag{35}$$

Integrating this equation gives an expression for the elongation:

$$\delta_C = \frac{P}{Et_C} \int_0^{x_{C_{max}}} \frac{dx_C}{w_{C_{min}} + 2R_1 - 2\sqrt{R_1^2 - \left(x_{A_{max}} + x_{B_{max}} + x_C\right)^2} - 2\left(y_{A_{max}} + y_{B_{max}}\right)}$$

$$= \frac{P}{Et_C} \int_0^{x_{C_{max}}} \frac{dx_C}{w_{A_{min}} + 2R_1 - 2\sqrt{R_1^2 - \left(x_{A_{max}} + x_{B_{max}} + x_C\right)^2}} \qquad (36)$$

where $w_{A_{min}}$, R_1, $x_{A_{max}}$, $x_{B_{max}}$, and t_C are all constants of known value. Again, since the equation is not directly integrable, it is necessary to make the geometric simplifications that were made on Sections A and B. After correcting y_C' for the difference between the curved edge and its chord, the cross-sectional area becomes

$$A_C = \left[w_{C_{min}} - \left(R_1 - 1/2\sqrt{4\,R_1^2 - p_C^2} \right) + 2y_C' \right] t_C$$

$$= w_{C_{min}} t_C - \left(R_1 - 1/2\sqrt{4\,R_1^2 - p_C^2} \right) t_C + 2y_C' t_C \qquad (37)$$

Now

$$y_C' = x_C \tan \beta_C = x_C \left(\frac{y_{C_{max}}}{x_{C_{max}}} \right) \qquad (38)$$

where $x_{C_{max}}$ can be determined from known specimen dimensions

and $y_{C_{max}}$ can be determined from $x_{C_{max}}$ and the known value of R_1. Therefore let

$$w_{C_{min}} t_C - \left(R_1 - 1/2 \sqrt{4 R_1^2 - p_C^2} \right) t_C = j_C \tag{39}$$

and

$$2t_C \tan \beta_C = k_C \tag{40}$$

The cross-sectional area of Section C then becomes

$$A_C = j_C + k_C x_C \tag{41}$$

and

$$C = \frac{P}{E} \int_0^{x_{C_{max}}} \frac{dx_C}{j_C + k_C x_C} \tag{42}$$

$$= \frac{P}{E} \left[\frac{1}{k_C} \ln (j_C + k_C x_C) \right]_0^{x_{C_{max}}} \tag{43}$$

B-3 Gage-Length Correction Factor

From Figures B-1 and B-2, it can be seen that the total elongation between points J and J' is

$$\delta_{J-J'} = \delta_G + 2 (\delta_A + \delta_B + \delta_C) \tag{44}$$

Therefore, the ratio Q between $\delta_{J-J'}$ and $\delta_{K-K'}$ is

$$Q = \frac{\delta_{K-K'}}{\delta_{J-J'}} = \frac{\delta_G}{\delta_G + 2(\delta_A + \delta_B + \delta_C)} \tag{45}$$

where δ_G, as indicated in Equation 1, is given by

$$\delta_G = \frac{Px}{AE} = \frac{P}{E}\,\frac{x_G}{A_G} \tag{46}$$

BLANK PAGE

APPENDIX C

COMPREHENSIVE DATA PRESENTATION

Page No. Index to Figures and Tables

Type of Information	Material and Condition																	
	A356-T6 L	6061-T6 L	6061-T6 LW	6061-T6 TW	6061-T6 LW*	6061-T6 TW*	7075-T6 L	347C L	347 L	347 LW	440C L	A-286 L	X-750 L	713C L	Has.C L	A-110-AT T	A-110-AT TW	D-979
Tensile and Shear Test Data	93	113	131	149	167	185	203	221	239	257	277	283	303	323	341	359	377	395
Stress-Strain Curves:																		
Extensometer	94	114	132	150	168	186	204	222	240	258	-	284	304	324	342	360	378	
Expanded Scale	-	115	-	-	-	-	-	-	241	259	-	285	305	-	343	361	-	
Comparison	95	-	133	151	-	-	-	-	-	260	-	286	306	-	-	-	-	
X-Ray Diffraction Data	96	116	134	152	169	187	205	223	242	261	-	287	307	325	344	362	379	
3X Macrophotograph of Fractured Specimen	98	117	135	153	170	188	206	224	243	262	278	288	308	326	345	363	380	
100X Optical Micrograph of Unstrained Area	99	118	136	154	171	189	207	225	244	263	-	289	309	327	346	364	381	
1000X Optical Micrograph of Unstrained Area	100	119	137	155	172	190	208	226	245	264	-	290	310	328	347	365	382	
100X Optical Micrograph of Strained Area	101	120	138°	156°	173°	191°	209	227	246	265°	-	291	311	329	348	366	383°	
1000X Optical Micrograph of Strained Area	102	121	139°	157°	174°	192°	210	228	247	266°	-	292	312	330	349	367	384°	
100X Optical Micrograph of Fracture Edge	103	122	140	158	175	193	211	229	248	267	-	293	313	331	350	368	385	
1000X Optical Micrograph of Fracture Edge	104	123	141	159	176	194	212	230	249	268	-	294	314	332	351	369	386	
15000X Electron Micrograph of Unstrained Area	105	124	142	160	177	195	213	231	250	269	-	295	315	333	352	370	387	
15000X Electron Micrograph of Strained Area	106	125	143	161	178	196	214	232	251	270	-	296	316	334	353	371	388	
4200X Fractograph of Center of Fracture	107	126	144	162	179	197	215	233	252	271	-	297	317	335	354	372	390	
4200X Fractograph of Edge of Fracture	108	127	145	163	180	198	216	235	253	272	-	298	318	336	355	373	391	
4200X Fractograph of Notched Specimen	109	128	146	164	181	199	217	236	254	273	279	299	319	337	356	374	392	

* As welded

° Shows parent and weld interface instead of general strained area

APPENDIX C

COMPREHENSIVE DATA PRESENTATION

This section contains a presentation of all detail data for the eighteen different material/condition combinations tested. These eighteen combinations are listed on the facing page, along with the first page of the section in which the data appear. Limited data are provided for two of the materials: D-979 was tested only in shear; and all unnotched tensile specimens of 440-C failed in the grip rather than in the reduced cross section. The data presented on all other material/condition combinations fall into two basic categories: mechanical-property measurements and metallographic examination.

1. Mechanical Properties

All specimens were tested to fracture, with the applied load and the resulting strain being recorded continuously. Three methods of strain measurement were utilized: extensometer, rod-movement, and strain gage. These are described in Section 2.2.8.2. A comparison of these methods is presented for a selected number of materials. The primary strain method was considered to be the extensometer, which measured the strain that occurred between the specimen shoulders. To obtain the strain that occurred within the 2-in. gage length, it was necessary to consider the specimen geometry and calculate a correction factor. An explanation of this correction factor is presented in Section 3.2 and described in detail in Appendix B. This factor was applied to all strain data presented.

The detail data are presented for each irradiated specimen, and the average values are compared with the average values from nonirradiated control data obtained from Reference 8. A statistical analysis of these data is presented in Section 3.1.

The stress-strain relationship for each material condition was plotted and is presented in this appendix.

2. Metallographic Examination

The purpose of the metallographic examination was to determine if the test environment can change the mechanisms of flow, fracture, and/or phase of engineering alloys.

The metallographic examination of the irradiated specimens was performed by the General Dynamics Engineering Test Laboratory. The examination of the preirradiated control specimens was accomplished by the Aerojet General Corporation. Only that work accomplished by General Dynamics is presented in this report. A radiation-effects comparison of these data will be performed by Aerojet General Corporation.

The metallographic data for each material/condition combination presented in this appendix consist of the following:

1. X-ray diffraction analysis of the strained and unstrained areas.
2. Macrophotographs at 3X of the fracture.
3. Optical micrographs at 100X and 1,000X of the strained and unstrained areas.
4. Electron micrographs at 15,000X of the strained and unstrained areas.
5. Electron fractographs at 4,200X of notched and unnotched specimens.

For the convenience of the reader whose field is not metallography, a brief glossary of terms (Refs. 9 and 10) is presented below:

Acicular	A needle-like structure.
Cleavage Fracture	Fracture which exhibits little or no plastic deformation and occurs along well-defined crystallographic lattice planes.
Cleavage Plane	A crystallographic lattice plane along which cleavage occurs.
Dendrite	A crystal condition exhibiting a pine-tree-like patterm.
Dimple	Concave depression on the fracture surface resulting from microvoid coalescence. As the result of the state of stress during fracture, the dimple shape may be elongated, oval, or equiaxed.
Equiaxed	Grains having essentially the same dimensions in all directions.
Eutectic	An alloy having components in such proportions that the melting point is the lowest possible with those components.
Fatigue Striation	A surface marking on a fatigue fracture representing the advance of the crack front during one cycle of loading.
Glide Plane Decohesion	Separation of material by glide along a slip plane.
Inclusion	Usually a foreign material - such as sulfides, oxides, or silicates - that has been induced during the melting operation.
Intermetallic	Formed compounds within the alloy due to the chemical composition and/or heat treatment of the alloy.
Matrix	The background or majority structure.

Microvoid	Microscopic cavities formed in the metal during the fracturing process.
Quasi-Cleavage	A fracture resembling cleavage but exhibiting some plastic deformation.
Ripple Pattern	Partially smoothed-out areas of serpentine glide.
Serpentine Glide	An inwoven pattern of glide plane decohesion steps.
Twinning	A condition where a part of the crystal changes lattice orientation relative to the remainder of the crystal.

Aluminum A356-T6
Condition L

BLANK PAGE

Table C-1
Tensile and Shear Test Data

Material Aluminum A356-T6 Specimen Condition L

Averaged Data (-423°F)		
Unnotched Specimens	Control	Irradiated
Ultimate Strength (ksi)	44.7	42.8
0.2% Yield Strength (ksi)	31.0	46.9
Elongation in Gage Length (%)	1.5	2.03
Reduction in Area (%)	2.8	0.77
Ultimate Shear Strength (ksi)	50.4	45.7
Notched Specimens		
Ultimate Strength (ksi)	39.7	43.2
Ratios		
Notched- Ult./Unnotched-Ult.	0.88	0.81
Notched-Ult./Unnotched-Yield	1.28	1.01

Unnotched Specimens				
Specimen Number	Ult. Tensile Strength(ksi)	Yield Strength 0.2% Offset (ksi)	Reduction in Area (%)	Elongation (%)
5	51.7	42.5	0.26	1.77
6	55.5	----	1.86	2.83
9	50.7	41.0	0.40	1.77
10	53.4	45.0	0.54	1.77

Notched Specimens		Shear Specimens	
Specimen Number	Ult. Tensile Strength (ksi)	Specimen Number	Ult. Shear Strength (ksi)
17	39.7	1	46.3
18	43.4	2	45.2
21	46.2	3	45.4
22	43.5	4	Broke on rebound

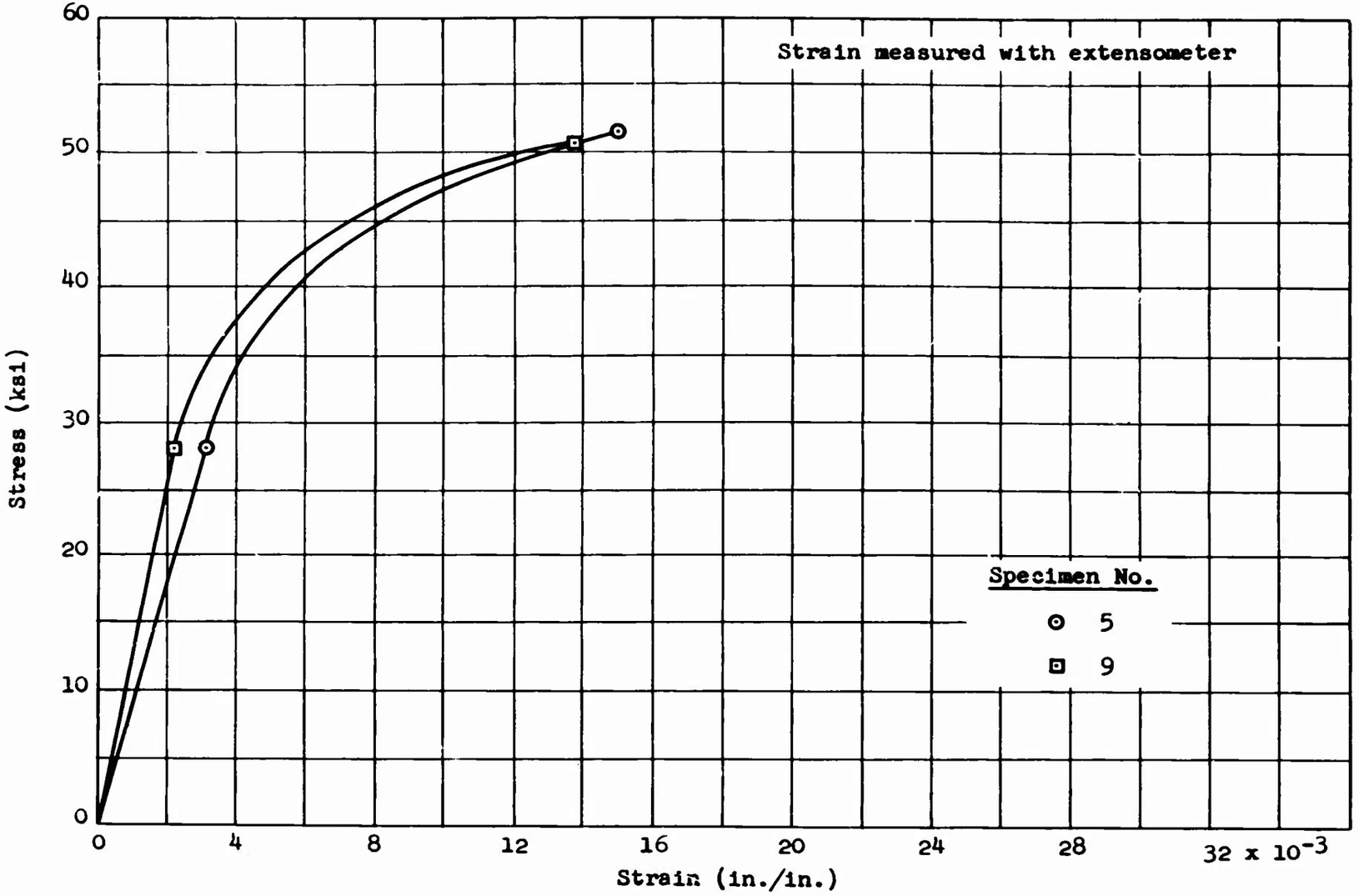

Figure C-1 Aluminum A356-T6, Condition LU: Stress-Strain Curves

NPC 23,435

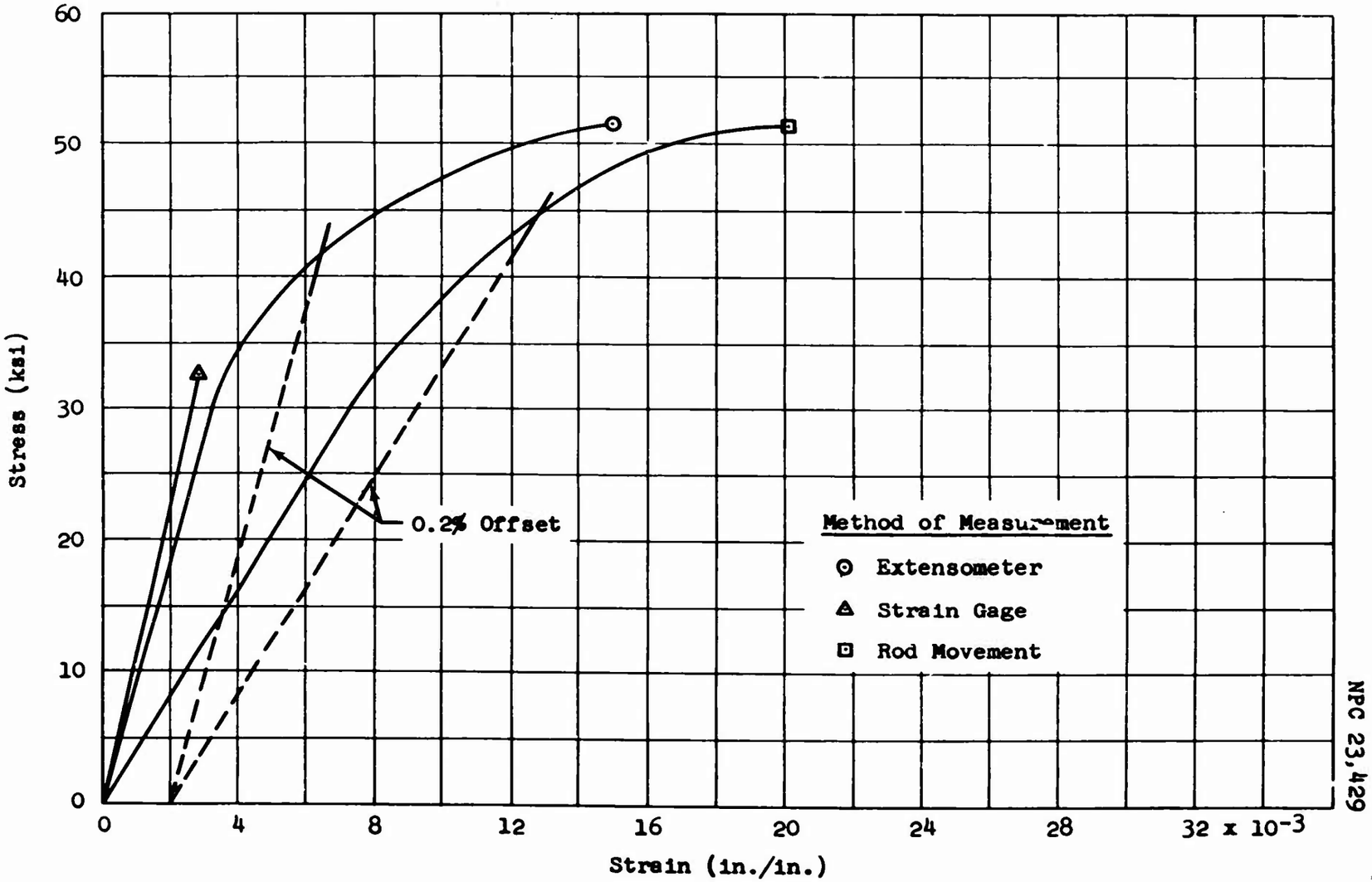

Figure C-2 Aluminum A356-T6, Condition LU: Comparison of Strain-Measurement Methods

Table C-2
X-Ray Diffraction Data

Material Aluminum A356-T6 Specimen LU 10

	STRAINED AREA		UNSTRAINED AREA	
DIFFRACTION PATTERN				
Miller Indices (hkl)	Interlattice Spacing, d (Å)	Relative Intensity (%)	Interlattice Spacing, d (Å)	Relative Intensity (%)
111	2.34	100	2.34	55
200	2.03	10	2.03	25
220	1.43	2	1.44	100
311	1.22	5	1.22	33
222	1.17	2	1.17	6
331	0.93	10		

LATTICE PARAMETER (Å)

111	4.05	4.05
200	4.06	4.06
220	4.04	4.07
311	4.05	4.05
222	4.05	4.05
331	4.05	--

MICROSTRESS, $\Delta\theta$

0.25° (2θ = 78.2°)	0.26° (2θ = 78.1°)
0.13° (2θ = 38.35°)	0.14° (2θ = 38.35°)

Table C-2 (cont'd)

X-Ray Diffraction Data

Material Silicon Specimen LU 10

	STRAINED AREA		UNSTRAINED AREA	
DIFFRACTION PATTERN				
Miller Indices (hkl)	Interlattice Spacing, d (Å)	Relative Intensity (%)	Interlattice Spacing, d (Å)	Relative Intensity (%)
111	3.14	100	3.15	70
220	1.92	30	1.92	35
311	1.64	20	1.64	20
422	1.10	5	1.11	5
440	0.94	6	--	--
531	0.91	45	0.91	100
620	--	--	0.85	8
533	--	--	0.83	20

LATTICE PARAMETER (Å)

MICROSTRESS, $\Delta\theta$

METALLOGRAPHIC STUDY

Material Aluminum A356-T6 Neg.No. None

Specimen LU 10 Neg.Mag. 3X

Etchant None Photo Enlargement None

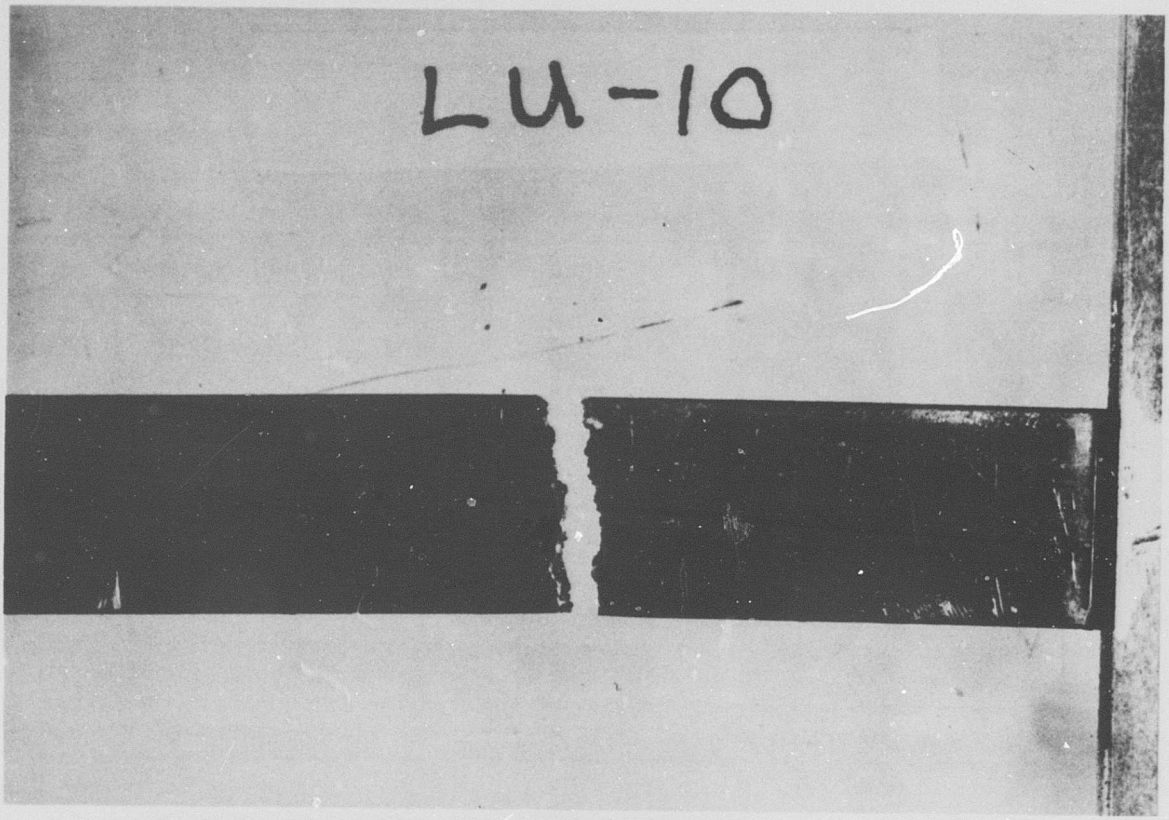

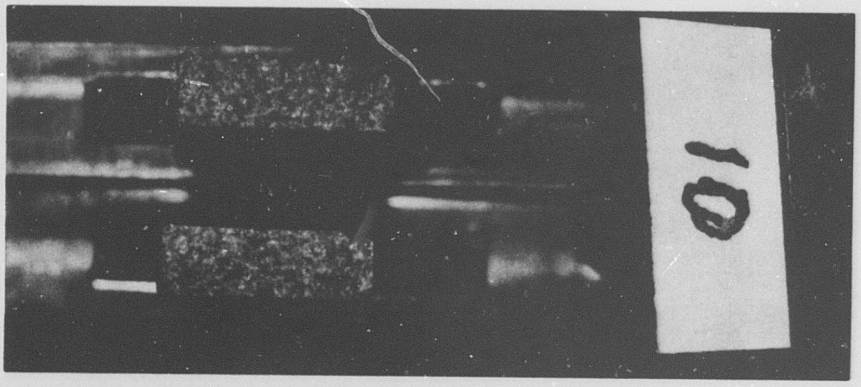

Figure C-3 Aluminum A356-T6, Condition L: Macrophotograph Showing 3X Magnification of Specimen

METALLOGRAPHIC STUDY

Material Aluminum A356-T6 Neg.No. W20

Specimen LU 10 Neg.Mag. 100X

Etchant Keller's Photo Enlargement None

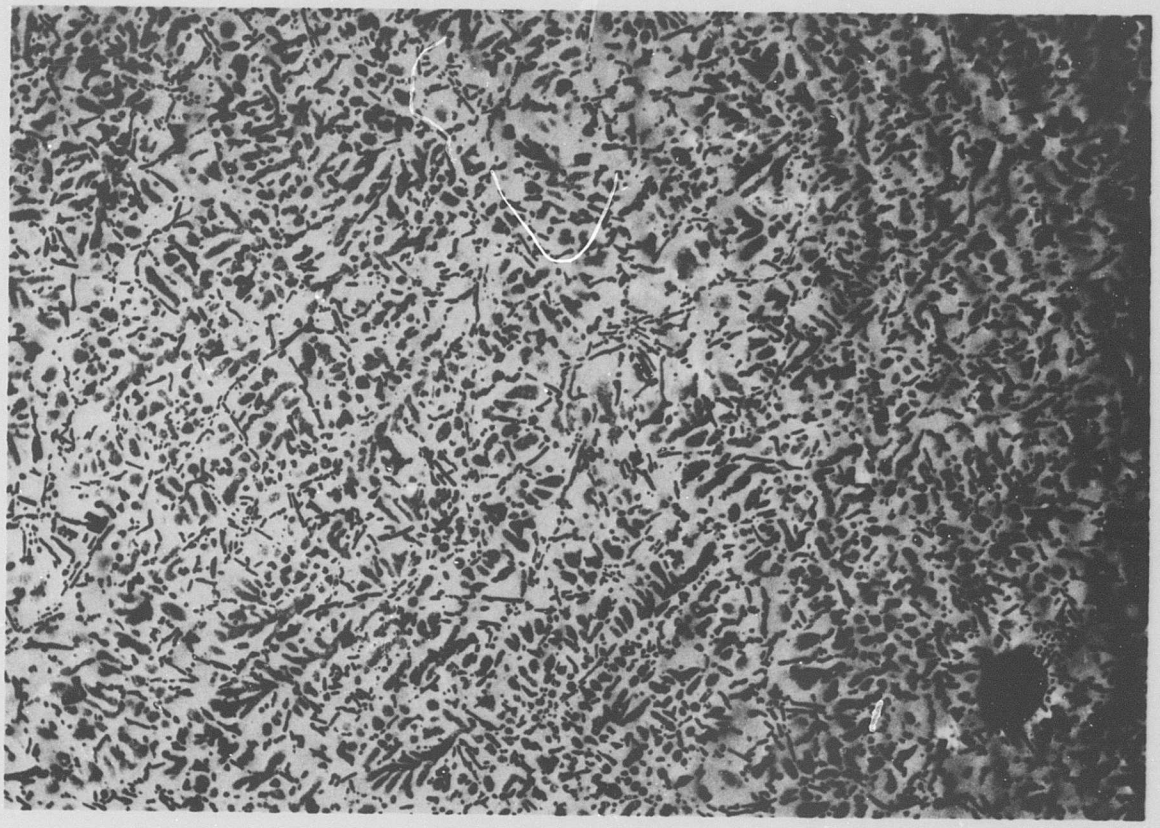

COMMENTS

The microstructure shows a solid-solution aluminum matrix with an intermetallic Al-Si. The cored structure is typical of castings.

Figure C-4 Aluminum A356-T6, Condition L: Optical Micrograph Showing 100X Magnification of Unstrained Area

METALLOGRAPHIC STUDY

Material Aluminum A356-T6 Neg.No. W28

Specimen LU 10 Neg.Mag. 1,000X

Etchant Keller's Photo Enlargement None

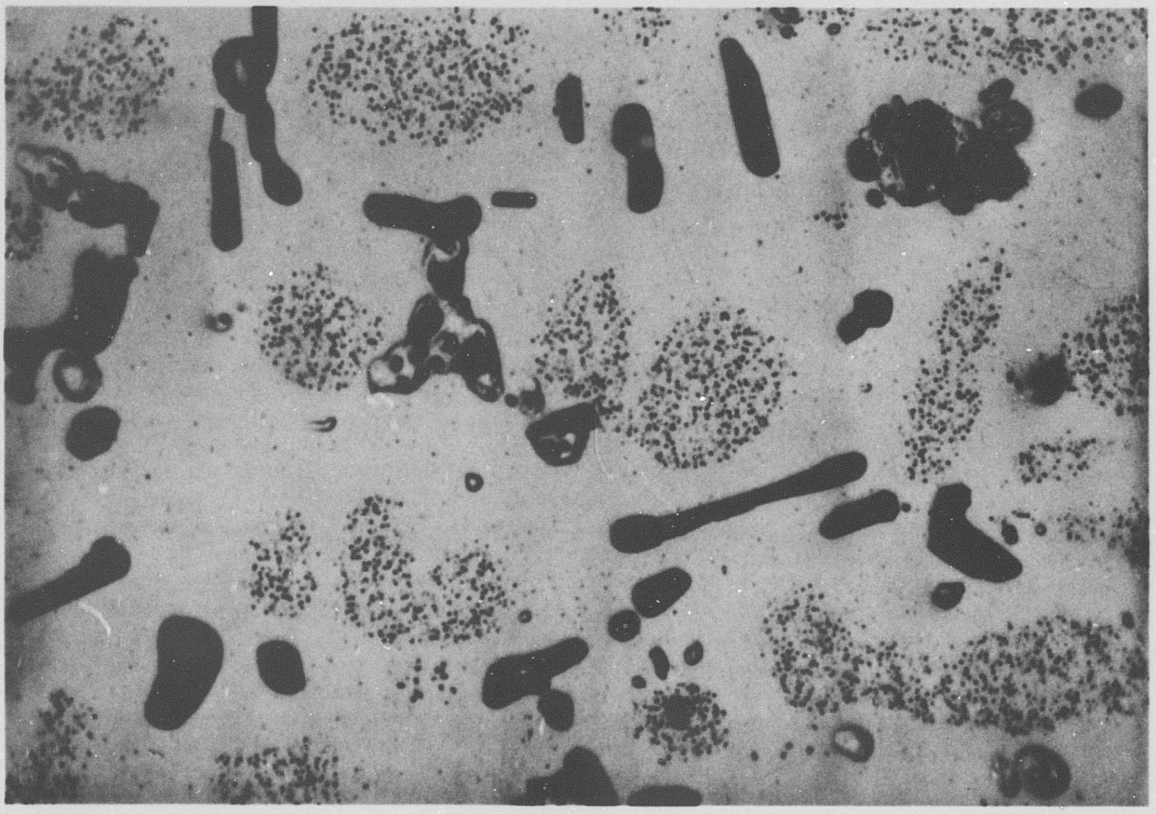

COMMENTS

The microstructure shows a solid-solution aluminum matrix containing intermetallic Al-Si. The cored structure is typical of castings.

Figure C-5 Aluminum A356-T6, Condition L: Optical Micrograph Showing 1,000X Magnification of Unstrained Area

METALLOGRAPHIC STUDY

Material Aluminum A356-T6 Neg.No. W42

Specimen LU 10 Neg.Mag. 100X

Etchant Keller's Photo Enlargement None

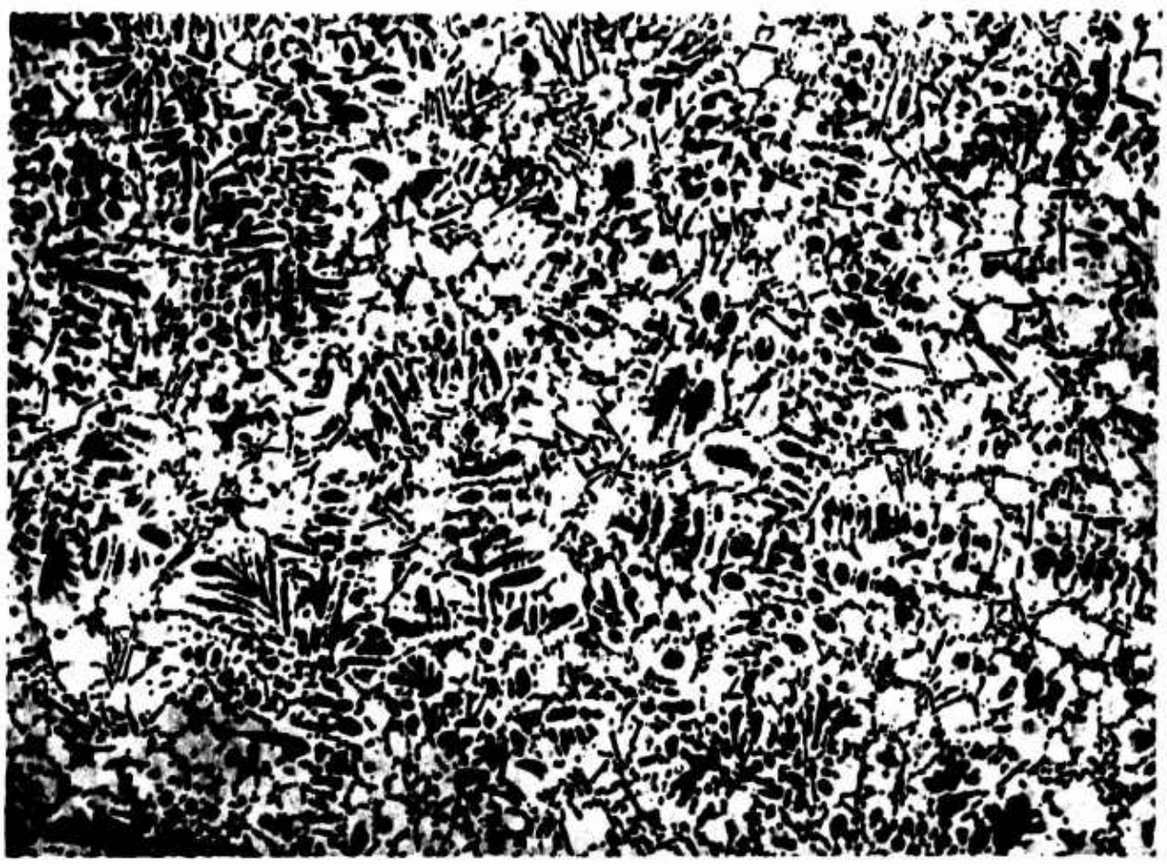

COMMENTS

The microstructure shows a solid-solution aluminum matrix with an intermetallic Al-Si. The cored structure is typical of castings.

Figure C-6 Aluminum A356-T6, Condition L: Optical Micrograph Showing 100X Magnification of General Strained Area

METALLOGRAPHIC STUDY

Material Aluminum A356-T6 Neg.No. W46

Specimen LU 10 Neg.Mag. 1,000X

Etchant Keller's Photo Enlargement None

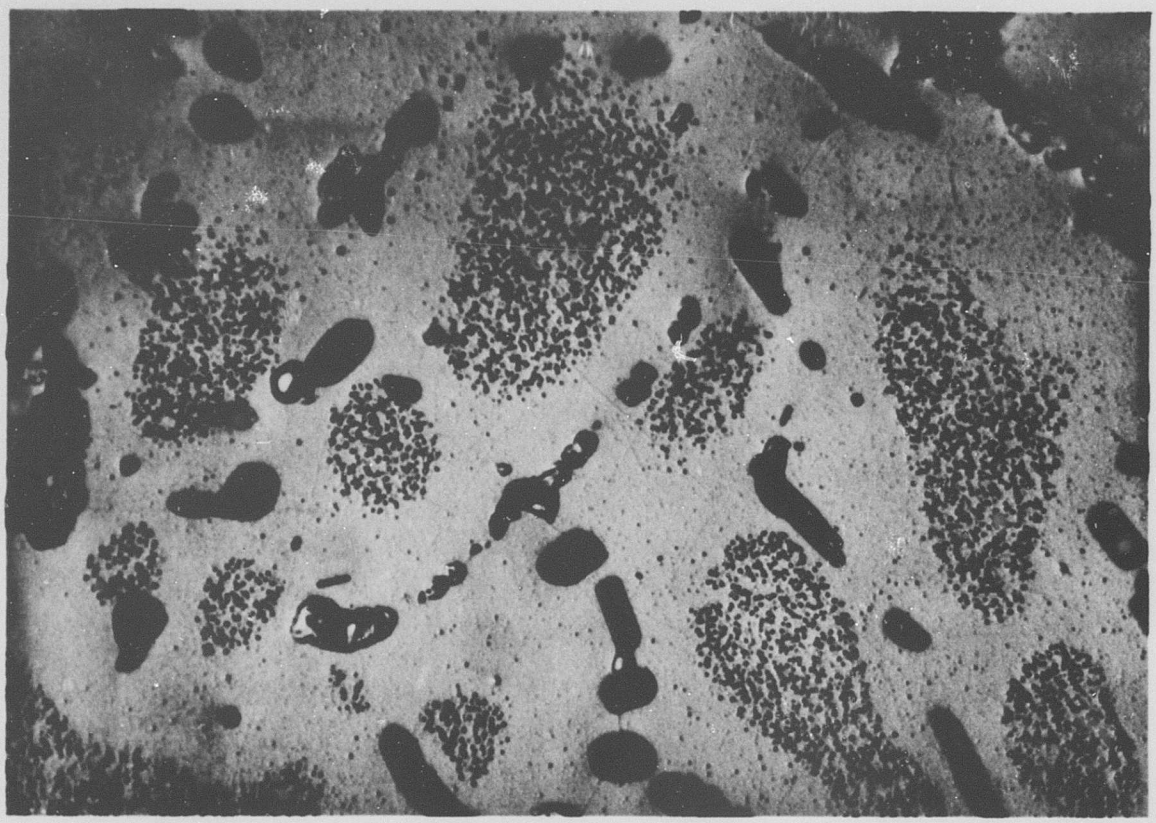

COMMENTS

The microstructure shows a solid-solution aluminum matrix with an intermetallic Al-Si. The cored structure is typical of castings.

Figure C-7 Aluminum A356-T6, Condition L: Optical Micrograph Showing 1,000X Magnification of General Strained Area

METALLOGRAPHIC STUDY

Material Aluminum A356-T6 Neg.No. W43

Specimen LU 10 Neg.Mag. 100X

Etchant Keller's Photo Enlargement None

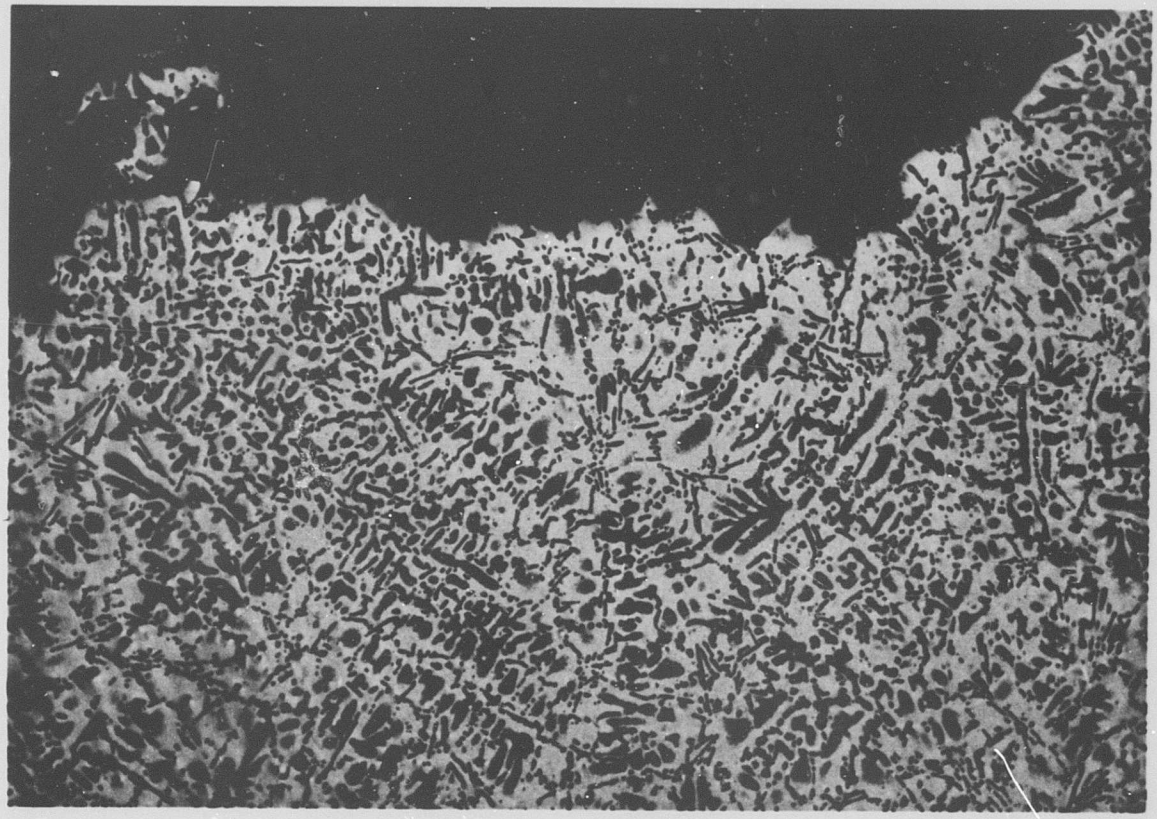

COMMENTS

The microstructure shows a solid-solution aluminum matrix with intermetallic Al-Si. The fracture is transgranular, occurring at the solid-solution-aluminum/intermetallic Al-Si interface and through the Al-Si eutectic.

Figure C-8 Aluminum A356-T6, Condition L: Optical Micrograph Showing 100X Magnification of Fracture Edge

METALLOGRAPHIC STUDY

Material Aluminum A356-T6 Neg.No. W47

Specimen LU 10 Neg.Mag. 1,000X

Etchant Keller's Photo Enlargement None

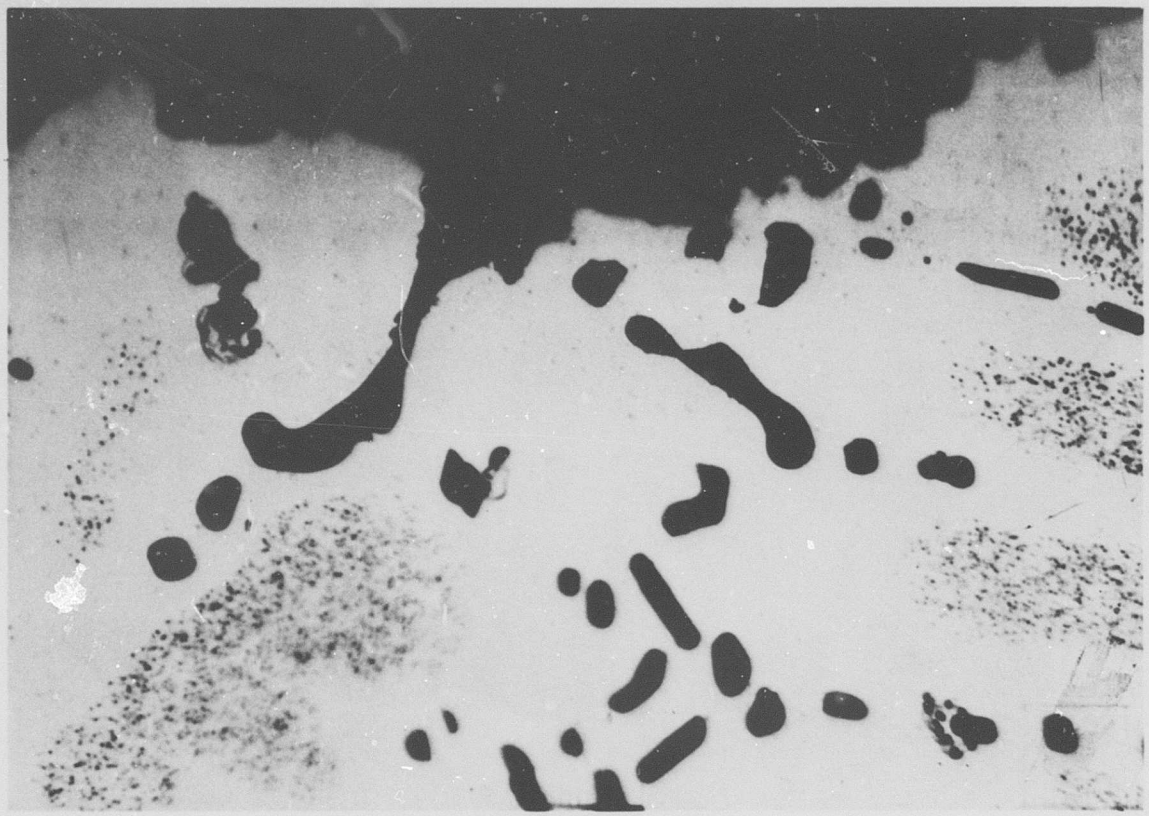

COMMENTS

The microstructure shows a solid-solution aluminum matrix with intermetallic Al-Si. The transgranular fracture occurred at the solid-solution-aluminum/ intermetallic Al-Si interface and through the Al-Si eutectic.

Figure C-9 Aluminum A356-T6, Condition L: Optical Micrograph Showing 1,000X Magnification of Fracture Edge

METALLOGRAPHIC STUDY

Material Aluminum A356-T6 Neg.No. W47

Specimen LU 10 Neg.Mag. 1,000X

Etchant Keller's Photo Enlargement None

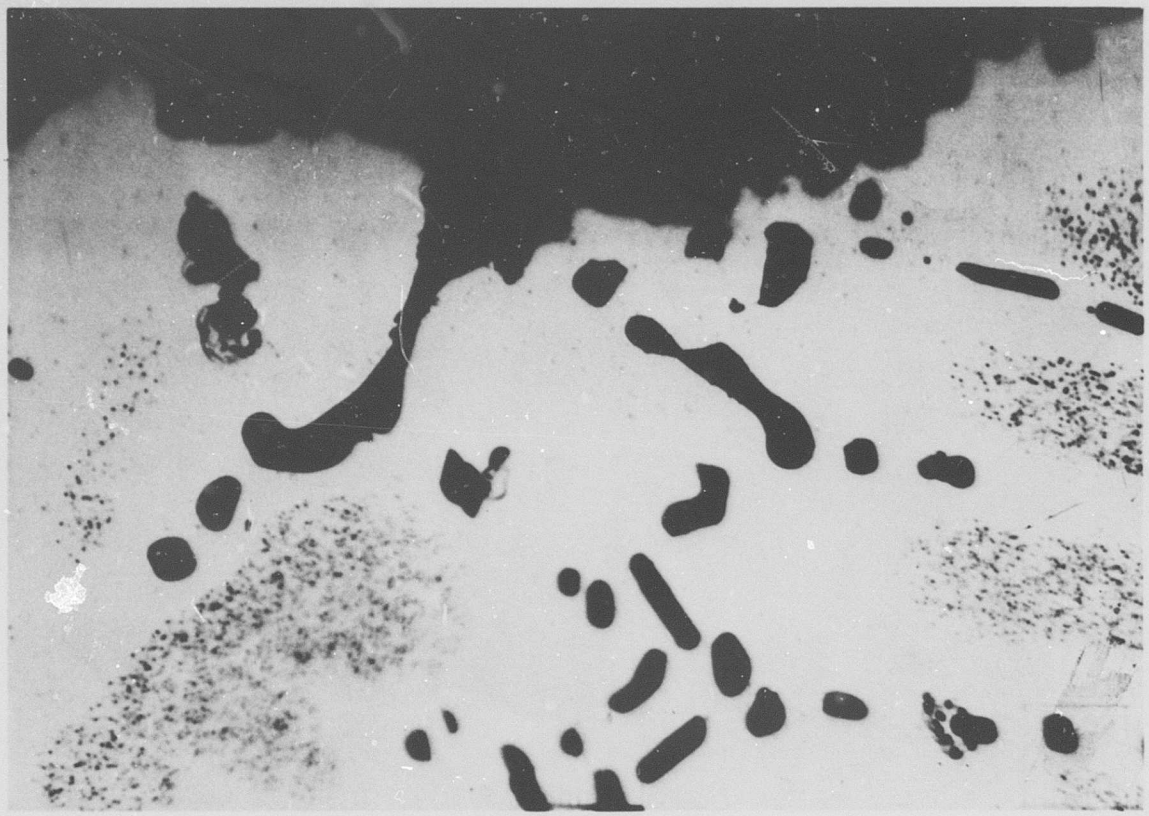

COMMENTS

The microstructure shows a solid-solution aluminum matrix with intermetallic Al-Si. The transgranular fracture occurred at the solid-solution-aluminum/ intermetallic Al-Si interface and through the Al-Si eutectic.

Figure C-9 Aluminum A356-T6, Condition L: Optical Micrograph Showing 1,000X Magnification of Fracture Edge

METALLOGRAPHIC STUDY

Material Aluminum A356-T6 Neg.No. 103-10

Specimen LU 10 Neg.Mag. 7,500X

Etchant Keller's Photo Enlargement 2X

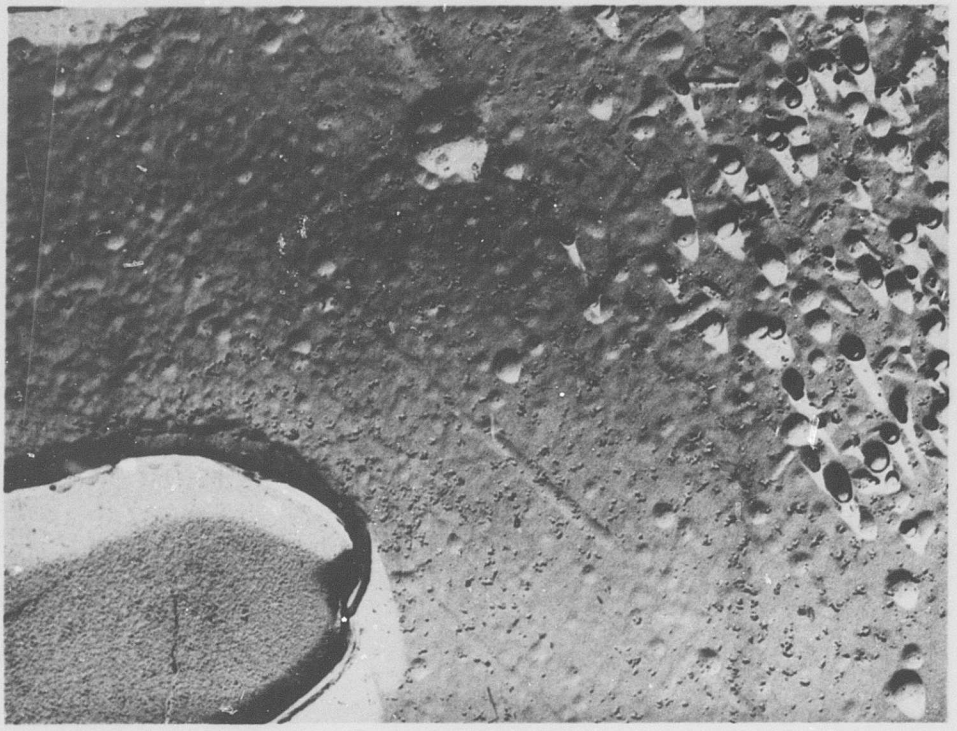

COMMENTS

The microstructure shows the Al-Si eutectic (lower left) and solid-solution aluminum with insolubles (right). Note strain lines between the eutectic and the insolubles.

Figure C-11 Aluminum A356-T6, Condition L: Electron Micrograph Showing 15,000X Magnification of Strained Area

METALLOGRAPHIC STUDY

Material Aluminum A356-T6 Neg.No. 95-4

Specimen LU 10 Neg.Mag. 2,100X

Etchant None Photo Enlargement 2X

COMMENTS

The topography at the center of the fracture is characterized by the brittle cleavage fracture of the Al-Si eutectic and by what is probably failure along the interface between the eutectic and the matrix.

Figure C-12 Aluminum A356-T6, Condition L: Electron Fractograph Showing 4,200X Magnification at Center of Fracture

METALLOGRAPHIC STUDY

Material Aluminum A356-T6 Neg.No. 95-6

Specimen LU 10 Neg.Mag. 2,100X

Etchant None Photo Enlargement 2X

COMMENTS

The topography near the edge of the fracture is made up mainly of brittle intermetallic fractures and separation along the interface between the Al-Si eutectic and the matrix. A few areas show shallow microvoid failures of the matrix.

Figure C-13 Aluminum A356-T6, Condition L: Electron Fractograph Showing 4,200X Magnification Near Edge of Fracture

METALLOGRAPHIC STUDY

Material Aluminum A356-T6 Neg.No. 97-5

Specimen LN 18 Neg.Mag. 2,100X

Etchant None Photo Enlargement 2X

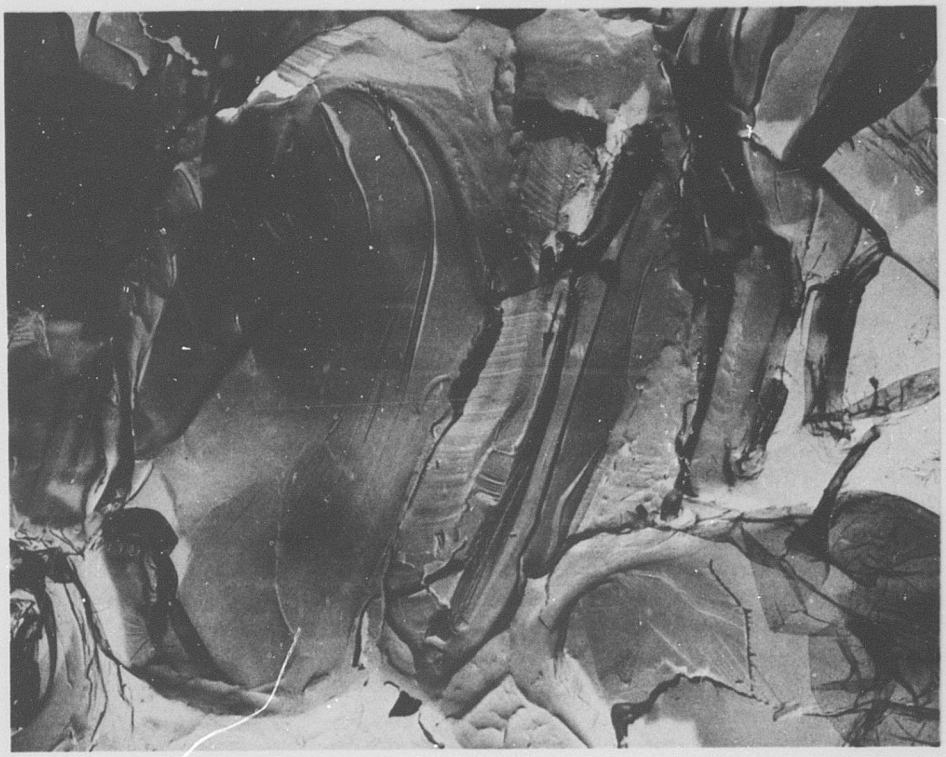

COMMENTS

The notched specimen fracture displays the same characteristics as the unnotched fractures: brittle intermetallic failure, eutectic matrix separation, and isolated areas of shallow micro-voids.

Figure C-14 Aluminum A356-T6, Condition L: Electron Fractograph Showing 4,200X Magnification of Notched Fracture

Aluminum 6061-T6
Condition L

Table C-3

Tensile and Shear Test Data

Material Aluminum 6061-T6 Specimen Condition L

Averaged Data (-423°F)		
Unnotched Specimens	Control	Irradiated
Ultimate Strength (ksi)	64.7	69.0
0.2% Yield Strength (ksi)	46.5	55.0
Elongation in Gage Length (%)	34.4	28.1
Reduction in Area (%)	24.1	32.6
Ultimate Shear Strength (ksi)	49.8	52.3
Notched Specimens		
Ultimate Strength (ksi)	61.4	65.8
Ratios		
Notched-Ult./Unnotched-Ult.	0.95	0.95
Notched-Ult./Unnotched-Yield	1.32	1.19

Unnotched Specimens				
Specimen Number	Ult. Tensile Strength (ksi)	Yield Strength 0.2% Offset (ksi)	Reduction in Area (%)	Elongation (%)
2-77	64.5	49.8	29.2	20.2
2-78	72.6	57.3	30.9	19.8
R-82	71.6	57.0	36.1	18.8
R-83	63.6	51.0	34.3	15.4
761	72.8	60.0	32.7	16.3

Notched Specimens		Shear Specimens	
Specimen Number	Ult. Tensile Strength (ksi)	Specimen Number	Ult. Shear Strength (ksi)
2-89	62.1	1	53.2
2-90	71.9	2	52.7
2-93	60.9	3	50.0
2-94	68.2	4	53.4

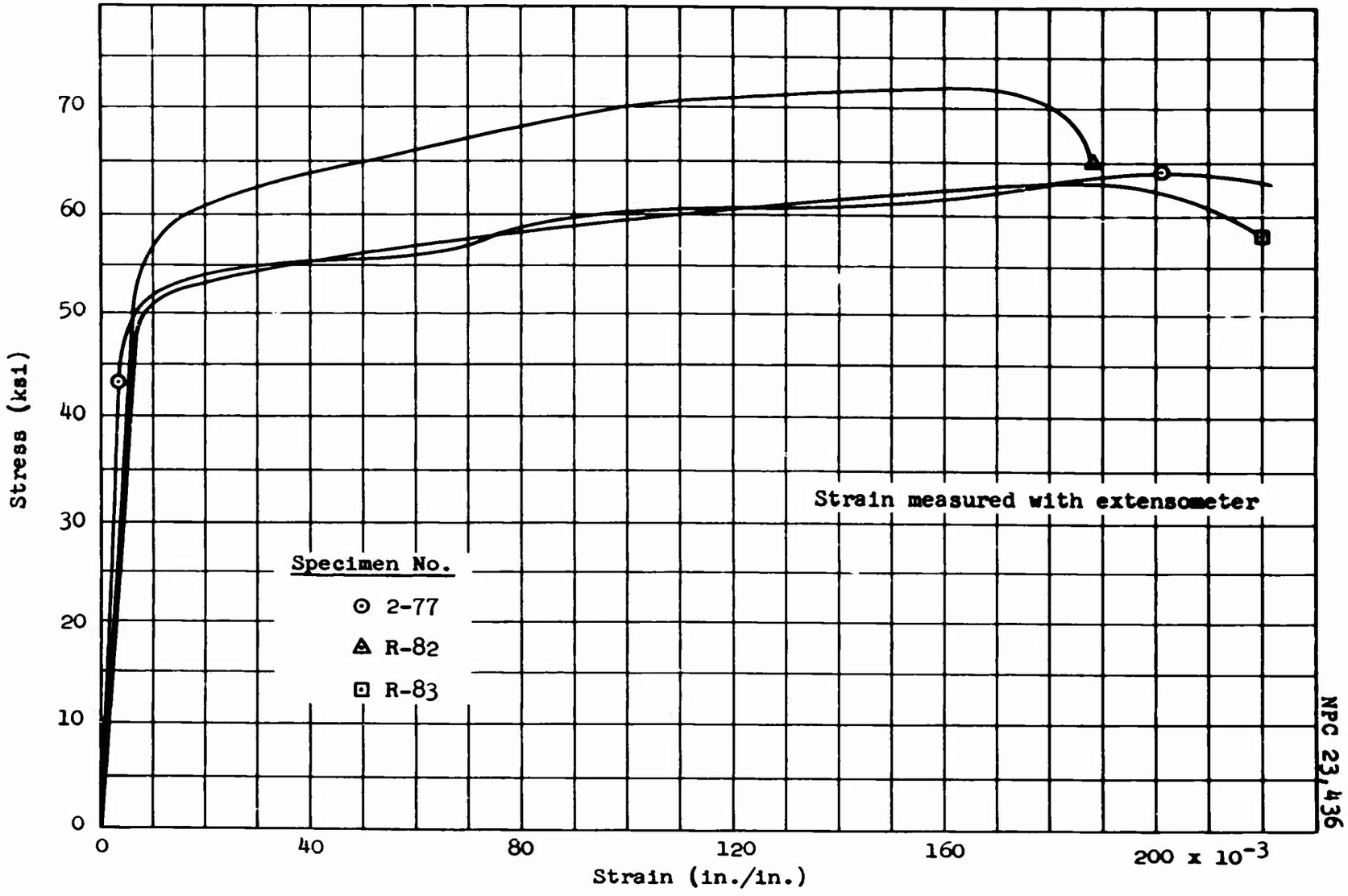

Figure C-15 Aluminum 6061-T6, Condition LU: Stress-Strain Curves

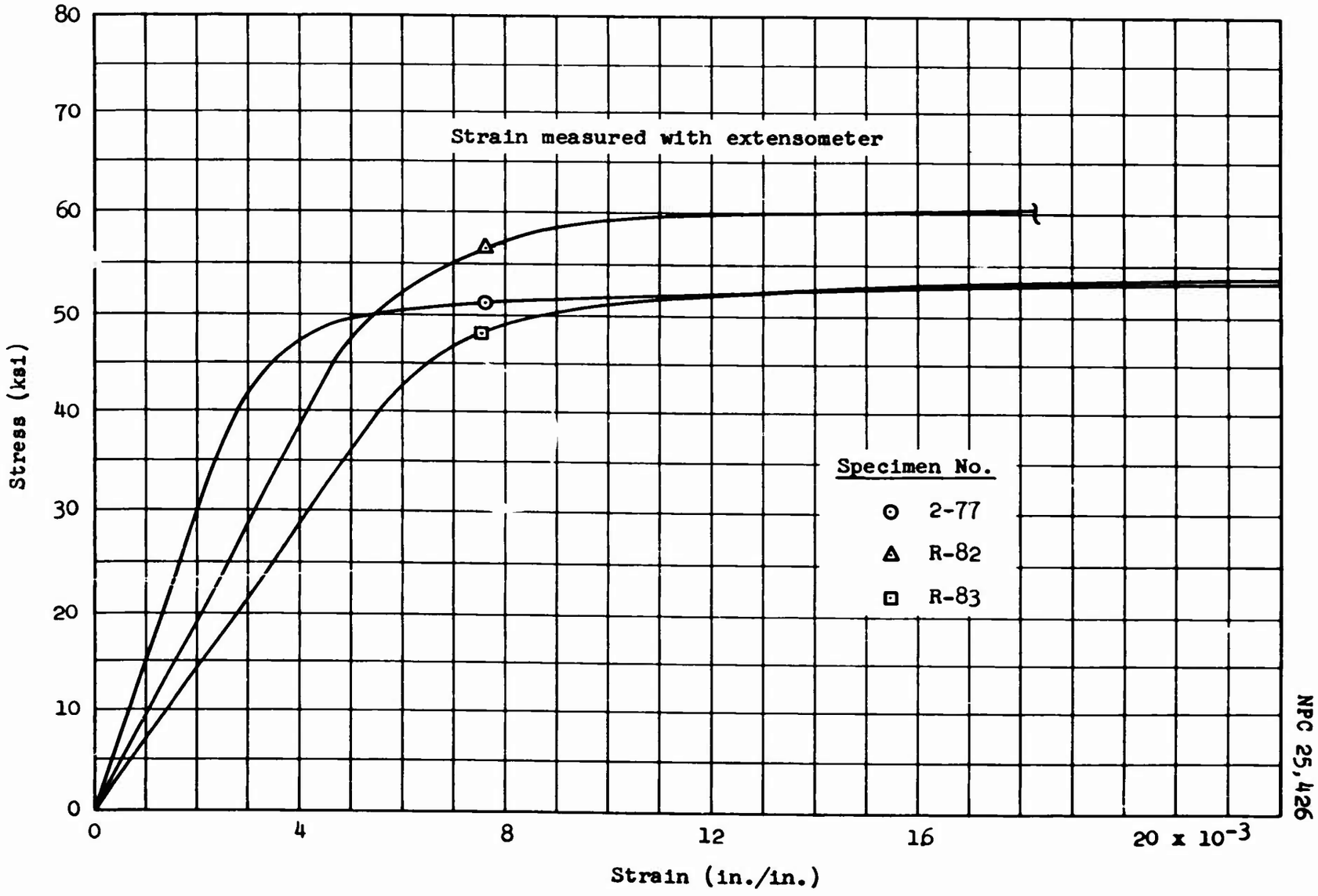

Figure C-16 Aluminum 6061-T6, Condition LU: Stress-Strain Curves (Expanded Scale)

Table C-4
X-Ray Diffraction Data

Material Aluminum 6061-T6 Specimen LU R-83

	STRAINED AREA		UNSTRAINED AREA	
DIFFRACTION PATTERN				
Miller Indices (hkl)	Interlattice Spacing, d (Å)	Relative Intensity (%)	Interlattice Spacing, d (Å)	Relative Intensity (%)
111	2.34	20	2.34	60
200	2.03	100	2.03	100
220	1.40	30	1.40	55
311	1.20	15	1.20	30
222				
400	1.00	5	1.00	3
331	0.92	2	0.92	6

LATTICE PARAMETER (Å)		
111	4.05	4.05
200	4.06	4.06
220	3.96	3.96
311	3.98	3.98
222	-	-
400	4.00	4.00
331	4.01	4.01

MICROSTRESS, $\Delta\theta$	
0.30° (2θ = 80.2°)	0.23° (2θ = 80.0°)
0.19° (2θ = 44.7°)	0.16° (2θ = 44.65°)
No Peak (2θ = 78°)	No Peak (2θ = 78°)

METALLOGRAPHIC STUDY

Material Aluminum 6061-T6 Neg.No. None

Specimen LU R-83 Neg.Mag. 3X

Etchant None Photo Enlargement None

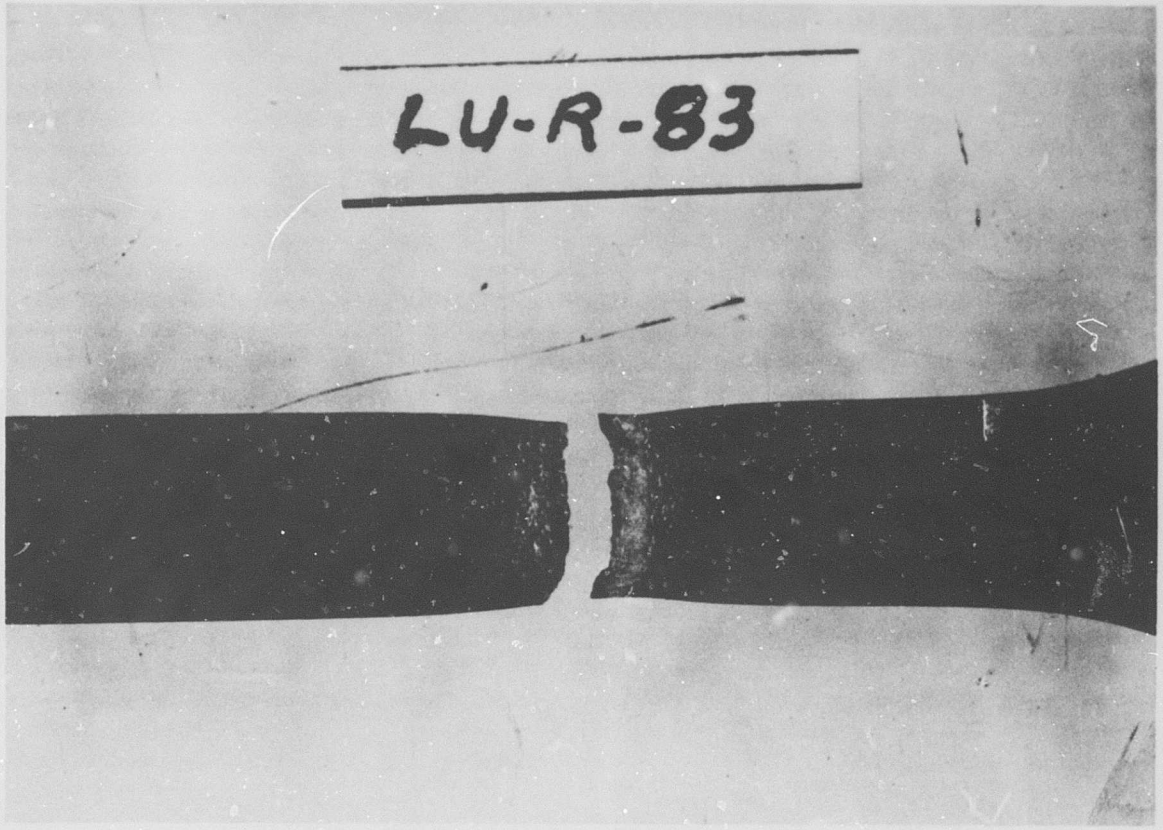

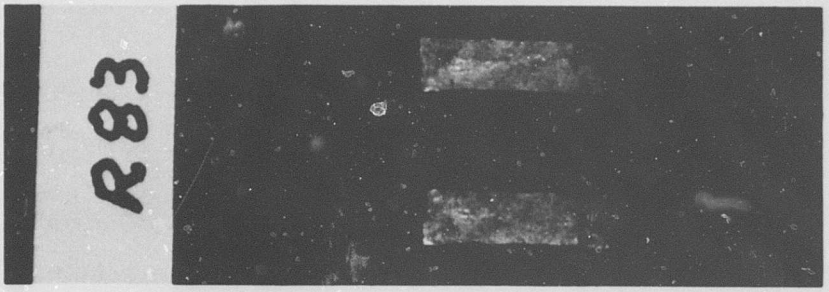

Figure C-17 Aluminum 6061-T6, Condition L: Macrophotograph Showing 3X Magnification of Specimen

METALLOGRAPHIC STUDY

Material Aluminum 6061-T6 Neg.No. W18

Specimen LU R-83 Neg.Mag. 100X

Etchant Keller's Photo Enlargement None

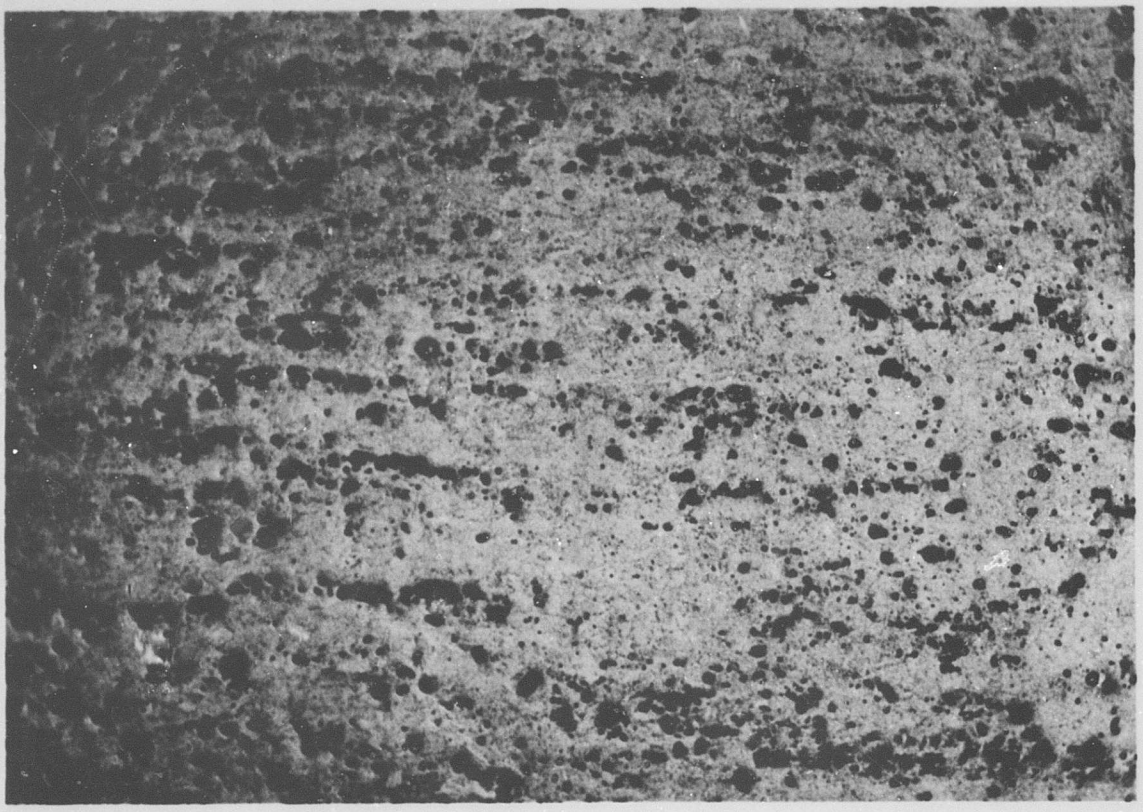

COMMENTS

The microstructure shows the solid-solution aluminum matrix. The matrix contains fine Mg-Si precipitate and intermetallic compounds.

Figure C-18 Aluminum 6061-T6, Condition L: Optical Micrograph Showing 100X Magnification of Unstrained Area

METALLOGRAPHIC STUDY

Material	Aluminum 6061-T6	Neg.No.	W30
Specimen	LU R-83	Neg.Mag.	1,000X
Etchant	Keller's	Photo Enlargement	None

COMMENTS

The microstructure shows the solid-solution aluminum matrix with fine Mg-Si precipitate and intermetallic compounds. The precipitate outlining the grain boundary resembles that produced during a slack quenching in heat treatment.

Figure C-19 Aluminum 6061-T6, Condition L: Optical Micrograph Showing 1,000X Magnification of Unstrained Area

METALLOGRAPHIC STUDY

Material Aluminum 6061-T6 Neg.No. W62

Specimen LU R-83 Neg.Mag. 100X

Etchant Keller's Photo Enlargement None

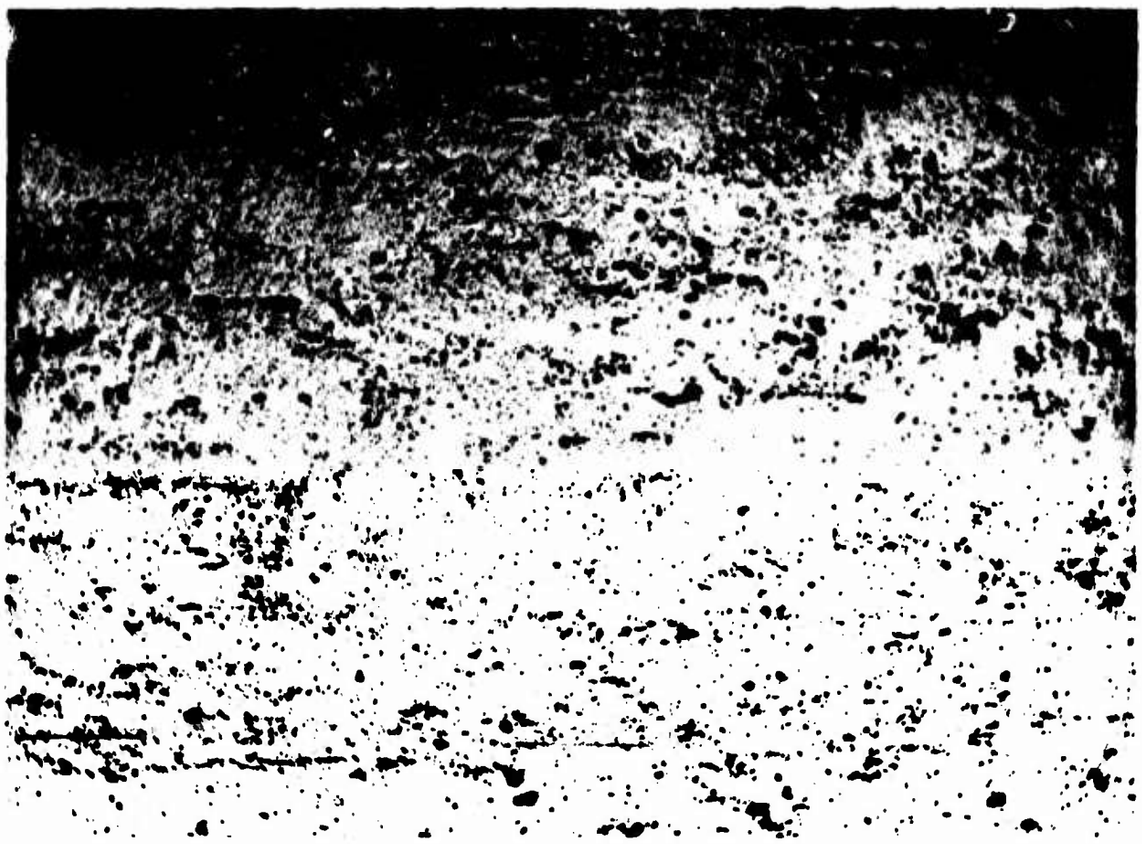

COMMENTS

The microstructure shows the solid-solution aluminum matrix. Fine Mg-Si precipitate and intermetallic compounds can be seen.

Figure C-20 Aluminum 6061-T6, Condition L: Optical Micrograph Showing 100X Magnification of General Strained Area

METALLOGRAPHIC STUDY

Material	Aluminum 6061-T6	Neg.No.	W54
Specimen	LU R-83	Neg.Mag.	1,000X
Etchant	Keller's	Photo Enlargement	None

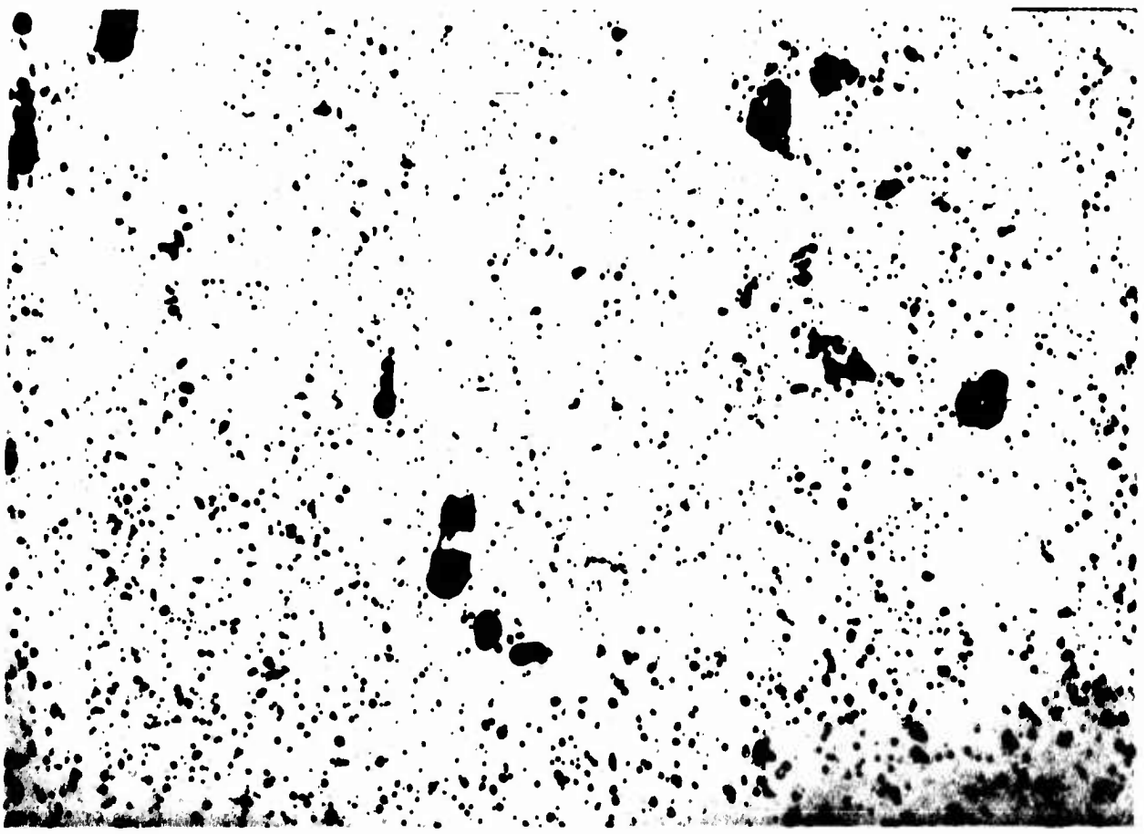

COMMENTS

The microstructure shows the solid-solution aluminum matrix with fine Mg-Si precipitate and intermetallic compounds.

Figure C-21 Aluminum 6061-T6, Condition L: Optical Micrograph Showing 1,000X Magnification of General Strained Area

METALLOGRAPHIC STUDY

Material Aluminum 6061-T6 Neg.No. W63

Specimen LU R-83 Neg.Mag. 100X

Etchant Keller's Photo Enlargement None

COMMENTS

The microstructure shows the solid-solution aluminum matrix containing a fine Mg-Si precipitate and intermetallic compounds. The fracture is transgranular.

Figure C-22 Aluminum 6061-T6, Condition L: Optical Micrograph Showing 100X Magnification of Fracture Edge

METALLOGRAPHIC STUDY

Material Aluminum 6061-T6 Neg.No. W55

Specimen LU R-83 Neg.Mag. 1,000X

Etchant Keller's Photo Enlargement None

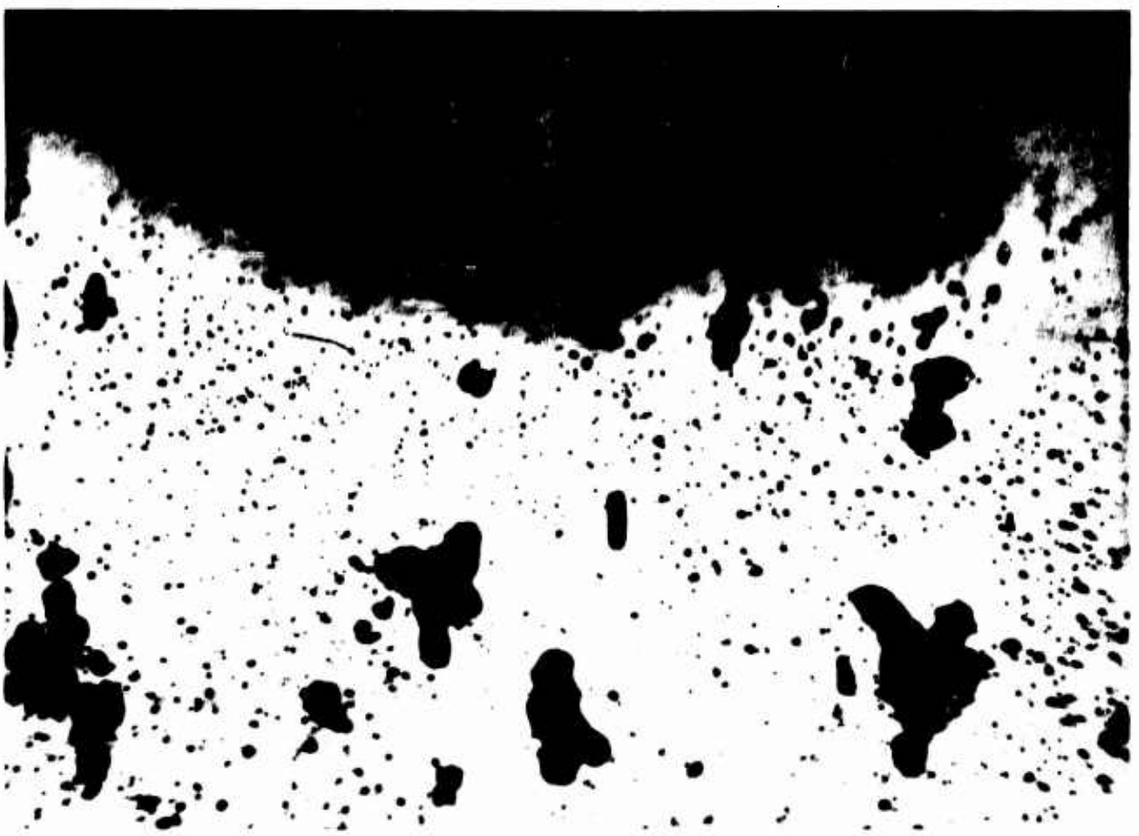

COMMENTS

The microstructure shows the solid-solution aluminum matrix containing fine Mg-Si precipitate and intermetallic compounds. The fracture is transgranular.

Figure C-23 Aluminum 6061-T6, Condition L: Optical Micrograph Showing 1,000X Magnification of Fracture Edge

METALLOGRAPHIC STUDY

Material Aluminum 6061-T6 Neg.No. 101-4

Specimen LU R-83 Neg.Mag. 7,500X

Etchant Keller's Photo Enlargement 2X

COMMENTS

The microstructure is typical of a solid-solution aluminum alloy with insolubles.

Figure C-24 Aluminum 6061-T6, Condition L: Electron Micrograph Showing 15,000X Magnification of Unstrained Area

METALLOGRAPHIC STUDY

Material Aluminum 6061-T6 Neg.No. 101-8

Specimen LU R-83 Neg.Mag. 7,500X

Etchant Keller's Photo Enlargement 2X

COMMENTS

The microstructure shows the solid-solution aluminum matrix, insolubles, and grain boundaries. The grain-boundary particles are normally not seen unless a slack quench has been performed.

Figure C-25 Aluminum 6061-T6, Condition L: Electron Micrograph Showing 15,000X Magnification of Strained Area

METALLOGRAPHIC STUDY

Material Aluminum 6061-T6 Neg.No. 96-8

Specimen LU R-83 Neg.Mag. 2,100X

Etchant None Photo Enlargement 2X

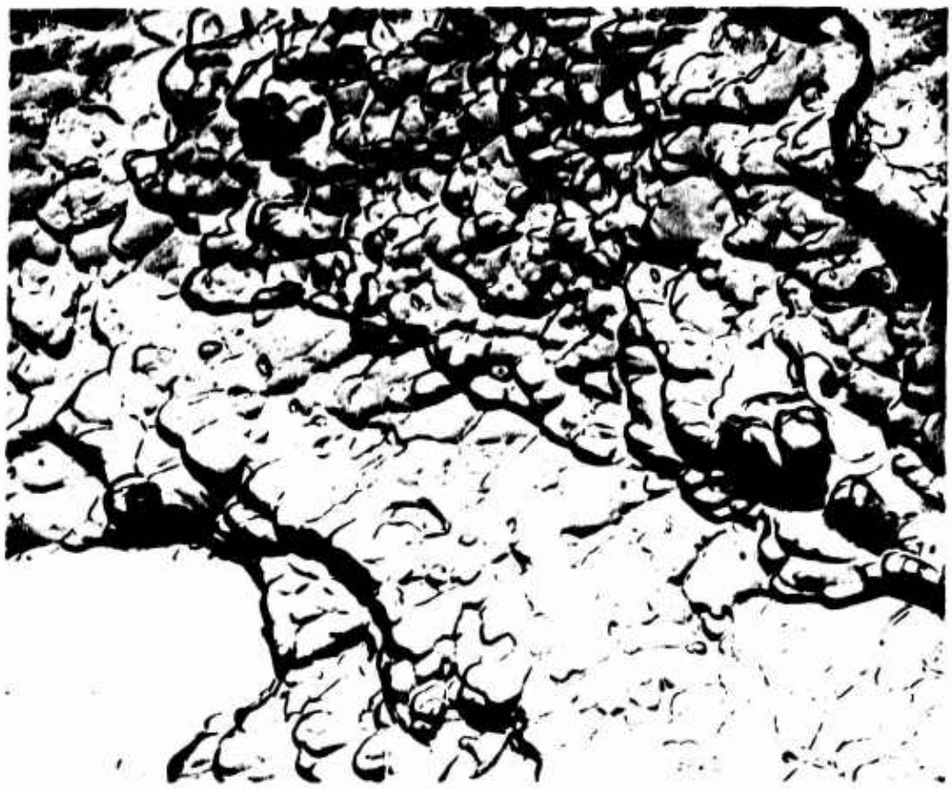

COMMENTS

The fracture surface at the center of the specimen is made up almost entirely of oriented dimples formed by microvoid coalescence. The flat area in the lower, left-hand corner represents the fracture of a brittle intermetallic compound.

Figure C-26 Aluminum 6061-T6, Condition L: Electron Fractograph Showing 4,200X Magnification at Center of Fracture

METALLOGRAPHIC STUDY

Material Aluminum 6061-T6 Neg.No. 96-11

Specimen LU R-83 Neg.Mag. 2,100X

Etchant None Photo Enlargement 2X

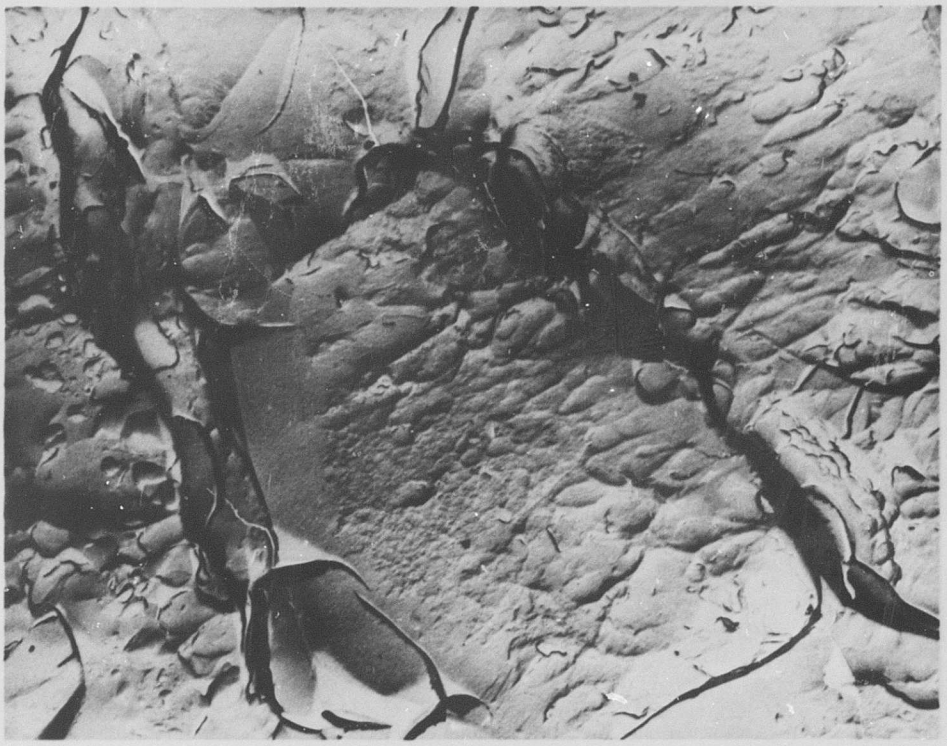

COMMENTS

The fracture surface near the edge consists of shallow dimples, intermetallic-compound failures, and intermetallic-compound/parent-metal interface failures.

Figure C-27 Aluminum 6061-T6, Condition L: Electron Fractograph Showing 4,200X Magnification Near Edge of Fracture

METALLOGRAPHIC STUDY

Material Aluminum 6061-T6 Neg.No. 99-6

Specimen LN 2-89 Neg.Mag. 2,100X

Etchant None Photo Enlargement 2X

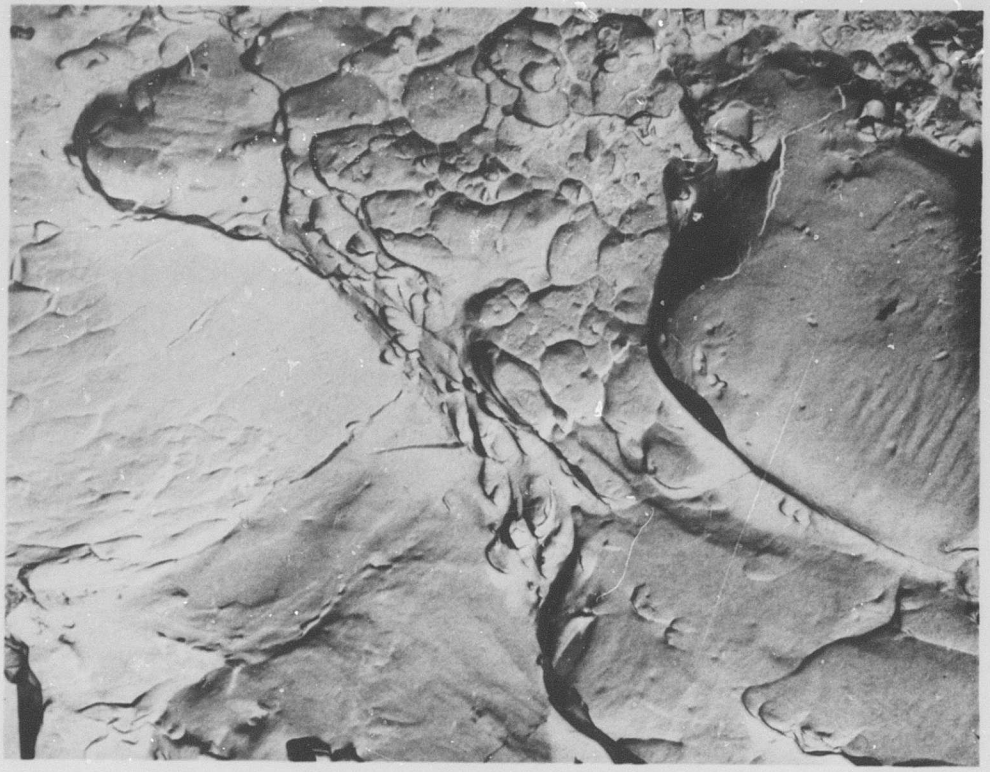

COMMENTS

The fracture consists of oriented and non-oriented microvoids. The area on the right shows some serpentine glide.

Figure C-28 Aluminum 6061-T6, Condition L: Electron Fractograph Showing 4,200X Magnification of Notched Fracture

Aluminum 6061-T6
Condition LW

BLANK PAGE

Table C-5
Tensile and Shear Test Data

Material Aluminum 6061-T6 Specimen Condition LW

Averaged Data (-423°F)		
Unnotched Specimens	Control	Irradiated
Ultimate Strength (ksi)	68.9	66.7
0.2% Yield Strength (ksi)	56.9	52.6
Elongation in Gage Length (%)	6.0	5.5
Reduction in Area (%)	11.9	10.8
Ultimate Shear Strength (ksi)	49.8	52.3
Notched Specimens		
Ultimate Strength (ksi)	57.3	67.6
Ratios		
Notched-Ult./Unnotched-Ult.	0.83	1.01
Notched-Ult./Unnotched-Yield	1.07	1.29

Unnotched Specimens				
Specimen Number	Ult. Tensile Strength(ksi)	Yield Strength 0.2% Offset (ksi)	Reduction in Area (%)	Elongation (%)
3-78	73.9	57.1	9.9	7.4
3-80	72.8	53.0	18.4	9.2
3-82	65.3	54.9	9.1	4.6
R-84	54.8	45.5	5.9	.88

Notched Specimens		Shear Specimens*	
Specimen Number	Ult. Tensile Strength (ksi)	Specimen Number	Ult. Shear Strength (ksi)
3-90	66.6		
3-92	68.8		
3-94	68.6		
3-96	66.2		

*Not Applicable

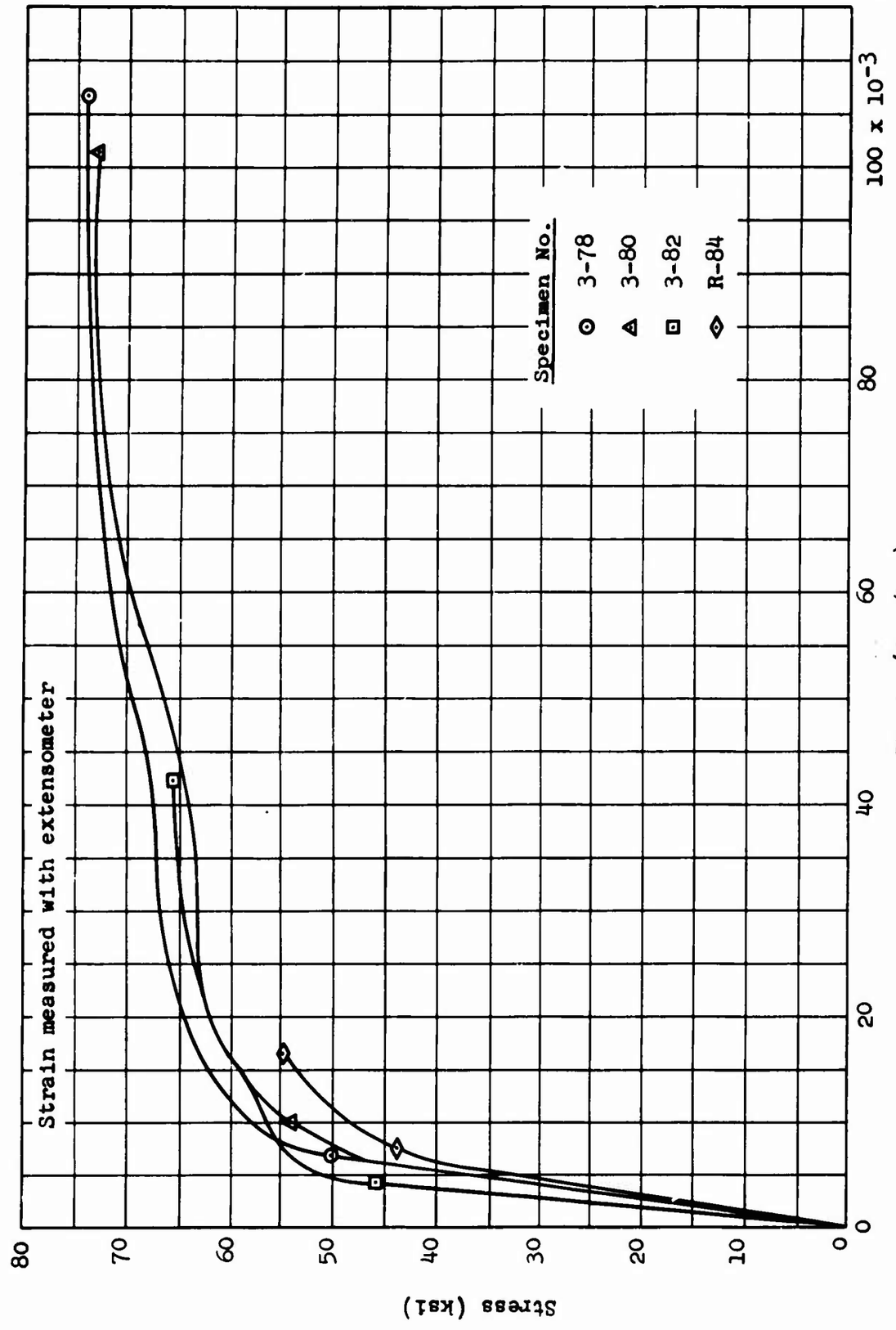

Figure C-29 Aluminum 6061-T6, Condition LWU: Stress-Strain Curves

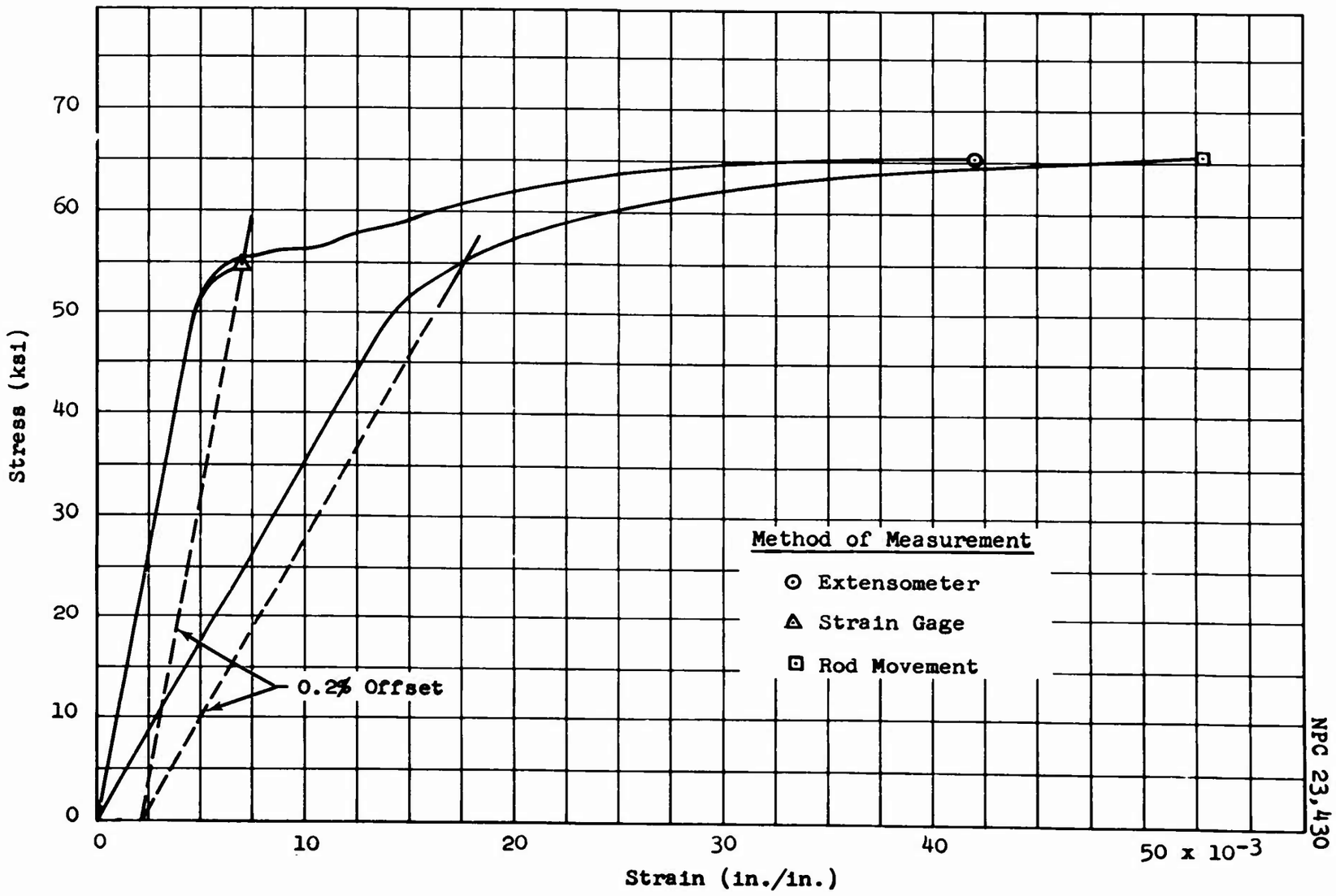

Figure C-30 Aluminum 6061-T6, Condition LWU: Comparison of Strain-Measurement Methods

Table C-6

X-Ray Diffraction Data

Material Aluminum 6061-T6 Specimen LWU 3-80

	STRAINED AREA		UNSTRAINED AREA	
DIFFRACTION PATTERN				
Miller Indices (hkl)	Interlattice Spacing, d (Å)	Relative Intensity (%)	Interlattice Spacing, d (Å)	Relative Intensity (%)
111	2.34	21	2.35	7
200	2.03	100	2.25 2.03	2 100
220	1.43	14	1.44	25
311	1.22	9	1.22	4
222				
400	1.01	3	1.01	8
331	0.93	2	0.91	2

LATTICE PARAMETER (Å)		
111	4.05	4.07
200	4.06	4.06
220	4.04	4.07
311	4.05	4.05
222	-	-
400	4.04	4.04
331	4.05	3.97

MICROSTRESS, $\Delta\theta$	
0.28° (2θ = 78°)	0.23° (2θ = 78°)
0.20° (2θ = 44.6°)	0.15° (2θ = 44.6°)

METALLOGRAPHIC STUDY

Material Aluminum 6061-T6 Neg.No. None

Specimen LWU 3-80 Neg.Mag. 3X

Etchant None Photo Enlargement None

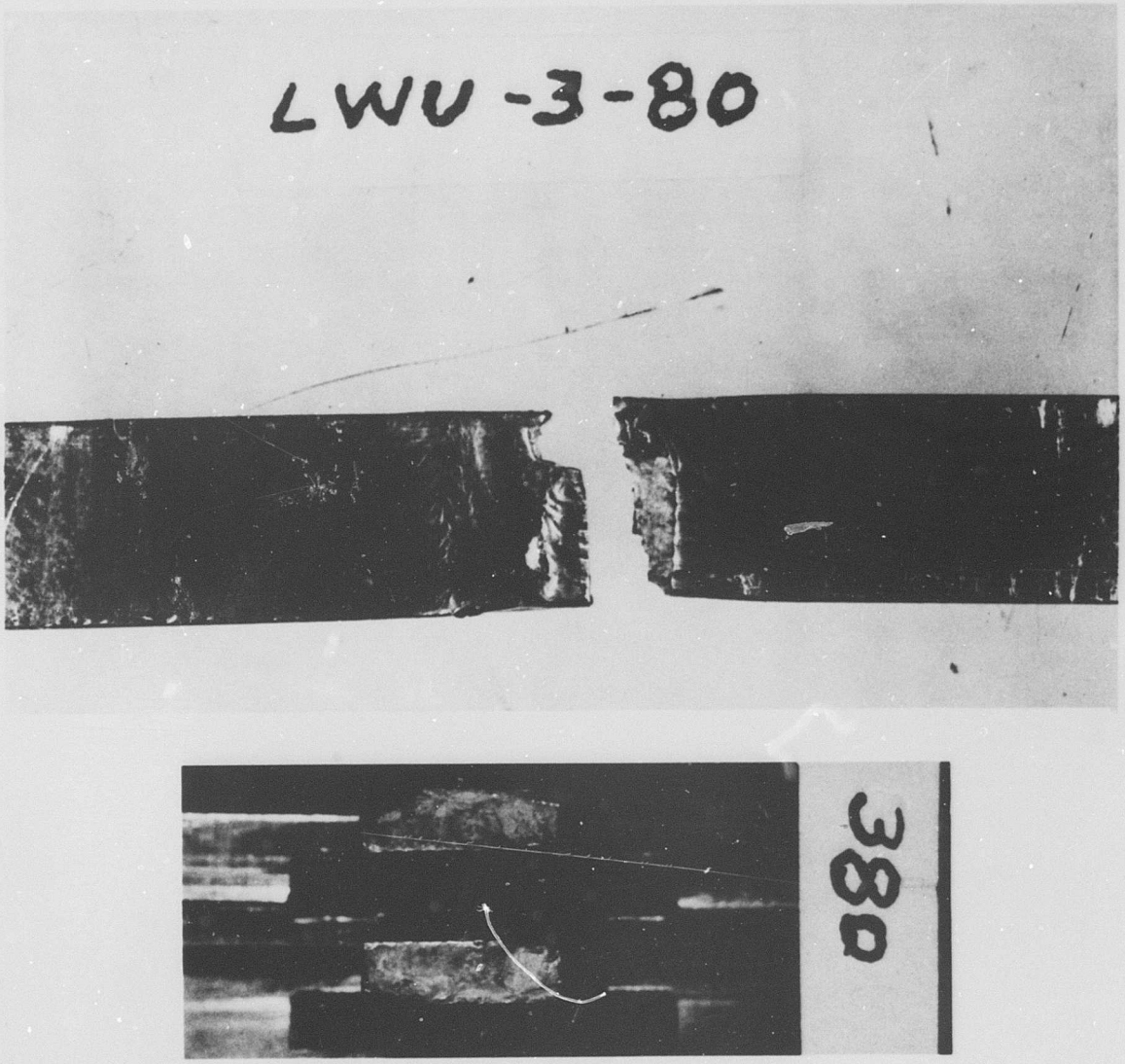

Figure C-31 Aluminum 6061-T6, Condition LW: Macrophotograph Showing 3X Magnification of Specimen

METALLOGRAPHIC STUDY

Material Aluminum 6061-T6 Neg.No. W21

Specimen LWU 3-80 Neg.Mag. 100X

Etchant Keller's Photo Enlargement None

COMMENTS

The microstructure shows the solid-solution aluminum matrix with inclusions and Al-Si eutectic.

Figure C-32 Aluminum 6061-T6, Condition LW: Optical Micrograph Showing 100X Magnification of Unstrained Area

METALLOGRAPHIC STUDY

Material Aluminum 6061-T6 Neg.No. W27

Specimen LWU 3-80 Neg.Mag. 1,000X

Etchant Keller's Photo Enlargement None

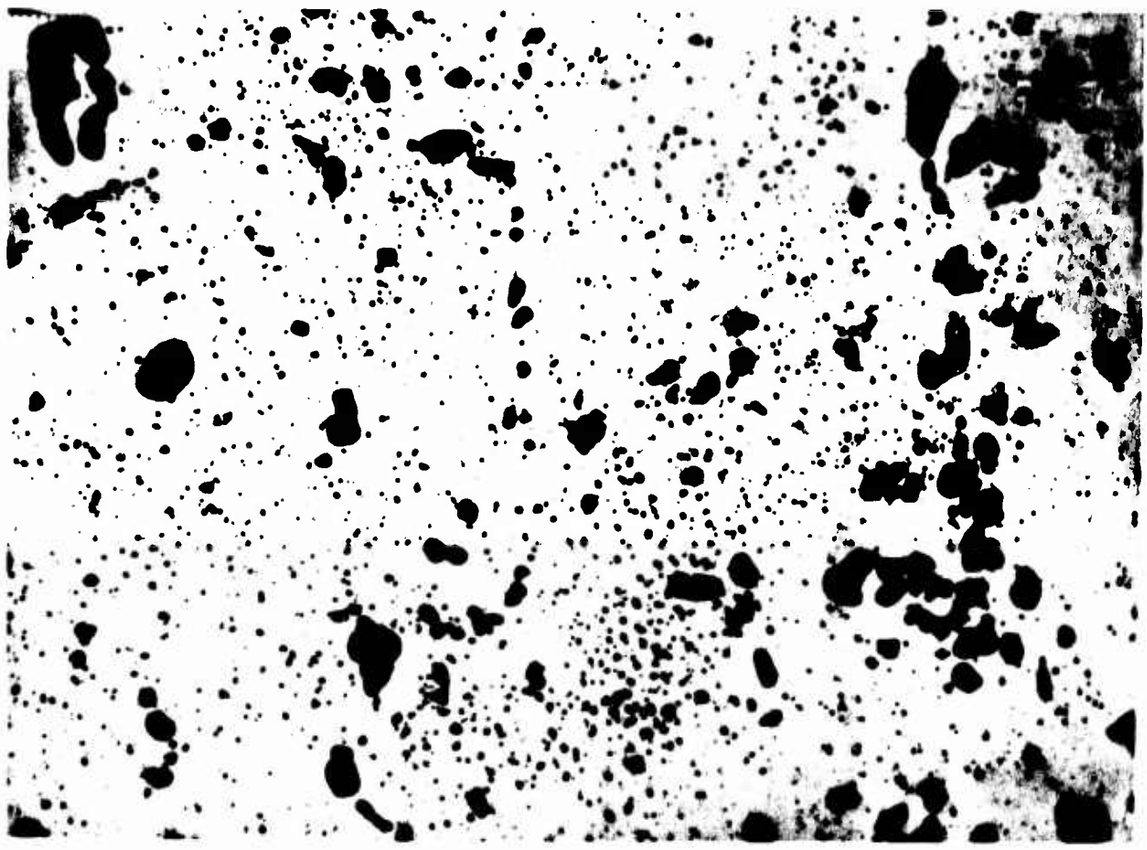

COMMENTS

The microstructure shows the solid-solution aluminum matrix containing inclusions and Al-Si eutectic.

Figure C-33 Aluminum 6061-T6, Condition LW: Optical Micrograph Showing 1,000X Magnification of Unstrained Area

METALLOGRAPHIC STUDY

Material	Aluminum 6061-T6	Neg.No.	W39
Specimen	LWU 3-80	Neg.Mag.	100X
Etchant	Keller's	Photo Enlargement	None

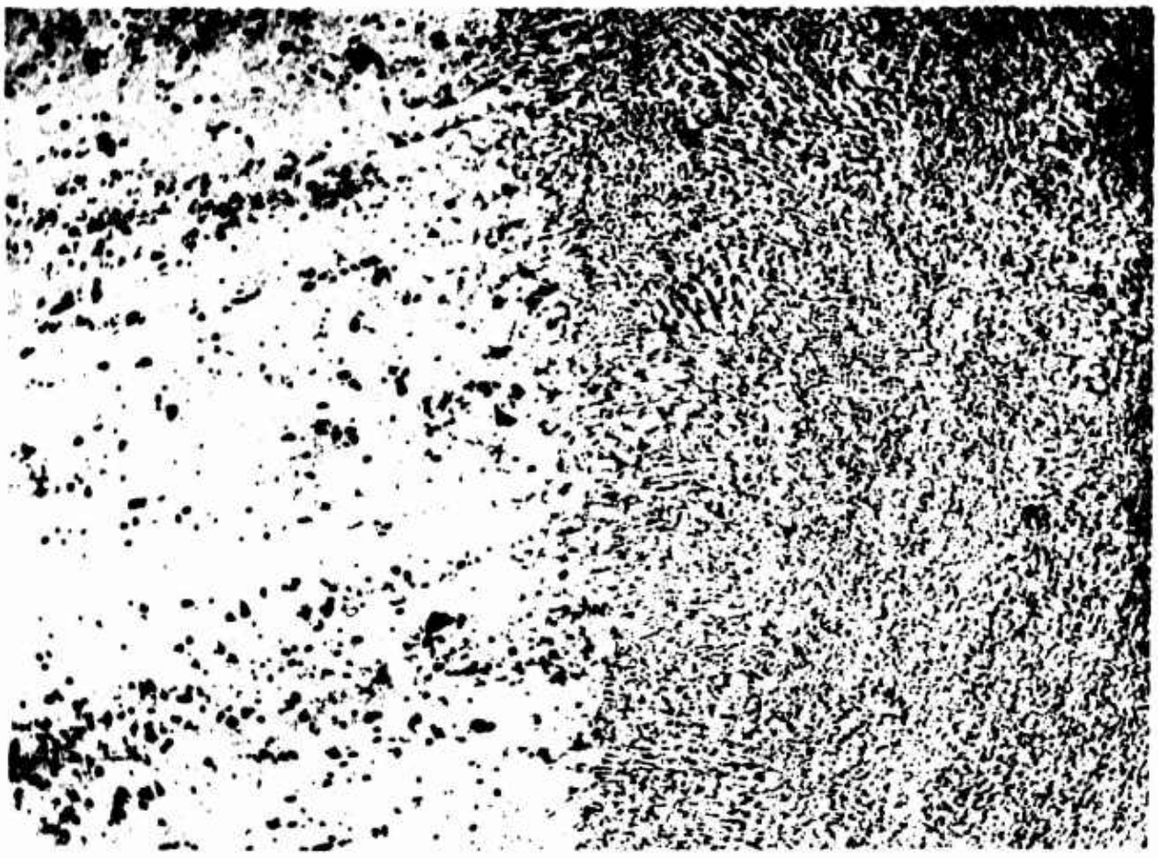

COMMENTS

The microstructure shows the parent metal (left) and weld metal (right) interface. Note the pronounced grain boundaries of the heat-affected zone in the matrix.

Figure C-34 Aluminum 6061-T6, Condition LW: Optical Micrograph Showing 100X Magnification of Parent Metal and Weld Interface

METALLOGRAPHIC STUDY

Material Aluminum 6061-T6 Neg.No. W36

Specimen LWU 3-80 Neg.Mag. 1,000X

Etchant Keller's Photo Enlargement None

COMMENTS

The microstructure shows the solid-solution aluminum matrix, the Al-Si eutectic, and inclusions. Note the clarification of the grain boundaries of the heat-affected zone in the matrix.

Figure C-35 Aluminum 6061-T6, Condition LW: Optical Micrograph Showing 1,000X Magnification of Parent Metal and Weld Interface

METALLOGRAPHIC STUDY

Material Aluminum 6061-T6 Neg.No. W38

Specimen LWU 3-80 Neg.Mag. 100X

Etchant Keller's Photo Enlargement None

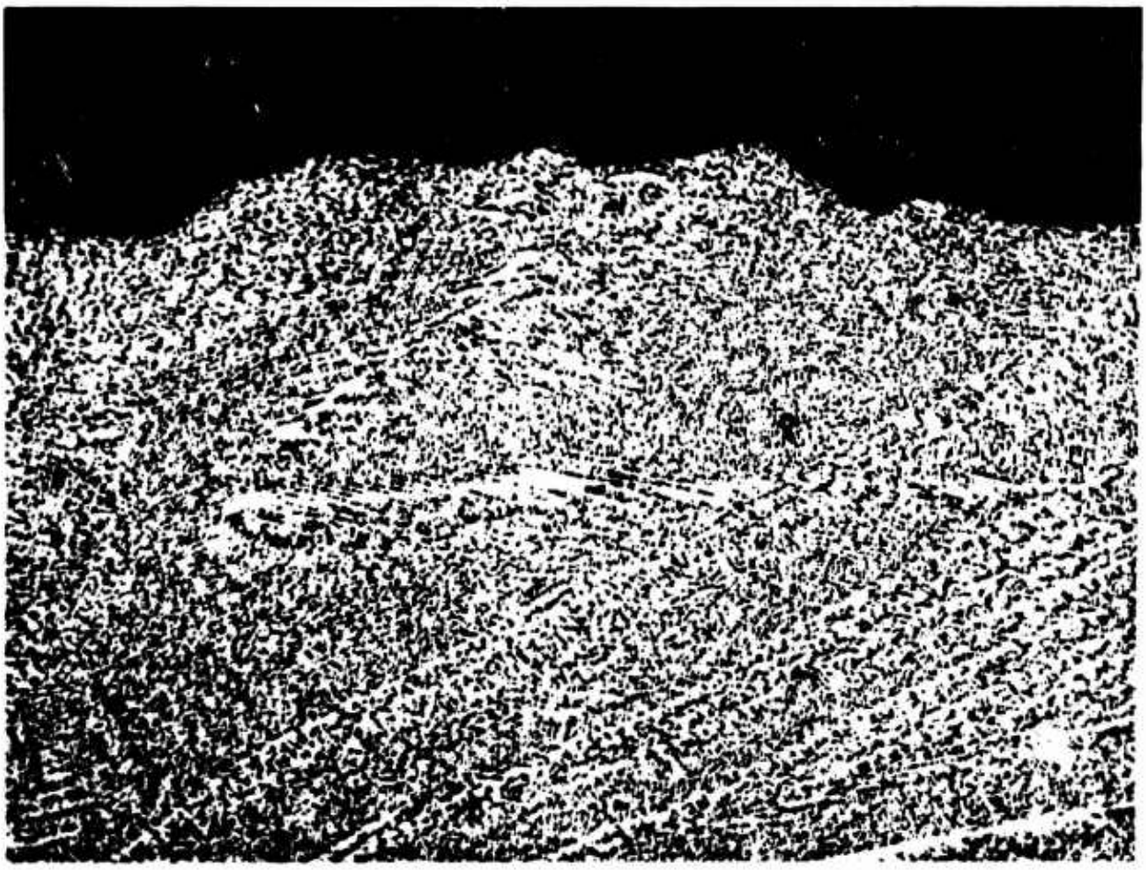

COMMENTS

The microstructure shows the dendritic pattern in the weld zone and the transgranular nature of the fracture through the weld.

Figure C-36 Aluminum 6061-T6, Condition LW: Optical Micrograph Showing 100X Magnification of Fracture Edge

METALLOGRAPHIC STUDY

Material Aluminum 6061-T6 Neg.No. W37

Specimen LWU 3-80 Neg.Mag. 1,000X

Etchant Keller's Photo Enlargement None

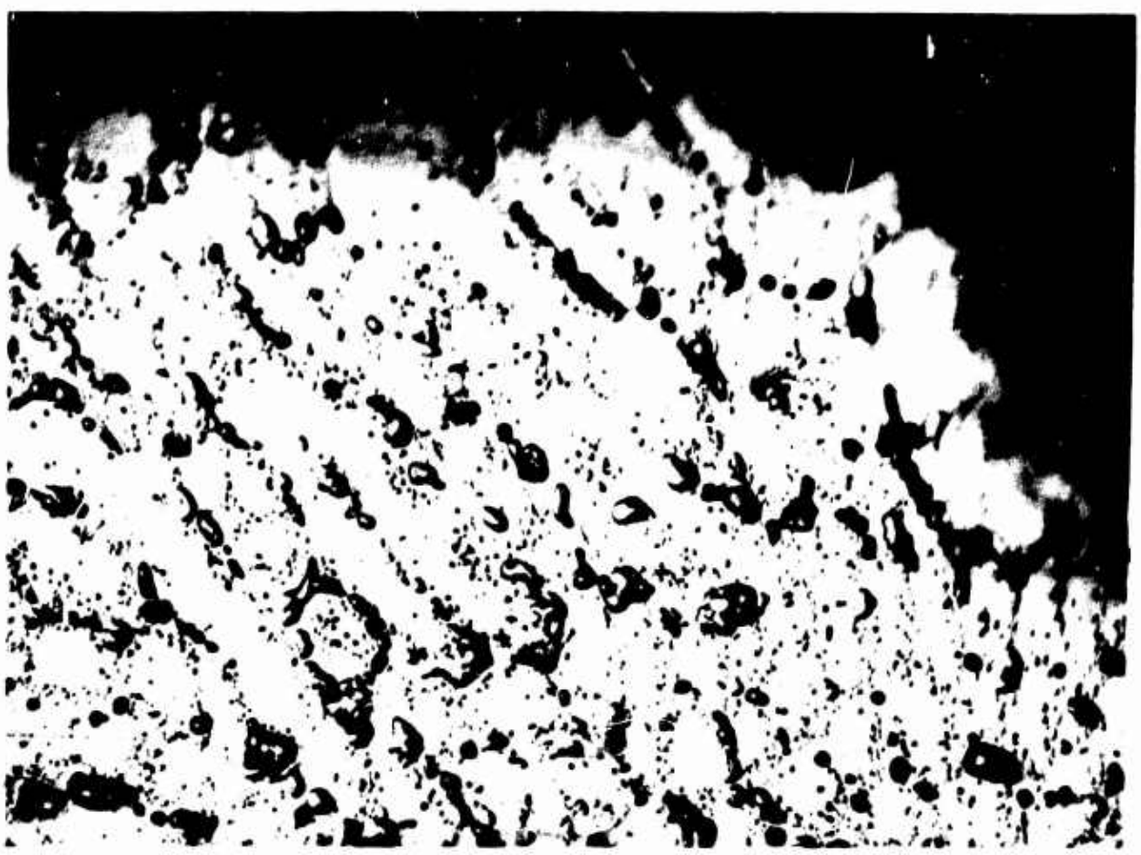

COMMENTS

The microstructure shows the aluminum matrix, the Al-Si eutectic, and the transgranular nature of the fracture through the weld.

Figure C-37 Aluminum 6061-T6, Condition LW: Optical Micrograph Showing 1,000X Magnification of Fracture Edge

METALLOGRAPHIC STUDY

Material Aluminum 6061-T6 Neg.No. 101-5

Specimen LWU 3-80 Neg.Mag. 7,500X

Etchant Keller's Photo Enlargement 2X

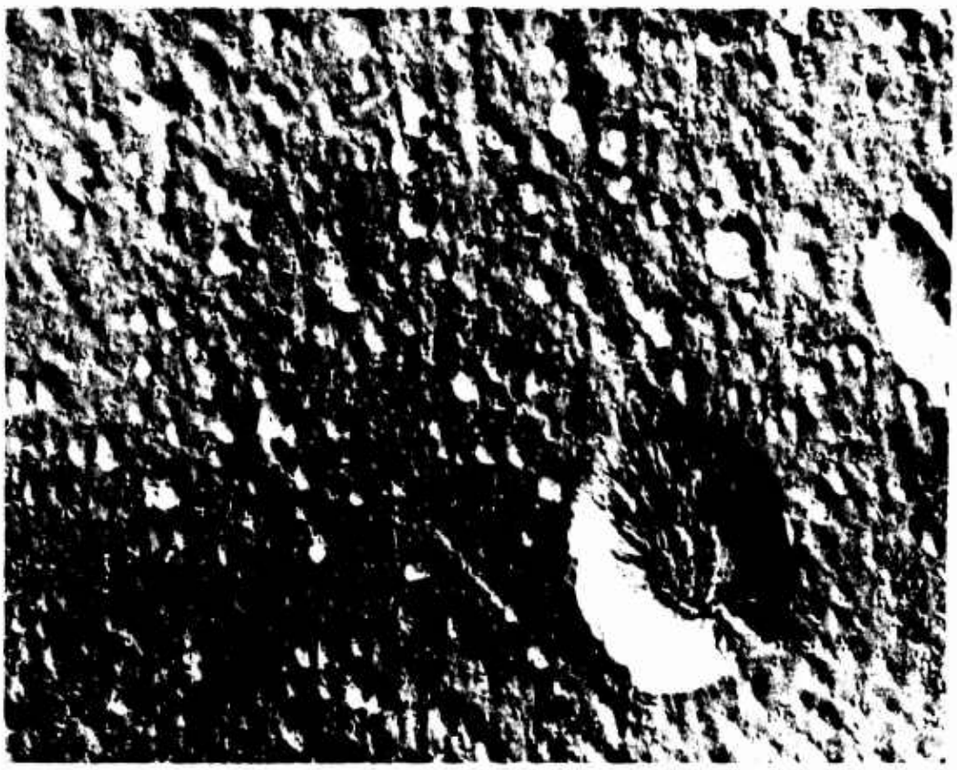

COMMENTS

The microstructure shows the solid-solution aluminum matrix with insolubles. Note the large circular inclusion site.

Figure C-38 Aluminum 6061-T6, Condition LW: Electron Micrograph Showing 15,000X Magnification of Unstrained Area

METALLOGRAPHIC STUDY

Material Aluminum 6061-T6 Neg.No. 104-3

Specimen LWU 3-80 Neg.Mag. 7,500X

Etchant Keller's Photo Enlargement 2X

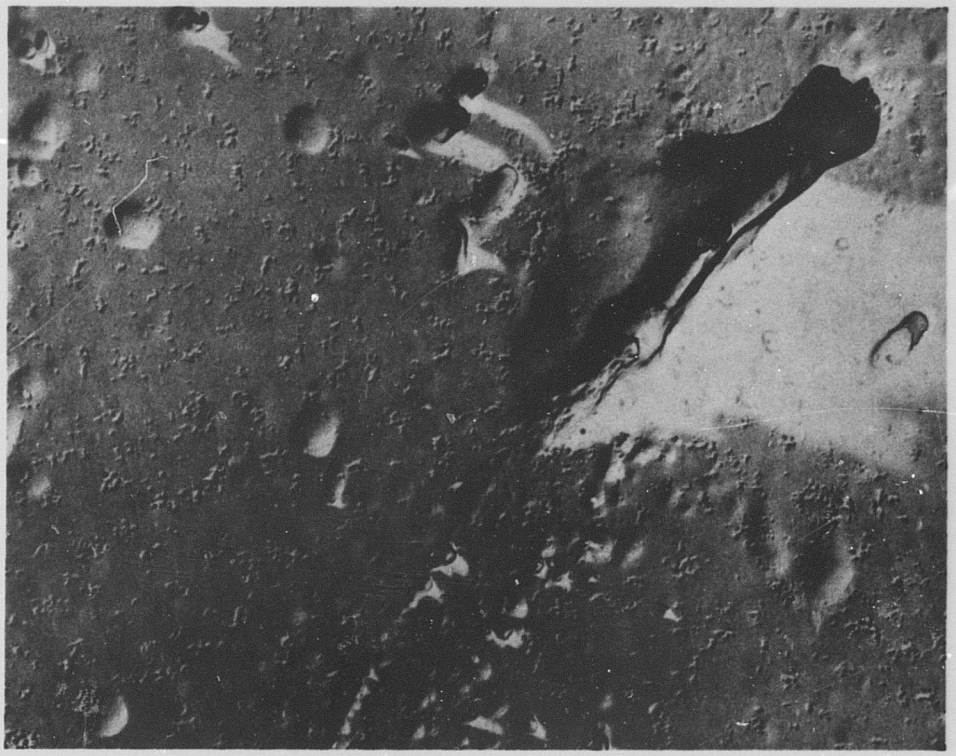

COMMENTS

The microstructure shows the solid-solution aluminum matrix; the Al-Si eutectic, and insolubles.

Figure C-39 Aluminum 6061-T6, Condition LW: Electron Micrograph Showing 15,000X Magnification of Strained Area

METALLOGRAPHIC STUDY

Material Aluminum 6061-T6 Neg.No. 92-11

Specimen LWU 3-80 Neg.Mag. 2,100X

Etchant None Photo Enlargement 2X

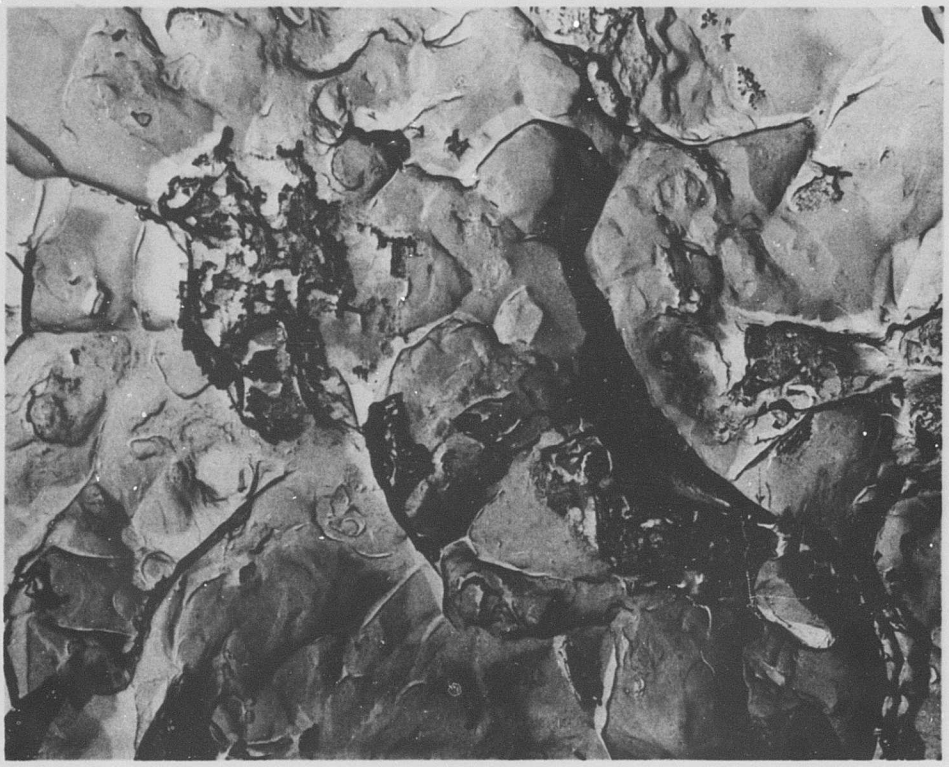

COMMENTS

The topography at the center of the fracture has the characteristics of a dimple rupture. Failure occurred along the eutectic/matrix interface and through the eutectic.

Figure C-40 Aluminum 6061-T6, Condition LW: Electron Fractograph Showing 4,200X Magnification at Center of Fracture

METALLOGRAPHIC STUDY

Material	Aluminum 6061-T6	Neg.No.	92-12
Specimen	LWU 3-80	Neg.Mag.	2,100X
Etchant	None	Photo Enlargement	2X

COMMENTS

The topography near the edge of the fracture is composed of an oriented dimple rupture. Areas of probable oxidation can be noted.

Figure C-41 Aluminum 6061-T6, Condition LW: Electron Fractograph Showing 4,200X Magnification Near Edge of Fracture

METALLOGRAPHIC STUDY

Material	Aluminum 6061-T6	Neg.No.	99-9
Specimen	LWN 3-90	Neg.Mag.	2,100X
Etchant	None	Photo Enlargement	2X

COMMENTS

The notched fracture topography is made up of dimples, with eutectic at the base of the dimples. In some areas, the fracture appears to follow the eutectic/ matrix interface.

Figure C-42 Aluminum 6061-T6, Condition LW: Electron Fractograph Showing 4,200X Magnification of Notched Fracture

Aluminum 6061-T6
Condition TW

BLANK PAGE

Table C-7

Tensile and Shear Test Data

Material Aluminum 6061-T6 Specimen Condition TW

Averaged Data (-423°F)		
Unnotched Specimens	Control	Irradiated
Ultimate Strength (ksi)	67.3	71.6
0.2% Yield Strength (ksi)	47.4	57.6
Elongation in Gage Length (%)	9.0	7.34
Reduction in Area (%)	16.3	21.6
Ultimate Shear Strength (ksi)	49.8	52.3
Notched Specimens		
Ultimate Strength (ksi)	56.5	65.2
Ratios		
Notched-Ult./Unnotched-Ult.	0.84	0.91
Notched-Ult./Unnotched-Yield	1.19	1.13

Unnotched Specimens				
Specimen Number	Ult. Tensile Strength(ksi)	Yield Strength 0.2% Offset (ksi)	Reduction in Area (%)	Elongation (%)
3-31	74.5	59.0	23.1	6.7
3-32	73.3	57.8	14.5	9.2
3-35	65.1	57.0	22.9	4.1
3-36	73.8	56.5	25.7	9.4

Notched Specimens		Shear Specimens*	
Specimen Number	Ult. Tensile Strength (ksi)	Specimen Number	Ult. Shear Strength (ksi)
3-42	62.4		
3-44	68.0		
3-46	65.0		
3-48	Broke on rebound		

*Not Applicable

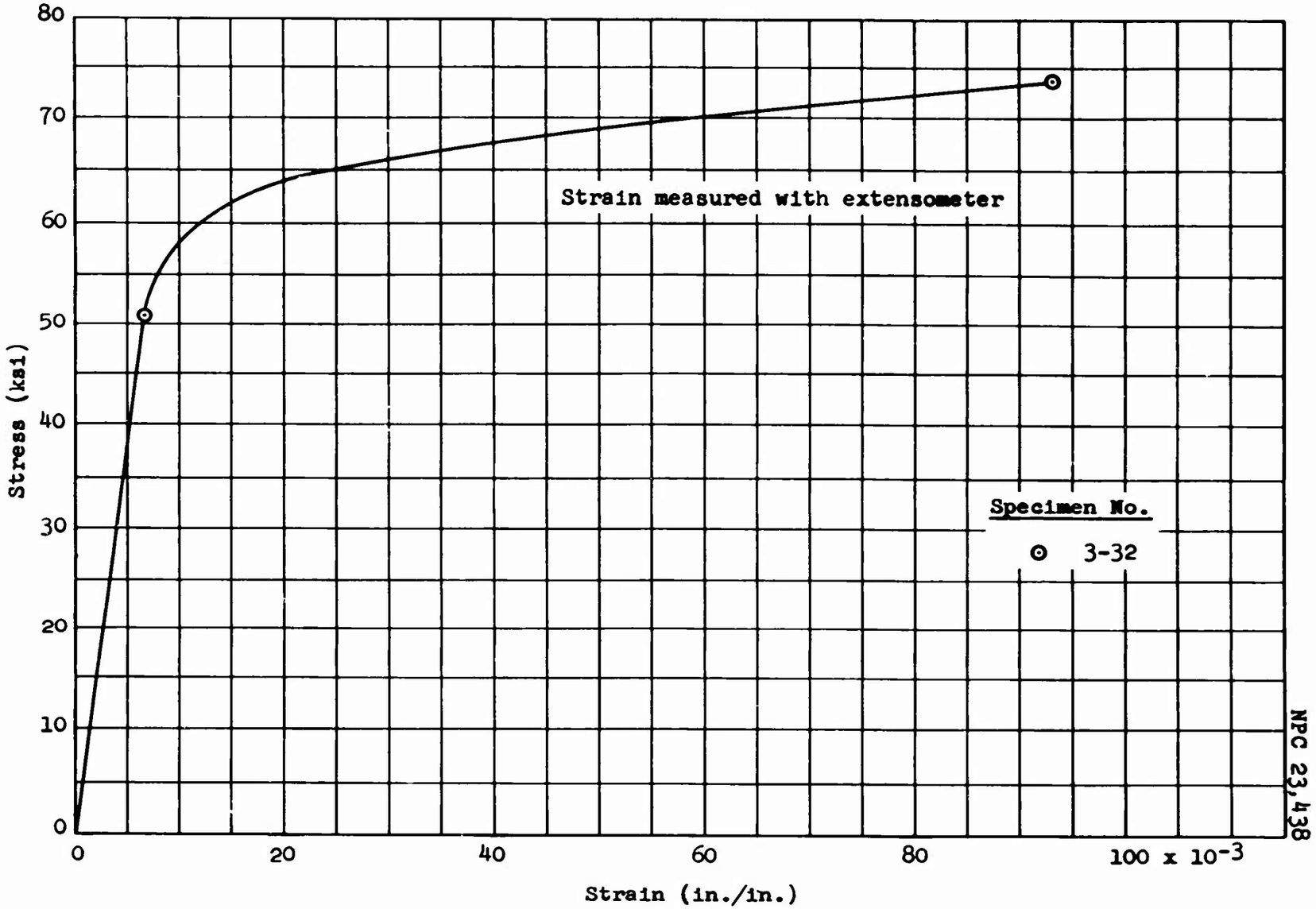

Figure C-43 Aluminum 6061-T6, Condition TWU: Stress-Strain Curves

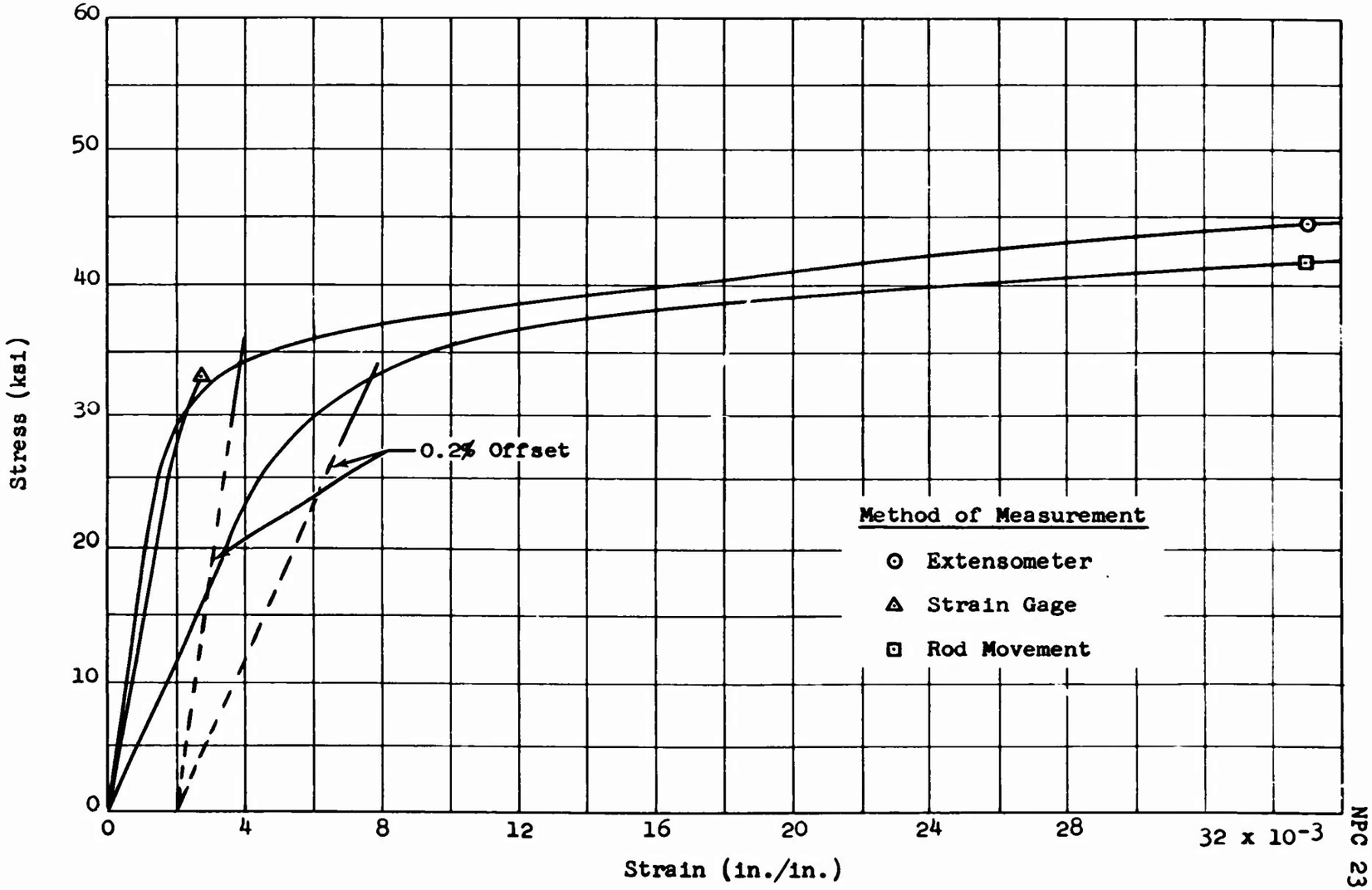

Figure C-44 Aluminum 6061-T6, Condition TWU: Comparison of Strain-Measurement Methods

Table C-8

X-Ray Diffraction Data

Material Aluminum 6061-T6 Specimen TWU 3-36

	STRAINED AREA		UNSTRAINED AREA	
DIFFRACTION PATTERN				
Miller Indices (hkl)	Interlattice Spacing, d (Å)	Relative Intensity (%)	Interlattice Spacing, d (Å)	Relative Intensity (%)
111	2.34	25	2.35	35
200	2.03	100	2.25 2.03	2 100
220	1.43	30	1.44	20
311	1.22	10	1.22	78
222	1.17	1	1.17	2
400	1.01	4	1.01	5
331	0.93	3	0.93	2

LATTICE PARAMETER (Å)		
111	40.5	4.07
200	4.06	4.06
220	4.04	4.07
311	4.05	4.05
222	4.05	4.05
400	4.04	4.04
331	4.05	4.05

MICROSTRESS, $\Delta\theta$	
0.27° (2θ = 78.2°)	0.18° (2θ = 78.0°)
0.18° (2θ = 44.7°)	0.13° (2θ = 44.5°)

METALLOGRAPHIC STUDY

Material Aluminum 6061-T6 Neg.No. None

Specimen TWU 3-36 Neg.Mag. 3X

Etchant None Photo Enlargement None

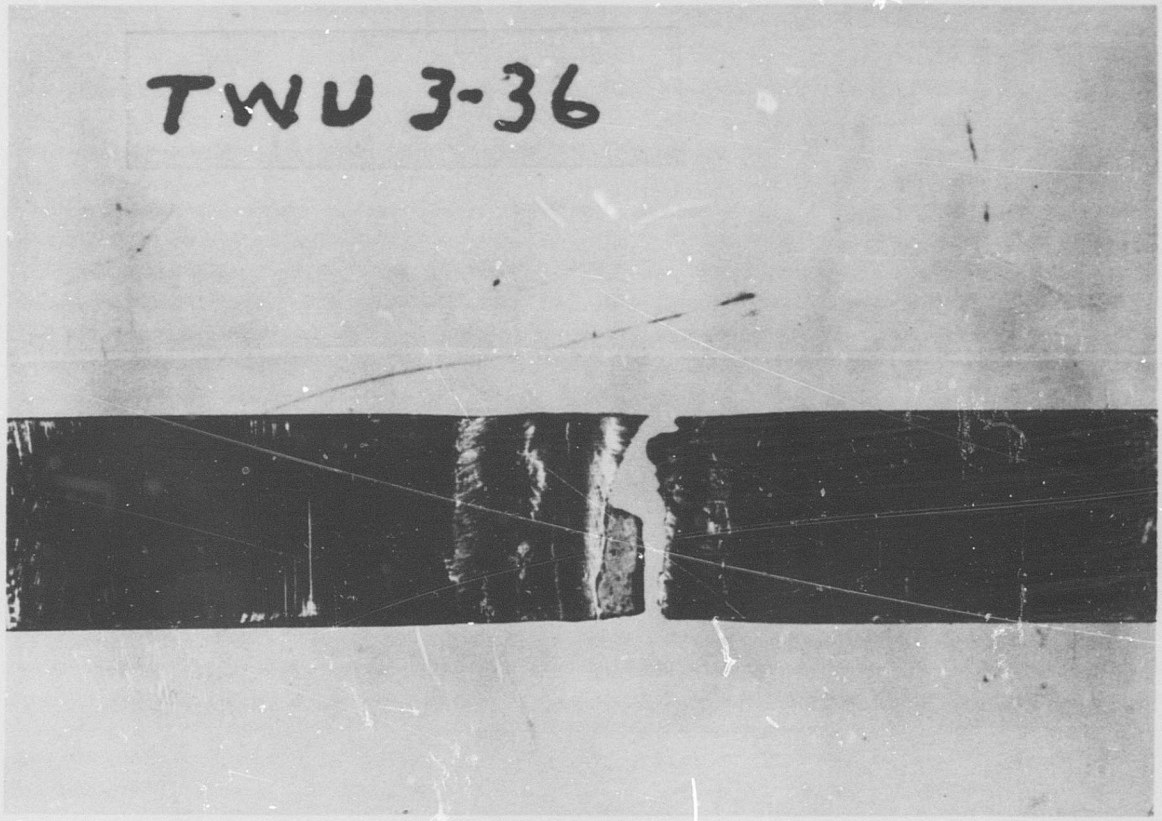

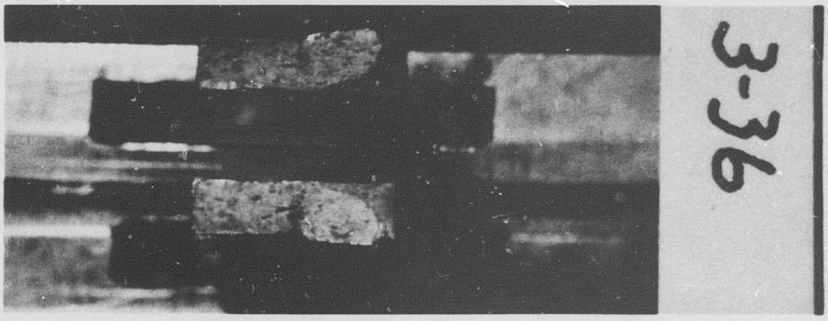

Figure C-45 Aluminum 6061-T6, Condition TW: Macrophotograph Showing 3X Magnification of Specimen

METALLOGRAPHIC STUDY

Material	Aluminum 6061-T6	Neg.No.	W19
Specimen	TWU 3-36	Neg.Mag.	100X
Etchant	Keller's	Photo Enlargement	None

COMMENTS

The microstructure shows the aluminum matrix with inclusions and Al-Si eutectic.

Figure C-46 Aluminum 6061-T6, Condition TW: Optical Micrograph Showing 100X Magnification of Unstrained Area

METALLOGRAPHIC STUDY

Material Aluminum 6061-T6 Neg.No. None

Specimen TWU 3-36 Neg.Mag. 3X

Etchant None Photo Enlargement None

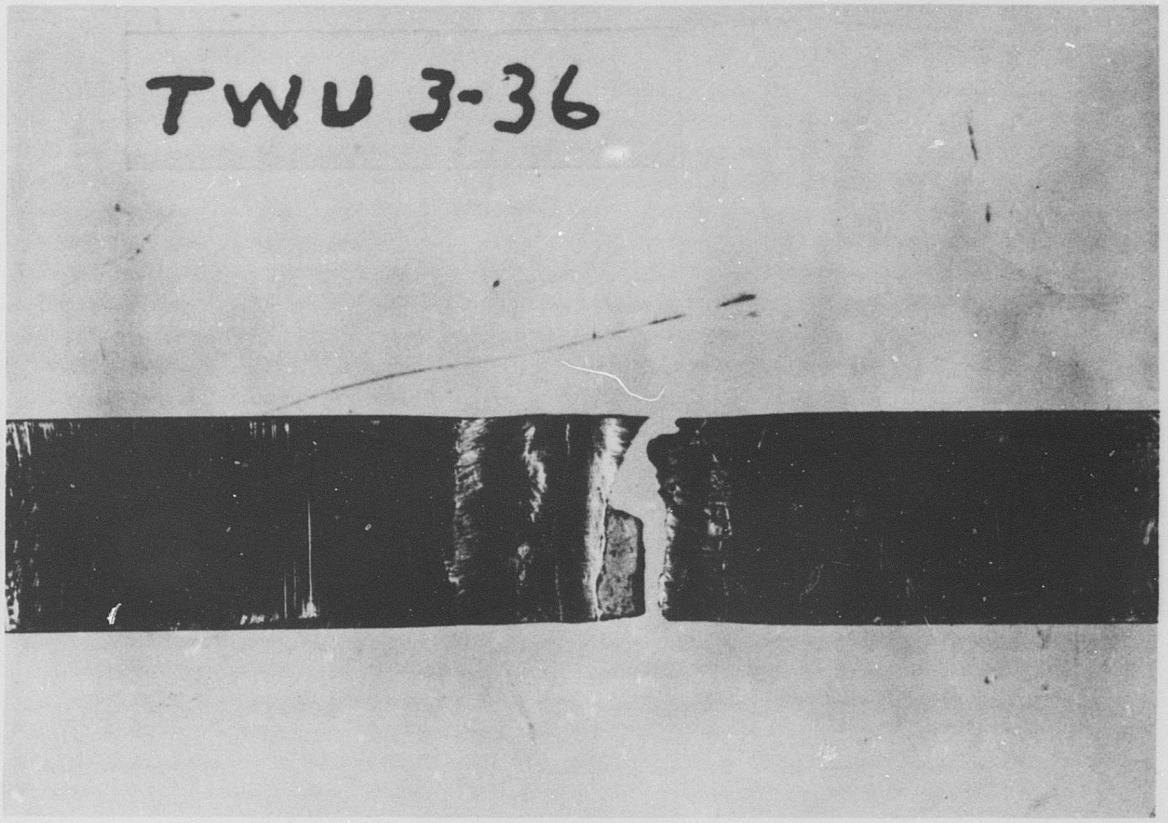

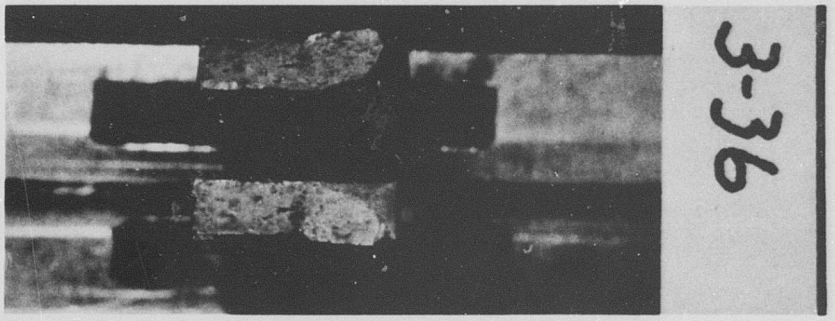

Figure C-45 Aluminum 6061-T6, Condition TW: Macrophotograph Showing 3X Magnification of Specimen

METALLOGRAPHIC STUDY

Material	Aluminum 6061-T6	Neg.No.	W19
Specimen	TWU 3-36	Neg.Mag.	100X
Etchant	Keller's	Photo Enlargement	None

COMMENTS

The microstructure shows the aluminum matrix with inclusions and Al-Si eutectic.

Figure C-46 Aluminum 6061-T6, Condition TW: Optical Micrograph Showing 100X Magnification of Unstrained Area

METALLOGRAPHIC STUDY

Material Aluminum 6061-T6 Neg.No. W29

Specimen TWU 3-36 Neg.Mag. 1,000X

Etchant Keller's Photo Enlargement None

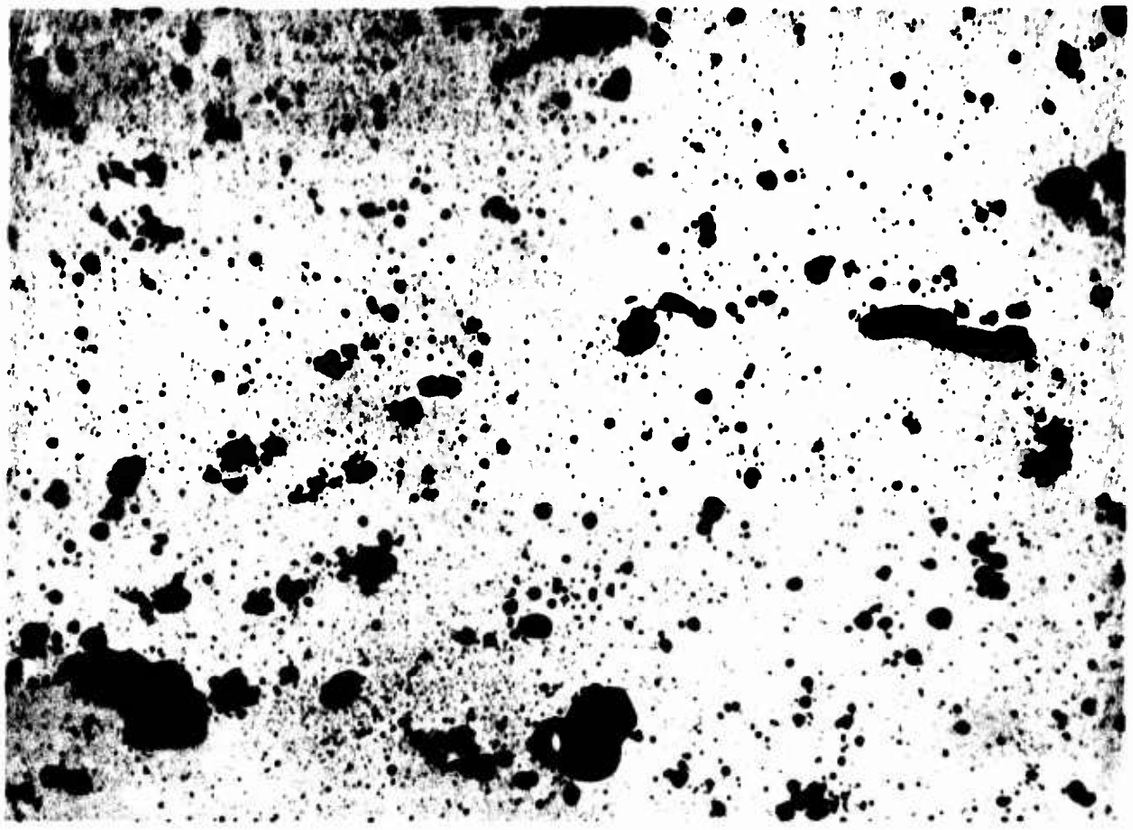

COMMENTS

The microstructure shows the aluminum matrix containing inclusions and Al-Si eutectic.

Figure C-47 Aluminum 6061-T6, Condition TW: Optical Micrograph Showing 1,000X Magnification of Unstrained Area

METALLOGRAPHIC STUDY

Material Aluminum 6061-T6 Neg.No. W50

Specimen TWU 3-36 Neg.Mag. 100X

Etchant Keller's Photo Enlargement None

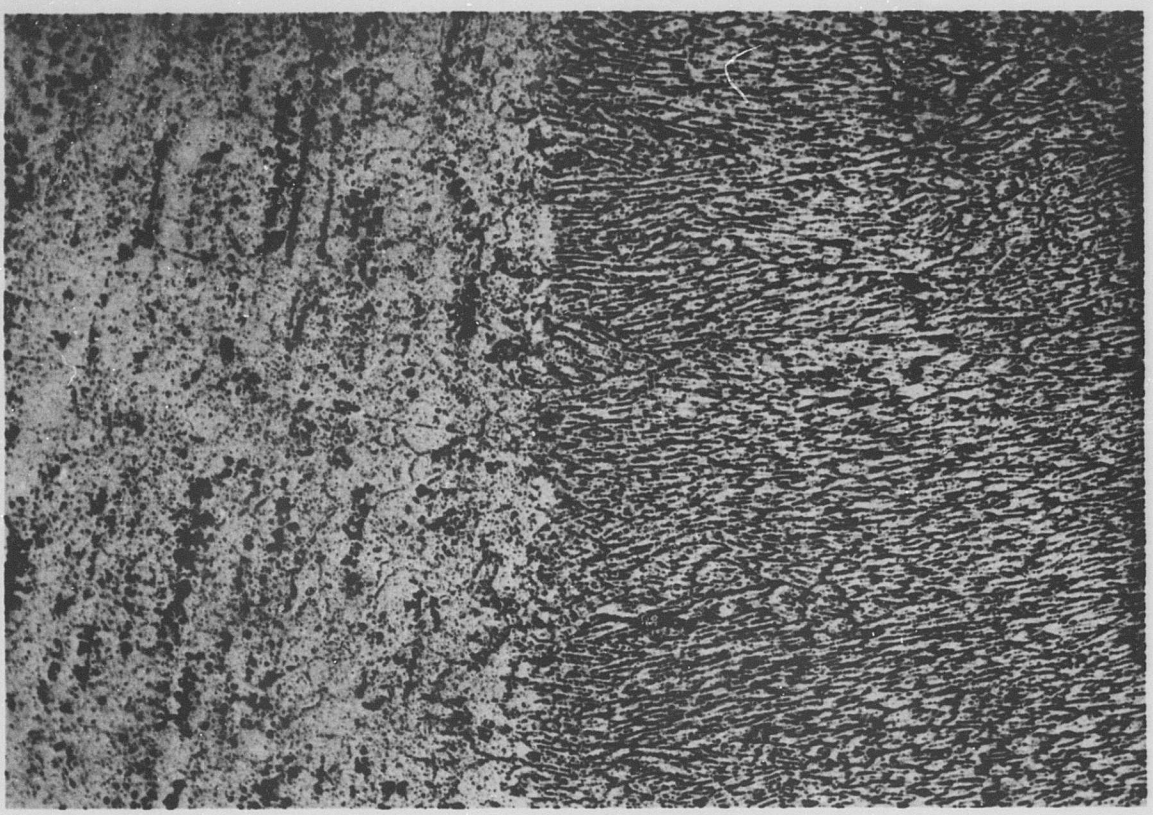

COMMENTS

The microstructure shows, on the left, the aluminum matrix, eutectic, and inclusions and, on the right, the columnar structure of the weld metal. The grain boundaries are accentuated in the heat-affected zone of the matrix.

Figure C-48 Aluminum 6061-T6, Condition TW: Optical Micrograph Showing 100X Magnification of Parent Metal and Weld Interface

METALLOGRAPHIC STUDY

Material Aluminum 6061-T6 Neg.No. W49

Specimen TWU 3-36 Neg.Mag. 1,000X

Etchant Keller's Photo Enlargement None

COMMENTS

The microstructure of the parent metal/weld interface shows the aluminum matrix with inclusions and eutectic.

Figure C-49 Aluminum 6061-T6, Condition TW: Optical Micrograph Showing 1,000X Magnification of Parent Metal and Weld Interface

METALLOGRAPHIC STUDY

Material	Aluminum 6061-T6	Neg.No.	W51
Specimen	TWU 3-36	Neg.Mag.	100X
Etchant	Keller's	Photo Enlargement	None

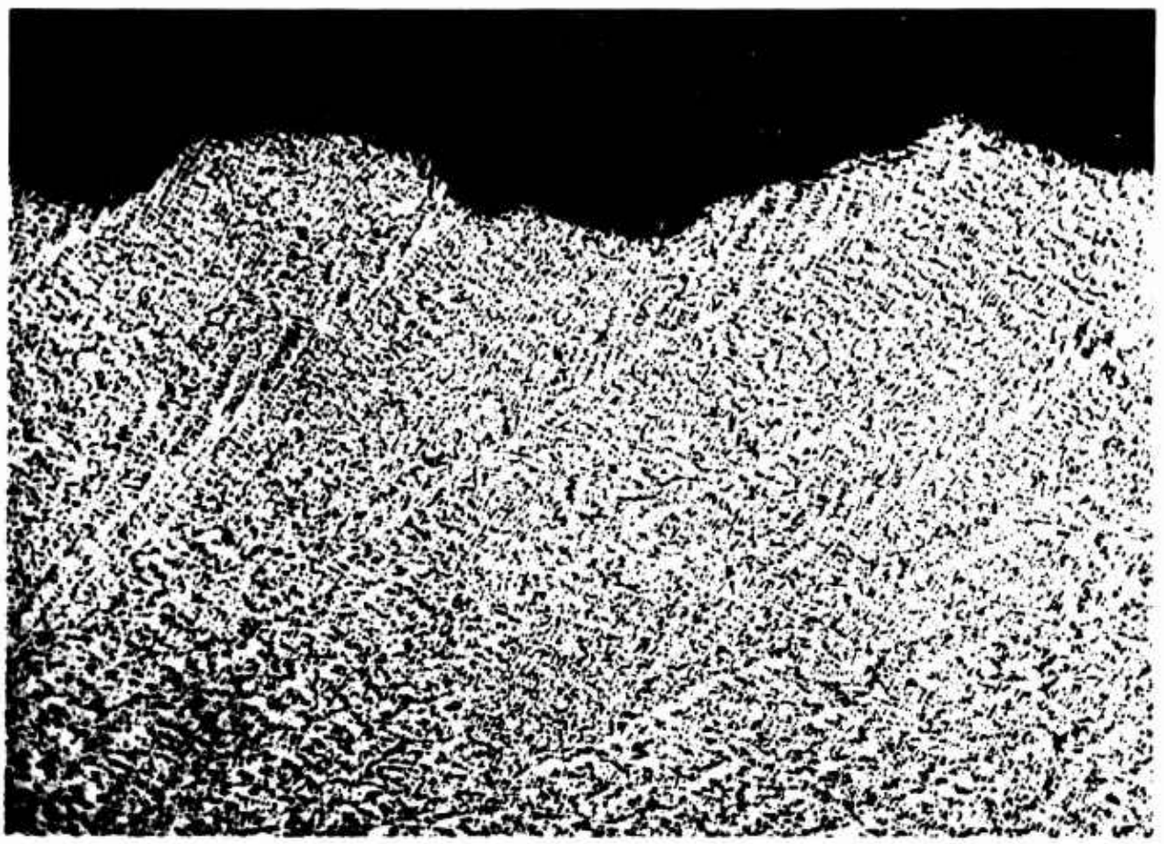

COMMENTS

The microstructure of the fracture edge shows the dendritic aluminum matrix with eutectic. The fracture was transgranular and through the weld.

Figure C-50 Aluminum 6061-T6, Condition TW: Optical Micrograph Showing 100X Magnification of Fracture Edge

METALLOGRAPHIC STUDY

Material Aluminum 6061-T6 Neg.No. W48

Specimen TWU 3-36 Neg.Mag. 1,000X

Etchant Keller's Photo Enlargement None

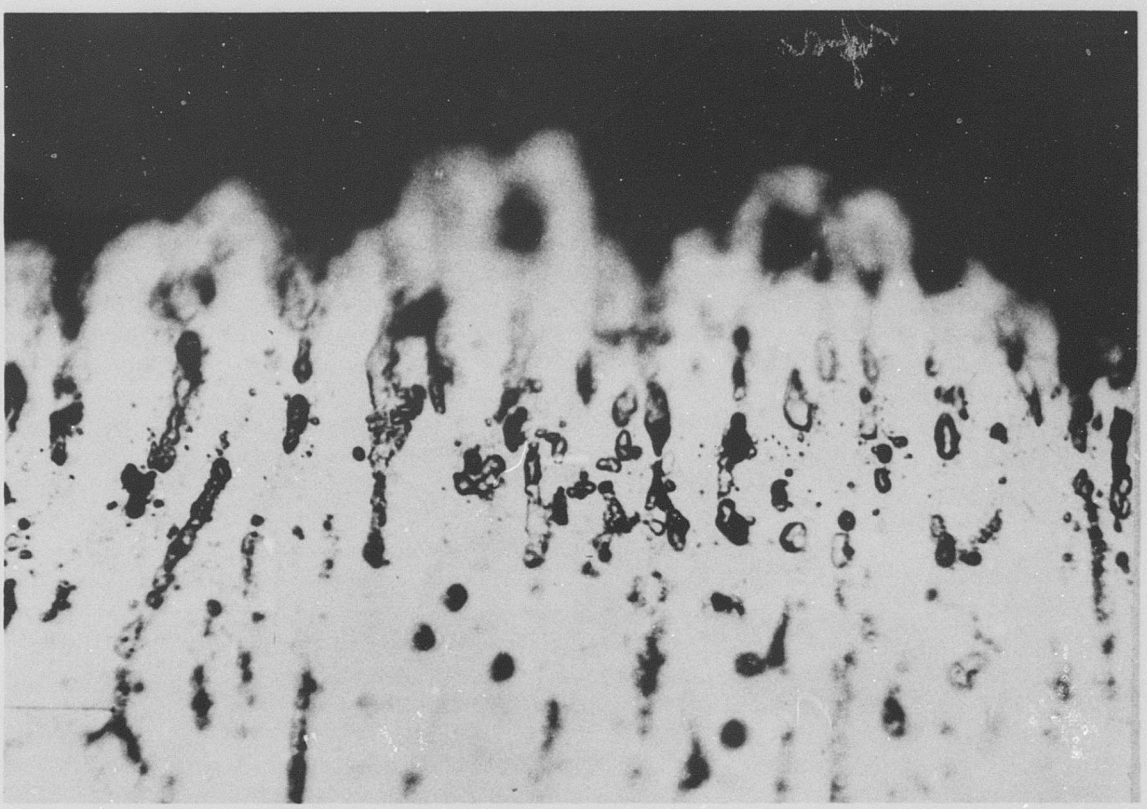

COMMENTS

The microstructure of the fracture edge shows the aluminum matrix with eutectic. The fracture was transgranular and through the weld.

Figure C-51 Aluminum 6061-T6, Condition TW: Optical Micrograph Showing 1,000X Magnification of Fracture Edge

METALLOGRAPHIC STUDY

Material Aluminum 6061-T6 Neg.No. 102-3

Specimen TWU 3-36 Neg.Mag. 7,500X

Etchant Keller's Photo Enlargement 2X

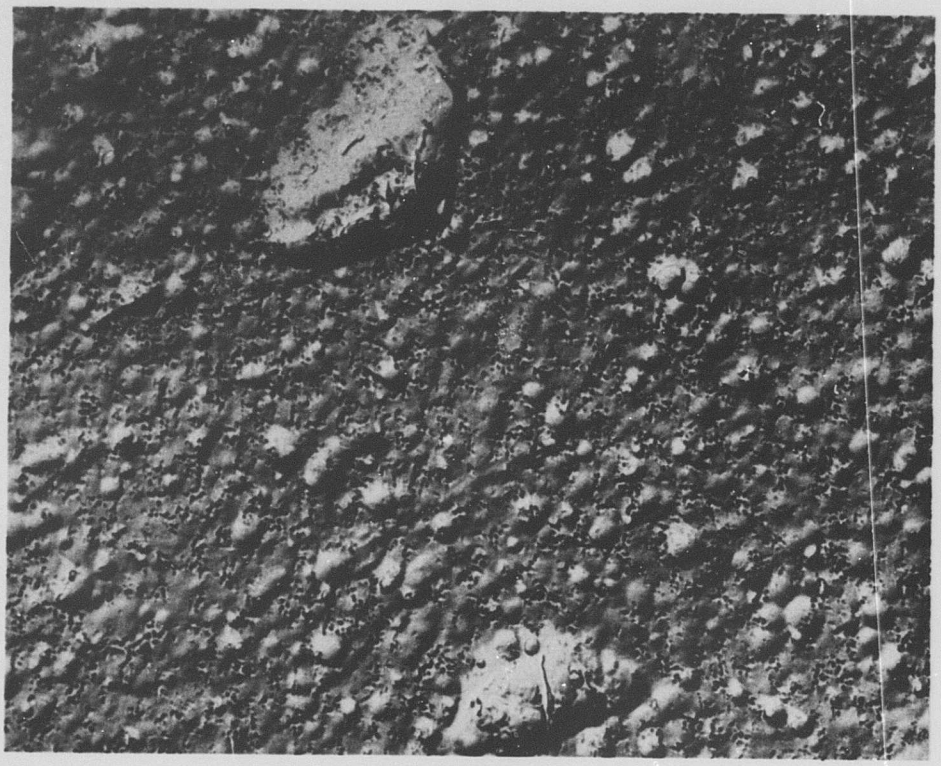

COMMENTS

The electron micrograph of an unstrained area shows the general structure of a solid-solution aluminum matrix with insolubles.

Figure C-52 Aluminum 6061-T6, Condition TW: Electron Micrograph Showing 15,000X Magnification of Unstrained Area

METALLOGRAPHIC STUDY

Material	Aluminum 6061-T6	Neg.No.	102-1
Specimen	TWU 3-36	Neg.Mag.	7,500X
Etchant	Keller's	Photo Enlargement	2X

COMMENTS

The electron micrograph of the weld area shows a matrix of solid-solution aluminum, eutectic in the grain boundary, and insolubles.

Figure C-53. Aluminum 6061-T6, Condition TW: Electron Micrograph Showing 15,000X Magnification of Strained Area

METALLOGRAPHIC STUDY

Material Aluminum 6061-T6 Neg.No. 96-1

Specimen TWU 3-36 Neg.Mag. 2,100X

Etchant None Photo Enlargement 2X

COMMENTS

The fracture surface at the center of the specimen is characterized by the brittle fracture at the eutectic and the failure at the eutectic/matrix interface. Note the directional effect.

Figure C-54 Aluminum 6061-T6, Condition TW: Electron Fractograph Showing 4,200X Magnification at Center of Fracture

METALLOGRAPHIC STUDY

Material Aluminum 6061-T6 Neg.No. 96-3

Specimen TWU 3-36 Neg.Mag. 2,100X

Etchant None Photo Enlargement 2X

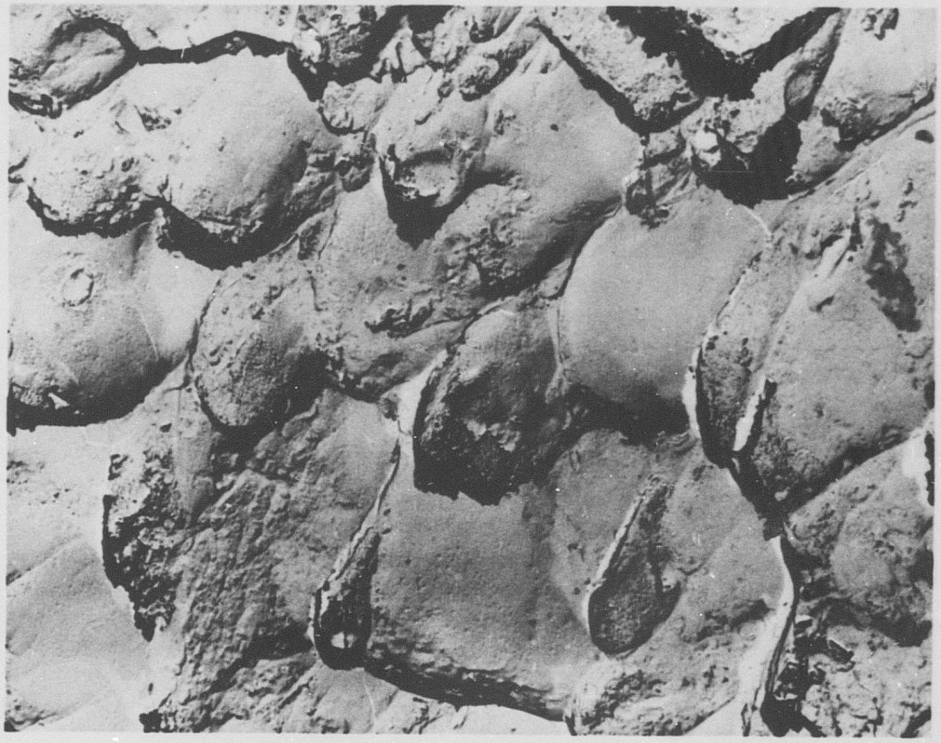

COMMENTS

The surface near the edge of the fracture shows an oriented dimple rupture. There is evidence of failure through and around the eutectic. The surface condition is thought to be oxidation.

Figure C-55 Aluminum 6061-T6, Condition TW: Electron Fractograph Showing 4,200X Magnification Near Edge of Fracture

METALLOGRAPHIC STUDY

Material	Aluminum 6061-T6	**Neg.No.**	99-2
Specimen	TWN 3-46	**Neg.Mag.**	2,100X
Etchant	None	**Photo Enlargement**	2X

COMMENTS

The notched specimen fracture surface shows a dimple rupture with eutectic at the origins of the voids. In some areas the fracture appears to follow the eutectic/matrix interface.

Figure C-56 Aluminum 6061-T6, Condition TW: Electron Fractograph Showing 4,200X Magnification of Notched Fracture

Aluminum 6061-T6
Condition LW
(As welded)

BLANK PAGE

Table C-9
Tensile and Shear Test Data

Material Aluminum 6061-T6 Specimen Condition LW (as welded)

Averaged Data (-423°F)		
Unnotched Specimens	Control	Irradiated
Ultimate Strength (ksi)	61.5	44.1
0.2% Yield Strength (ksi)	34.3	34.4
Elongation in Gage Length (%)	13.76	3.4
Reduction in Area (%)	23.7	3.7
Ultimate Shear Strength (ksi)		
Notched Specimens		
Ultimate Strength (ksi)	42.1	41.1
Ratios		
Notched-Ult./Unnotched-Ult.	0.68	0.93
Notched-Ult./Unnotched-Yield	1.23	1.19

Unnotched Specimens				
Specimen Number	Ult. Tensile Strength(ksi)	Yield Strength 0.2% Offset (ksi)	Reduction in Area (%)	Elongation (%)
724	43.1	35.2	5.1	3.2
725	47.2	31.0	4.9	4.1
726	38.2	35.7	2.0	1.4
760	47.9	35.5	2.9	4.9

Notched Specimens		Shear Specimens*	
Specimen Number	Ult. Tensile Strength (ksi)	Specimen Number	Ult. Shear Strength (ksi)
727	35.2		
728	42.3		
3-114	45.6		

*Not Applicable

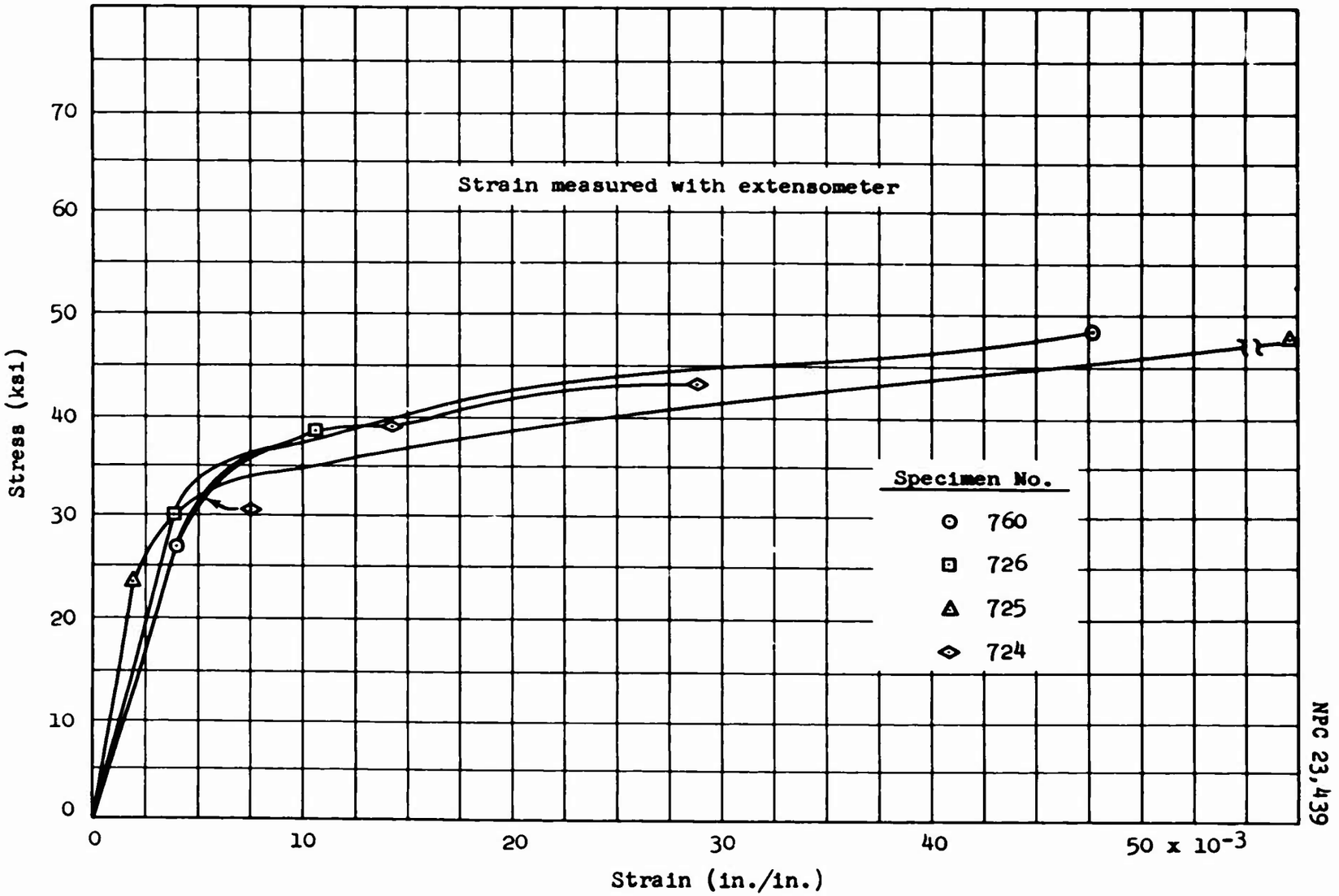

Figure C-57 Aluminum 6061-T6, Condition LWU (as welded): Stress-Strain Curves

Table C-10
X-Ray Diffraction Data

Material Aluminum 6061-T6 Specimen LWU 726

	STRAINED AREA		UNSTRAINED AREA	
DIFFRACTION PATTERN				
Miller Indices (hkl)	Interlattice Spacing, d (Å)	Relative Intensity (%)	Interlattice Spacing, d (Å)	Relative Intensity (%)
111	2.34	30	2.34	50
200	2.03	100	2.03	100
220	1.43	8	1.43	35
311	1.22	10	1.22	18
222	1.17	3	1.17	2
400	1.01	7	1.01	6
331	0.93	3	0.93	6

LATTICE PARAMETER (Å)		
111	4.05	4.05
200	4.06	4.06
220	4.04	4.04
311	4.05	4.05
222	4.05	4.05
400	4.04	4.04
331	4.05	4.05

MICROSTRESS, $\Delta\theta$	
0.21° (2θ = 78.15°)	0.23° (2θ = 78.1°)
0.15° (2θ = 44.7°)	0.17° (2θ = 44.6°)

METALLOGRAPHIC STUDY

Material Aluminum 6061-T6 Neg.No. None

Specimen LWU 726 Neg.Mag. 3X

Etchant None Photo Enlargement None

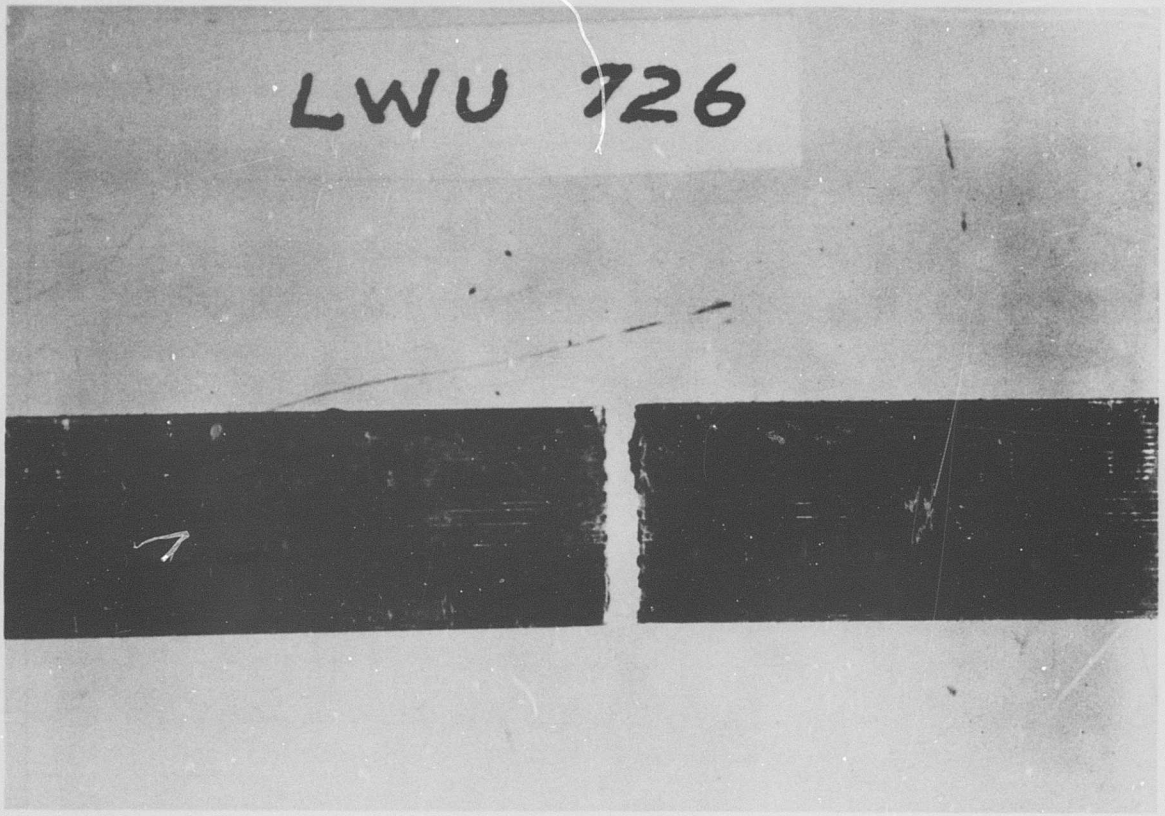

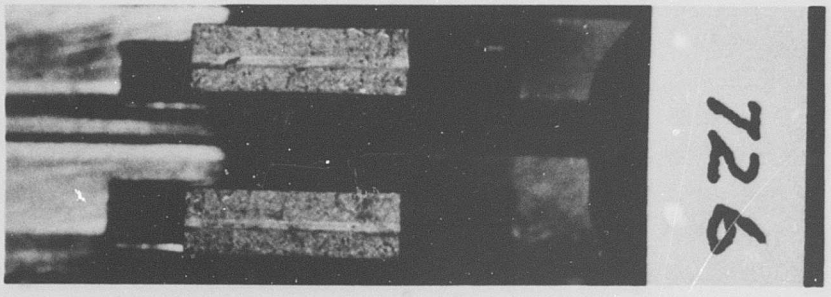

Figure C-58 Aluminum 6061-T6, Condition LW (as welded): Macrophotograph Showing 3X Magnification of Specimen

METALLOGRAPHIC STUDY

Material Aluminum 6061-T6 Neg.No. W31

Specimen LWU 726 Neg.Mag. 100X

Etchant Keller's Photo Enlargement None

COMMENTS

The microstructure shows a solid-solution aluminum matrix, Al-Si eutectic, and insolubles.

Figure C-59 Aluminum 6061-T6, Condition LW (as welded): Optical Micrograph Showing 100X Magnification of Unstrained Area

METALLOGRAPHIC STUDY

Material	Aluminum 6061-T6	Neg.No.	W26
Specimen	LWU 726	Neg.Mag.	1,000X
Etchant	Keller's	Photo Enlargement	None

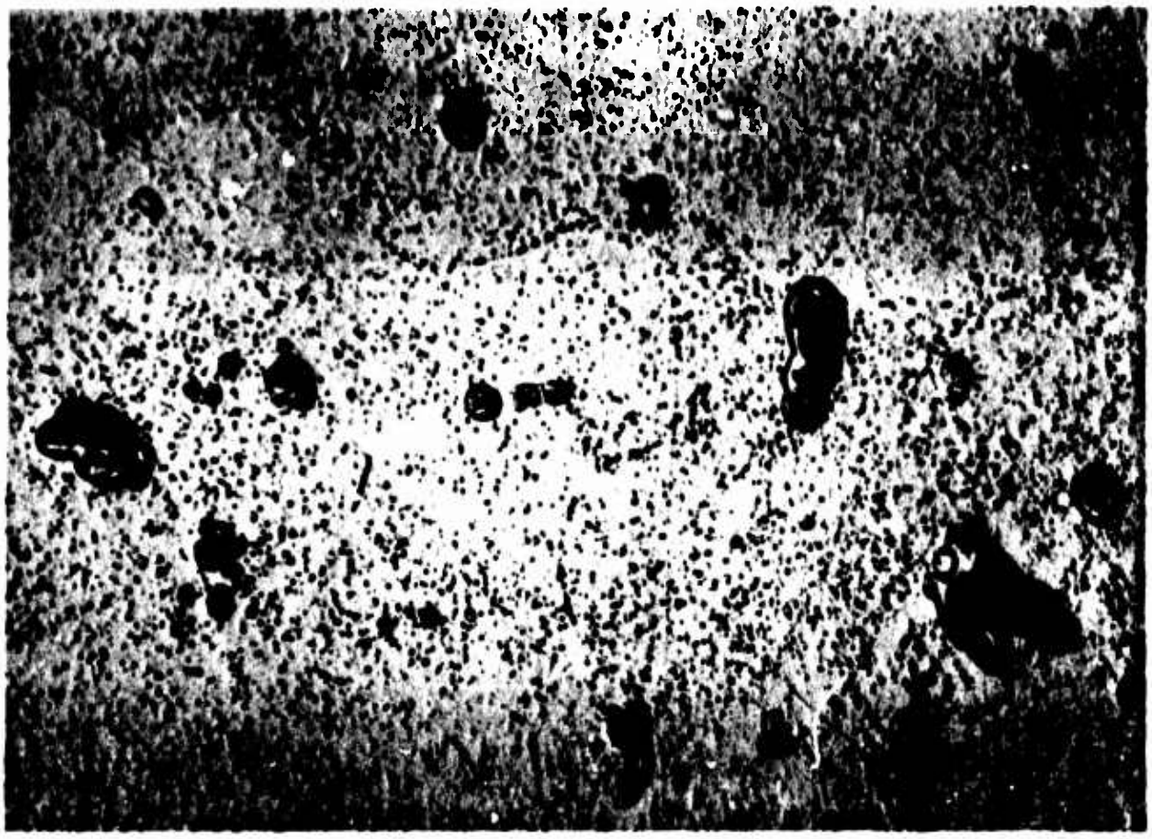

COMMENTS

The microstructure shows the solid-solution aluminum matrix containing the Al-Si eutectic and insolubles.

Figure C-60 Aluminum 6061-T6, Condition LW (as welded): Optical Micrograph Showing 1,000X Magnification of Unstrained Area

METALLOGRAPHIC STUDY

Material Aluminum 6061-T6 Neg.No. W61

Specimen LWU 726 Neg.Mag. 100X

Etchant Keller's Photo Enlargement None

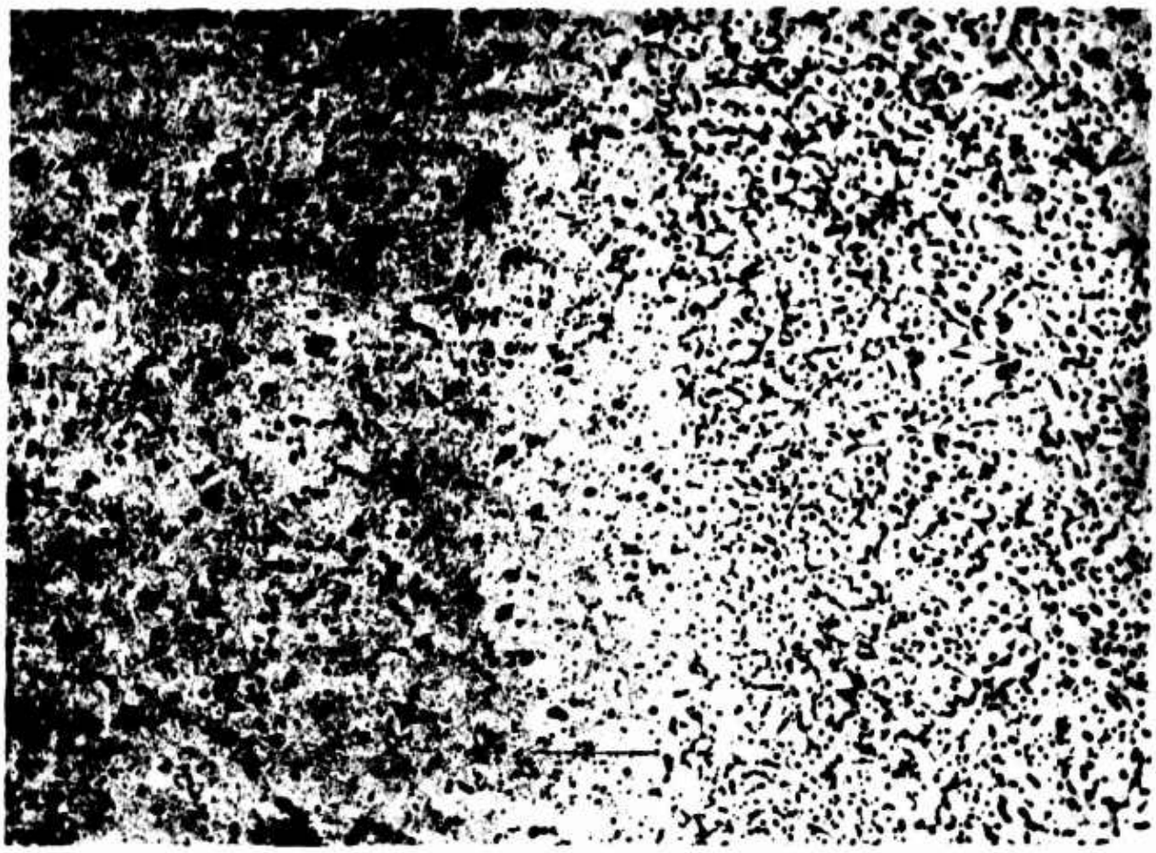

COMMENTS

The microstructure shows the structure of the "as-welded" material, the heat-affected zone, and the base material.

Figure C-61 Aluminum 6061-T6, Condition LW (as welded): Optical Micrograph Showing 100X Magnification of Parent Metal and Weld Interface

METALLOGRAPHIC STUDY

Material Aluminum 6061-T6 Neg.No. W52

Specimen LWU 726 Neg.Mag. 1,000X

Etchant Keller's Photo Enlargement None

COMMENTS

The microstructure shows the solid-solution aluminum matrix, the Al-Si eutectic in the grain boundaries of the weld material, and insoluble particles.

Figure C-62 Aluminum 6061-T6, Condition LW (as welded): Optical Micrograph Showing 1,000X Magnification of Parent Metal and Weld Interface

METALLOGRAPHIC STUDY

Material Aluminum 6061-T6 Neg.No. W60

Specimen LWU 726 Neg.Mag. 100X

Etchant Keller's Photo Enlargement None

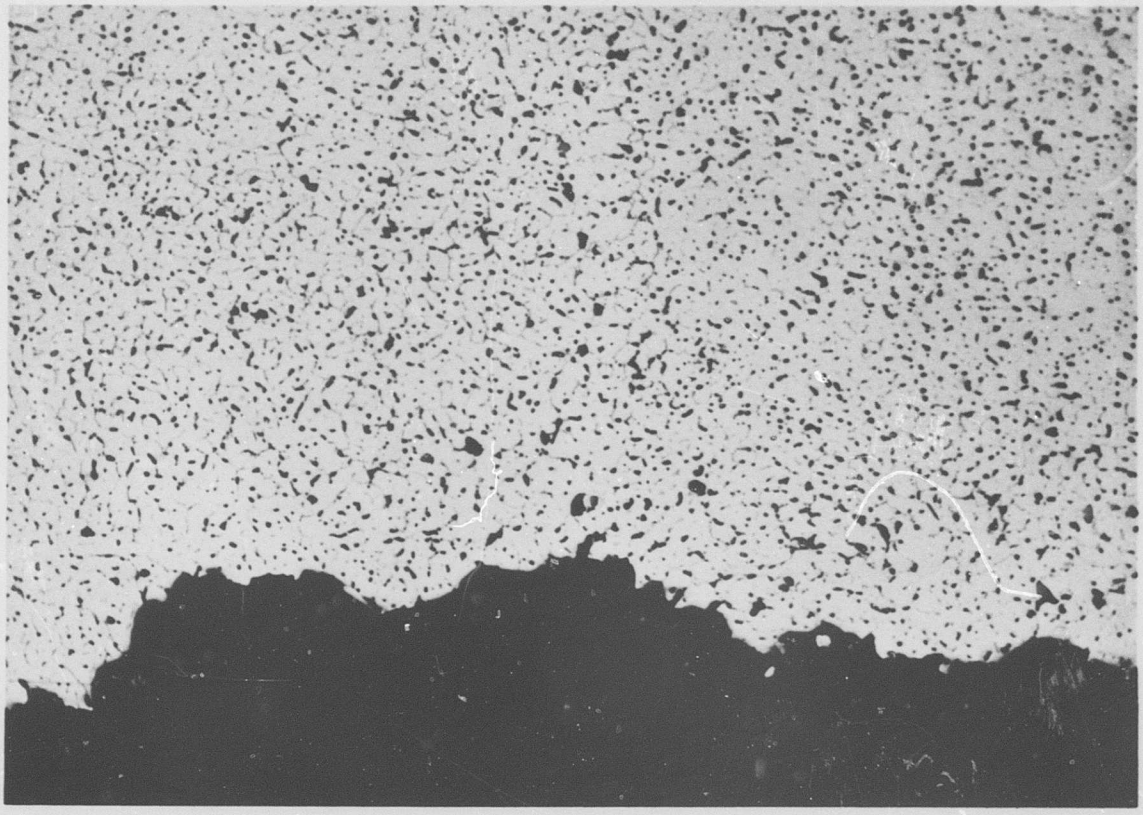

COMMENTS

The microstructure shows the structure of the untreated weld material. The fracture path appears to be partly intergranular and partly transgranular.

Figure C-63 Aluminum 6061-T6, Condition LW (as welded): Optical Micrograph Showing 100X Magnification of Fracture Edge

METALLOGRAPHIC STUDY

Material Aluminum 6061-T6 Neg.No. W53

Specimen LWU 726 Neg.Mag. 1,000X

Etchant Keller's Photo Enlargement None

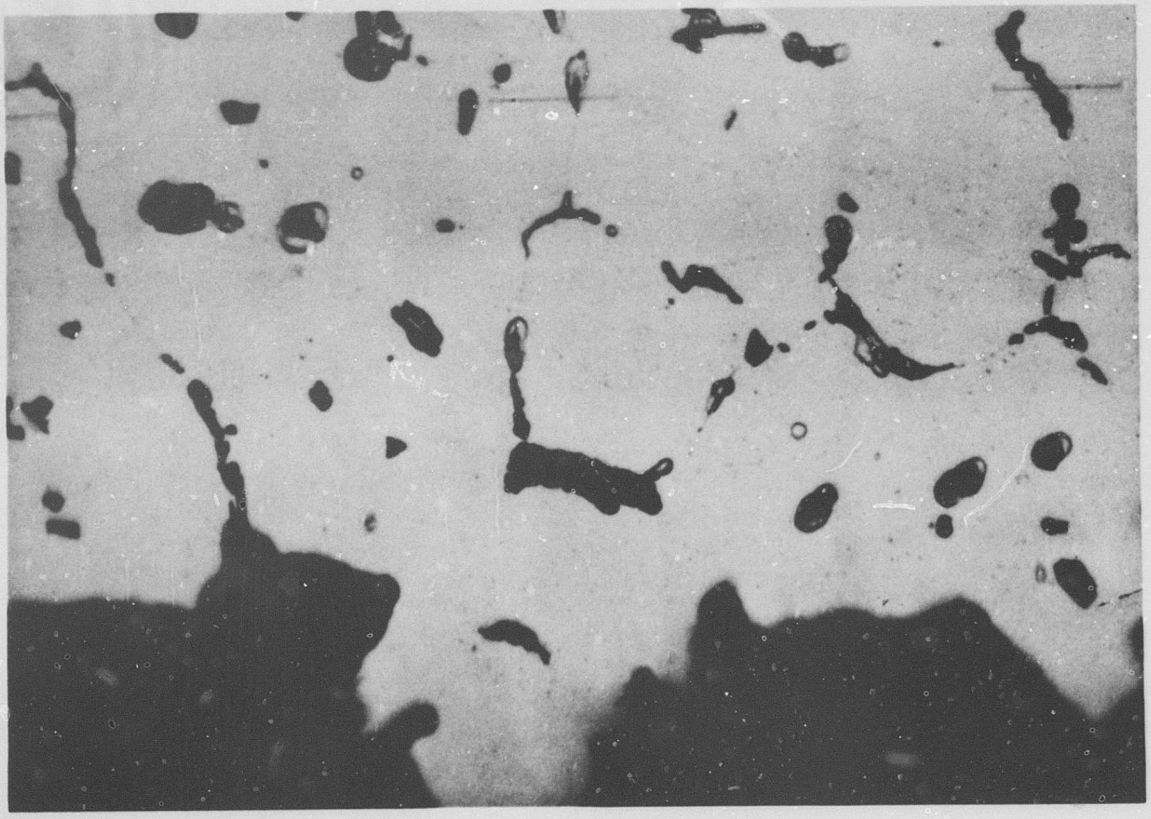

COMMENTS

The microstructure shows the aluminum-matrix, the Al-Si eutectic in the grain boundaries, and insolubles. The fracture edge is not clear, but the fracture path appears to be intergranular and transgranular.

Figure C-64 Aluminum 6061-T6, Condition LW (as welded): Optical Micrograph Showing 1,000X Magnification of Fracture Edge

METALLOGRAPHIC STUDY

Material	Aluminum 6061-T6	Neg.No.	101-10
Specimen	LWU 726	Neg.Mag.	7,500X
Etchant	Keller's	Photo Enlargement	2X

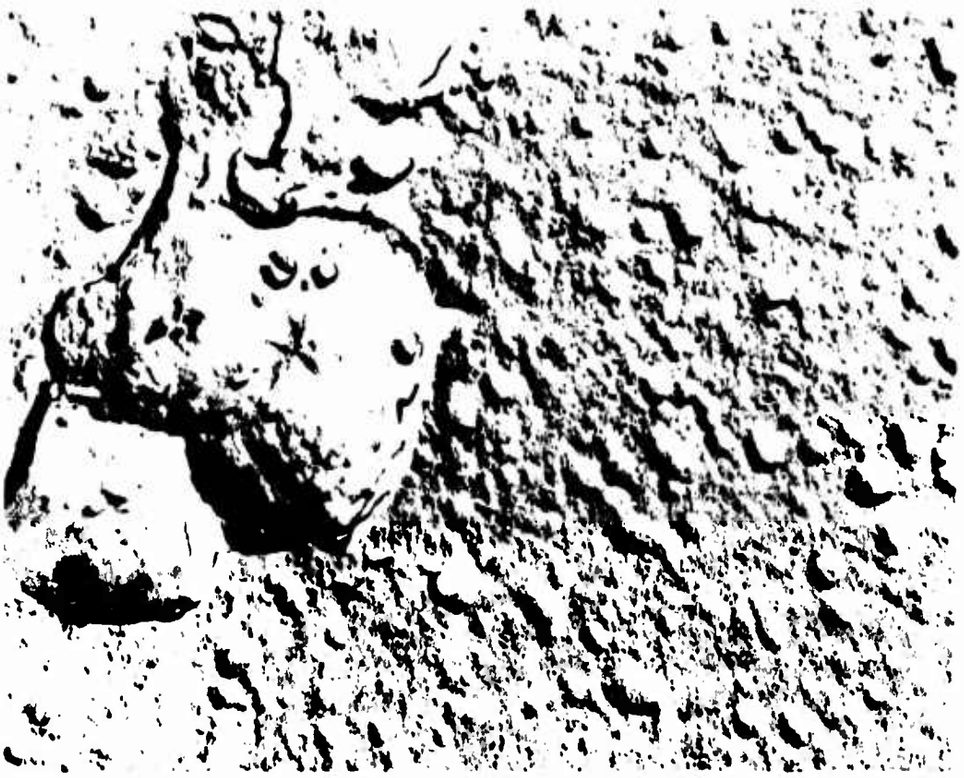

COMMENTS

The microstructure shows the solid-solution aluminum matrix and a large inclusion site.

Figure C-65 Aluminum 6061-T6, Condition LW (as welded): Electron Micrograph Showing 15,000X Magnification of Unstrained Area

METALLOGRAPHIC STUDY

Material	Aluminum 6061-T6	Neg.No.	106-1
Specimen	LWU 726	Neg.Mag.	7,500X
Etchant	Keller's	Photo Enlargement	2X

COMMENTS

The microstructure of the weld area shows the solid-solution aluminum matrix and a grain boundary containing Al-Si eutectic.

Figure C-66 Aluminum 6061-T6, Condition LW (as welded): Electron Micrograph Showing 15,000X Magnification of Strained Area

METALLOGRAPHIC STUDY

Material Aluminum 6061-T6 Neg.No. 94-9

Specimen LWU 726 Neg.Mag. 2,100X

Etchant None Photo Enlargement 2X

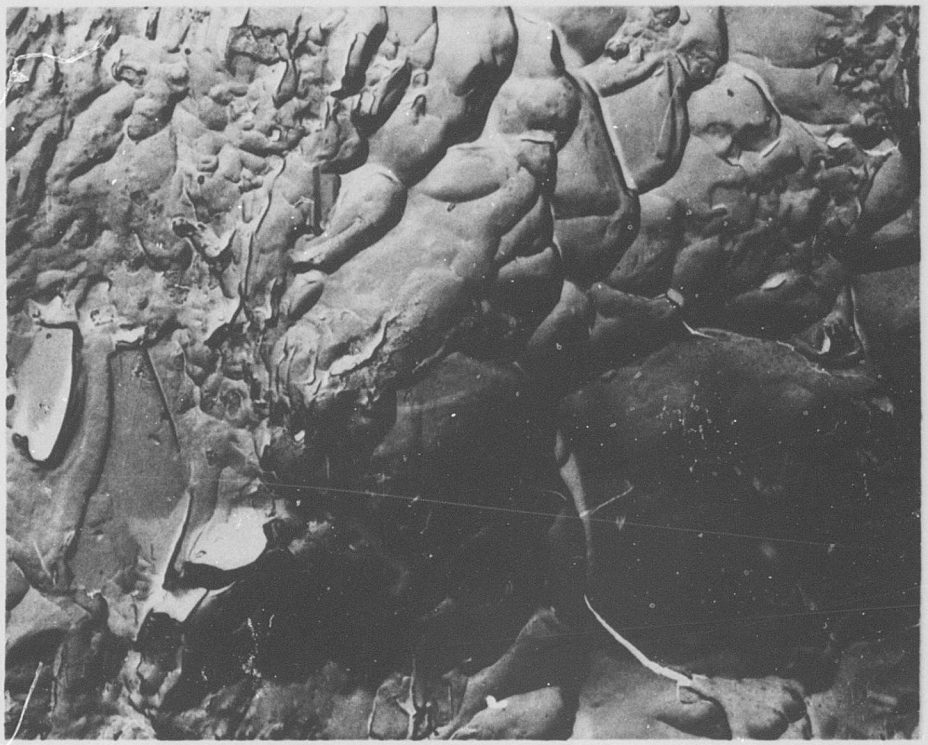

COMMENTS

The fractograph of this area near the center of the specimen shows a dimple rupture. Certain areas show the failure through the brittle eutectic; the fracture was transgranular within this area.

Figure C-67 Aluminum 6061-T6, Condition LW (as welded): Electron Fractograph Showing 4,200X Magnification at Center of Fracture

METALLOGRAPHIC STUDY

Material Aluminum 6061-T6 Neg.No. 94-10

Specimen LWU 726 Neg.Mag. 2,100X

Etchant None Photo Enlargement 2X

COMMENTS

The fracture shown in this photo, taken of an area near the edge, is almost entirely through and around the brittle eutectic phase.

Figure C-68 Aluminum 6061-T6, Condition LW (as welded): Electron Fractograph Showing 4,200X Magnification Near Edge of Fracture

METALLOGRAPHIC STUDY

Material Aluminum 6061-T6 Neg.No. 99-10

Specimen LWN 727 Neg.Mag. 2,100X

Etchant None Photo Enlargement 2X

COMMENTS

The fracture of the notched specimen is through and around the brittle eutectic.

Figure C-69 Aluminum 6061-T6, Condition LW (as welded): Electron Fractograph Showing 4,200X Magnification of Notched Fracture

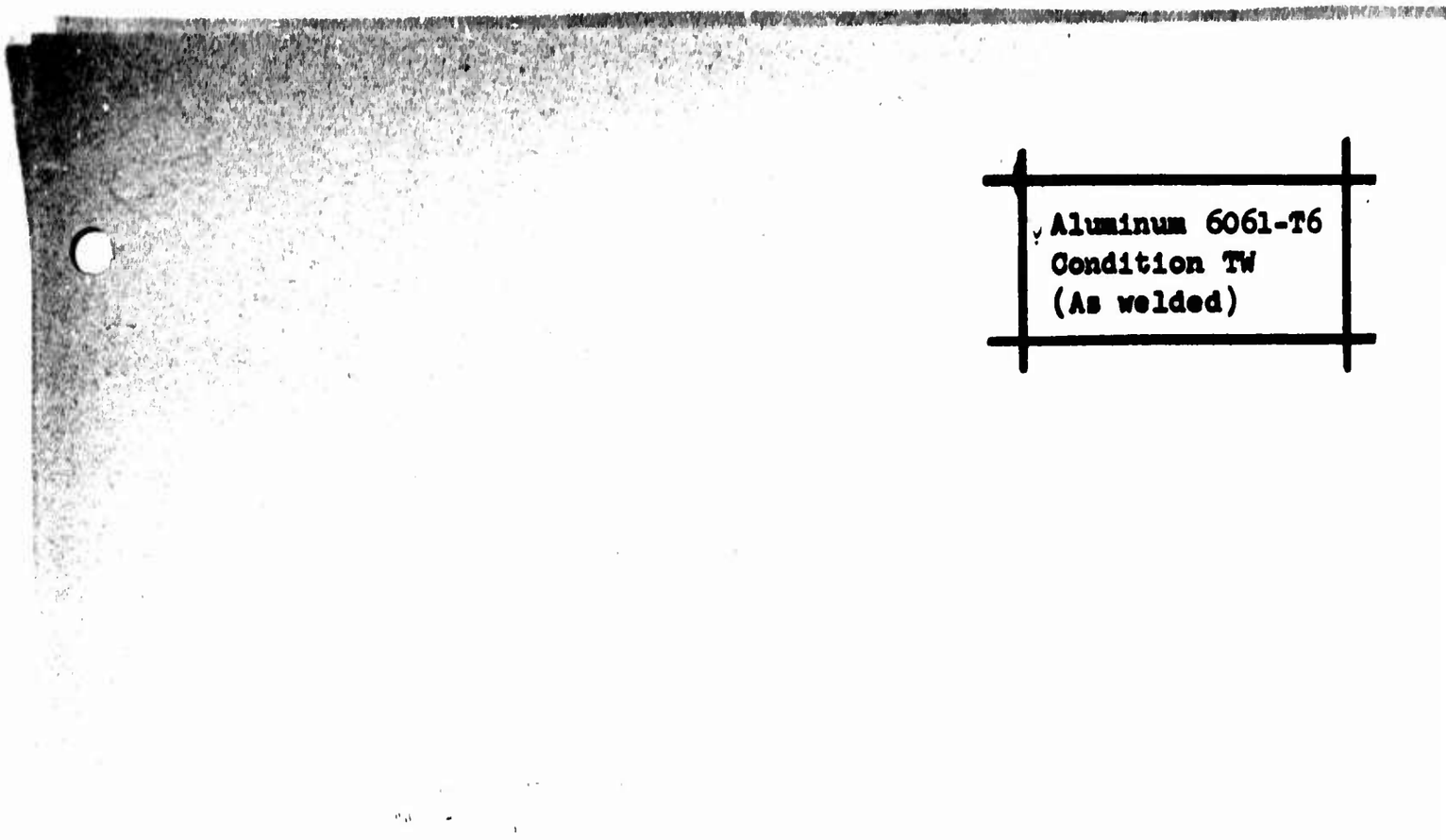
Aluminum 6061-T6
Condition TW
(As welded)

Table C-11
Tensile and Shear Test Data

Material Aluminum 6061-T6 Specimen Condition TW (as welded)

Averaged Data (-423°F)		
Unnotched Specimens	Control	Irradiated
Ultimate Strength (ksi)	54.9	45.8
0.2% Yield Strength (ksi)	34.4	30.6
Elongation in Gage Length (%)	6.8	5.4
Reduction in Area (%)	12.5	5.4
Ultimate Shear Strength (ksi)		
Notched Specimens		
Ultimate Strength (ksi)	31.8	37.9
Ratios		
Notched-Ult./Unnotched-Ult.	0.58	0.83
Notched-Ult./Unnotched-Yield	0,92	1.24

Unnotched Specimens				
Specimen Number	Ult. Tensile Strength(ksi)	Yield Strength 0.2% Offset (ksi)	Reduction in Area (%)	Elongation (%)
717	48.0	34.5	5.2	4.7
718	43.4	29.8	5.2	4.7
719	45.8	28.5	5.5	6.7
720	46.1	29.6	5.6	5.6

Notched Specimens		Shear Specimens*	
Specimen Number	Ult. Tensile Strength (ksi)	Specimen Number	Ult. Shear Strength (ksi)
288	47.5		
721	36.3		
722	32.2		
723	35.9		

*Not Applicable

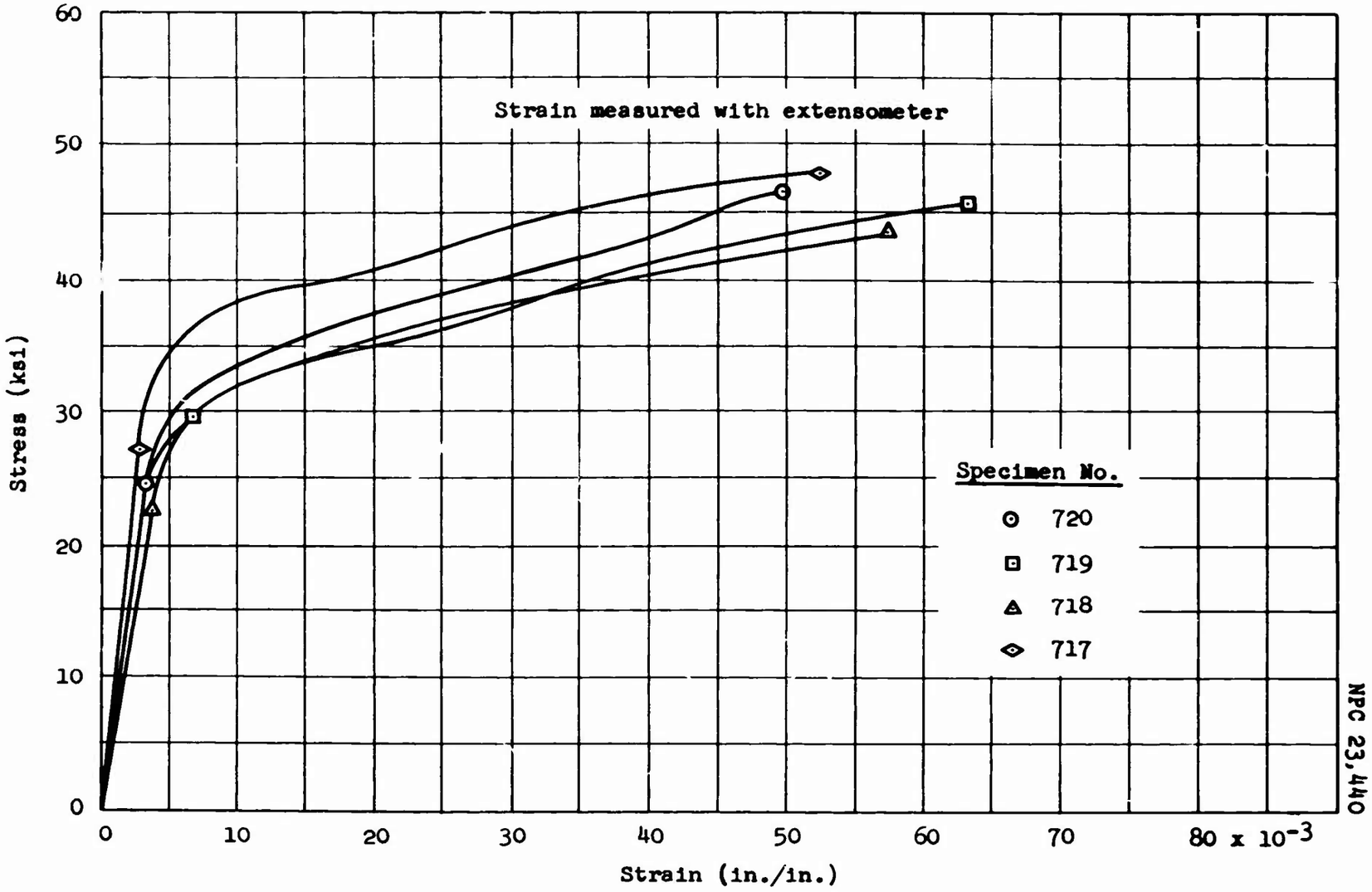

Figure C-70 Aluminum 6061-T6, Condition TWU (as welded): Stress-Strain Curves

Table C-12
X-Ray Diffraction Data

Material Aluminum 6061-T6 Specimen TWU 717

	STRAINED AREA		UNSTRAINED AREA	
DIFFRACTION PATTERN				
Miller Indices (hkl)	Interlattice Spacing, d (Å)	Relative Intensity (%)	Interlattice Spacing, d (Å)	Relative Intensity (%)
111	2.34	20	2.35	65
200	2.03	100	2.03	100
220	1.43	15	1.43	55
311	1.22	10	1.22	30
222			1.17	4
400	1.01	4	1.01	5
331	0.93	3	0.93	6

LATTICE PARAMETER (Å)		
111	4.05	4.07
200	4.06	4.06
220	4.04	4.04
311	4.05	4.05
222	-	4.05
400	4.04	4.04
331	4.05	4.05

MICROSTRESS, $\Delta\theta$	
0.23° (2θ = 78.0°)	0.23° (2θ = 78.05°)
0.16° (2θ = 44.6°)	0.16° (2θ = 44.55°)

METALLOGRAPHIC STUDY

Material Aluminun 6061-T6 Neg.No. None

Specimen TWU 717 Neg.Mag. 3X

Etchant None Photo Enlargement None

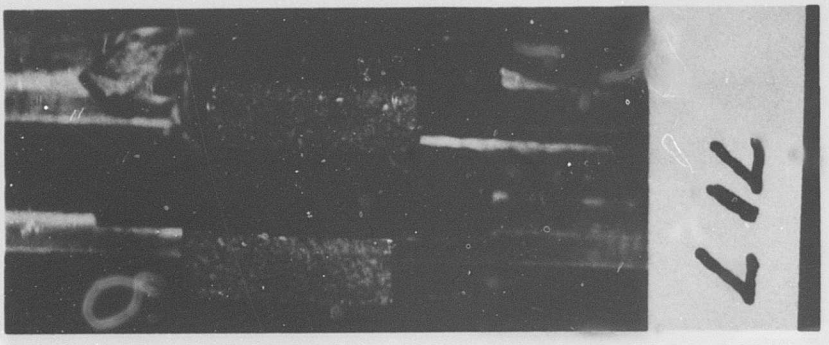

Figure C-71 Aluminum 6061-T6, Condition TW (as welded): Macrophotograph Showing 3X Magnification of Specimen

METALLOGRAPHIC STUDY

Material Aluminum 6061-T6 Neg.No. W16

Specimen TW J 717 Neg.Mag. 100X

Etchant Keller's Photo Enlargement None

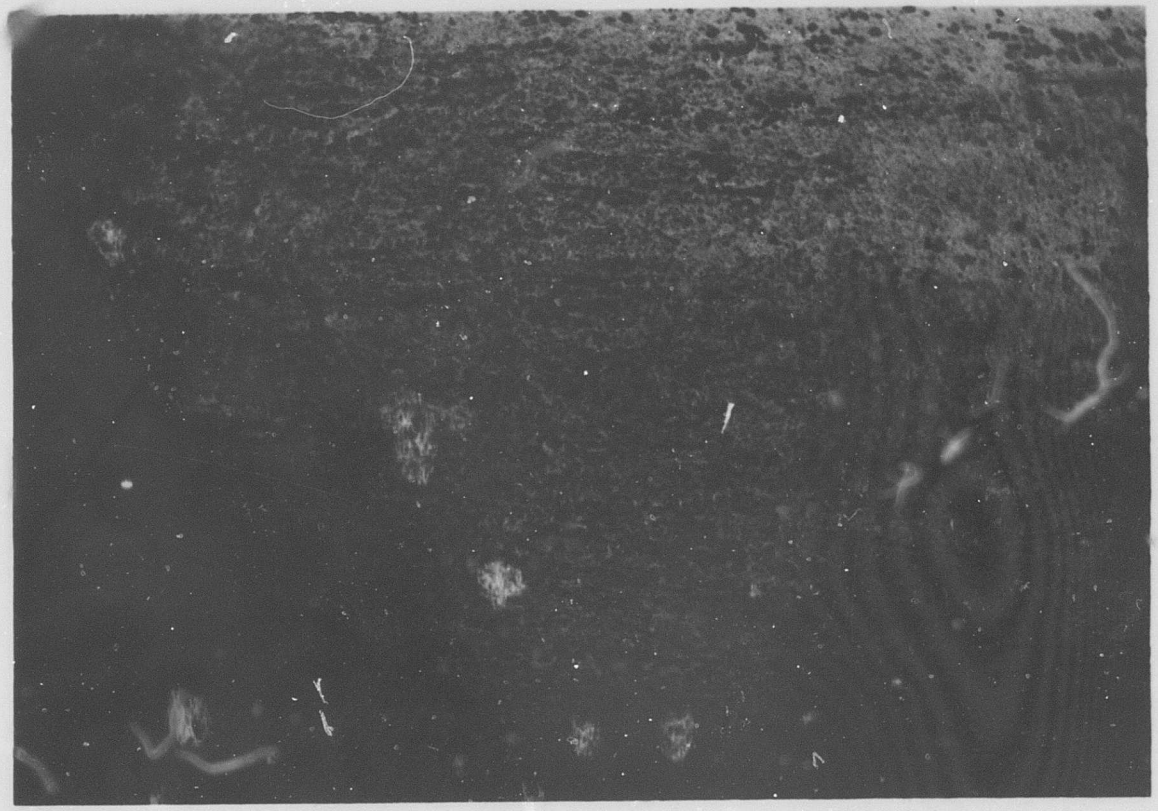

COMMENTS

The microstructure in the unstrained area shows the solid-solution aluminum matrix and insolubles.

Figure C-72 Aluminum 6061-T6, Condition TW (as welded): Optical Micrograph Showing 100X Magnification of Unstrained Area

METALLOGRAPHIC STUDY

Material Aluminum 6061-T6 Neg.No. W23

Specimen TWU 717 Neg.Mag. 1,000X

Etchant Keller's Photo Enlargement None

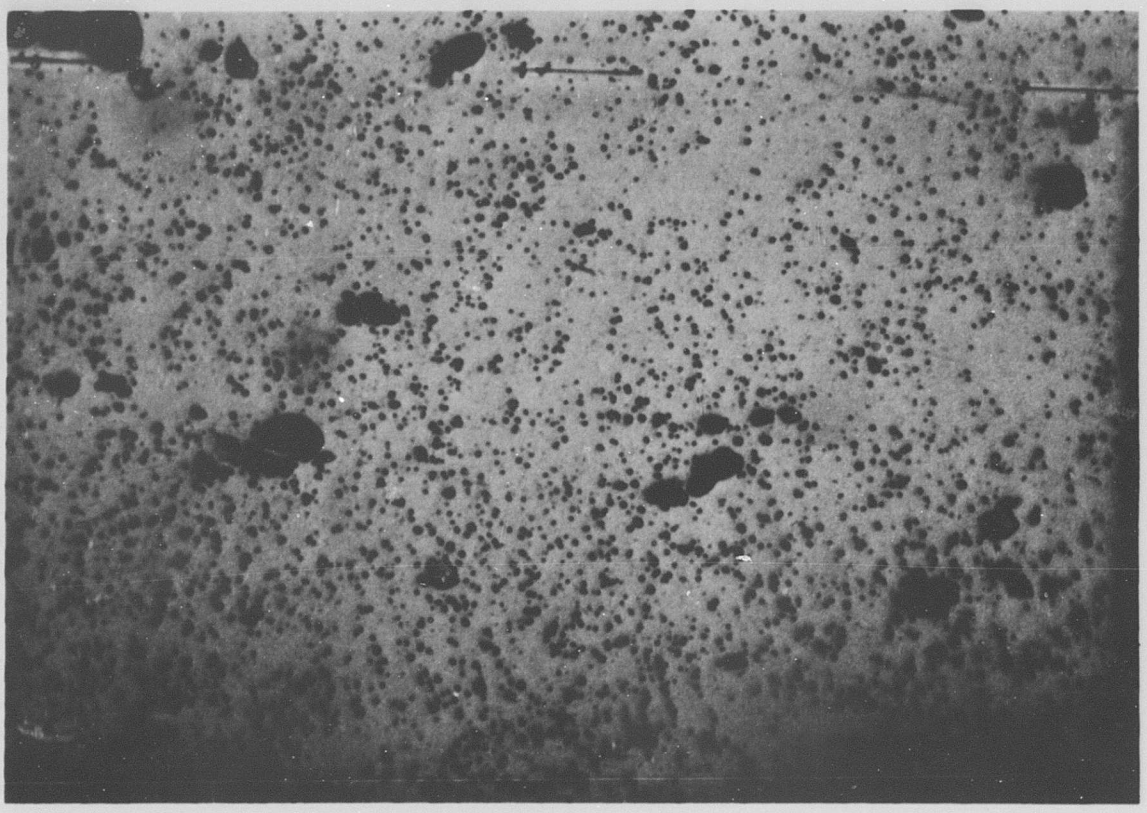

COMMENTS

The microstructure in the unstrained area shows the solid-solution aluminum matrix and insolubles.

Figure C-73 Aluminum 6061-T6, Condition TW (as welded): Optical Micrograph Showing 1,000X Magnification of Unstrained Area

METALLOGRAPHIC STUDY

Material Aluminum 6061-T6 Neg.No. W40

Specimen TWU 717 Neg.Mag. 100X

Etchant Keller's Photo Enlargement None

COMMENTS

The microstructure shows the normal matrix and the cast structure of the weld at the weld/ matrix interface.

Figure C-74 Aluminum 6061-T6, Condition TW (as welded) Optical Micrograph Showing 100X Magnification of Parent Metal and Weld Interface

METALLOGRAPHIC STUDY

Material Aluminum 6061-T6 Neg.No. W44

Specimen TWU 717 Neg.Mag. 1,000X

Etchant Keller's Photo Enlargement None

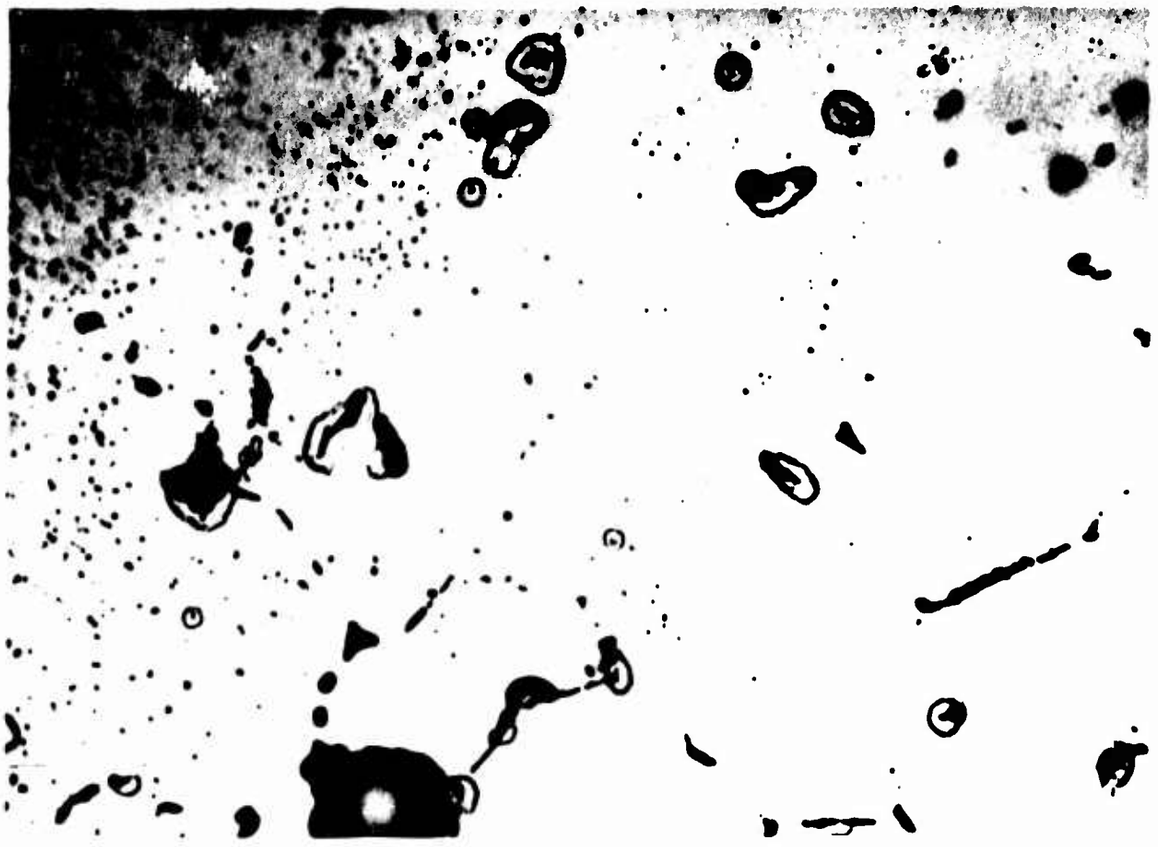

COMMENTS

The microstructure shows the solid-solution aluminum matrix, the weld-metal matrix, and the Al-Si eutectic.

Figure C-75 Aluminum 6061-T6, Condition TW (as welded): Optical Micrograph Showing 1,000X Magnification of Parent Metal and Weld Interface

METALLOGRAPHIC STUDY

Material Aluminum 6061-T6 Neg.No. W41

Specimen TWU 717 Neg.Mag. 100X

Etchant Keller's Photo Enlargement None

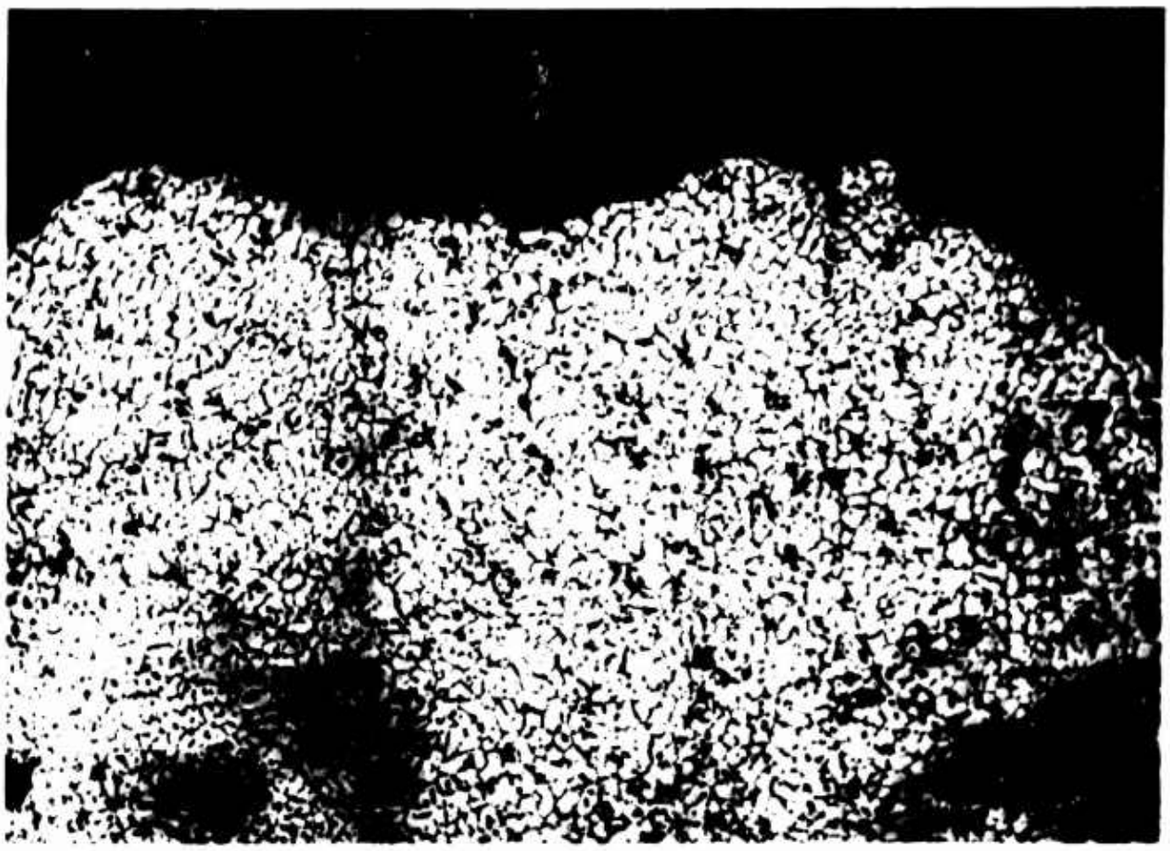

COMMENTS

The fracture profile shows a fracture path that is primarily intergranular through and along the brittle eutectic.

Figure C-76 Aluminum 6061-T6, Condition TW (as welded): Optical Micrograph Showing 100X Magnification of Fracture Edge

METALLOGRAPHIC STUDY

Material Aluminum 6061-T6 Neg.No. W45

Specimen TWU 717 Neg.Mag. 1,000X

Etchant Keller's Photo Enlargement None

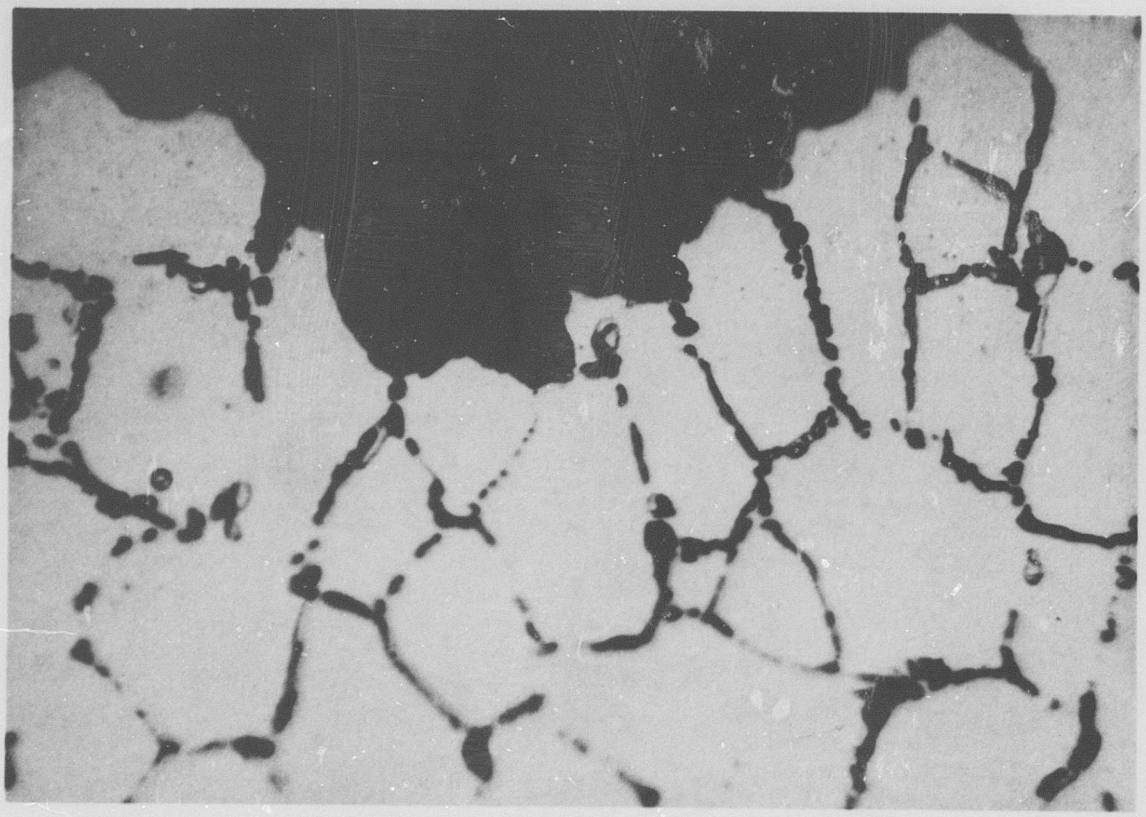

COMMENTS

The fracture profile shows a fracture path that is primarily intergranular through and along the brittle eutectic.

Figure C-77 Aluminum 6061-T6, Condition TW (as welded): Optical Micrograph Showing 1,000X Magnification of Fracture Edge

METALLOGRAPHIC STUDY

Material Aluminum 6061-T6 Neg.No. 101-7

Specimen TWU 717 Neg.Mag. 7,500X

Etchant Keller's Photo Enlargement 2X

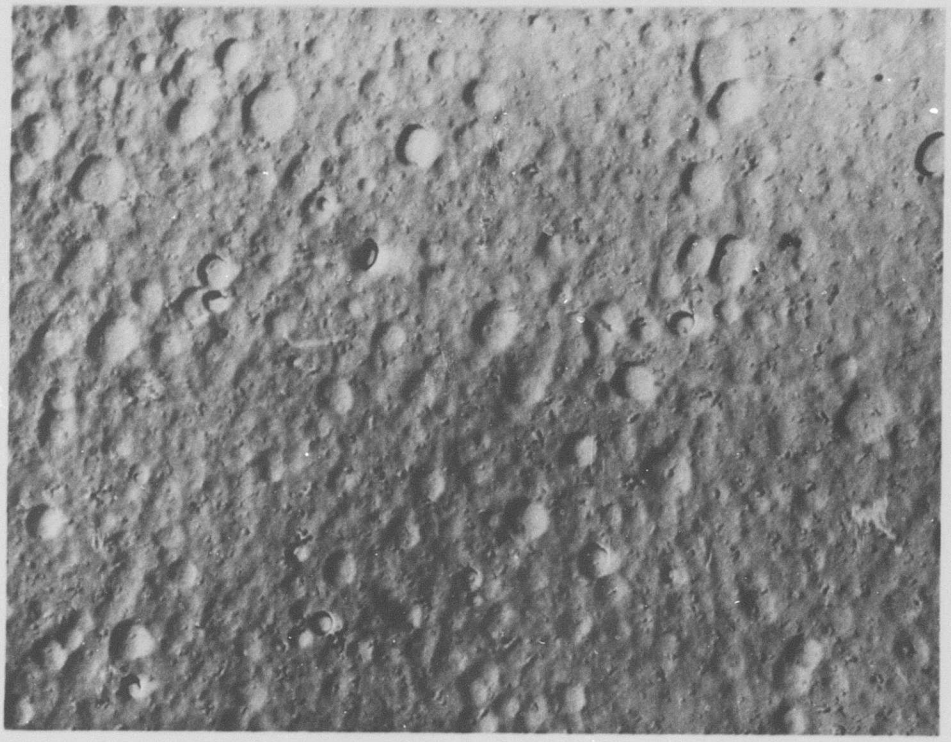

COMMENTS

The electron micrograph shows a typical, unstrained, solid-solution aluminum matrix with insolubles.

Figure C-78 Aluminum 6061-T6, Condition TW (as welded): Electron Micrograph Showing 15,000X Magnification of Unstrained Area

METALLOGRAPHIC STUDY

Material Aluminum 6061-T6 Neg.No. 105-7

Specimen TWU 717 Neg.Mag. 7,500X

Etchant Keller's Photo Enlargement 2X

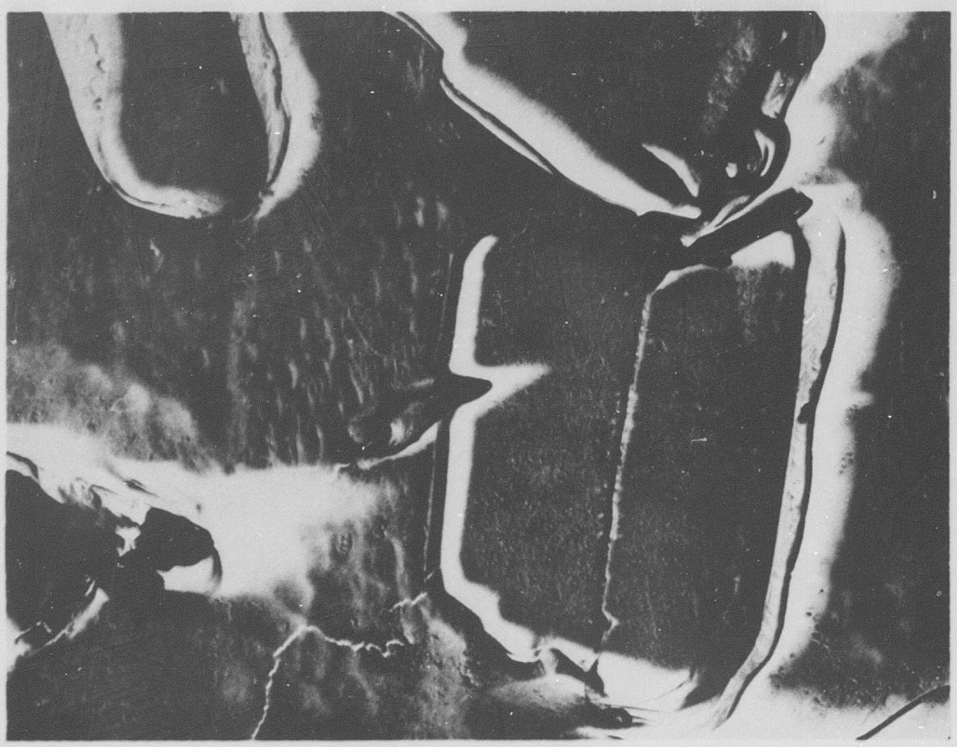

COMMENTS

The micrograph shows the weld matrix and the Al-Si eutectic.

Figure C-79 Aluminum 6061-T6, Condition TW (as welded): Electron Micrograph Showing 15,000X Magnification of Strained Area

METALLOGRAPHIC STUDY

Material Aluminum 6061-T6 Neg.No. 94-4

Specimen TWU 717 Neg.Mag. 2,100X

Etchant None Photo Enlargement 2X

COMMENTS

The fracture at the center of the specimen is mainly through the brittle eutectic and along the eutectic/matrix interface.

Figure C-80 Aluminum 6061-T6, Condition TW (as welded): Electron Fractograph Showing 4,200X Magnification at Center of Fracture

METALLOGRAPHIC STUDY

Material Aluminum 6061-T6 Neg.No. 94-5

Specimen TWU 717 Neg.Mag. 2,100X

Etchant None Photo Enlargement 2X

COMMENTS

The fracture at the edge of the specimen is the same as that seen at the center of the specimen, i.e., through and adjacent to the brittle eutectic.

Figure C-81 Aluminum 6061-T6, Condition TW (as welded): Electron Fractograph Showing 4,200X Magnification Edge of Fracture

METALLOGRAPHIC STUDY

Material Aluminum 6061-T6 Neg.No. 98-12

Specimen TWN 721 Neg.Mag. 2,100X

Etchant None Photo Enlargement 2X

COMMENTS

The picture shows a low-ductility fracture, mainly through the eutectic and along the eutectic/matrix interface.

Figure C-82 Aluminum 6061-T6, Condition TW (as welded): Electron Fractograph Showing 4,200X Magnification of Notched Fracture

Aluminum 7075-T6
Condition L

Table C-13
Tensile and Shear Test Data

Material Aluminum 7075-T6 Specimen Condition L

Averaged Data (-423°F)		
Unnotched Specimens	Control	Irradiated
Ultimate Strength (ksi)	110.4	113.4
0.2% Yield Strength (ksi)	99.1	104.3
Elongation in Gage Length (%)	6.4	4.1
Reduction in Area (%)	7.0	7.9
Ultimate Shear Strength (ksi)	95.2	80.3
Notched Specimens		
Ultimate Strength (ksi)	70.5	75.5
Ratios		
Notched-Ult./Unnotched-Ult.	0.64	0.67
Notched-Ult./Unnotched-Yield	0.71	0.72

Unnotched Specimens				
Specimen Number	Ult. Tensile Strength(ksi)	Yield Strength 0.2% Offset (ksi)	Reduction in Area (%)	Elongation (%)
101	111.1	102.0	9.4	5.0
102	111.6	104.0	7.5	3.5
105	115.4	104.5	6.7	3.4
106	115.5	106.5	8.0	4.6

Notched Specimens		Shear Specimens	
Specimen Number	Ult. Tensile Strength (ksi)	Specimen Number	Ult. Shear Strength (ksi)
113	69.0	1	83.1
114	77.6	2	83.1
117	80.2	3	79.1
118	75.3	4	75.8

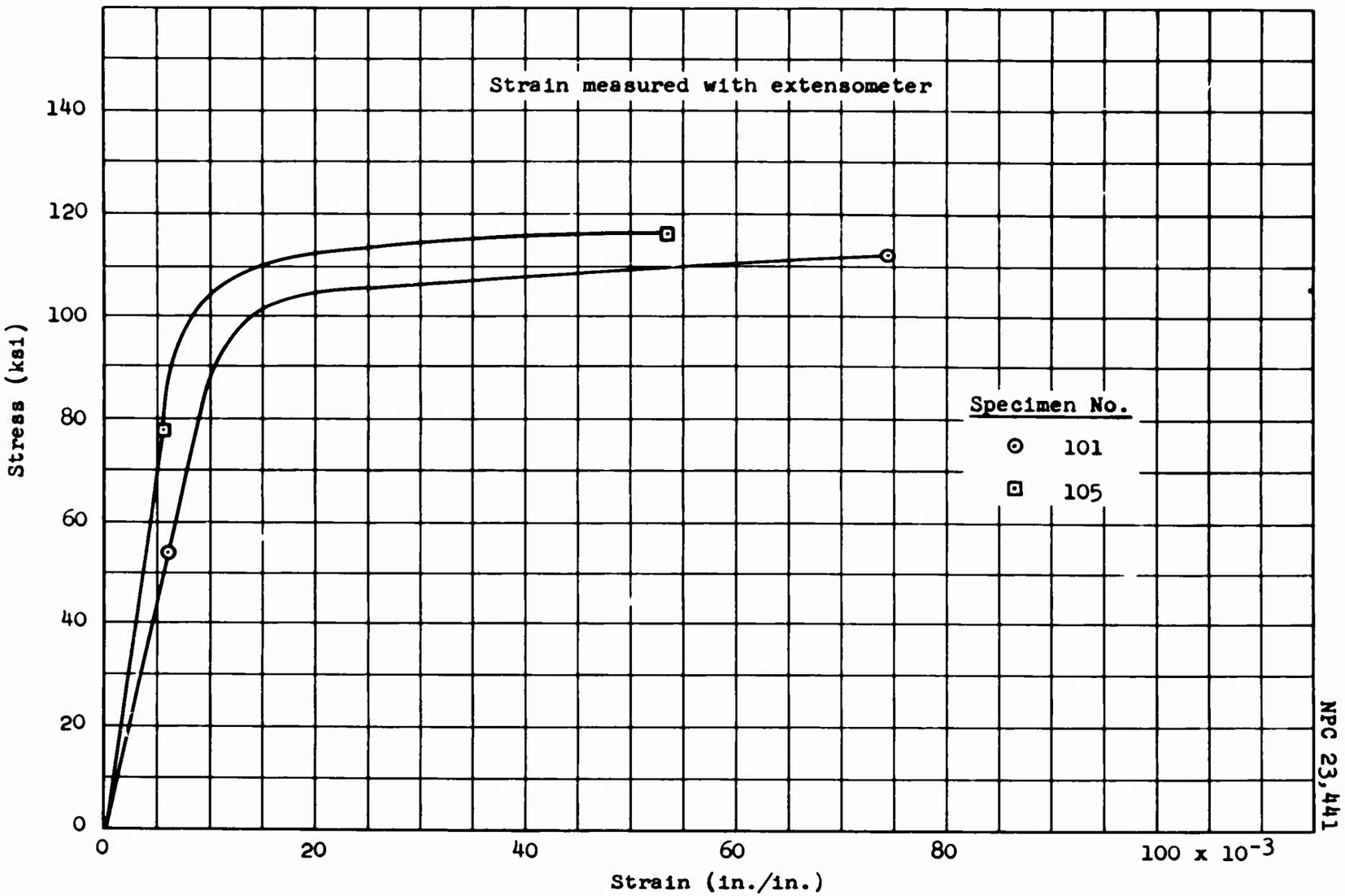

Figure C-83 Aluminum 7075-T6, Condition LU: Stress-Strain Curves

Table C-14
X-Ray Diffraction Data

Material Aluminum 7075-T6 Specimen LU 106

	STRAINED AREA		UNSTRAINED AREA	
DIFFRACTION PATTERN				
Miller Indices (hkl)	Interlattice Spacing, d (Å)	Relative Intensity (%)	Interlattice Spacing, d (Å)	Relative Intensity (%)
111	2.34	27	2.35	29
200	2.03	100	2.25 2.03	2 100
220	1.43	48	1.44	49
311	1.22	14	1.23	2
222			1.17	2
400	1.02	3	1.01	5
331	0.93	3	0.93	1
LATTICE PARAMETER (Å)				
111	4.05		4.07	
200	4.06		4.06	
220	4.04		4.07	
311	4.05		4.08	
222	-		4.05	
400	4.06		4.04	
331	4.05		4.05	
MICROSTRESS, $\Delta\theta$				
0.30° ($2\theta = 78.0^\circ$)			0.25° ($2\theta = 78.0^\circ$)	
0.20° ($2\theta = 44.6^\circ$)			0.16° ($2\theta = 44.55^\circ$)	

METALLOGRAPHIC STUDY

Material Aluminum 7075-T6 Neg.No. None

Specimen LU 106 Neg.Mag. 3X

Etchant None Photo Enlargement None

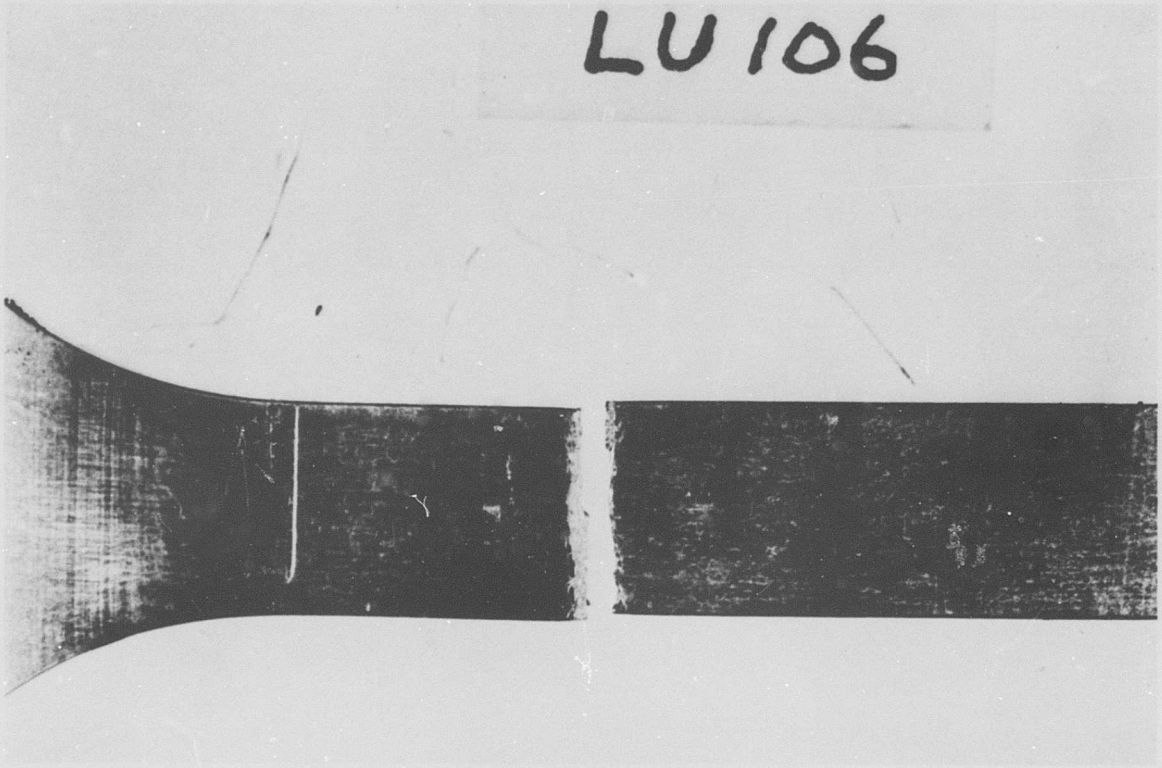

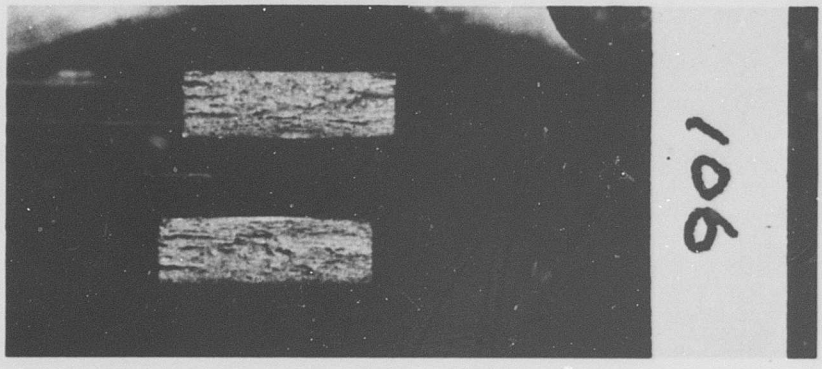

Figure C-84 Aluminum 7075-T6, Condition L: Macrophotograph Showing 3X Magnification of Specimen

METALLOGRAPHIC STUDY

Material Aluminum 7075-T6 Neg.No. W24

Specimen LU 106 Neg.Mag. 100X

Etchant Keller's Photo Enlargement None

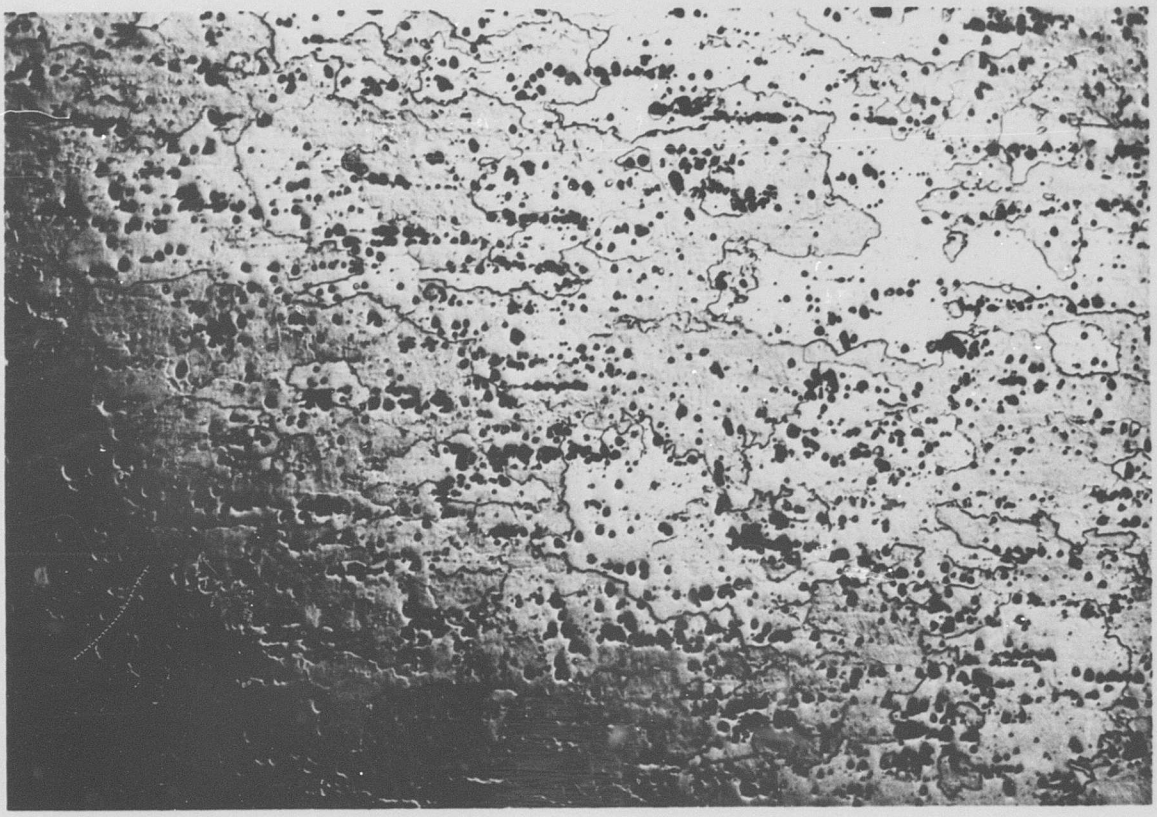

COMMENTS

The optical micrograph shows a structure typical of the 7075-T6 wrought material - solid-solution aluminum containing a fine precipitate and nonmetallic inclusions. The primary hardening constituent is a Zn-Mg intermetallic precipitate.

Figure C-85 Aluminum 7075-T6, Condition L: Optical Micrograph Showing 100X Magnification of Unstrained Area

METALLOGRAPHIC STUDY

Material Aluminum 7075-T6 Neg.No. W25

Specimen LU 106 Neg.Mag. 1,000X

Etchant Keller's Photo Enlargement None

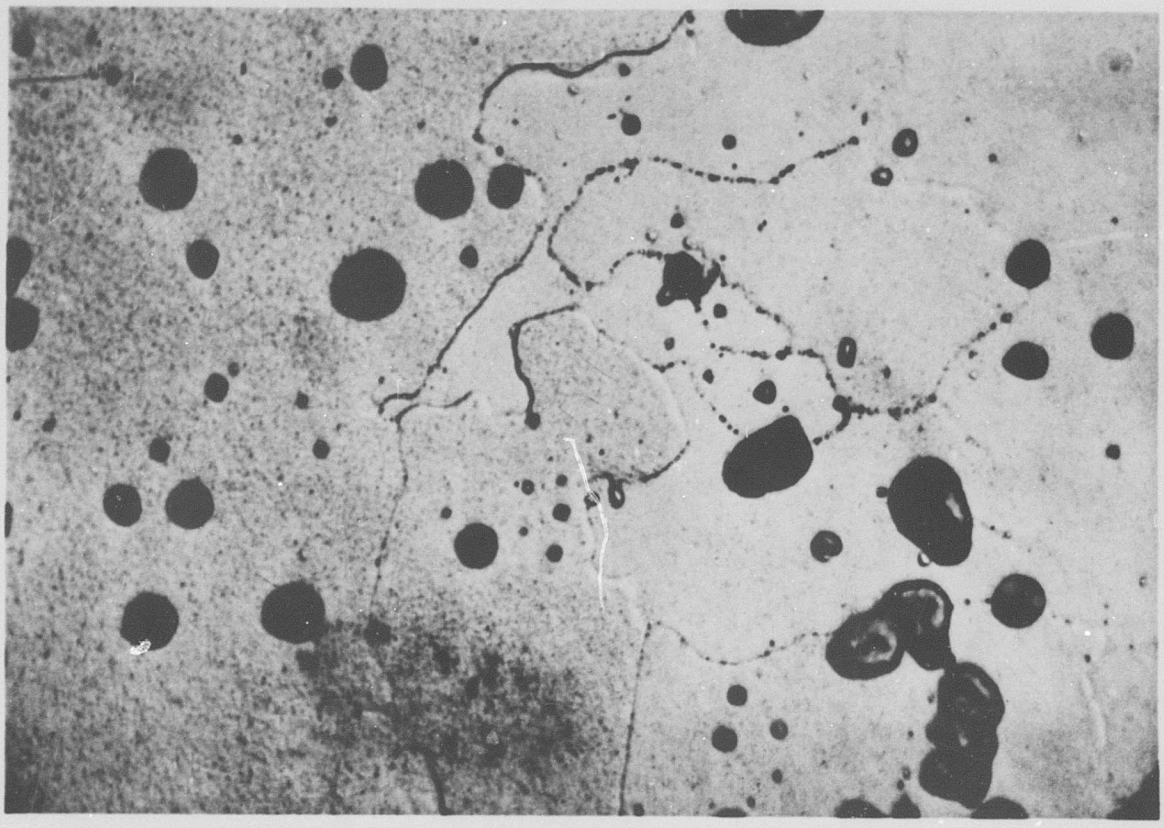

COMMENTS

The micrograph shows an unstrained area of the specimen. Fine precipitate particles and nonmetallic inclusions can be seen in the solid-solution aluminum matrix.

Figure C-86 Aluminum 7075-T6, Condition L: Optical Micrograph Showing 1,000X Magnification of Unstrained Area

METALLOGRAPHIC STUDY

Material Aluminum 7075-T6 Neg.No. W25

Specimen LU 106 Neg.Mag. 1,000X

Etchant Keller's Photo Enlargement None

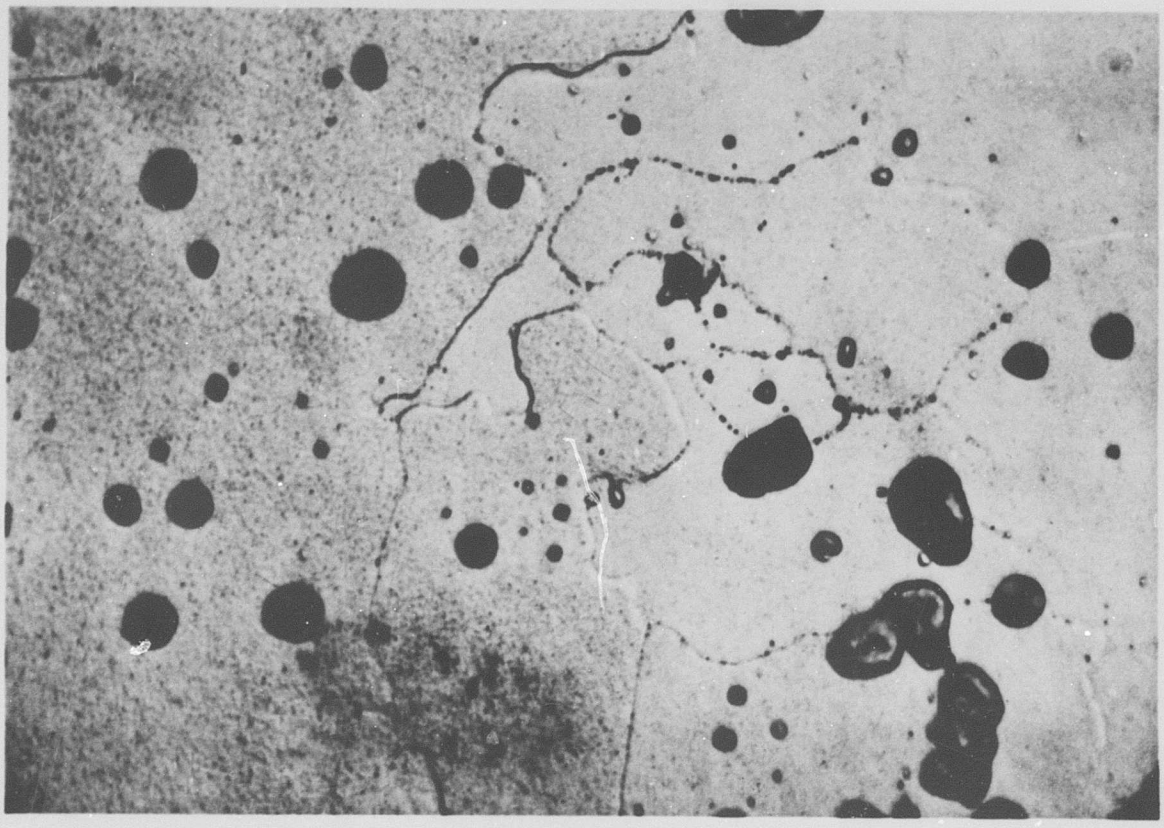

COMMENTS

The micrograph shows an unstrained area of the specimen. Fine precipitate particles and nonmetallic inclusions can be seen in the solid-solution aluminum matrix.

Figure C-86 Aluminum 7075-T6, Condition L: Optical Micrograph Showing 1,000X Magnification of Unstrained Area

METALLOGRAPHIC STUDY

Material Aluminum 7075-T6 Neg.No. W58

Specimen LU 106 Neg.Mag. 1,000X

Etchant Keller's Photo Enlargement None

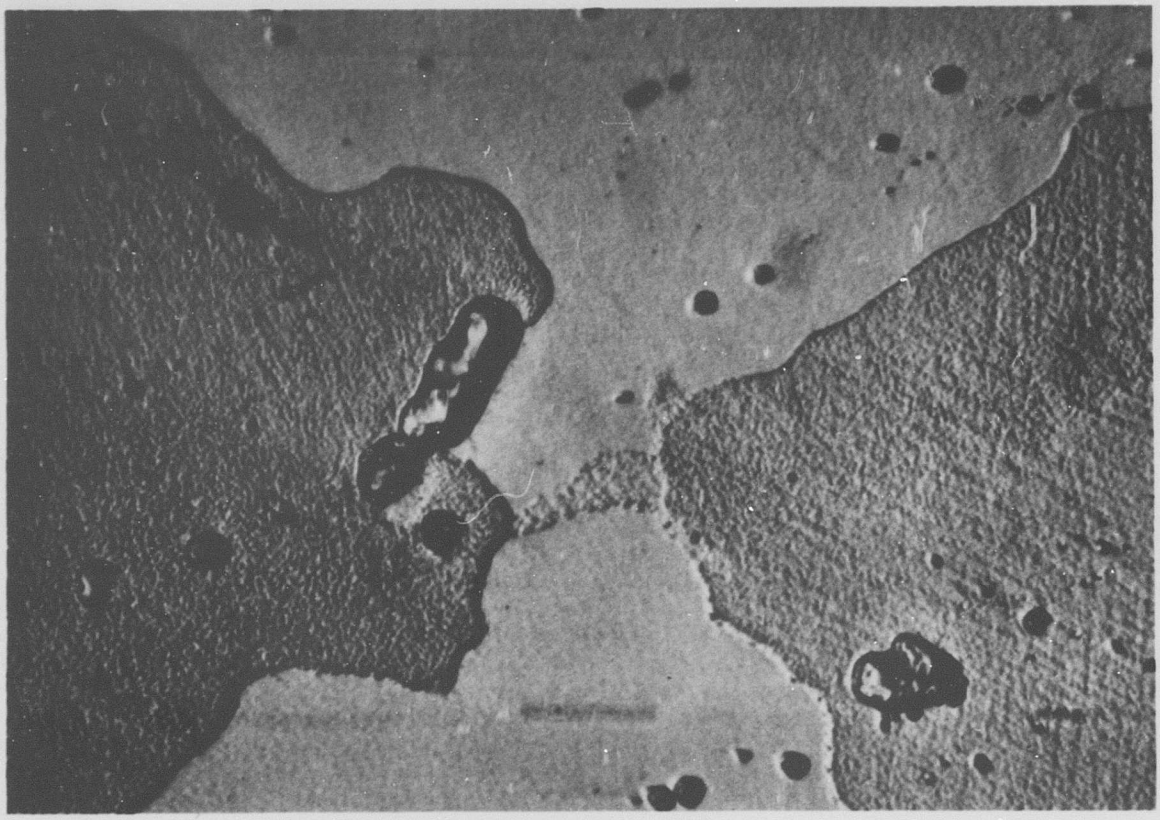

COMMENTS

The optical micrograph of a strained area shows fine precipitate particles and nonmetallic inclusions in solid-solution aluminum.

Figure C-88 Aluminum 7075-T6, Condition L: Optical Micrograph Showing 1,000X Magnification of General Strained Area

METALLOGRAPHIC STUDY

Material Aluminum 7075-T6 Neg.No. W56

Specimen LU 106 Neg.Mag. 100X

Etchant Keller's Photo Enlargement None

COMMENTS

The path of the fracture is primarily transgranular.

Figure C-89 Aluminum 7075-T6, Condition L: Optical Micrograph Showing 100X Magnification of Fracture Edge

METALLOGRAPHIC STUDY

Material Aluminum 7075-T6 Neg.No. W59

Specimen LU 106 Neg.Mag. 1,000X

Etchant Keller's Photo Enlargement None

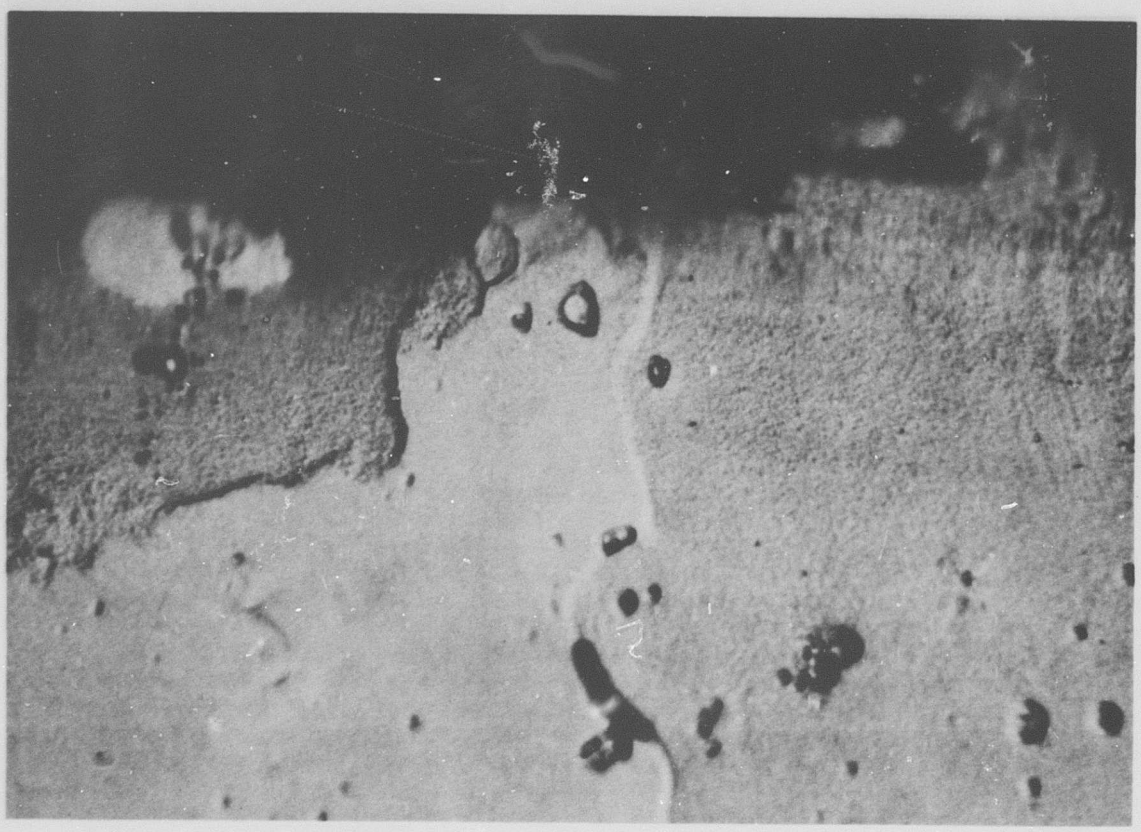

COMMENTS

The optical micrograph of the fracture profile shows the fracture to be primarily transgranular. Note the strain line revealed by the etchant.

Figure C-90 Aluminum 7075-T6, Condition L: Optical Micrograph Showing 1,000X Magnification of Fracture Edge

METALLOGRAPHIC STUDY

Material Aluminum 7075-T6 Neg.No. 102-4

Specimen LU 106 Neg.Mag. 7,500X

Etchant Keller's Photo Enlargement 2X

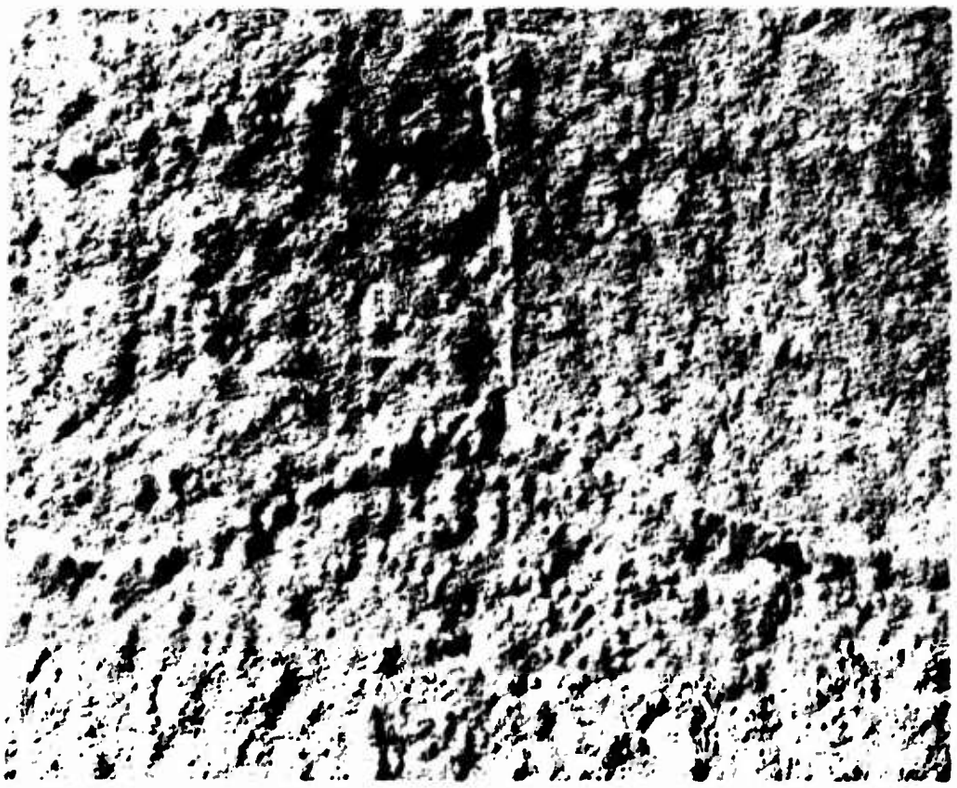

COMMENTS

The electron metallograph shows the solid-solution aluminum matrix with a grain-boundary intersection and fine insolubles.

Figure C-91 Aluminum 7075-T6, Condition L: Electron Micrograph Showing 15,000X Magnification of Unstrained Area

METALLOGRAPHIC STUDY

Material	Aluminum 7075-T6	Neg.No.	102-6
Specimen	LU 106	Neg.Mag.	7,500X
Etchant	Keller's	Photo Enlargement	2X

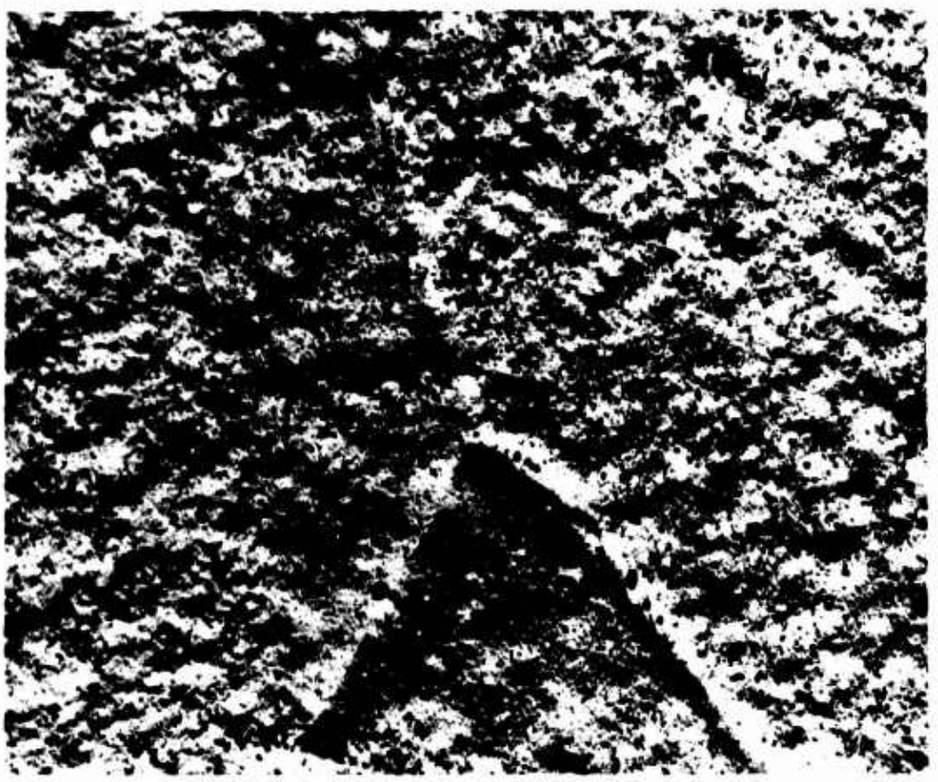

COMMENTS

The photograph shows the solid-solution aluminum matrix with grain boundaries and fine insolubles.

Figure C-92 Aluminum 7075-T6, Condition L: Electron Micrograph Showing 15,000X Magnification of Strained Area

METALLOGRAPHIC STUDY

Material	Aluminum 7075-T6	Neg.No.	95-11
Specimen	LU 106	Neg.Mag.	2,100X
Etchant	None	Photo Enlargement	2X

COMMENTS

The fractograph shows a microvoid and glide-plane decohesion fracture mode with some intergranular areas.

Figure C-93 Aluminum 7075-T6, Condition L: Electron Fractograph Showing 4,200X Magnification at Center of Fracture

METALLOGRAPHIC STUDY

Material	Aluminum 7075-T6	Neg.No.	95-8
Specimen	LU 106	Neg.Mag.	2,100X
Etchant	None	Photo Enlargement	2X

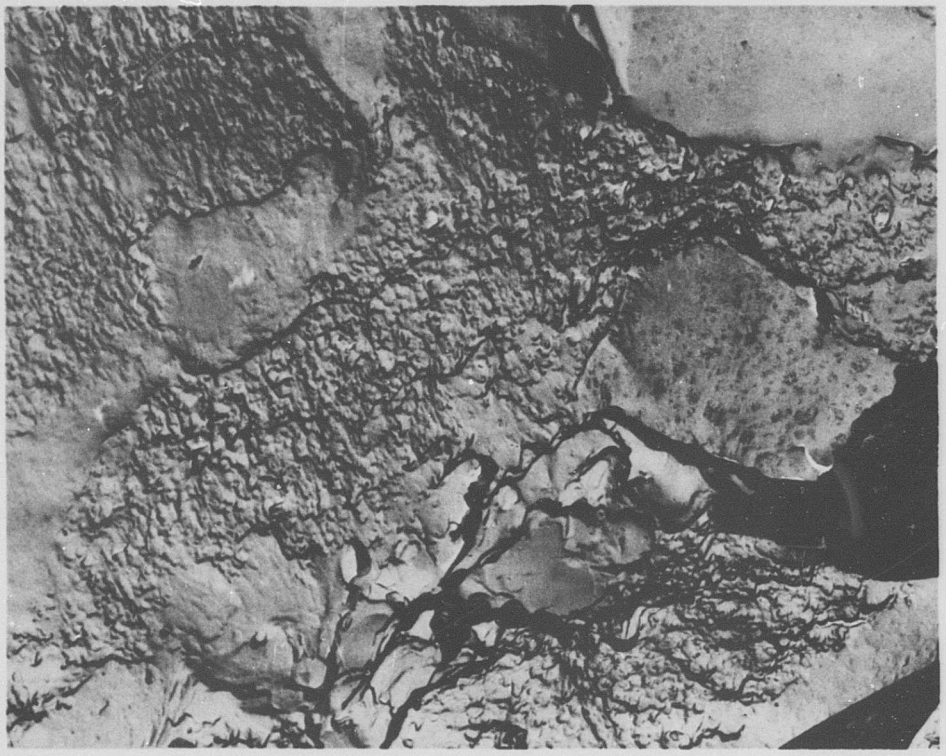

COMMENTS

The fracture near the edge of the specimen is made up of glide-plane decohesion, small oriented micro-voids, and some intergranular areas. The fracture of an intermetallic compound is apparent.

Figure C-94 Aluminum 7075-T6, Condition L: Electron Fractograph Showing 4,200X Magnification Near Edge of Fracture

METALLOGRAPHIC STUDY

Material Aluminum 7075-T6 Neg.No. 97-6

Specimen LN 113 Neg.Mag. 2,100X

Etchant None Photo Enlargement 2X

COMMENTS

This fractograph of the notched specimen shows small microvoid regions and some intergranular fracture.

Figure C-95 Aluminum 7075-T6, Condition L: Electron Fractograph Showing 4,200X Magnification of Notched Fracture

Stainless Steel 347C
Condition L

Table C-15
Tensile and Shear Test Data

Material Stainless Steel 347C Specimen Condition L

Averaged Data (-423°F)		
Unnotched Specimens	Control	Irradiated
Ultimate Strength (ksi)	117.3	115.4
0.2% Yield Strength (ksi)	83.0	80.2
Elongation in Gage Length (%)	7.7	7.3
Reduction in Area (%)	8.8	6.4
Ultimate Shear Strength (ksi)		
Notched Specimens		
Ultimate Strength (ksi)	99.2	102.3
Ratios		
Notched-Ult./Unnotched-Ult.	0.85	0.89
Notched-Ult./Unnotched-Yield	1.20	1.28

Unnotched Specimens				
Specimen Number	Ult. Tensile Strength(ksi)	Yield Strength 0.2% Offset (ksi)	Reduction in Area (%)	Elongation (%)
173	109.9	94.0	6.5	8.8
174	119.5	76.0	6.7	7.4
177	118.5	83.0	7.8	8.5
178	113.7	68.0	4.6	4.6

Notched Specimens		Shear Specimens*	
Specimen Number	Ult. Tensile Strength (ksi)	Specimen Number	Ult. Shear Strength (ksi)
185	98.0		
186	102.2		
189	100.4		
190	108.5		

*Not Applicable

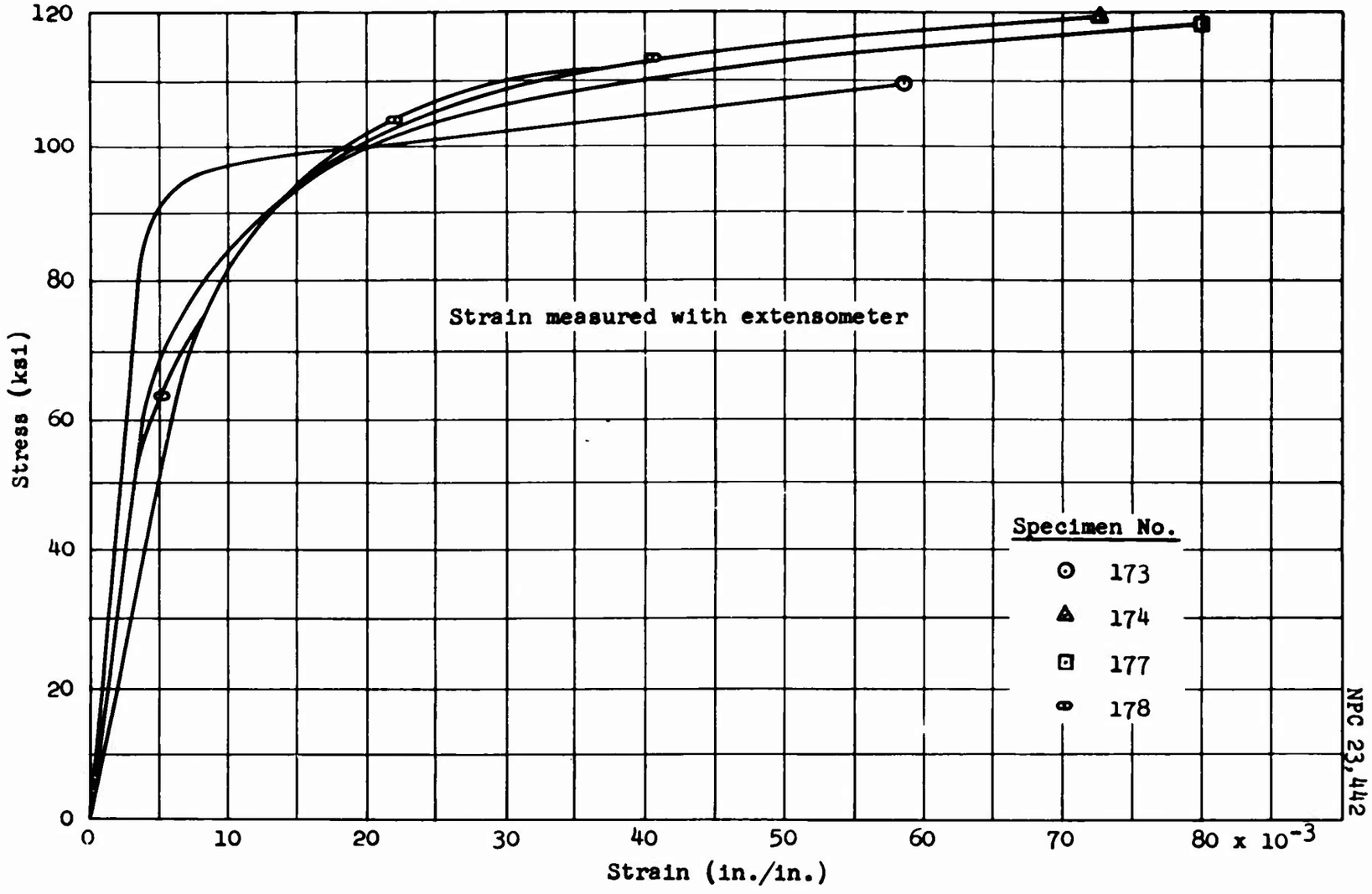

Figure C-96 Stainless Steel 347C, Condition LU: Stress-Strain Curves

Table C-16
X-Ray Diffraction Data

Material Stainless Steel 347C Specimen LU 178

	STRAINED AREA		UNSTRAINED AREA	
DIFFRACTION PATTERN				
Miller Indices (hkl)	Interlattice Spacing, d (Å)	Relative Intensity (%)	Interlattice Spacing, d (Å)	Relative Intensity (%)
111	2.09	100	2.08	100
110	2.03	21	2.03	10
200	1.80	50	1.44	5
220			1.25	5
211	1.17	26		

LATTICE PARAMETER (Å)		
111	3.62	3.60
110	2.87	2.87
200	3.60	2.88
220	-	3.54
211	2.87	-

MICROSTRESS, $\Delta\theta$	
0.15° (2θ = 50.8°)	0.13° (2θ = 51.0°)
No Peak (2θ = 129°)	No Peak (2θ = 129°)

METALLOGRAPHIC STUDY

Material Stainless Steel 347C Neg.No. None

Specimen LU 178 Neg.Mag. 3X

Etchant None Photo Enlargement None

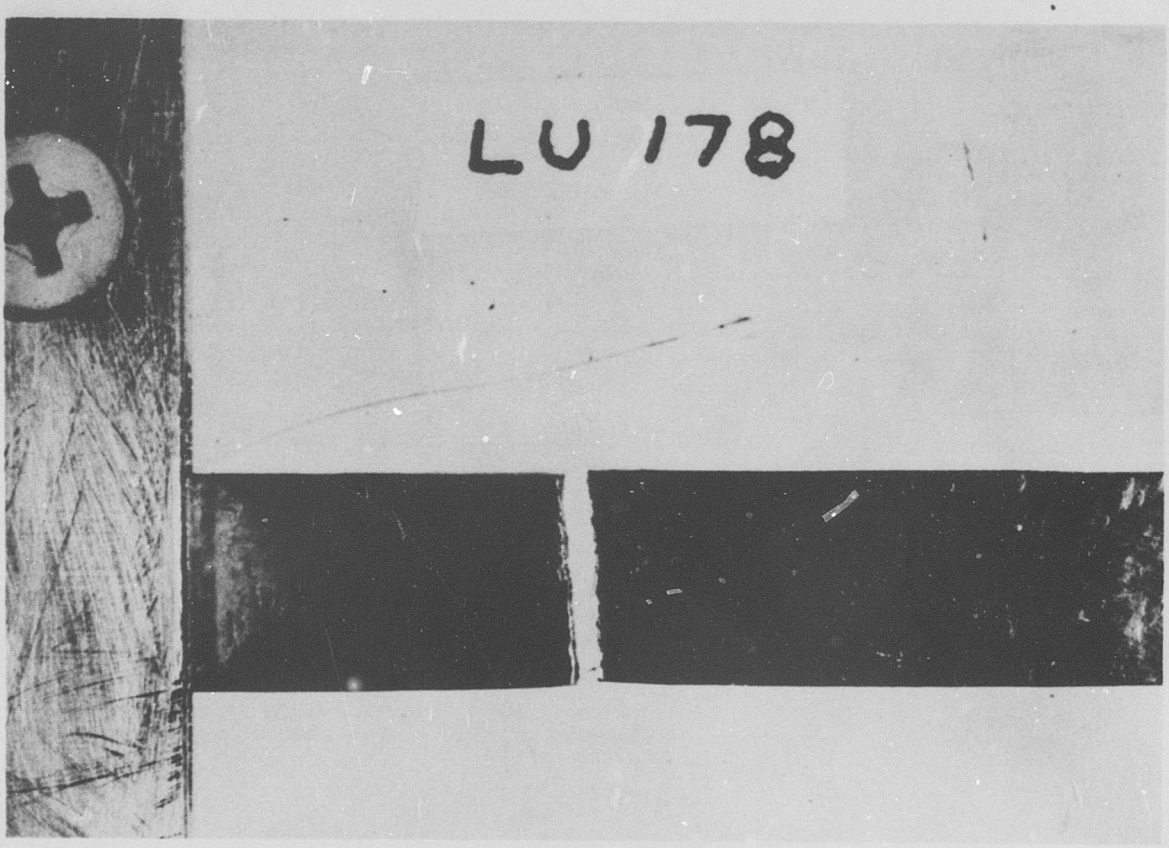

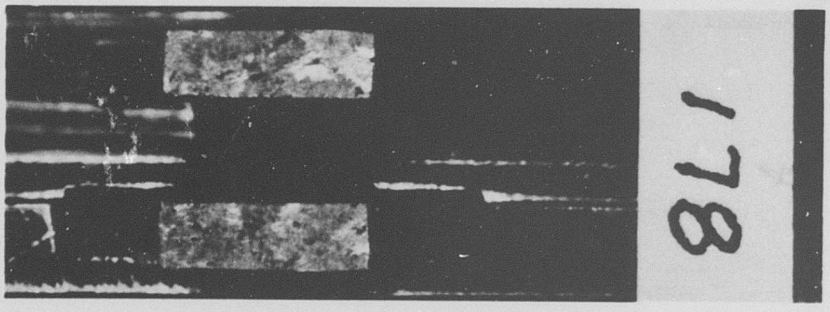

Figure C-97 Stainless Steel 347C, Condition L: Macrophotograph Showing 3X Magnification of Specimen

METALLOGRAPHIC STUDY

Material Stainless Steel 347C Neg.No. W8

Specimen LU 178 Neg.Mag. 100X

Etchant 10% Amonium Persulfate Photo Enlargement None

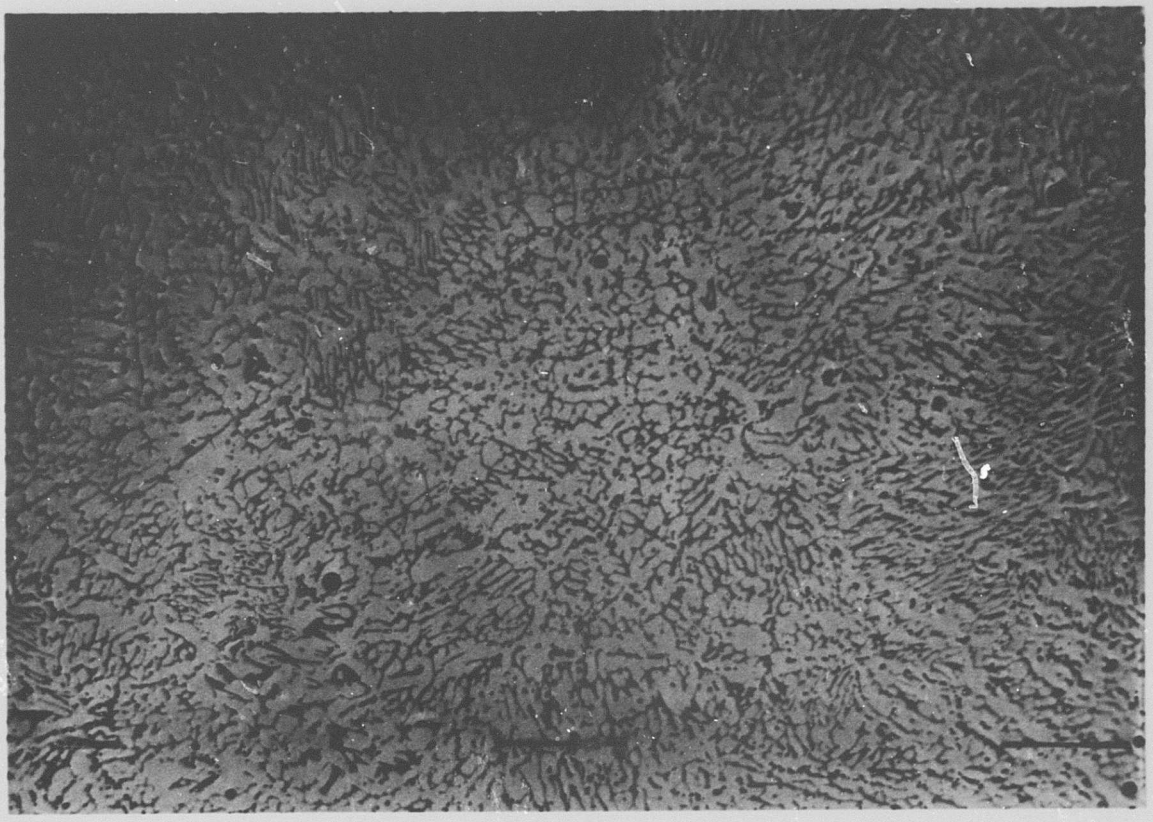

COMMENTS

The microstructure consists of a high Cr-Fe phase (dark) - carbides (black) in a matrix of austenite (light).

Figure C-98 Stainless Steel 347C, Condition L: Optical Micrograph Sh..ing 100X Magnification of Unstrained Area

METALLOGRAPHIC STUDY

Material Stainless Steel 347C Neg.No. 9W

Specimen LU 178 Neg.Mag. 1,000X

Etchant 10% Amonium Persulfate Photo Enlargement None

COMMENTS

The microstructure shows clearly the high Cr-Fe phase - carbides (black) in a matrix of austenite (light).

Figure C-99 Stainless Steel 347C, Condition L: Optical Micrograph Showing 1,000X Magnification of Unstrained Area

METALLOGRAPHIC STUDY

Material Stainless Steel 347C Neg.No. W6

Specimen LU 178 Neg.Mag. 100X

Etchant 10% Amonium Persulfate Photo Enlargement None

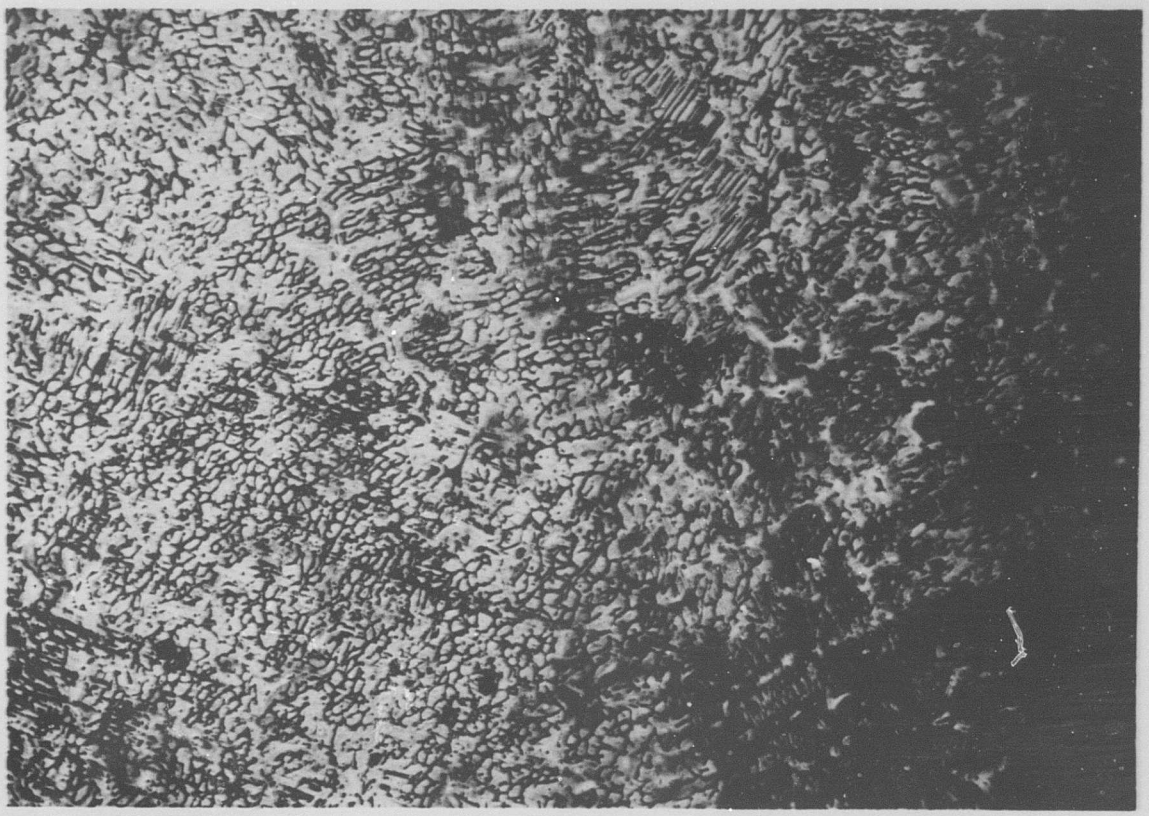

COMMENTS

The microstructure of a high Cr-Fe phase (dark) is shown - carbides (black) in a strained matrix of austenite. The areas of high strain exhibit general darkening due to preferential etching.

Figure C-100 Stainless Steel 347C, Condition L: Optical Micrograph Showing 100X Magnification of General Strained Area

METALLOGRAPHIC STUDY

Material Stainless Steel 347C Neg.No. W5

Specimen LU 178 Neg.Mag. 1,000X

Etchant 10% Amonium Persulfate Photo Enlargement None

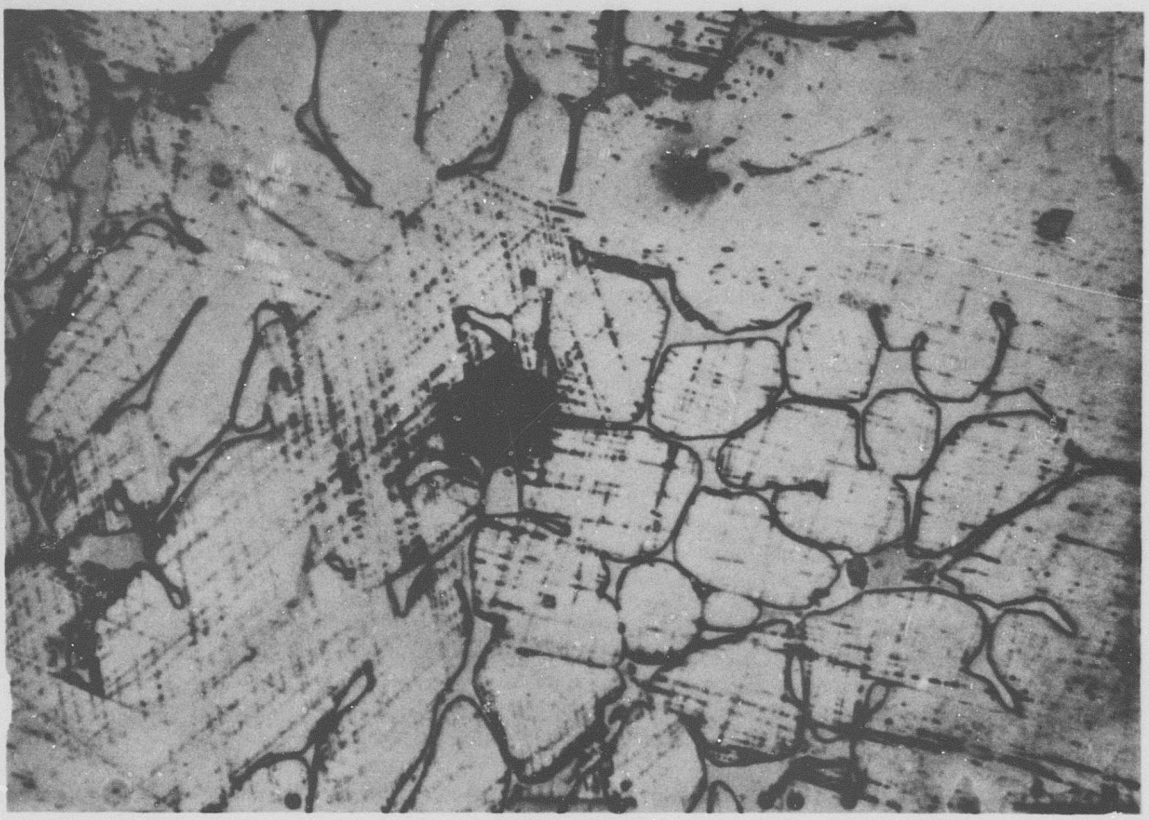

COMMENTS

The microstructure shown is a partially transformed austenite matrix with a high Cr-Fe grain boundary phase. The transformation occurs only on the austenitic slip planes.

Figure C-101 Stainless Steel 347C, Condition L: Optical Micrograph Showing 1,000X Magnification of General Strained Area

METALLOGRAPHIC STUDY

Material Stainless Steel 347C Neg.No. W7

Specimen LU 178 Neg.Mag. 100X

Etchant 10% Amonium Persulfate Photo Enlargement None

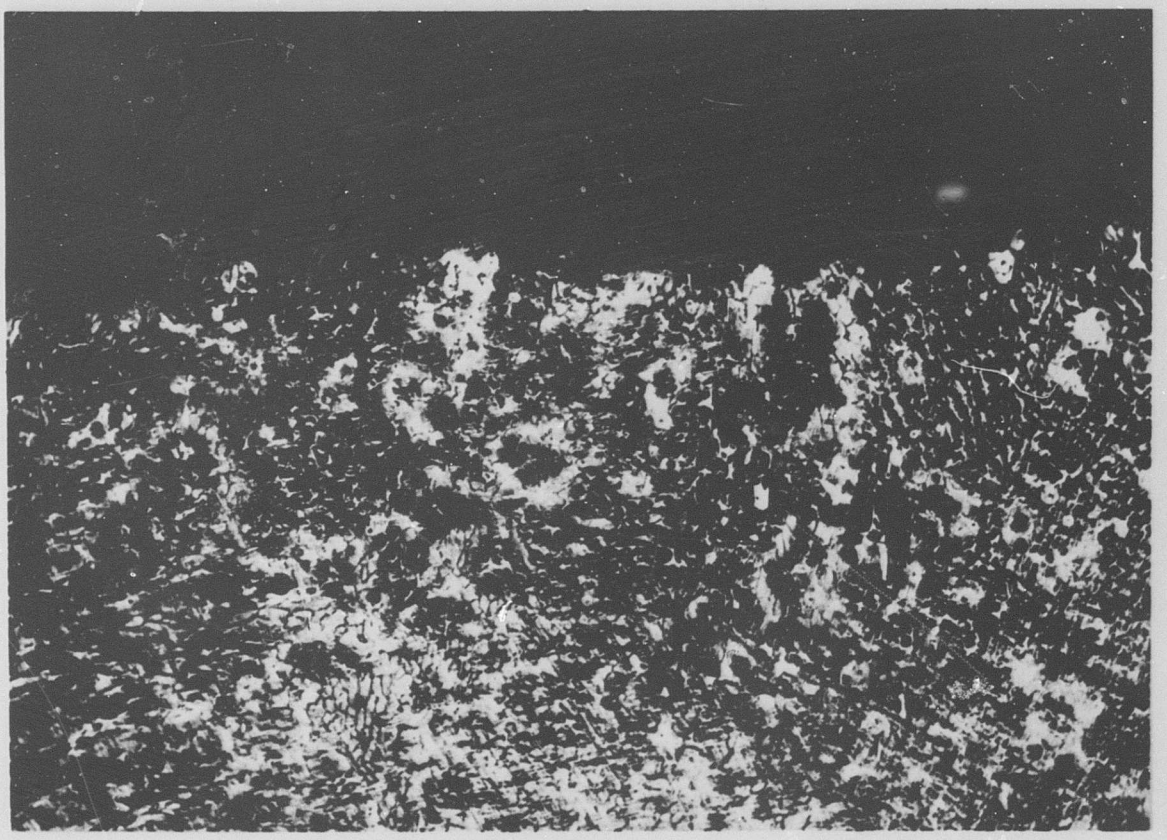

COMMENTS

The areas of high strain exhibit general darkening due to preferential etching.

Figure C-102 Stainless Steel 347C, Condition L: Optical Micrograph Showing 100X Magnification of Fracture Edge

METALLOGRAPHIC STUDY

Material Stainless Steel 347C Neg.No. W4

Specimen LU 178 Neg.Mag. 1,000X

Etchant 10% Amonium Persulfate Photo Enlargement None

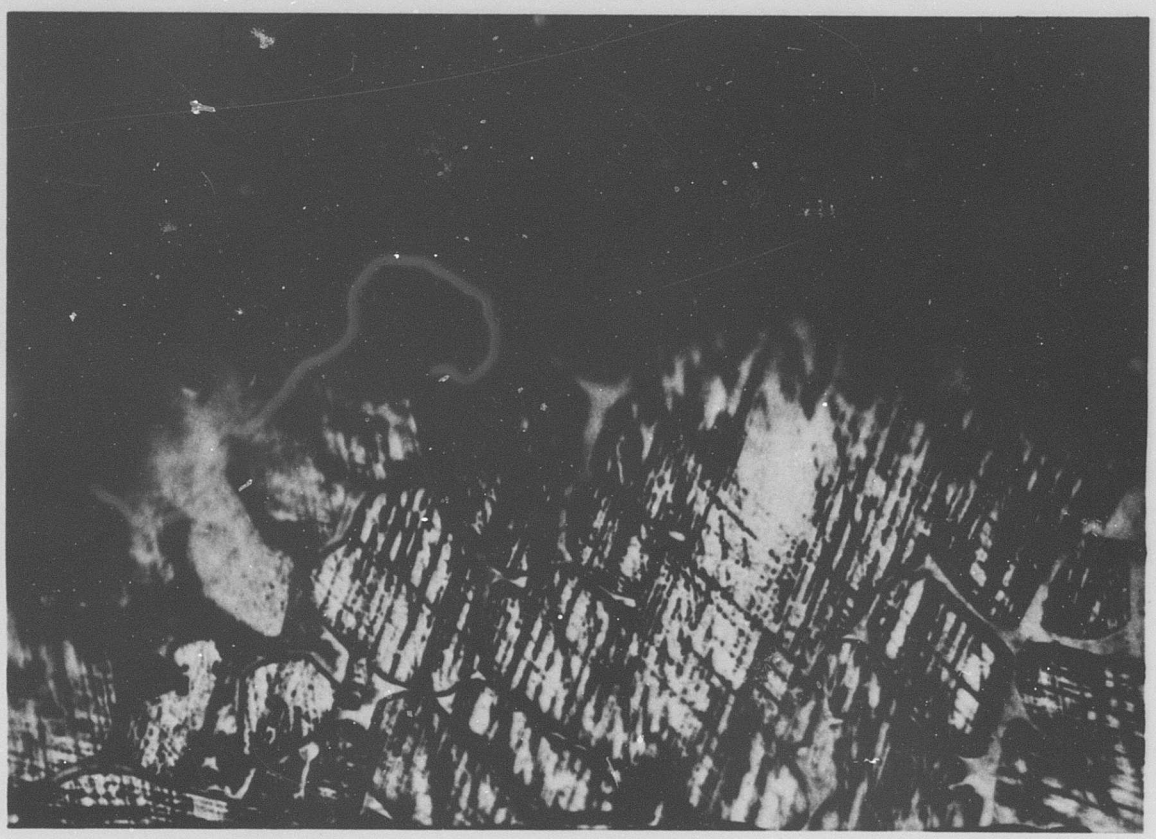

COMMENTS

The microstructure exhibits both intergranular and transgranular fractures. The austenite shows the high strain while the high Cr-Fe phase is not affected.

Figure C-103 Stainless Steel 347C, Condition L: Optical Micrograph Showing 1,000X Magnification of Fracture Edge

METALLOGRAPHIC STUDY

Material Stainless Steel 347C Neg.No. 103-4

Specimen LU 178 Neg.Mag. 7,500X

Etchant 10% Amonium Persulfate Photo Enlargement 2X

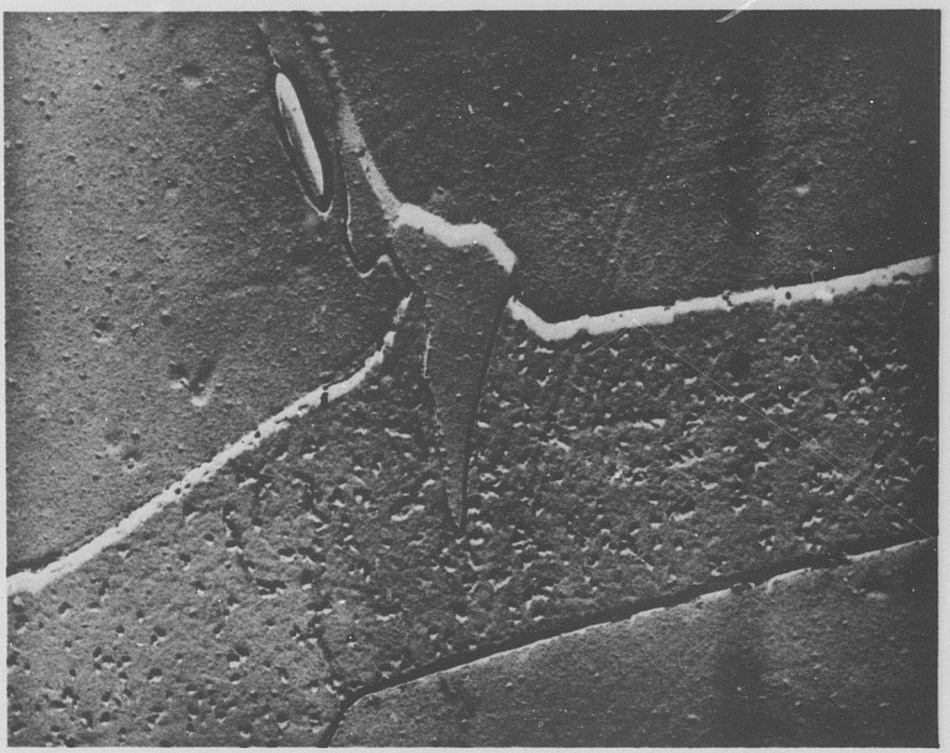

COMMENTS

The microstructure shows the austenite matrix with some chromium-rich ferrite. The large particle along the austenite grain boundary is a carbide, as are the smaller particles in the ferrite.

Figure C-104 Stainless Steel 347C, Condition L: Electron Micrograph Showing 15,000X Magnification of Unstrained Area

METALLOGRAPHIC STUDY

Material	Stainless Steel 347C	Neg.No.	103-6
Specimen	LU 178	Neg.Mag.	7,500X
Etchant	10% Amonium Persulfate	Photo Enlargement	2X

COMMENTS

The microstructure consists of the chromium-rich ferrite and austenite with partially transformed areas. The bands running through the austenite grains are (111) planes thought by other investigators (Refs. 11 & 12) to be made up of (hcp) or epsilon martensite. Alpha martensite is also present. It is felt that the different textured area near the ferrite/austenite interface is alpha martensite.

Figure C-105 Stainless Steel 347C, Condition L: Electron Micrograph Showing 15,000X Magnification of Strained Area

METALLOGRAPHIC STUDY

Material Stainless Steel 347C — Neg.No. 93-10

Specimen LU 178 — Neg.Mag. 2,100X

Etchant None — Photo Enlargement 2X

COMMENTS

The fracture surface of this area at the center of the specimen is made up of large quasi-cleavage facets and what appear to be grain-boundary fractures between the facets. The area in the middle of the photograph shows evidence of the failure of the high Cr-Fe phase. The area on the right represents the fracture of one large austenitic grain, quite possibly through or adjacent to the bands in Figure C-105 running through the austenite grain.

Figure C-106a Stainless Steel 347C, Condition L: Electron Fractograph Showing 4,200X Magnification at Center of Fracture

METALLOGRAPHIC STUDY

Material Stainless Steel 347C Neg.No. 93-11

Specimen LU 178 Neg.Mag. 2,100X

Etchant None Photo Enlargement 2X

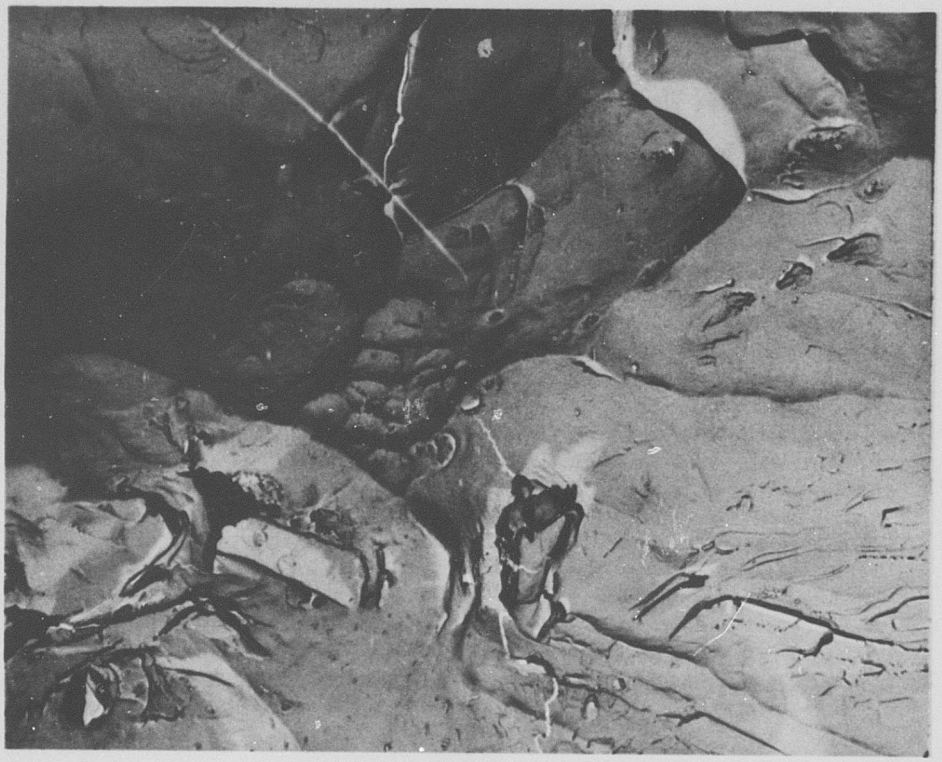

COMMENTS

The fracture surface in this area at the center of the specimen shows grain boundary fracture (in the upper left-hand corner), microvoid formation (at the center), and fracture through the ferrite phase (lower half of the picture).

Figure C-106b Stainless Steel 347C, Condition L: Electron Fractograph Showing 4,200X Magnification at Center of Fracture

METALLOGRAPHIC STUDY

Material Stainless Steel 347C Neg.No. 93-2

Specimen LU 178 Neg.Mag. 2,100X

Etchant None Photo Enlargement 2X

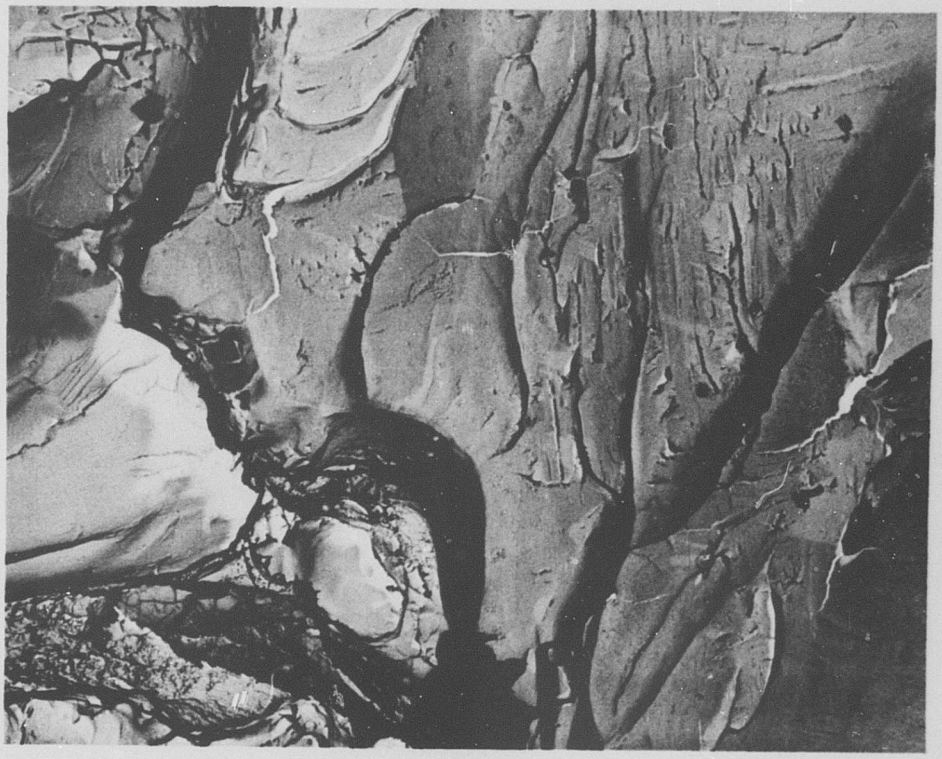

COMMENTS

The fracture surface at the edge of the specimen exhibited the same characteristics as at the center: large quasi-cleavage facets, some intergranular fracture at the austenite/ferrite interface, and isolated areas of microvoid fracture.

Figure C-107 Stainless Steel 347C, Condition L: Electron Fractograph Showing 4,200X Magnification Near Edge of Fracture

METALLOGRAPHIC STUDY

Material Stainless Steel 347C Neg.No. 100-5

Specimen LN 185 Neg.Mag. 2,100X

Etchant None Photo Enlargement 2X

COMMENTS

The fracture is a reflection of the cast structure. The individual facets are a very brittle cleavage type.

Figure C-108 Stainless Steel 347C, Condition L: Electron Fractograph Showing 4,200X Magnification of Notched Fracture

Stainless Steel 347
Condition L

BLANK PAGE

Table C-17
Tensile and Shear Test Data

Material Stainless Steel 347 Specimen Condition L

Averaged Data (-423°F)		
Unnotched Specimens	**Control**	**Irradiated**
Ultimate Strength (ksi)	No Data	227.0
0.2% Yield Strength (ksi)		84.5
Elongation in Gage Length (%)		35.0
Reduction in Area (%)		28.0
Ultimate Shear Strength (ksi)		150.2
Notched Specimens		
Ultimate Strength (ksi)		135.2
Ratios		
Notched- Ult./Unnotched-Ult.		0.6
Notched-Ult./Unnotched-Yield		1.60

Unnotched Specimens				
Specimen Number	Ult. Tensile Strength (ksi)	Yield Strength 0.2% Offset (ksi)	Reduction in Area (%)	Elongation (%)
701	235.6	91.0	29.1	35.4
702	246.5	74.0	28.5	36.8
703	220.8	89.0	30.0	37.0
704	205.3	84.0	23.9	30.8

Notched Specimens		Shear Specimens	
Specimen Number	Ult. Tensile Strength (ksi)	Specimen Number	Ult. Shear Strength (ksi)
705	130.8	1	151.8
706	134.3	2	146.4
707	140.4	3	154.7
708	135.1	4	147.9

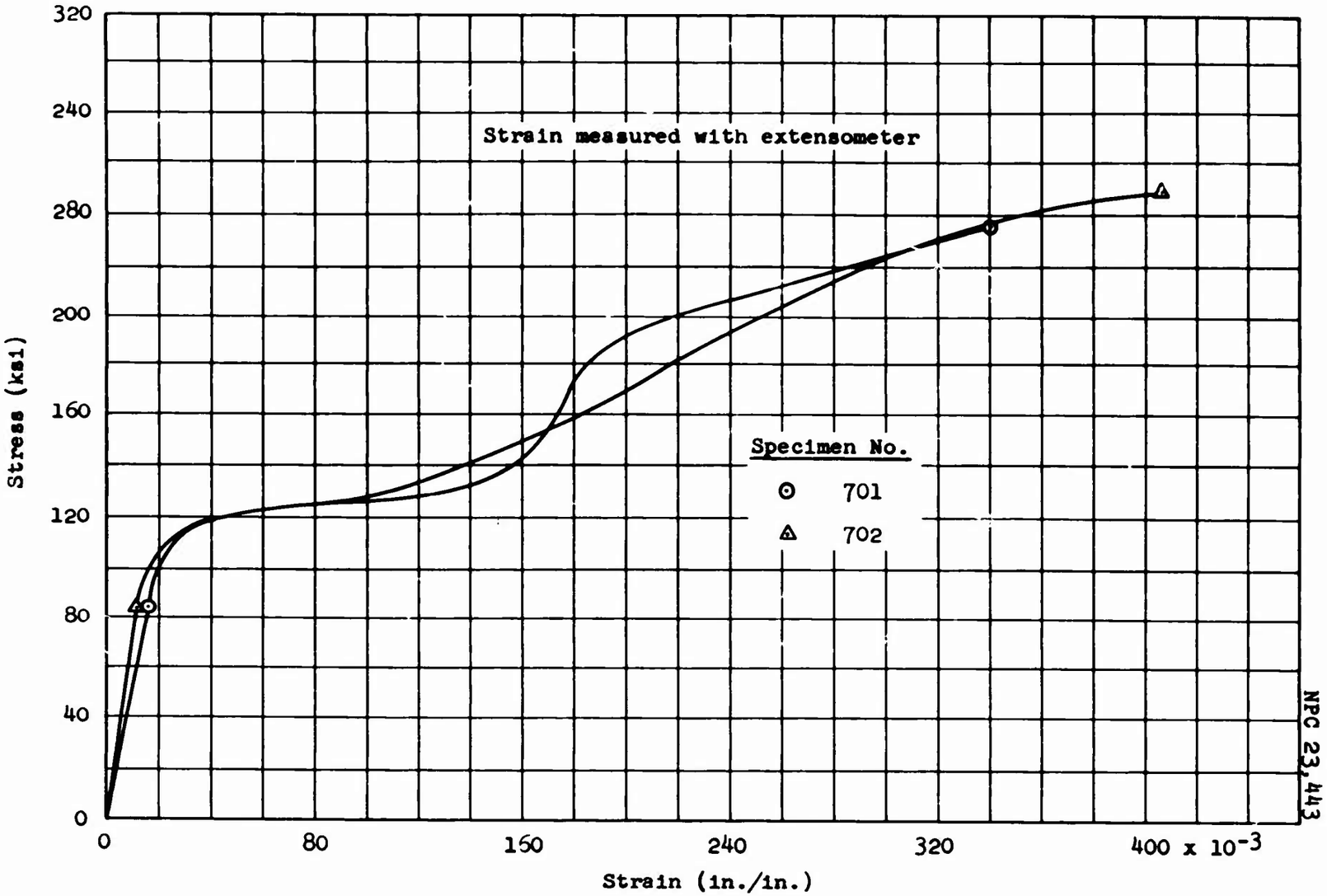

240

Figure C-109 Stainless Steel 347, Condition LU: Stress-Strain Curves

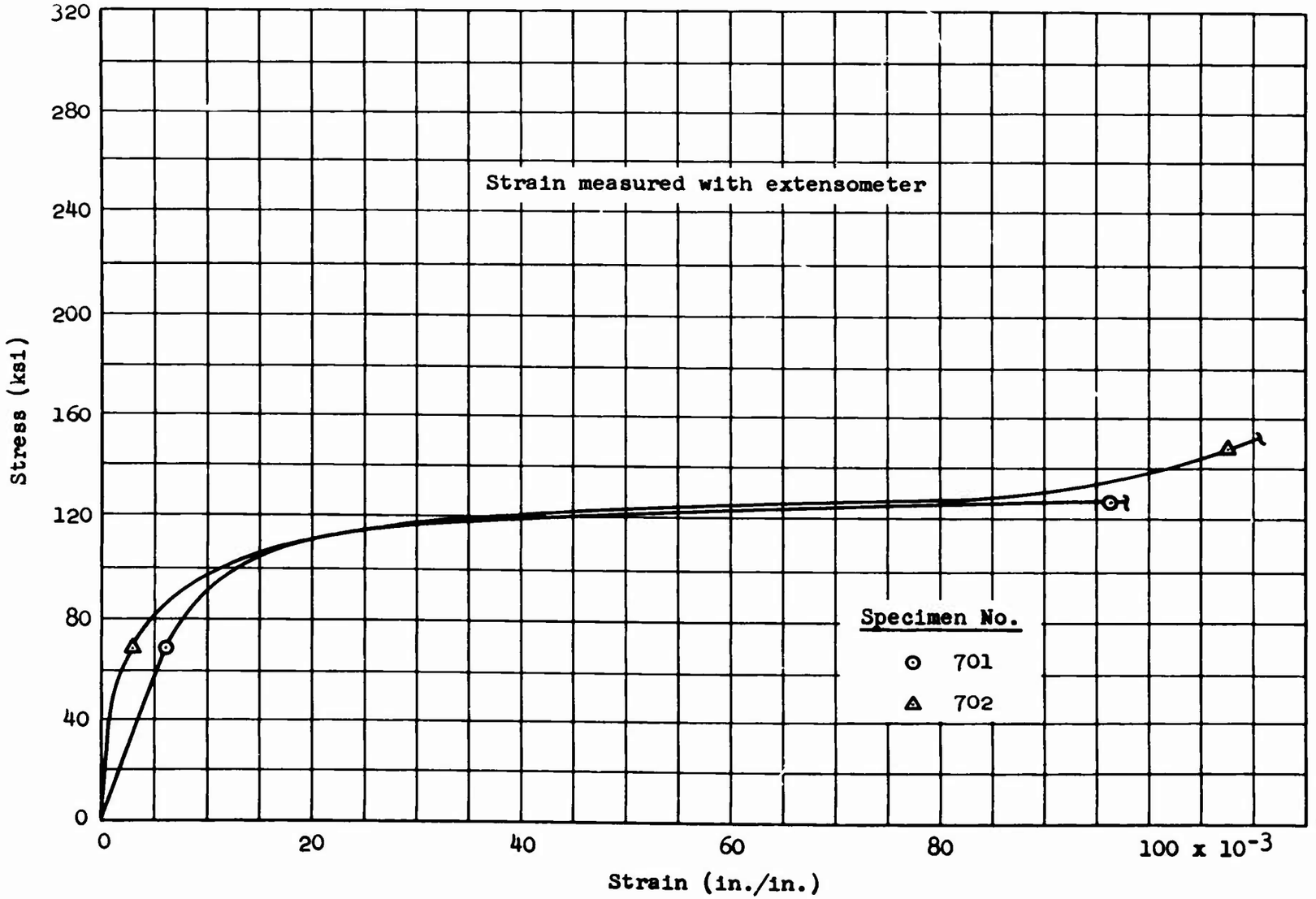

Figure C-110 Stainless Steel 347, Condition LU: Stress-Strain Curves (Expanded Scale)

Table C-18
X-Ray Diffraction Data

Material Stainless Steel 347 Specimen LU 702

	STRAINED AREA		UNSTRAINED AREA	
DIFFRACTION PATTERN				
Miller Indices (hkl)	Interlattice Spacing, d (Å)	Relative Intensity (%)	Interlattice Spacing, d (Å)	Relative Intensity (%)
111			2.08	100
110	2.03	100		
200			1.80	55
220			1.27	9
211	1.15	87	1.08	20

LATTICE PARAMETER (Å)		
111	-	3.60
110	3.52	-
200	-	3.60
220	-	3.59
211	2.82	-

MICROSTRESS, $\Delta\theta$	
0.33° (2θ = 52.4°)	0.14° (2θ = 52.4°)
No Peak (2θ = 129°)	No Peak (2θ = 129°)

METALLOGRAPHIC STUDY

Material Stainless Steel 347 Neg.No. None

Specimen LU 702 Neg.Mag. 3X

Etchant None Photo Enlargement None

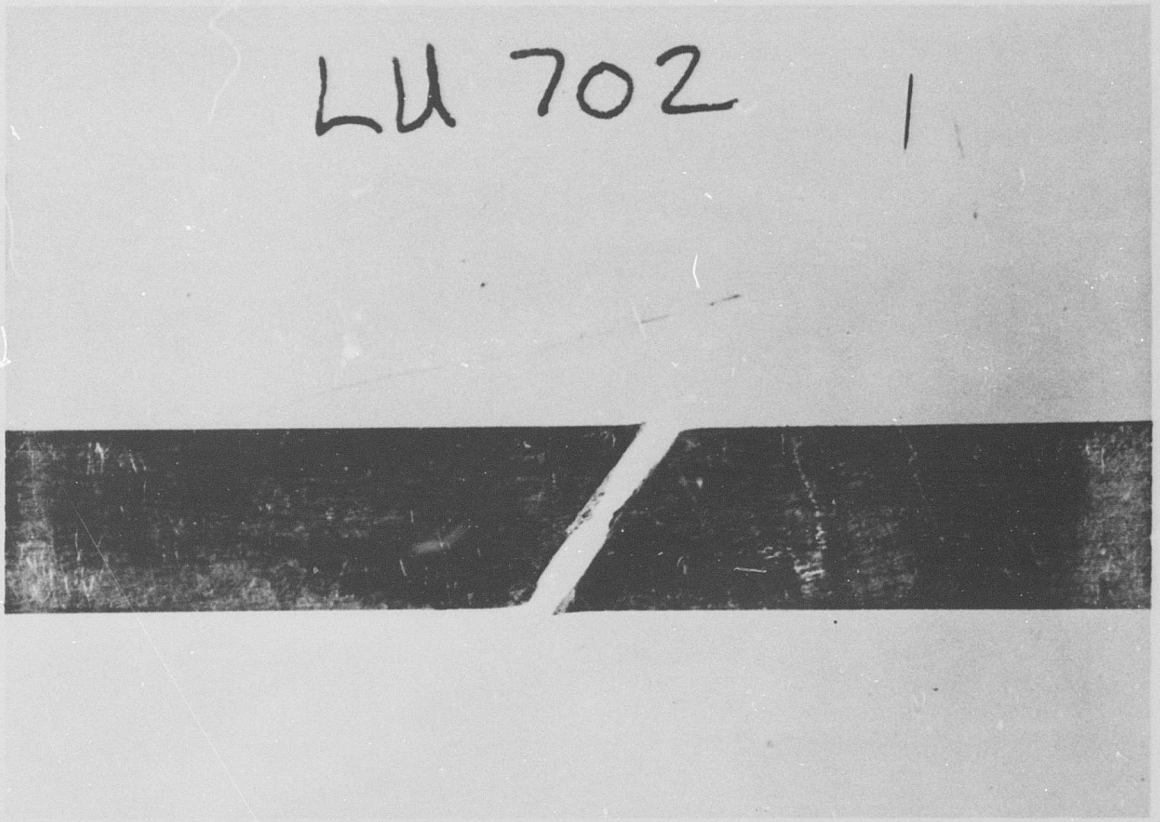

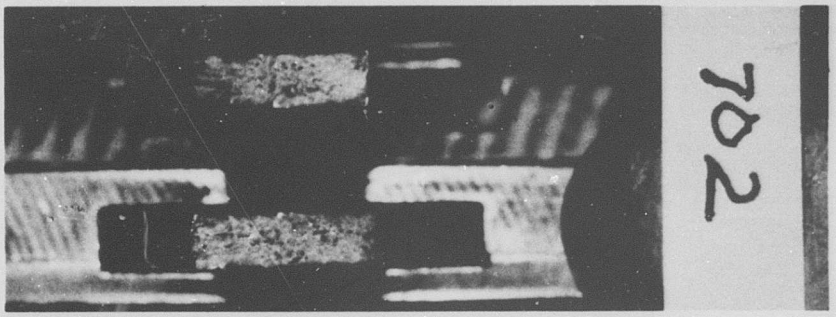

Figure C-111 Stainless Steel 347, Condition L: Macrophotograph Showing 3X Magnification of Specimen

METALLOGRAPHIC STUDY

Material Stainless Steel 347 Neg.No. W11

Specimen LU 702 Neg.Mag. 100X

Etchant 10% Amonium Persulfate Photo Enlargement None

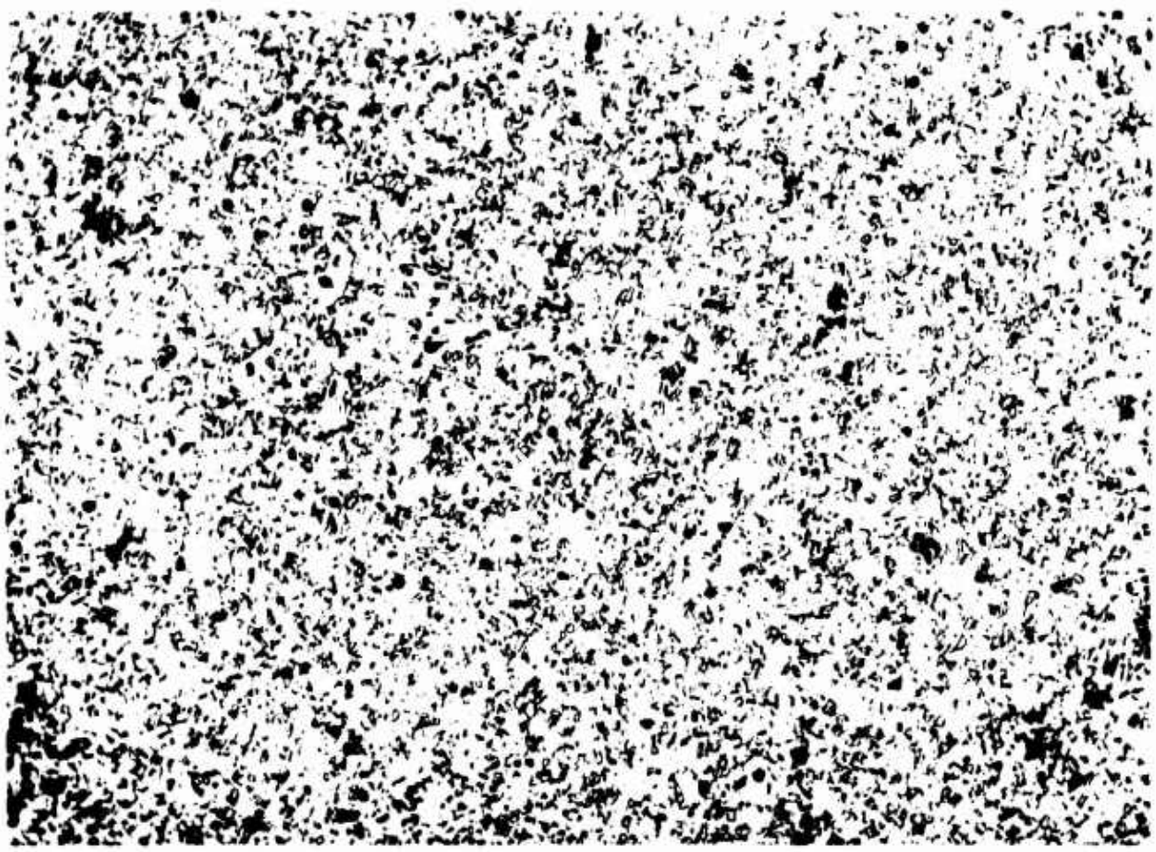

COMMENTS

The austenitic microstructure shows the original annealing twins and carbide dispersion.

Figure C-112 Stainless Steel 347, Condition L: Optical Micrograph Showing 100X Magnification of Unstrained Area

METALLOGRAPHIC STUDY

Material Stainless Steel 347 Neg.No. W10

Specimen LU 702 Neg.Mag. 1,000X

Etchant 10% Amonium Persulfate Photo Enlargement None

COMMENTS

The austenitic microstructure shows the original annealing twins and carbide dispersion. There appears to be some carbide (and grain boundary) sensitization.

Figure C-113 Stainless Steel 347, Condition L: Optical Micrograph Showing 1,000X Magnification of Unstrained Area

METALLOGRAPHIC STUDY

Material Stainless Steel 347 Neg.No. W70

Specimen LU 702 Neg.Mag. 100X

Etchant 10% Amonium Persulfate Photo Enlargement None

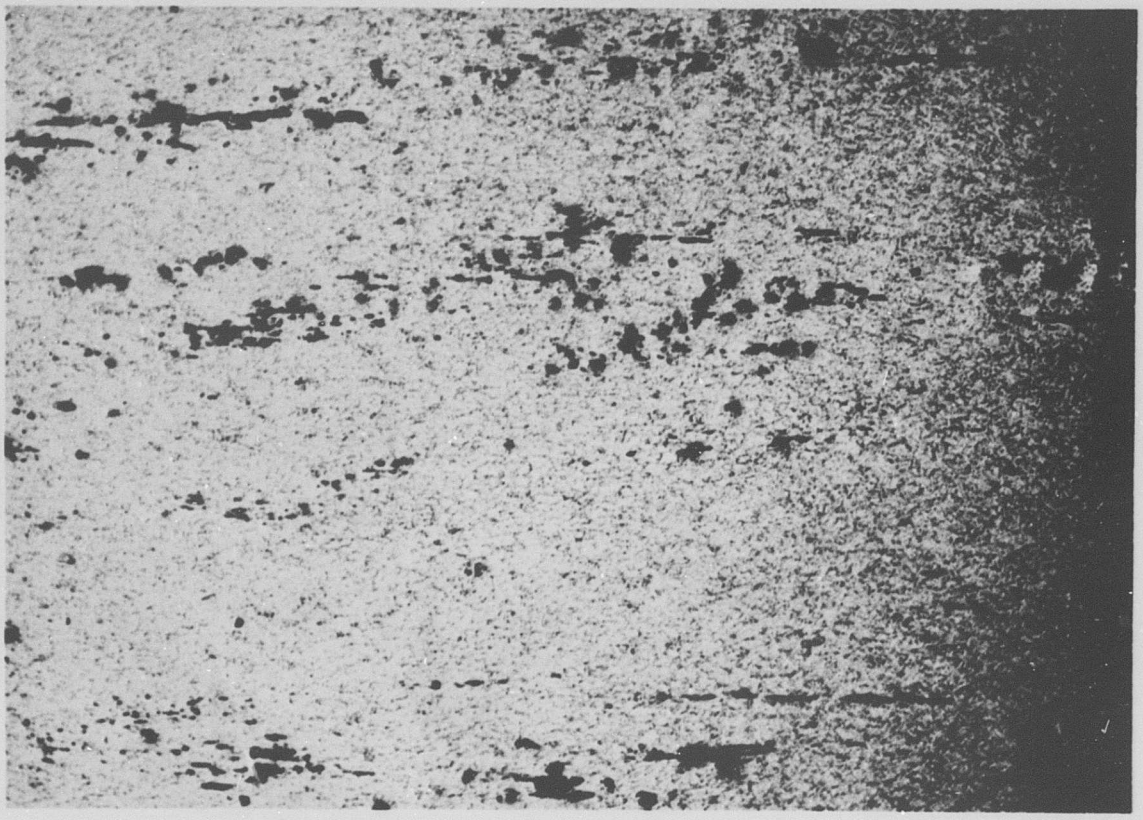

COMMENTS

The austenitic microstructure of a strained area shows large areas of nonmetallic inclusions.

Figure C-114 Stainless Steel 347, Condition L: Optical Micrograph Showing 100X Magnification of General Strained Area

METALLOGRAPHIC STUDY

Material Stainless Steel 347 Neg.No. W80

Specimen LU 702 Neg.Mag. 1,000X

Etchant 10% Amonium Persulfate Photo Enlargement None

COMMENTS

The austenitic microstructure shows carbide dispersion through the matrix.

Figure C-115 Stainless Steel 347, Condition L: Optical Micrograph Showing 1,000X Magnification of General Strained Area

METALLOGRAPHIC STUDY

Material Stainless Steel 347 Neg.No. W69

Specimen LU 702 Neg.Mag. 100X

Etchant 10% Amonium Persulfate Photo Enlargement None

COMMENTS

The optical micrograph of the fracture edge shows the austenitic microstructure with large areas of nonmetallic inclusions.

Figure C-116 Stainless Steel 347, Condition L: Optical Micrograph Showing 100X Magnification of Fracture Edge

METALLOGRAPHIC STUDY

Material Stainless Steel 347 Neg.No. W82

Specimen LU 702 Neg.Mag. 1,000X

Etchant 10% Amonium Persulfate Photo Enlargement None

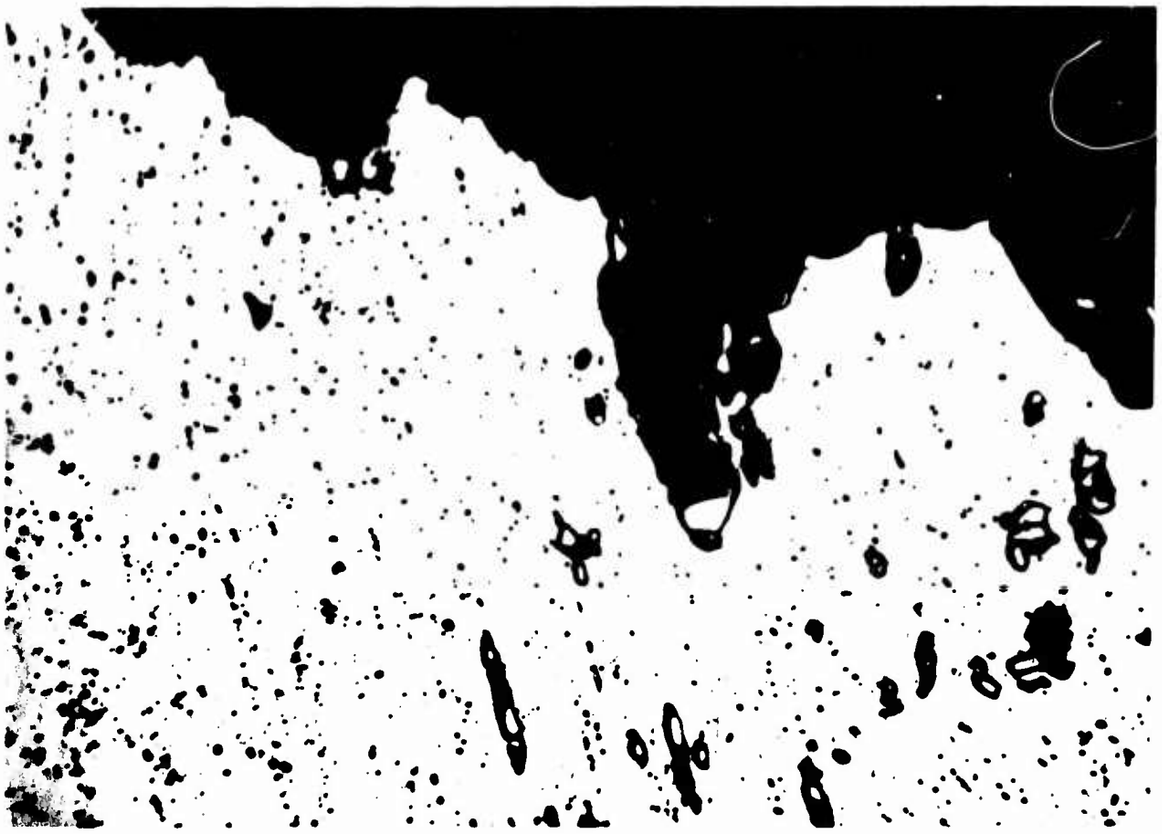

COMMENTS

The micrograph of the fracture edge shows the austenitic structure with large areas of non-metallic inclusions. The fracture is primarily transgranular.

Figure C-117 Stainless Steel 347, Condition L: Optical Micrograph Showing 1,000X Magnification of Fracture Edge

METALLOGRAPHIC STUDY

Material Stainless Steel 347 Neg.No. 103-1

Specimen LU 702 Neg.Mag. 7,500X

Etchant 10% Amonium Persulfate Photo Enlargement 2X

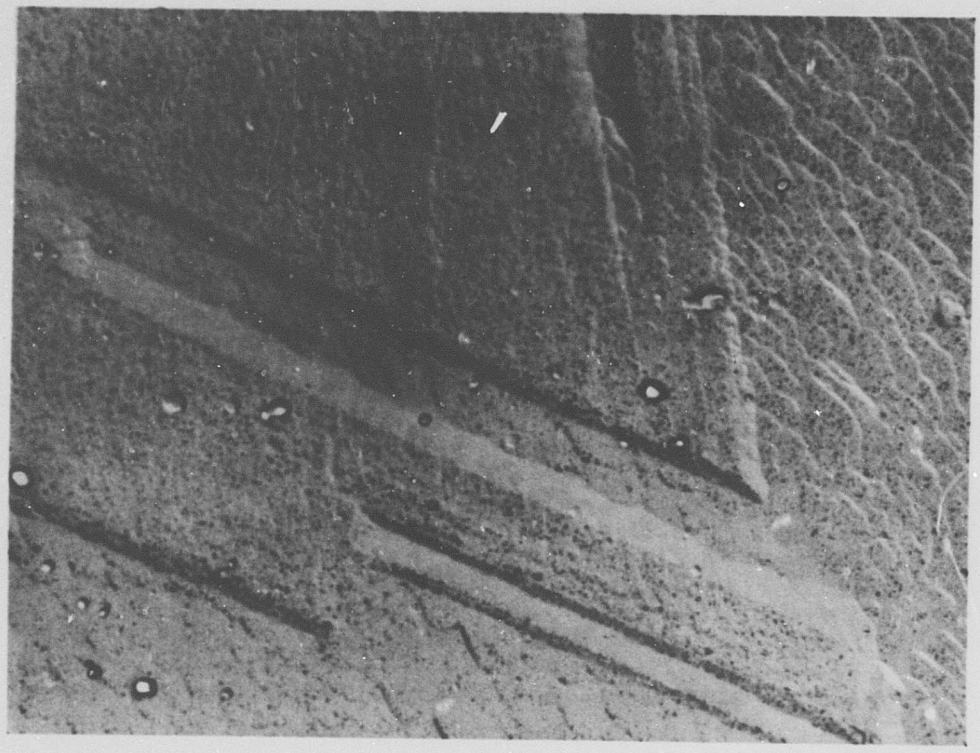

COMMENTS

The structure shows annealing twins in austenite and fine carbide dispersion. The texture reveals grain orientation.

Figure C-118 Stainless Steel 347, Condition L: Electron Micrograph Showing 15,000X Magnification of Unstrained Area

METALLOGRAPHIC STUDY

Material	Stainless Steel 347	Neg.No.	105-5
Specimen	LU 702	Neg.Mag.	7,500X
Etchant	10% Amonium Persulfate	Photo Enlargement	2X

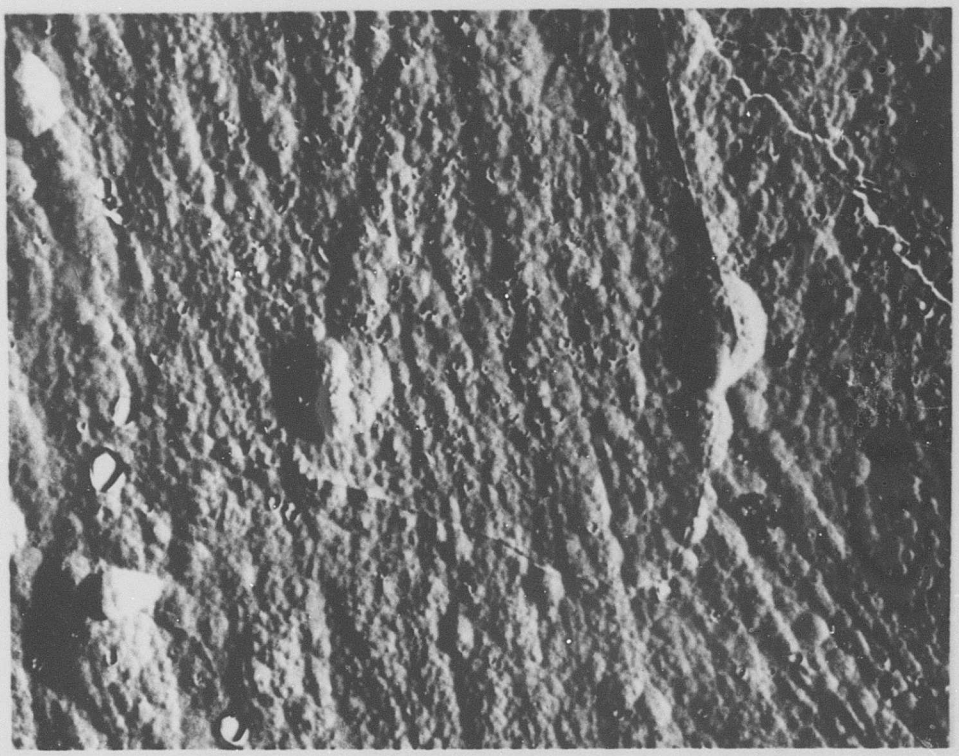

COMMENTS

The general structure shows austenitic grains and grain boundaries. Within the austenite there appears to be at least a partial transformation to martensite. The clearly defined particles are carbides. The large holes are carbides loosened during straining and removed during polishing.

Figure C-119 Stainless Steel 347, Condition L: Electron Micrograph Showing 15,000X Magnification of Strained Area

METALLOGRAPHIC STUDY

Material	Stainless Steel 347	Neg.No.	92-1
Specimen	LU 702	Neg.Mag.	2,100X
Etchant	None	Photo Enlargement	2X

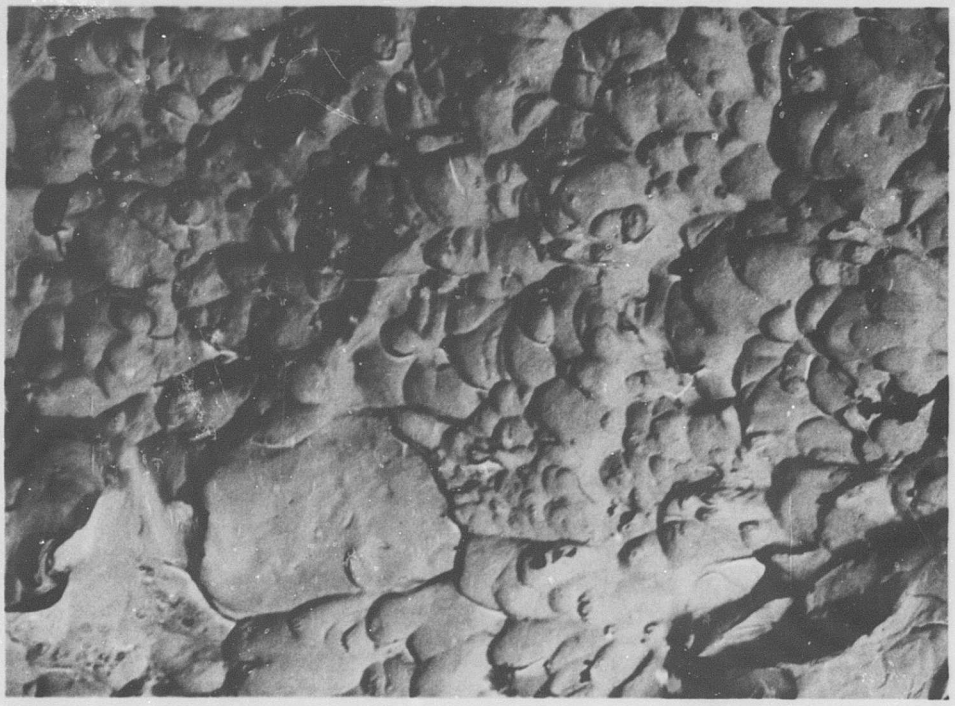

COMMENTS

The fracture surface at the center of the specimen is composed of nonoriented dimples of random size, indicating a ductile failure.

Figure C-120 Stainless Steel 347, Condition L: Electron Fractograph Showing 4,200X Magnification at Center of Fracture

METALLOGRAPHIC STUDY

Material Stainless Steel 347 Neg.No. 92-4

Specimen LU 702 Neg.Mag. 2,100X

Etchant None Photo Enlargement 2X

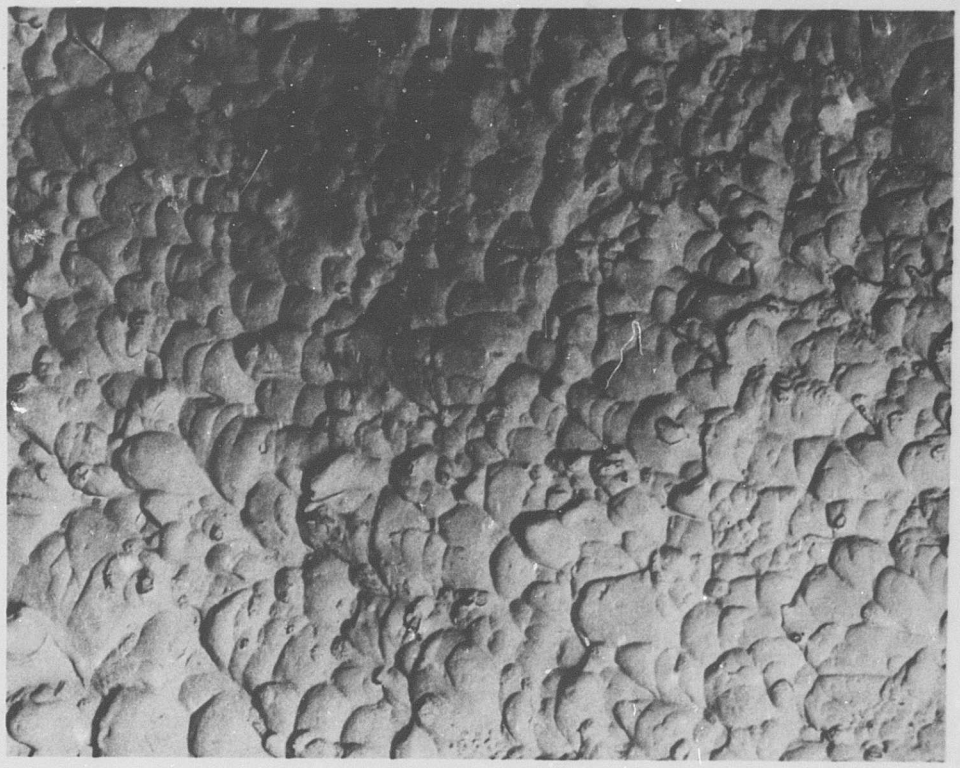

COMMENTS

The fracture surface near the edge of the specimen is composed of oriented dimples typical of a ductile shear failure. Many of the dimples contain particles, probably carbides.

Figure C-121 Stainless Steel 347, Condition L: Electron Fractograph Showing 4,200X Magnification Near Edge of Fracture

METALLOGRAPHIC STUDY

Material Stainless Steel 347 Neg.No. 97-9

Specimen LN 705 Neg.Mag. 2,100X

Etchant None Photo Enlargement 2X

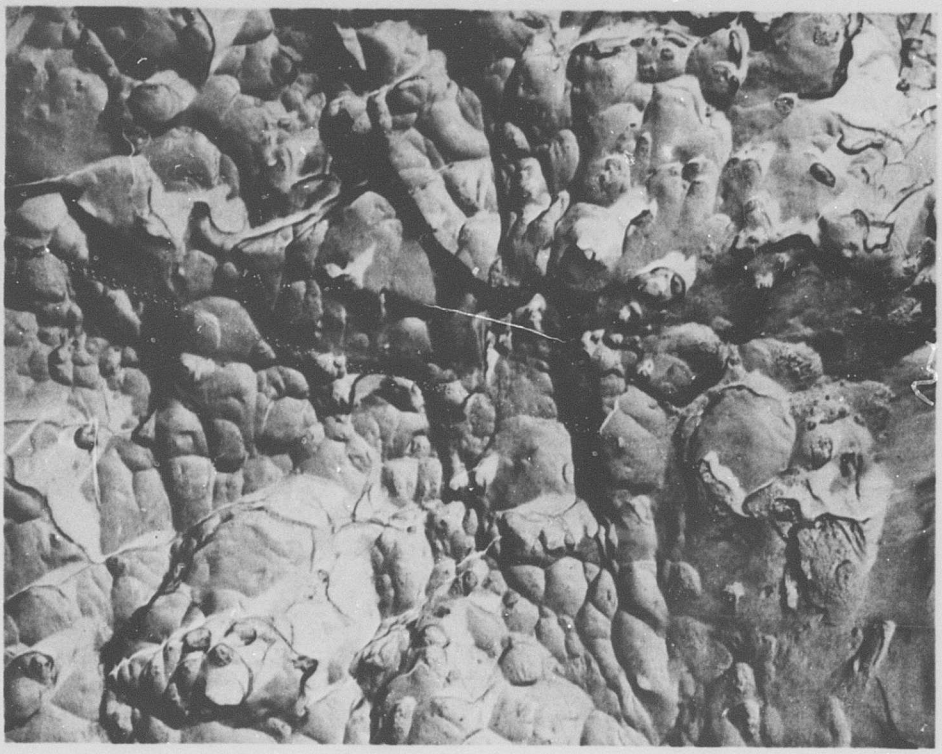

COMMENTS

The fractograph shows a completely microvoid type of fracture, indicating a ductile failure mode. The pitted appearance is probably due to oxidation.

Figure C-122 Stainless Steel 347, Condition L: Electron Fractograph Showing 4,200X Magnification of Notched Fracture

Stainless Steel 347
Condition LW

BLANK PAGE

Table C-19

Tensile and Shear Test Data

Material Stainless Steel 347 Specimen Condition LW

Averaged Data (-423°F)		
Unnotched Specimens	Control	Irradiated
Ultimate Strength (ksi)	224.2	229.5
0.2% Yield Strength (ksi)	97.0	63.0
Elongation in Gage Length (%)	27.1	28.2
Reduction in Area (%)	20.8	23.7
Ultimate Shear Strength (ksi)	152.4	150.2
Notched Specimens		
Ultimate Strength (ksi)	136.5	126.9
Ratios		
Notched-Ult./Unnotched-Ult.	0.61	0.55
Notched-Ult./Unnotched-Yield	1.41	2.01

Unnotched Specimens				
Specimen Number	Ult. Tensile Strength(ksi)	Yield Strength 0.2% Offset (ksi)	Reduction in Area (%)	Elongation (%)
198	227.0	60.0	35.2	26.4
200	226.5	63.0	19.1	26.7
202	224.3	54.0	20.0	29.5
204	240.1	75.0	20.3	30.0

Notched Specimens		Shear Specimens*	
Specimen Number	Ult. Tensile Strength (ksi)	Specimen Number	Ult. Shear Strength (ksi)
210	125.3		
212	124.8		
214	130.5		
216	Broke on rebound		

*Not Applicable

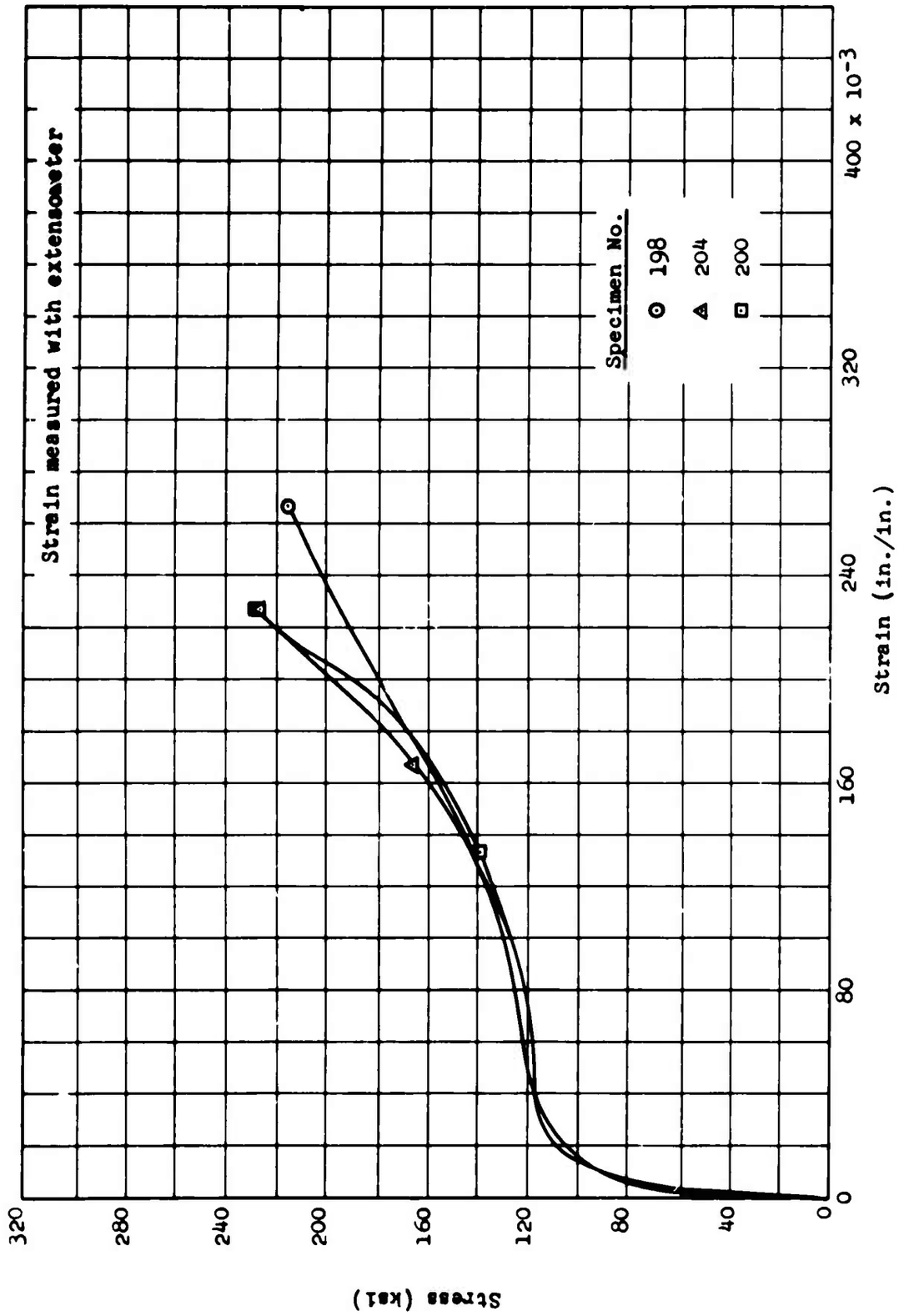

Figure C-123 Stainless Steel 347, Condition LWU: Stress-Strain Curves

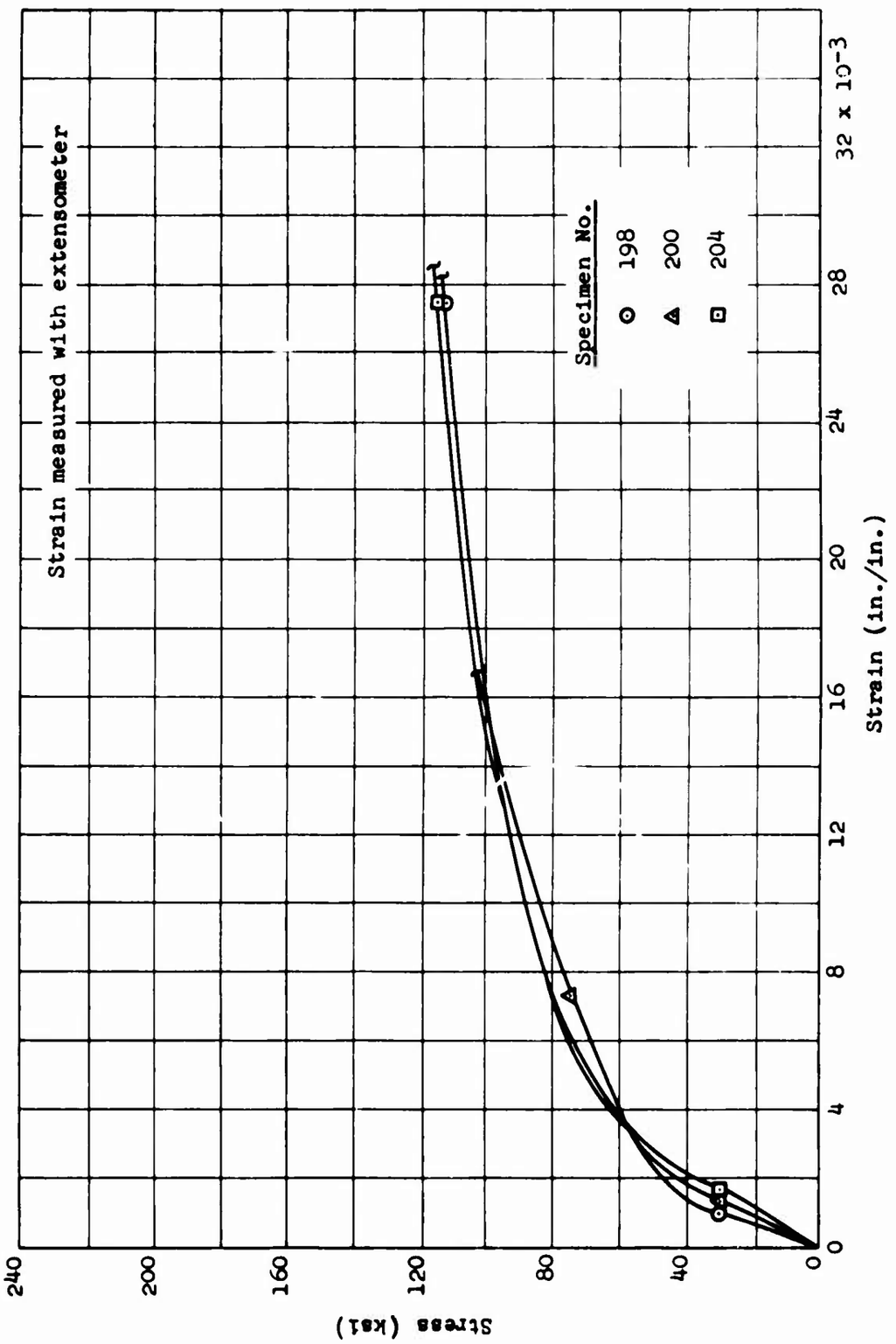

Figure C-124 Stainless Steel 347, Condition LWU: Stress-Strain Curves (Expanded Scale)

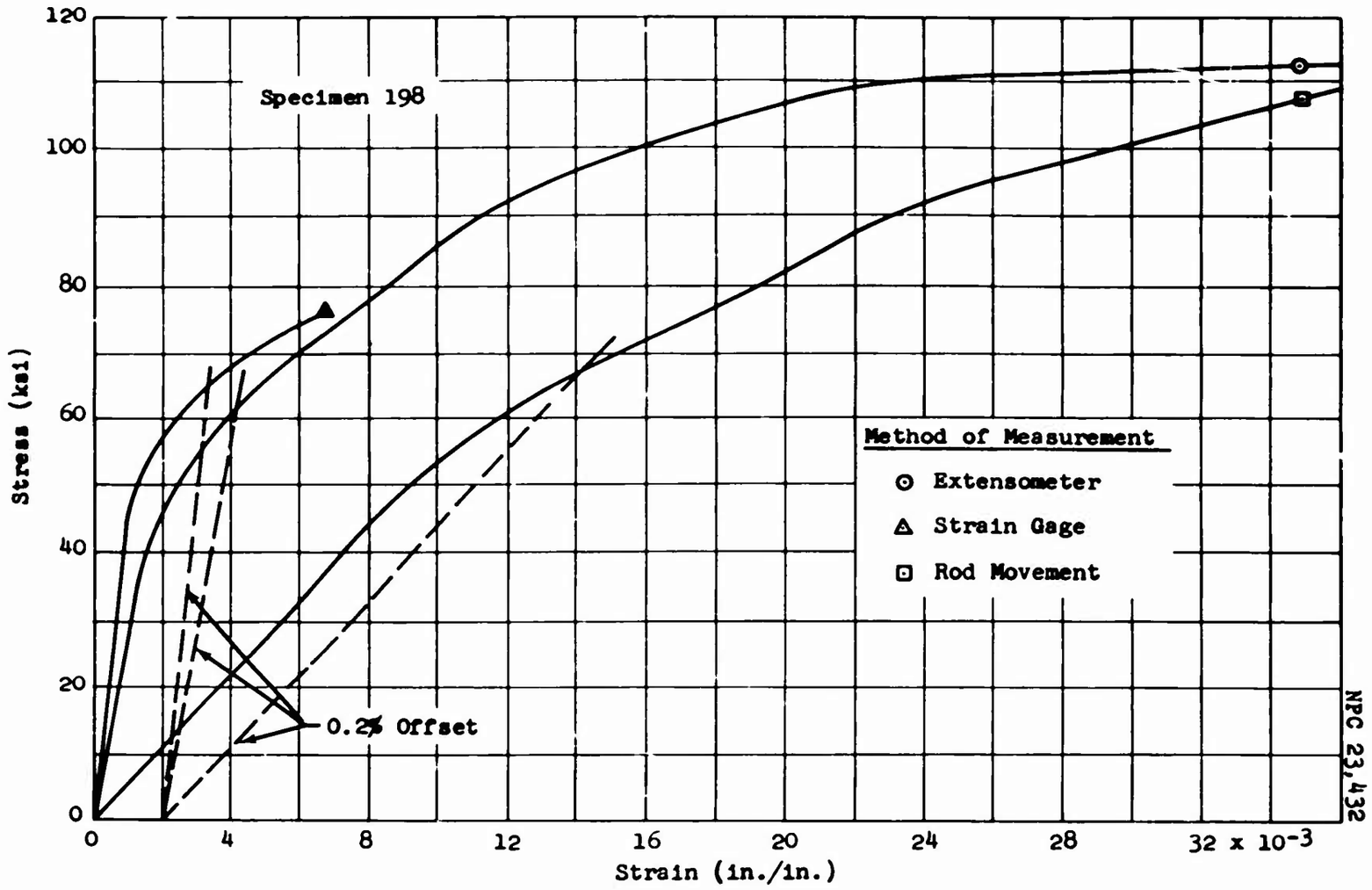

Figure C-125 Stainless Steel 347, Condition LWU: Comparison of Strain-Measurement Methods

Table C-20

X-Ray Diffraction Data

Material Stainless Steel 347 Specimen LWU 204

	STRAINED AREA		UNSTRAINED AREA	
DIFFRACTION PATTERN				
Miller Indices (hkl)	Interlattice Spacing, d (Å)	Relative Intensity (%)	Interlattice Spacing, d (Å)	Relative Intensity (%)
111			2.07	100
110	2.03	100		
200	1.44	25	1.80	60
220			1.27	15
211	1.17	40	1.08	20

LATTICE PARAMETER (Å)		
111	-	3.59
110	2.87	-
200	2.88	3.60
220	-	3.59
211	2.87	2.64

MICROSTRESS, $\Delta\theta$	
0.32° ($2\theta = 52.4^\circ$)	0.15° ($2\theta = 51.1^\circ$)
No Peak ($2\theta = 129^\circ$)	No Peak ($2\theta = 129^\circ$)

METALLOGRAPHIC STUDY

Material Stainless Steel 347 Neg.No. None

Specimen LWU 204 Neg.Mag. 3X

Etchant None Photo Enlargement None

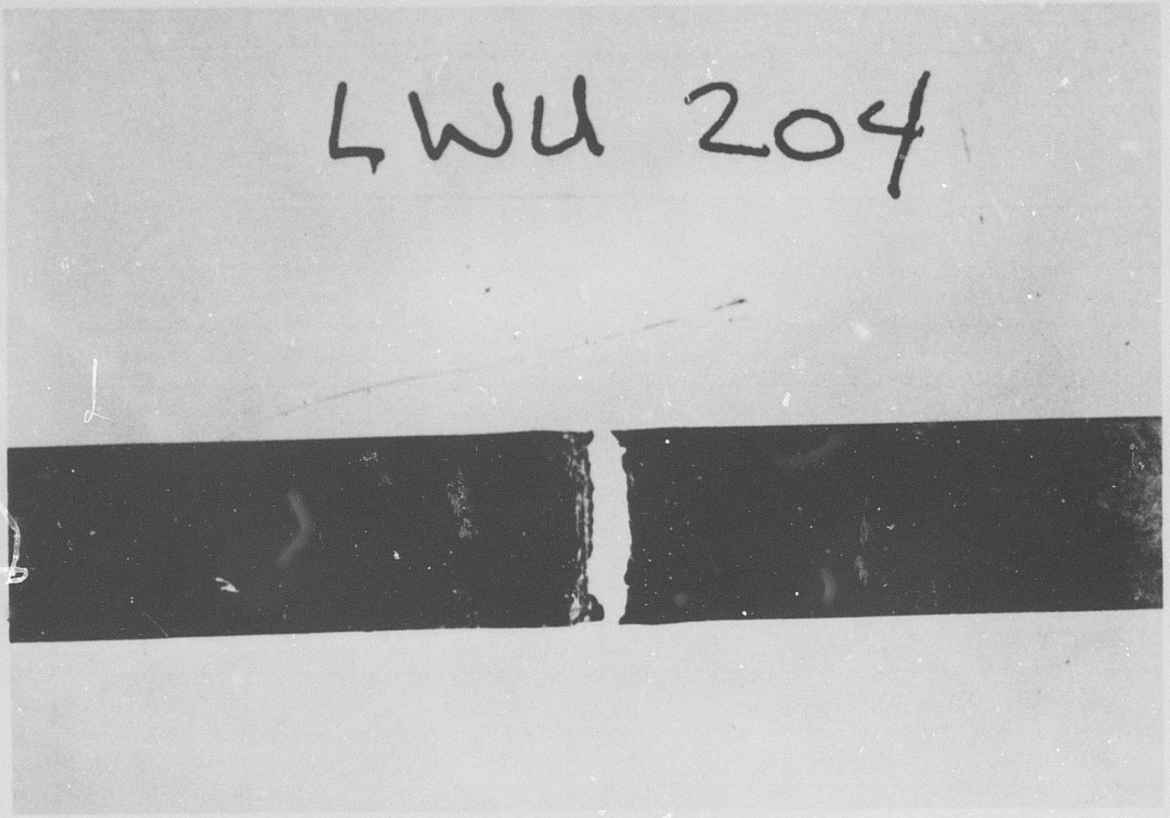

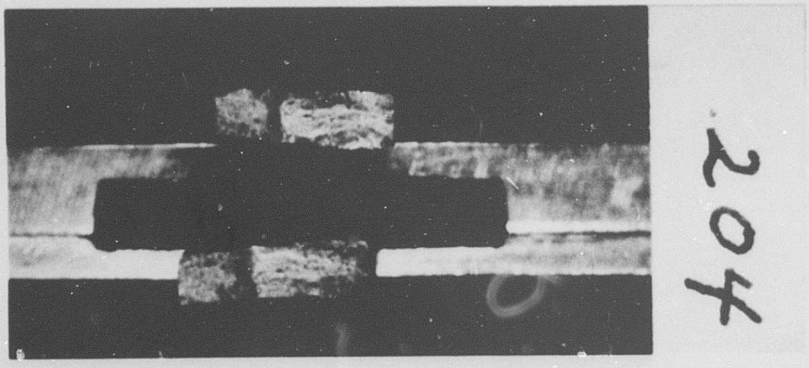

Figure C-126 Stainless Steel 347, Condition LW: Macrophotograph Showing 3X Magnification of Specimen

METALLOGRAPHIC STUDY

Material Stainless Steel 347 Neg.No. W17

Specimen LWU 204 Neg.Mag. 100X

Etchant 10% Amonium Persulfate Photo Enlargement None

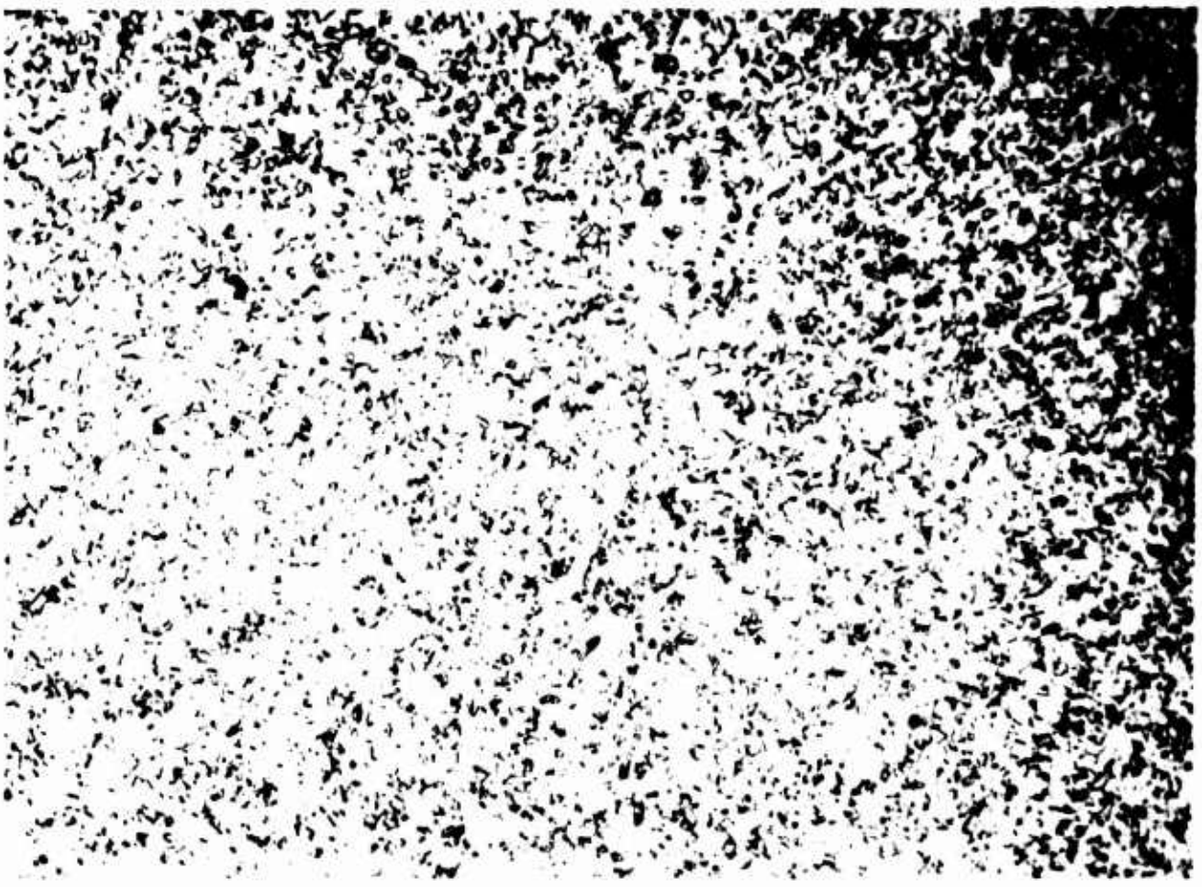

COMMENTS

The microstructure comprises an austenitic (gamma phase) matrix with fine carbides.

Figure C-127 Stainless Steel 347, Condition LW: Optical Microphotograph Showing 100X Magnification of Unstrained Area

METALLOGRAPHIC STUDY

Material	Stainless Steel 347	Neg.No.	W22
Specimen	LWU 204	Neg.Mag.	1,000X
Etchant	10% Amonium Persulfate	Photo Enlargement	None

COMMENTS

The microstructure shows an austenitic matrix with fine carbides. Annealing twins are seen through the austenite grain.

Figure C-128 Stainless Steel 347, Condition LW: Optical Micrograph Showing 1,000X Magnification of Unstrained Area

METALLOGRAPHIC STUDY

Material Stainless Steel 347 Neg.No. W2

Specimen LWU 204 Neg.Mag. 100X

Etchant 10% Amonium Persulfate Photo Enlargement None

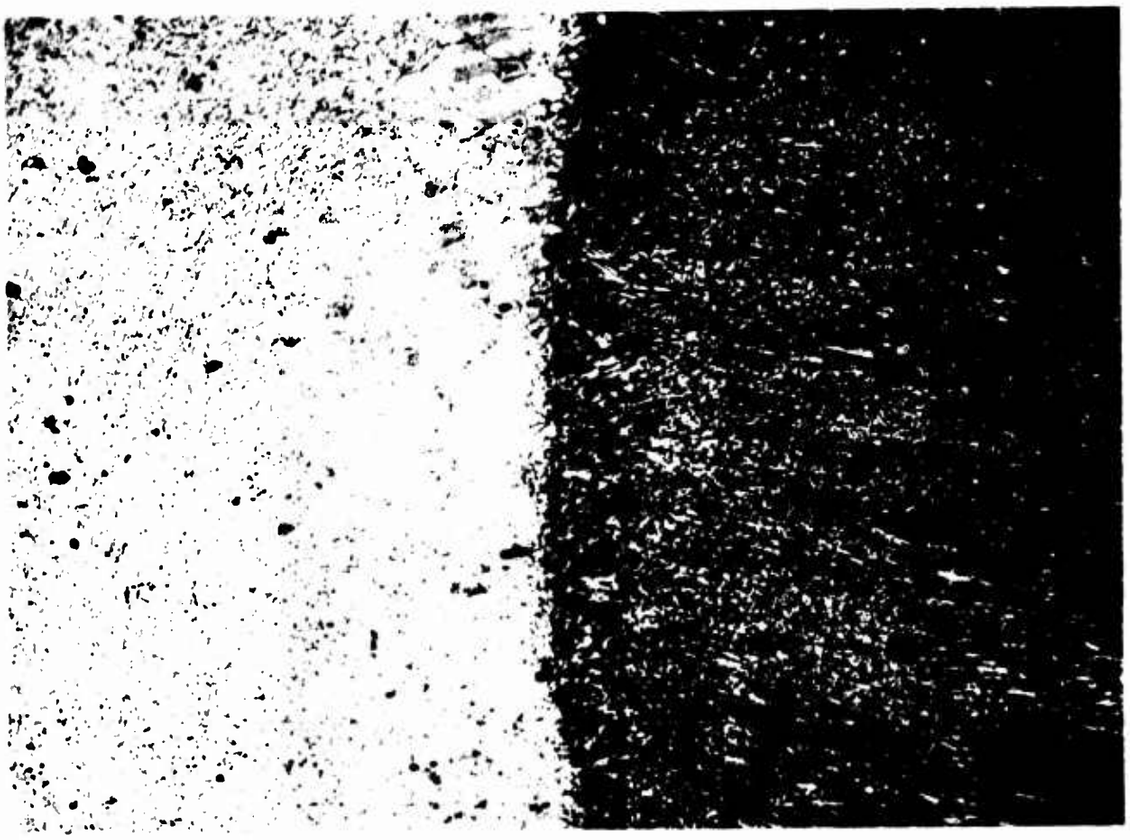

COMMENTS

The microstructure represents an austenite-ferrite matrix in the weld area, transition zone of austenite grain growth, and the austenite parent-metal matrix with fine carbide plus nonmetallic inclusions.

Figure C-129 Stainless Steel 347, Condition LW: Optical Micrograph Showing 100X Magnification of Parent Metal and Weld Interface

METALLOGRAPHIC STUDY

Material	Stainless Steel 347	Neg.No.	W74
Specimen	LWU 204	Neg.Mag.	1,000X
Etchant	10% Amonium Persulfate	Photo Enlargement	None

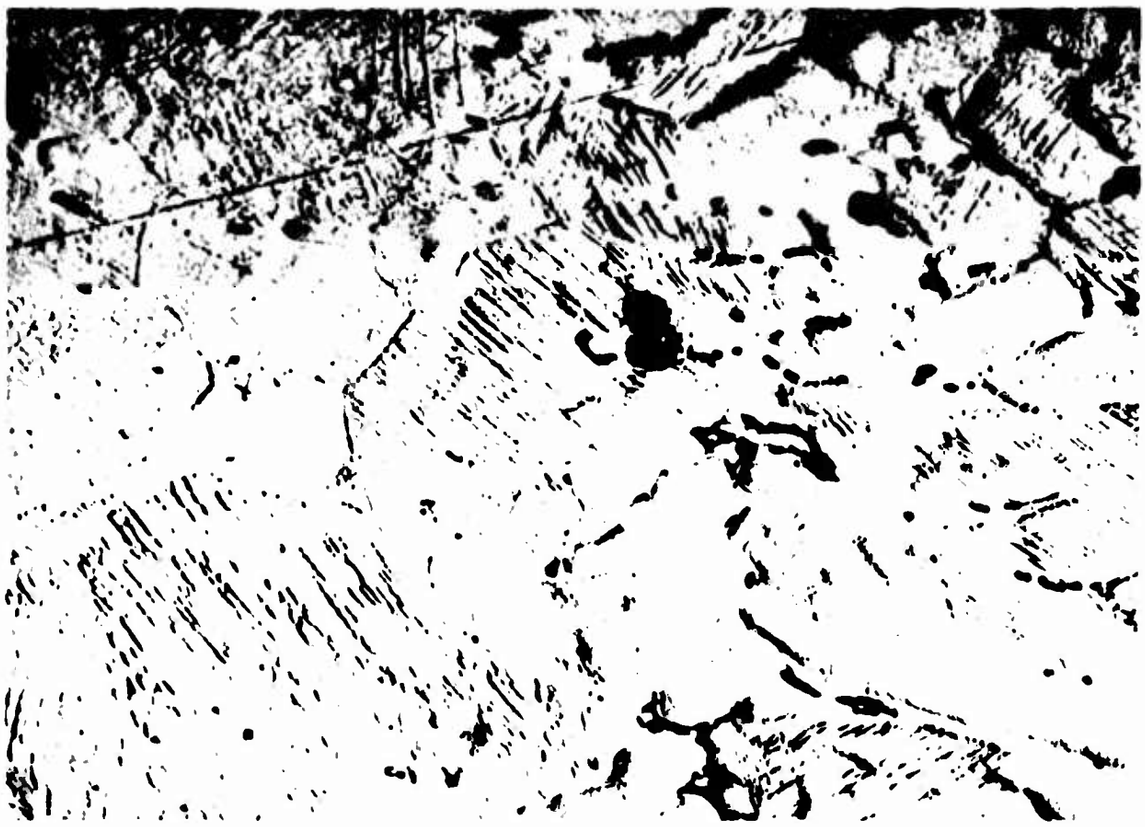

COMMENTS

The microstructure shows the transformed phase with the Cr-Fe phase at the grain boundaries in the weld area. The parent-metal microstructure (left) is transformed austenite (martensite). Note the strain lines.

Figure C-130 Stainless Steel 347, Condition LW: Optical Micrograph Showing 1,000X Magnification of Parent Metal and Weld Interface

METALLOGRAPHIC STUDY

Material Stainless Steel 347 Neg.No. W3

Specimen LWU 204 Neg.Mag. 100X

Etchant 10% Amonium Persulfate Photo Enlargement None

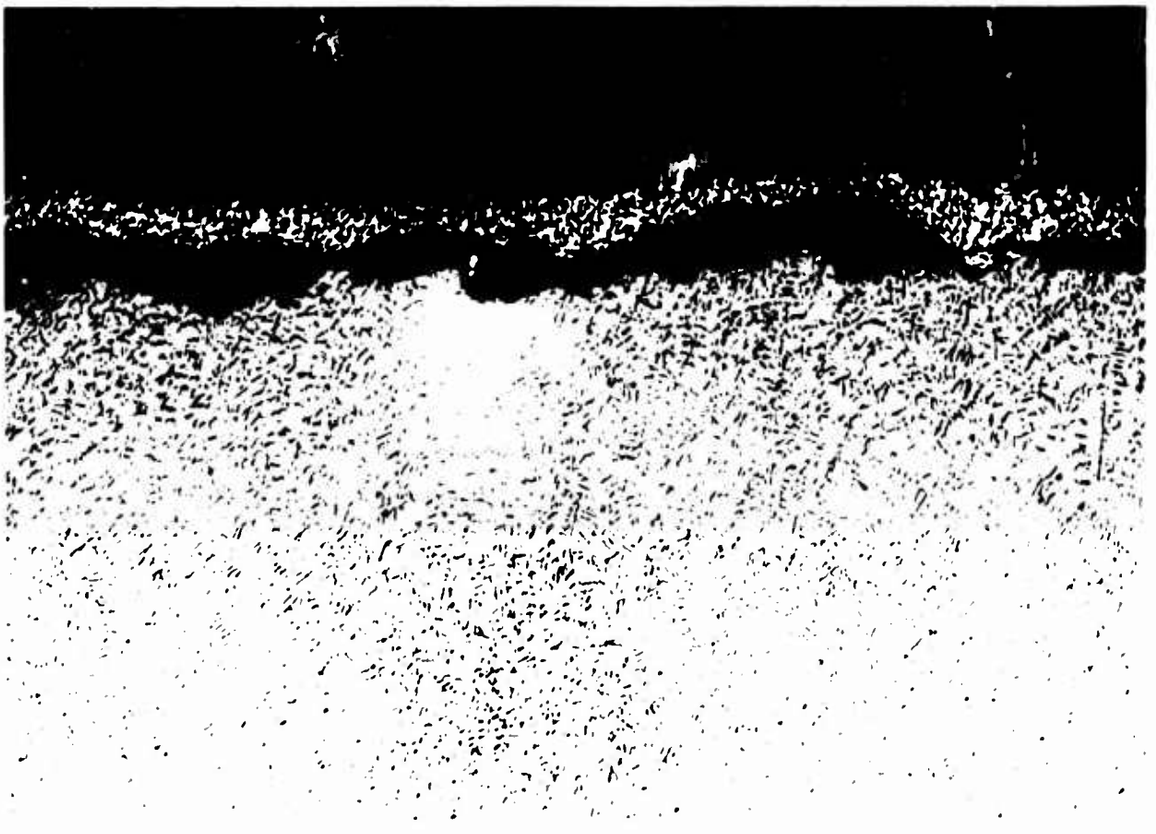

COMMENTS

The microstructure represents an austenite-ferrite matrix. Failure occurred through the weld metal.

Figure C-131 Stainless Steel 347, Condition LW: Optical Micrograph Showing 100X Magnification of Fracture Edge

METALLOGRAPHIC STUDY

Material	Stainless Steel 347	Neg.No.	W75
Specimen	LWU 204	Neg.Mag.	1,000X
Etchant	10% Amonium Persulfate	Photo Enlargement	None

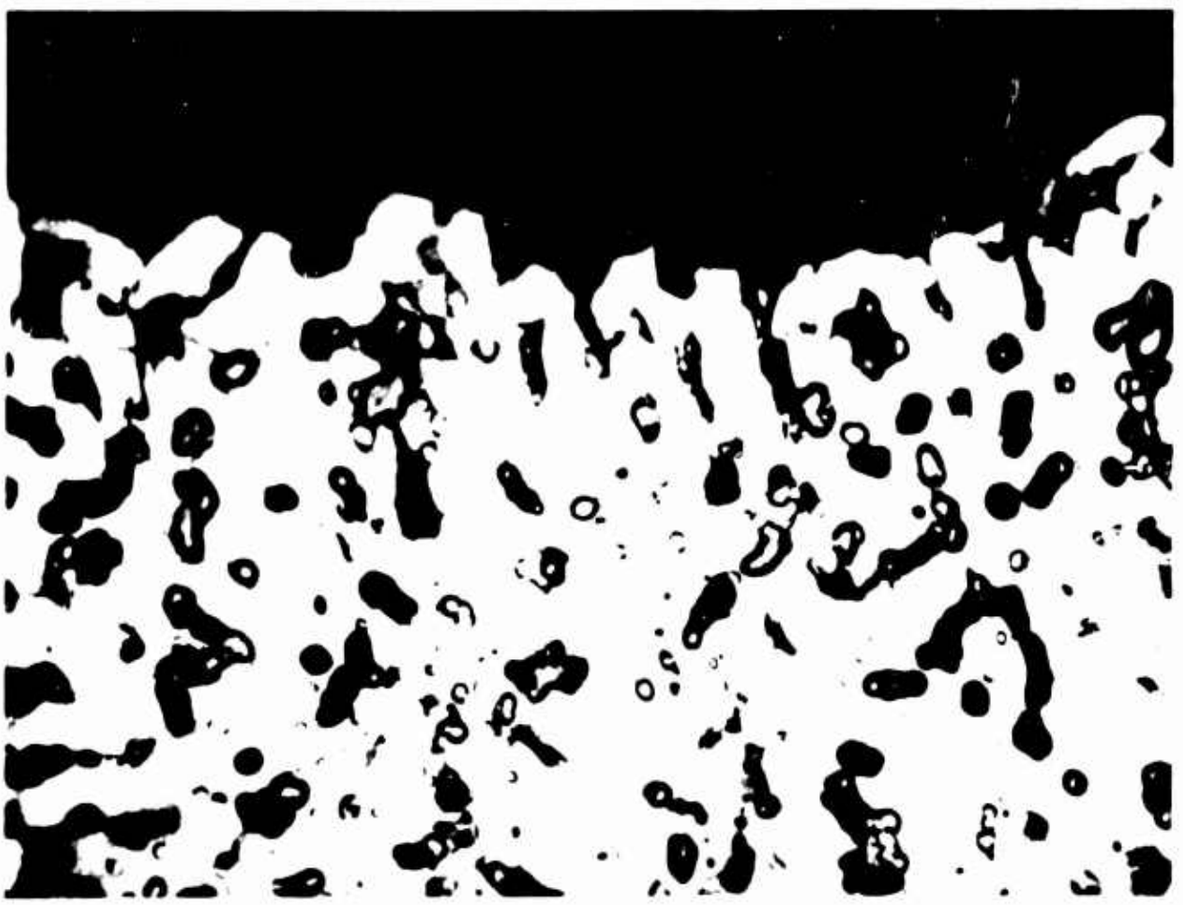

COMMENTS

The microstructure shows a transgranular fracture of the matrix. The high Cr-Fe phase lies at the grain boundary.

Figure C-132 Stainless Steel 347, Condition LW: Optical Micrograph Showing 1,000X Magnification of Fracture Edge

METALLOGRAPHIC STUDY

Material Stainless Steel 347 Neg.No. 102-10

Specimen LWU 204 Neg.Mag. 7,500X

Etchant 10% Amonium Persulfate Photo Enlargement 2X

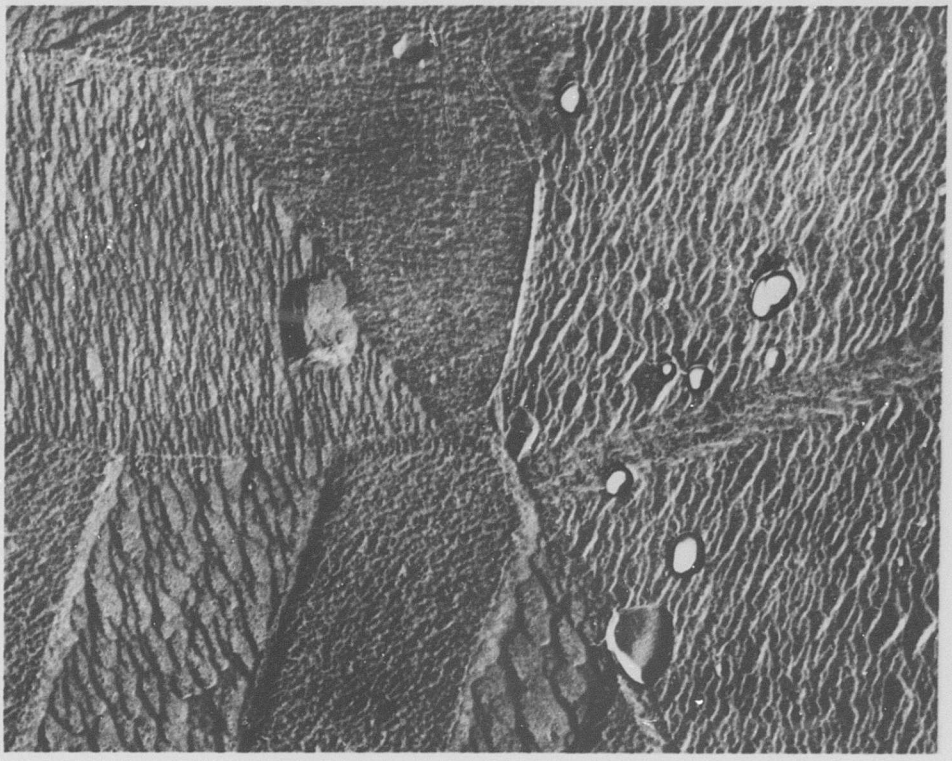

COMMENTS

The structure is austenite with annealing twins, carbides, and orientation texture.

Figure C-133 Stainless Steel 347, Condition LW: Electron Micrograph Showing 15,000X Magnification of Unstrained Area

METALLOGRAPHIC STUDY

Material Stainless Steel 347 Neg.No. 105-9

Specimen LWU 204 Neg.Mag. 7,500X

Etchant 10% Amonium Persulfate Photo Enlargement 2X

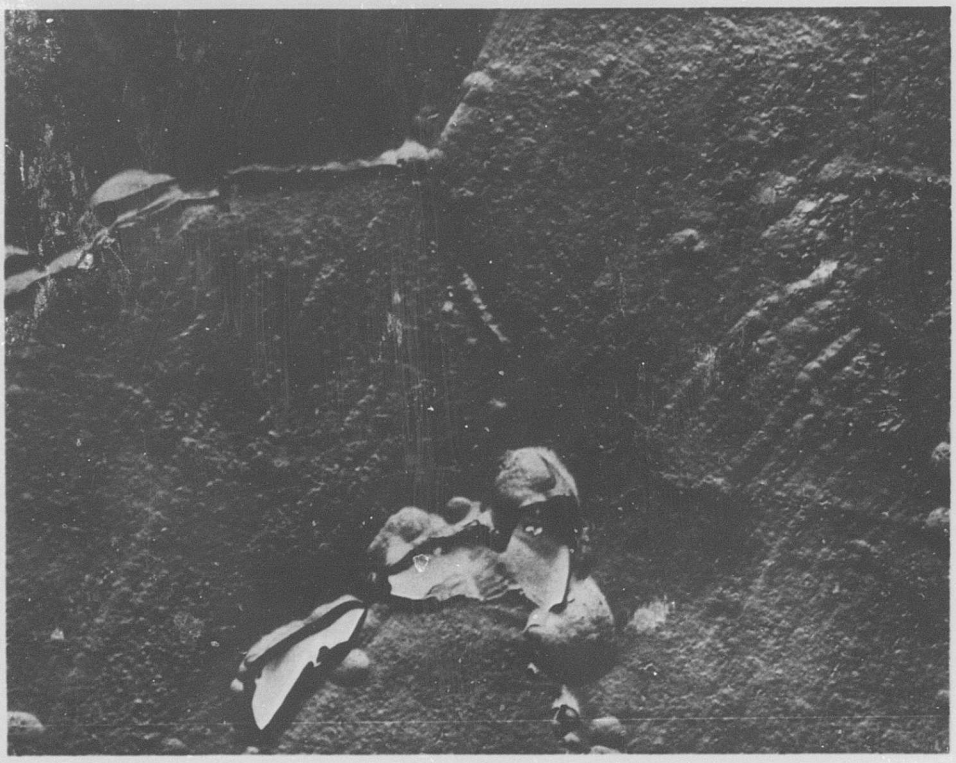

COMMENTS

The chromium-rich ferrite phase appears in the grain boundaries of the transformed austenite (martensite) phase.

Figure C-134 Stainless Steel 347, Condition LW: Electron Micrograph Showing 15,000X Magnification of Strained Area

METALLOGRAPHIC STUDY

Material Stainless Steel 347 Neg.No. 93-6

Specimen LWU 204 Neg.Mag. 2,100X

Etchant None Photo Enlargement 2X

COMMENTS

The fracture at the center is made up of microvoid and intergranular fractures. The intergranular facet in the center of the photograph shows a brittle ferrite particle that failed and was removed during replication. The smaller round particles present on the fracture represent carbides.

Figure C-135 Stainless Steel 347, Condition LW: Electron Fractograph Showing 4,200X Magnification at Center of Fracture

METALLOGRAPHIC STUDY

Material Stainless Steel 347 Neg.No. 93-8

Specimen LWU 204 Neg.Mag. 2,100X

Etchant None Photo Enlargement 2X

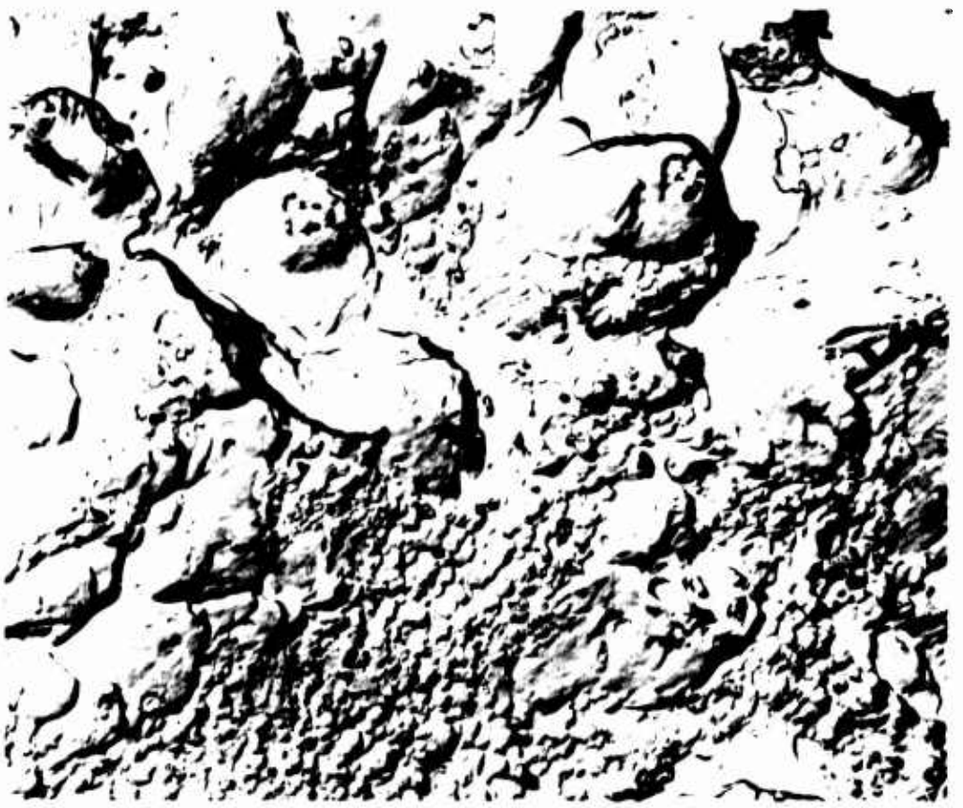

COMMENTS

The fracture at the edge of the specimen is made up of large and small oriented dimples, typical of a shear type of fracture. Some of the large dimples at the top of the photo have fractured ferrites at the tip. The smaller round particles in the dimples represent carbides.

Figure C-136 Stainless Steel 347, Condition LW: Electron Fractograph Showing 4,200X Magnification Near Edge of Fracture

METALLOGRAPHIC STUDY

Material Stainless Steel 347 Neg.No. 98-5

Specimen LWN 210 Neg.Mag. 2,100X

Etchant None Photo Enlargement 2X

COMMENTS

The fracture is composed mainly of quasi-cleavage facets; however, some small dimples are present. There are indications of plastic flow at the edge of the cleavage facets, indicating a semi-brittle rather than completely brittle failure mode.

Figure C-137a Stainless Steel 347, Condition LW: Electron Fractograph Showing 4,200X Magnification of Notched Fracture

METALLOGRAPHIC STUDY

Material Stainless Steel 347 Neg.No. 98-4

Specimen LWN 210 Neg.Mag. 2,100X

Etchant None Photo Enlargement 2X

COMMENTS

The fracture is composed mainly of large dimples, indicating that the fracture was ductile in this local area. Near the upper right-hand corner is an area that indicates localized segregation during welding and the fracture follows the cast structure produced. The pitted appearance that is present in isolated areas is oxidation.

Figure C-137b Stainless Steel 347, Condition LW: Electron Fractograph Showing 4,200X Magnification of Notched Fracture

Stainless Steel 440C
Condition L

BLANK PAGE

Table C-21

Tensile and Shear Test Data

Material Stainless Steel 440C Specimen Condition L

Averaged Data (-423°F)		
	Control	Irradiated
Unnotched Specimens		
Ultimate Strength (ksi)	The control specimens broke in such a way that tensile properties could not be measured satisfactorily.	All irradiated specimens failed in the grips.
0.2% Yield Strength (ksi)		
Elongation in Gage Length (%)		
Reduction in Area (%)		
Ultimate Shear Strength (ksi)		
Notched Specimens		
Ultimate Strength (ksi)		50.6
Ratios		
Notched-Ult./Unnotched-Ult.		
Notched-Ult./Unnotched-Yield		

Unnotched Specimens				
Specimen Number	Ult. Tensile Strength(ksi)	Yield Strength 0.2% Offset (ksi)	Reduction in Area (%)	Elongation (%)

Notched Specimens		Shear Specimens	
Specimen Number	Ult. Tensile Strength (ksi)	Specimen Number	Ult. Shear Strength (ksi)
604	51.4		
606	58.9		
608	49.3		
610	43.1		

METALLOGRAPHIC STUDY

Material Stainless Steel 440C Neg.No. None

Specimen LU 2-198 Neg.Mag. 1X

Etchant None Photo Enlargement None

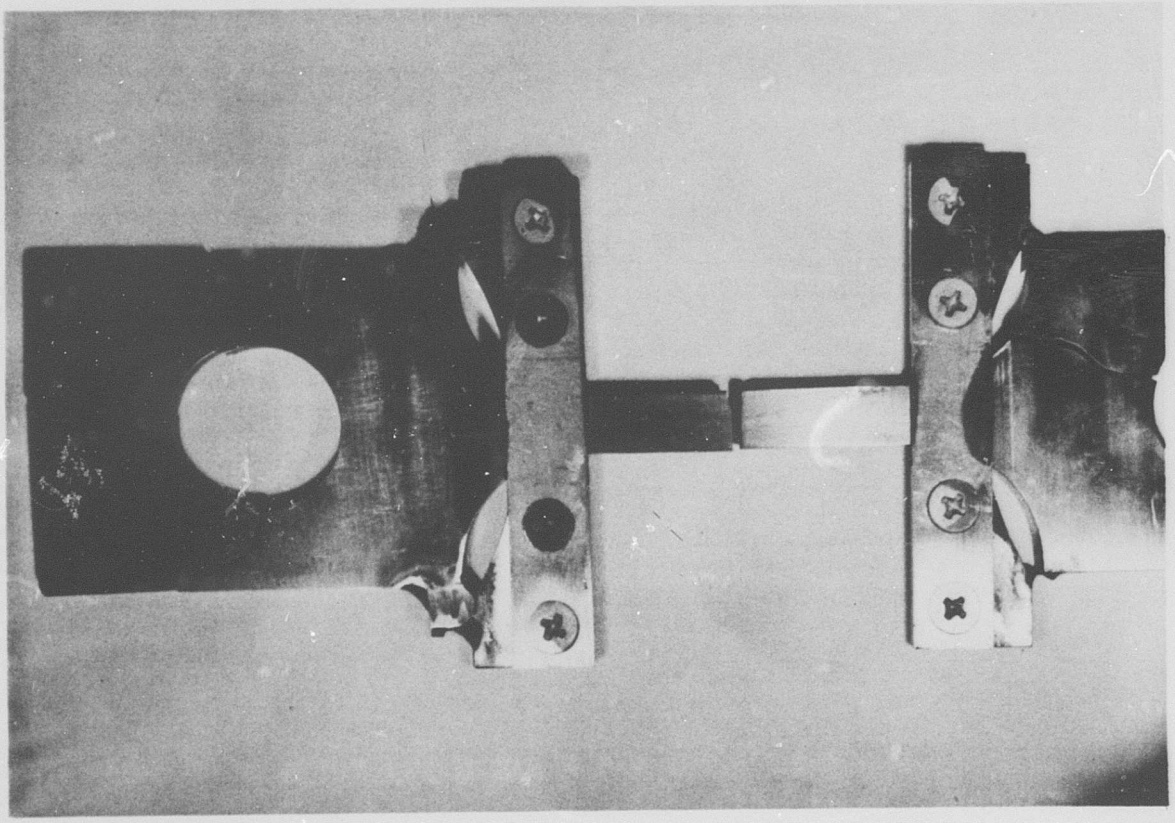

Figure C-138 Stainless Steel 440C, Condition L: Macrophotograph Showing 1X Magnification of Specimen

METALLOGRAPHIC STUDY

Material Stainless Steel 440C Neg.No. 98-6

Specimen LN 604 Neg.Mag. 2,100X

Etchant None Photo Enlargement 2X

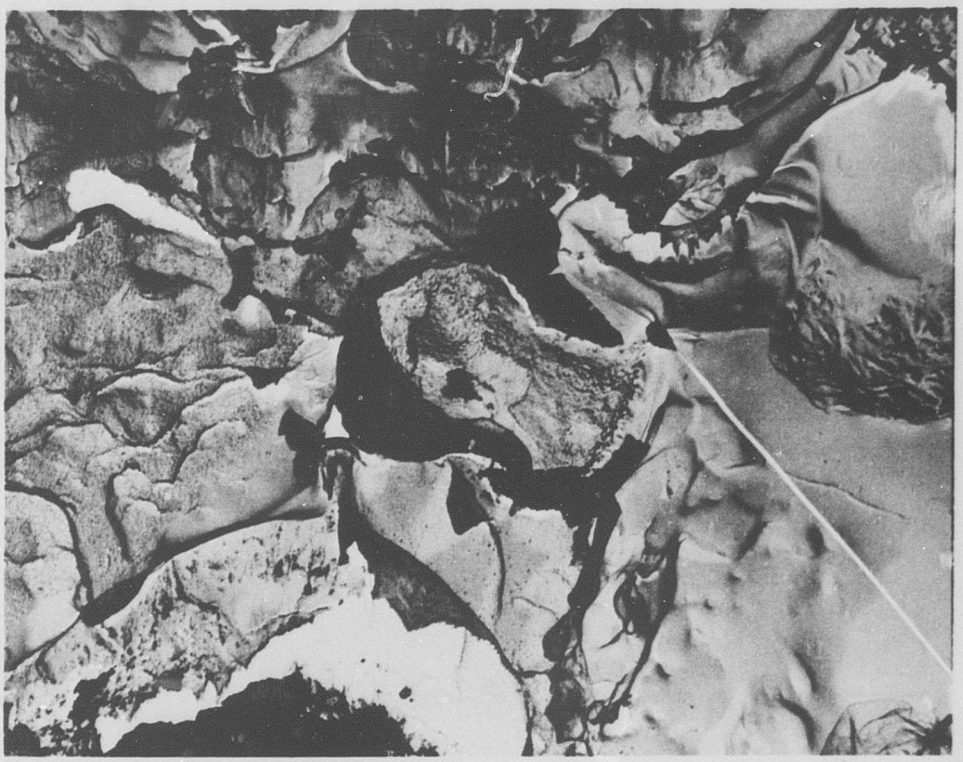

COMMENTS

The fracture surface indicates a failure through and around the brittle carbides and a low ductility fracture at the matrix. The area adjacent to the black extracted carbide is oxidized, probably as a result of depletion of the chromium during the carbide formation.

Figure C-139 Stainless Steel 440C, Condition L: Electron Fractograph Showing 4,200X Magnification of Notched Fracture

Stainless Steel A-286
Condition L

Table C-22

Tensile and Shear Test Data

Material Stainless Steel A-286 Specimen Condition L

Averaged Data (-423°F)		
Unnotched Specimens	**Control**	**Irradiated**
Ultimate Strength (ksi)	223.6	219.8
0.2% Yield Strength (ksi)	135.9	137.0
Elongation in Gage Length (%)	37.5	26.5
Reduction in Area (%)	31.0	32.2
Ultimate Shear Strength (ksi)	168.2	157.1
Notched Specimens		
Ultimate Strength (ksi)	185.8	188.6
Ratios		
Notched- Ult./Unnotched-Ult.	0.83	0.86
Notched- Ult./Unnotched- Yield	1.37	1.38

Unnotched Specimens				
Specimen Number	Ult. Tensile Strength(ksi)	Yield Strength 0.2% Offset (ksi)	Reduction in Area (%)	Elongation (%)
210	222.2	129.0	34.9	20.7
211	214.6	142.0	30.8	22.8
213	221.8	137.0	29.6	30.8
214	220.4	140.0	33.3	31.8

Notched Specimens		Shear Specimens	
Specimen Number	Ult. Tensile Strength (ksi)	Specimen Number	Ult. Shear Strength (ksi)
221	190.6	1	162.8
222	188.6	2	152.9
225	186.9	3	155.6
226	188.2	4	No Data*

*Ram Bottomed Out

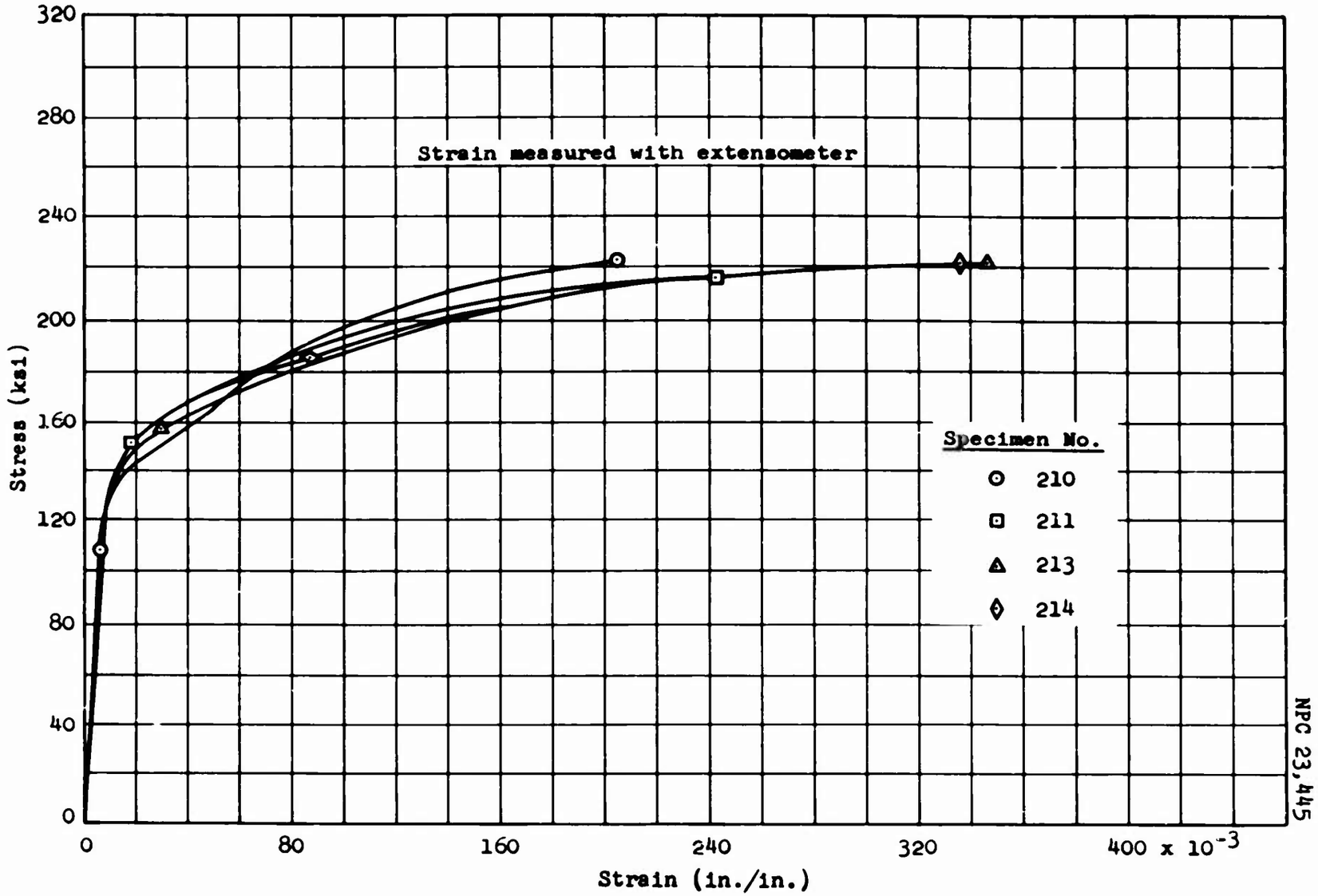

Figure C-140 Stainless Steel A-286, Condition LU: Stress-Strain Curves

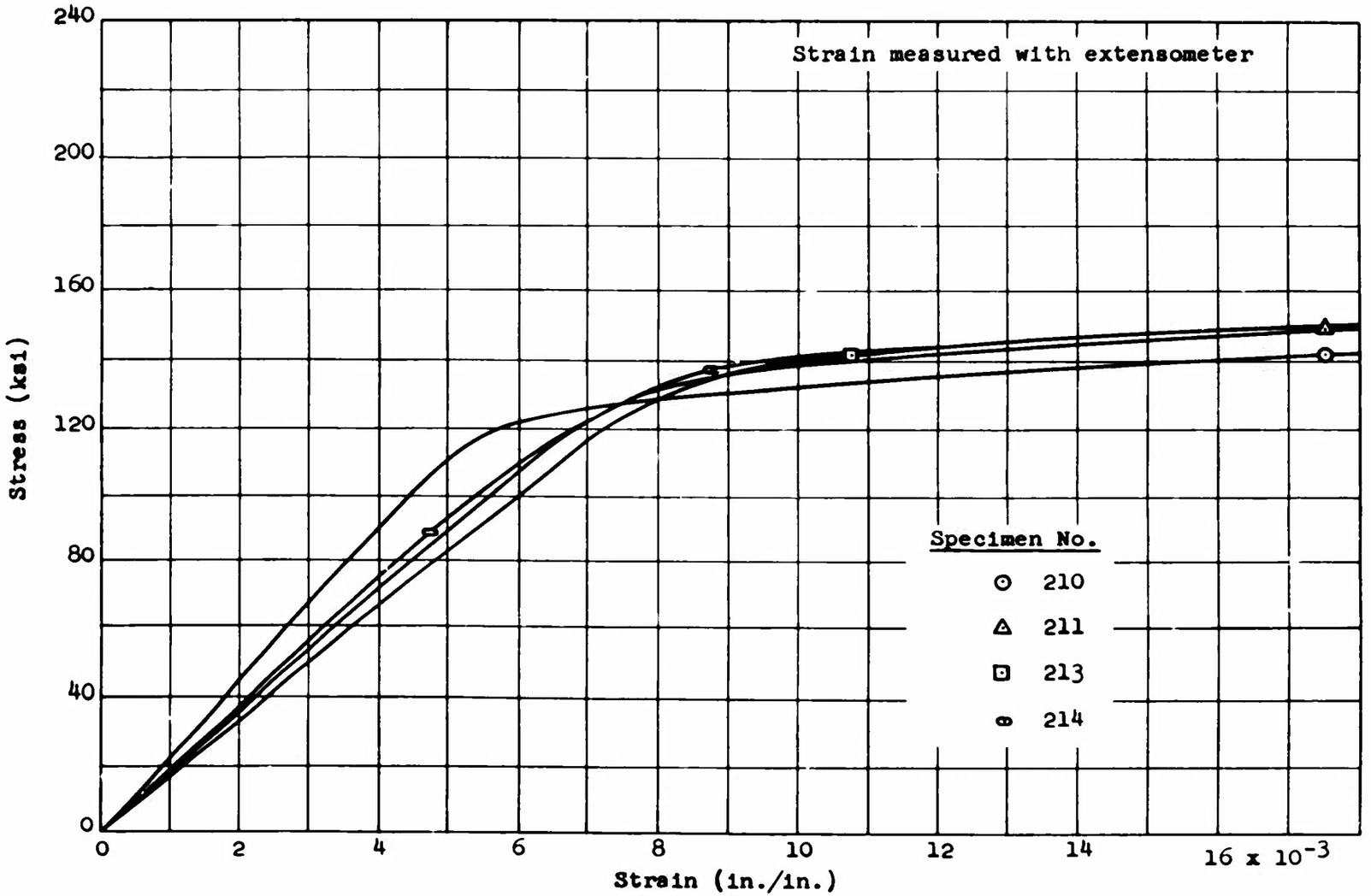

Figure C-141 Stainless Steel A-286, Condition LU: Stress-Strain Curves (Expanded Scale)

NPC 23,423

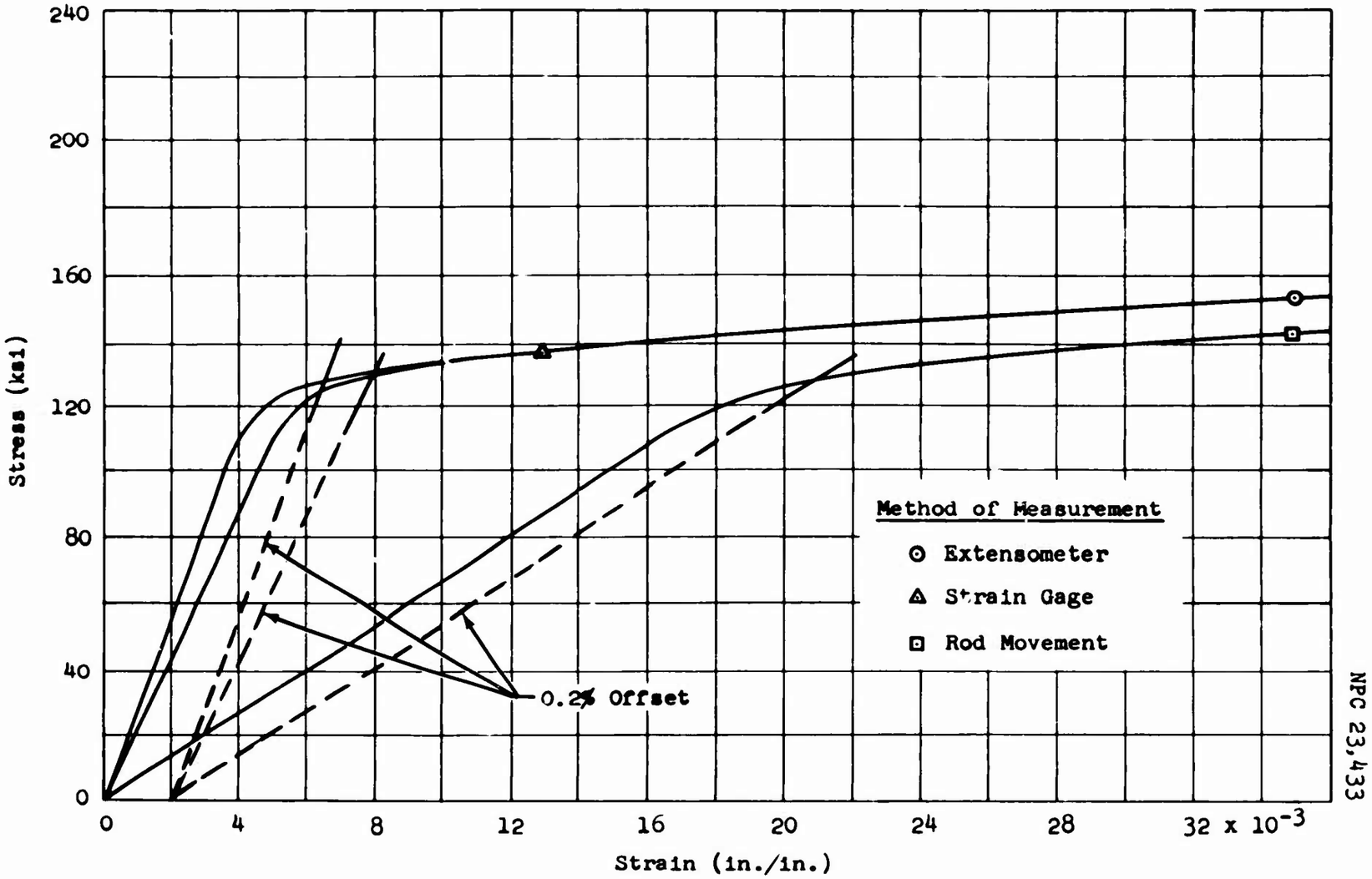

Figure C-142 Stainless Steel A-286, Condition LU: Comparison of Strain-Measurement Methods

Table C-23
X-Ray Diffraction Data

Material Stainless Steel A-286 Specimen LU 214

	STRAINED AREA		UNSTRAINED AREA	
DIFFRACTION PATTERN				
Miller Indices (hkl)	Interlattice Spacing, d (Å)	Relative Intensity (%)	Interlattice Spacing, d (Å)	Relative Intensity (%)
111	2.08	65	2.08	100
110				
200	1.79	65	1.80	50
220	1.27	100	1.27	43
211			1.08	40

LATTICE PARAMETER (Å)		
111	3.60	3.60
110	-	-
200	3.58	3.60
220	3.59	3.59
211	-	2.64

MICROSTRESS, $\Delta\theta$	
0.54° (2θ = 51.1°)	0.14°(2θ = 51.0°)
No Peak (2θ = 129°)	No Peak (2θ = 129°)

METALLOGRAPHIC STUDY

Material Stainless Steel A-286 Neg.No. None

Specimen LU 214 Neg.Mag. 3X

Etchant None Photo Enlargement None

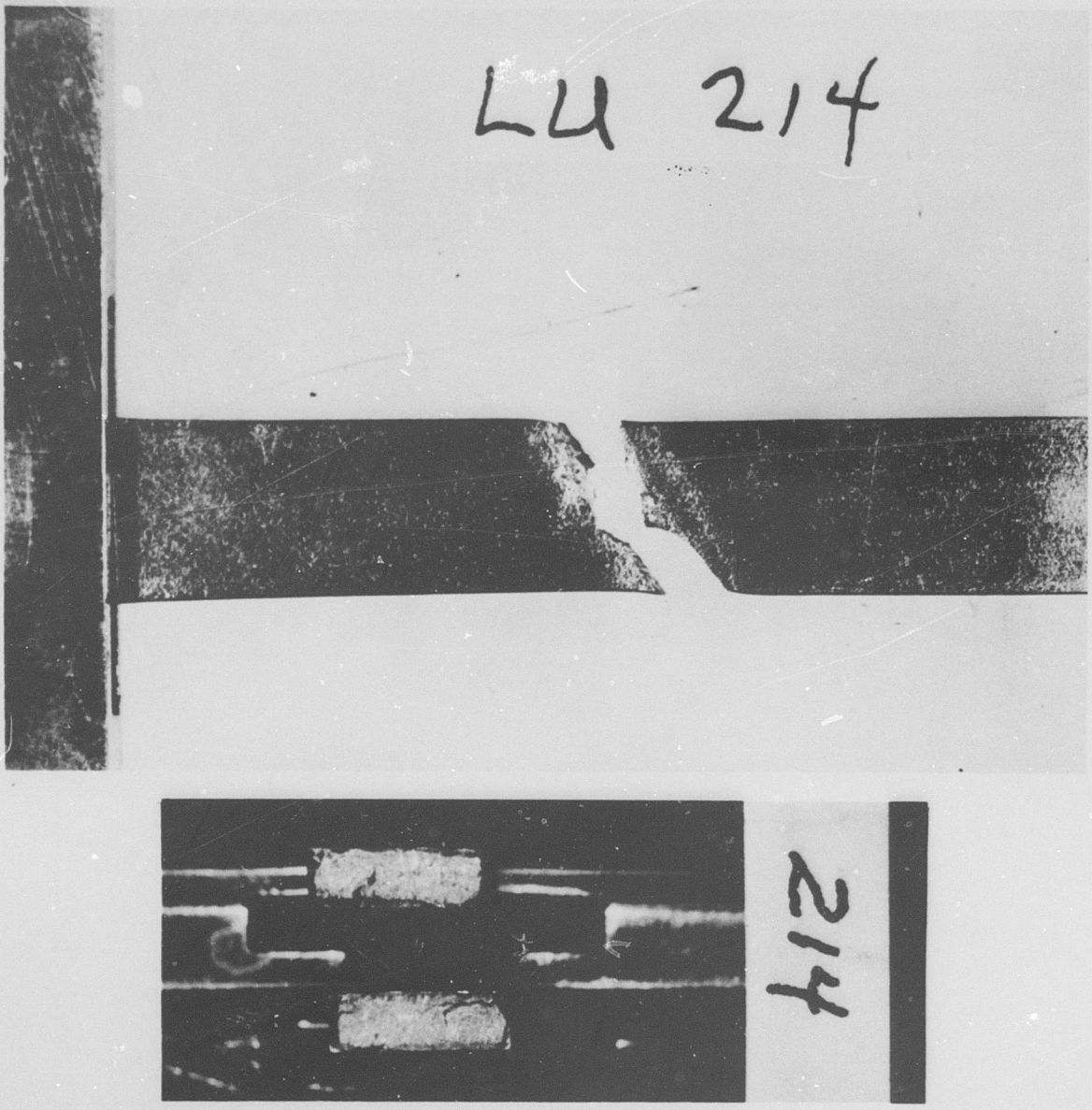

Figure C-143 Stainless Steel A-286, Condition L: Macrophotograph Showing 3X Magnification of Specimen

METALLOGRAPHIC STUDY

Material Stainless Steel A-286 Neg.No. W67

Specimen LU 214 Neg.Mag. 100X

Etchant 10% Oxalic Acid (electrolytic) Photo Enlargement None

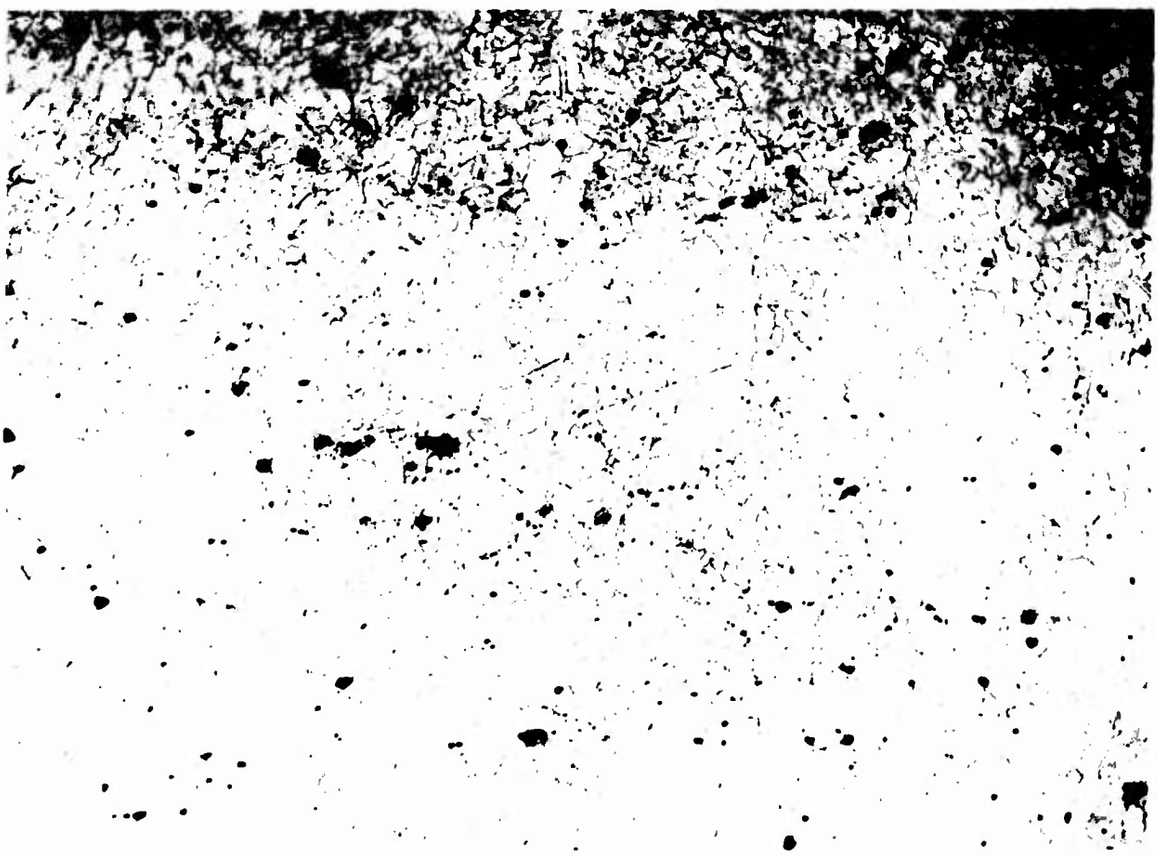

COMMENTS

The microstructure shows an austenitic matrix with dispersed carbides.

Figure C-144 Stainless Steel A-286, Condition L: Optical Micrograph Showing 100X Magnification of Unstrained Area

METALLOGRAPHIC STUDY

Material Stainless Steel A-286 Neg.No. None

Specimen LU 214 Neg.Mag. 3X

Etchant None Photo Enlargement None

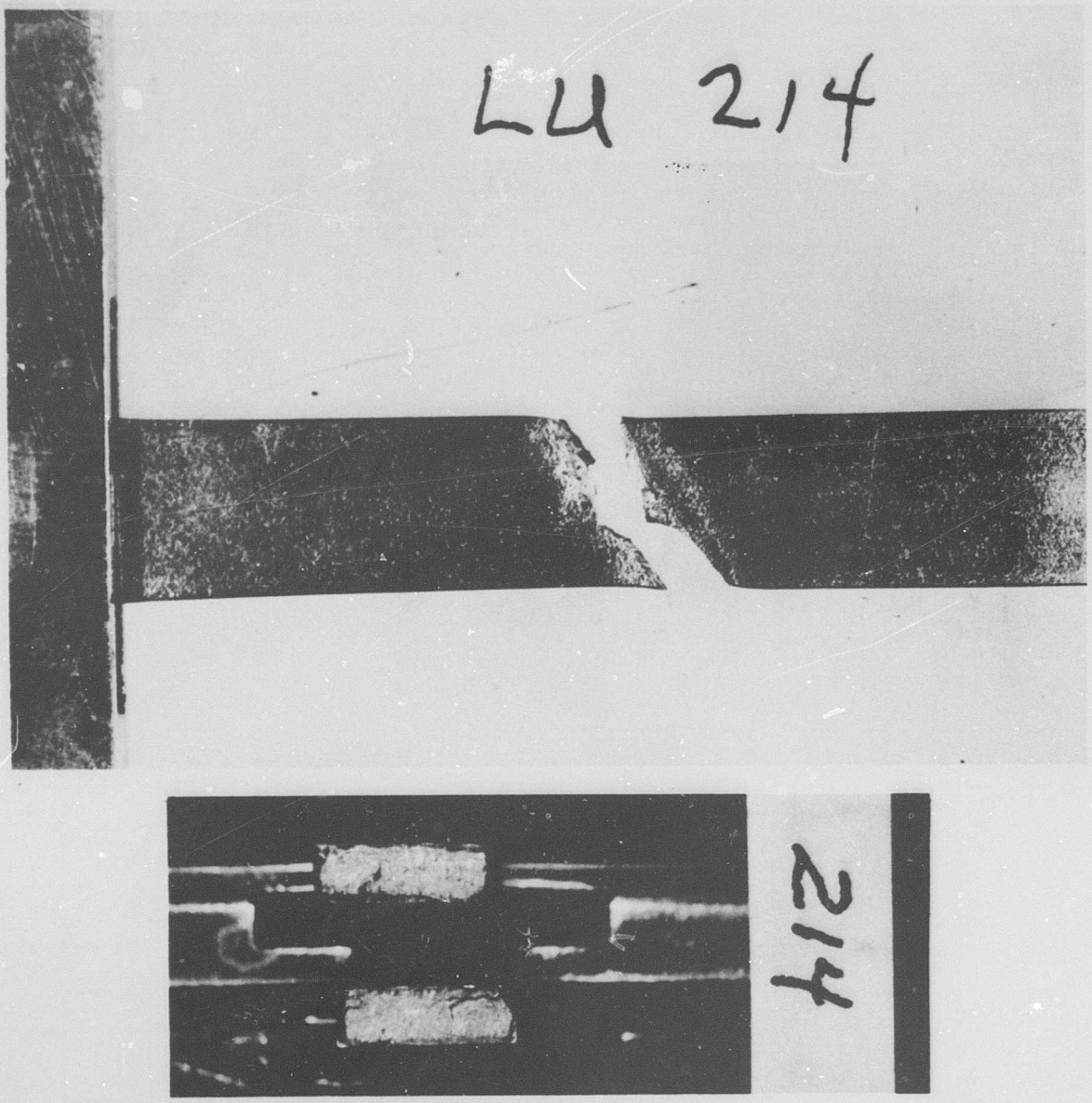

Figure C-143 Stainless Steel A-286, Condition L: Macrophotograph Showing 3X Magnification of Specimen

METALLOGRAPHIC STUDY

Material Stainless Steel A-286 Neg.No. W71

Specimen LU 214 Neg.Mag. 100X

Etchant 10% Oxalic Acid (electrolytic) Photo Enlargement None

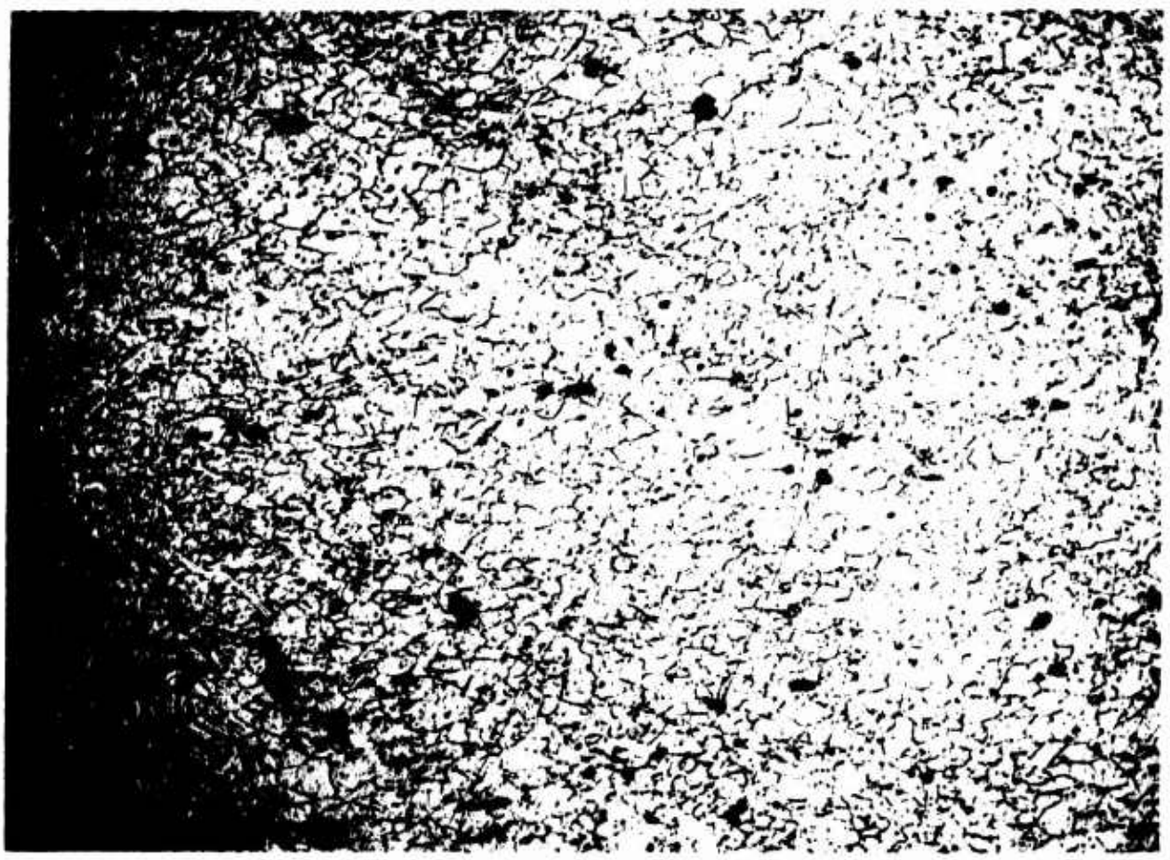

COMMENTS

The microstructure shows a deformed austenitic matrix, carbide dispersion, and strain lines in the grains.

Figure C-146 Stainless Steel A-286, Condition L: Optical Micrograph Showing 100X Magnification of General Strained Area

METALLOGRAPHIC STUDY

Material Stainless Steel A-286 Neg.No. W78

Specimen LU 214 Neg.Mag. 1,000X

Etchant 10% Oxalic Acid (electrolytic) Photo Enlargement None

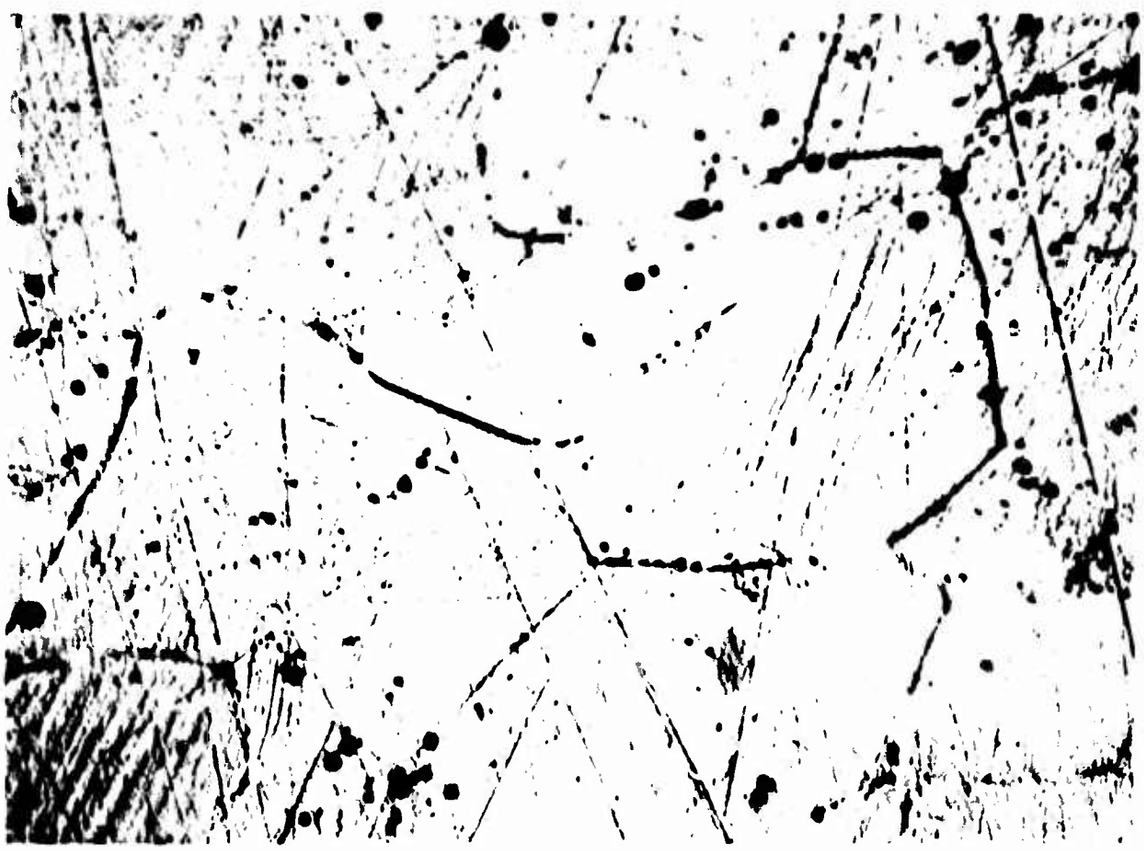

COMMENTS

The microstructure shows the deformed austenite matrix, carbide dispersions, and strain lines in the grains. Note the strain orientation variation within the original austenite grain.

Figure C-147 Stainless Steel A-286, Condition L: Optical Micrograph Showing 1,000X Magnification of General Strained Area

METALLOGRAPHIC STUDY

Material Stainless Steel A-286 Neg.No. W75

Specimen LU 214 Neg.Mag. 100X

Etchant 10% Oxalic Acid (electrolytic) Photo Enlargement None

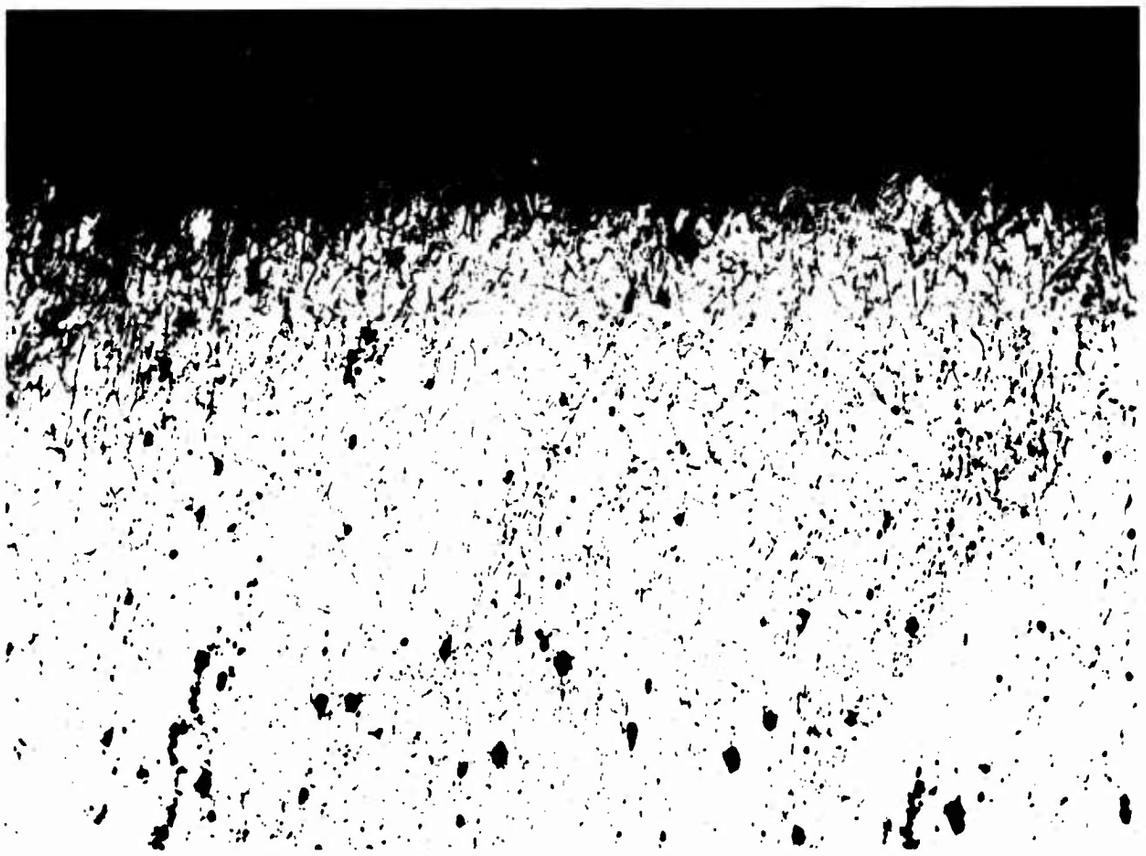

COMMENTS

The microstructure shows the deformed austenitic matrix, carbide dispersion, and strain lines in the grains. The fracture was primarily transgranular.

Figure C-148 Stainless Steel A-286, Condition L: Optical Micrograph Showing 100X Magnification of Fracture Edge

METALLOGRAPHIC STUDY

Material Stainless Steel A-286 Neg.No. W79

Specimen LU 214 Neg.Mag. 1,000X

Etchant 10% Oxalic Acid (electrolytic) Photo Enlargement None

COMMENTS

The microstructure shows the deformed austenite matrix, carbide dispersions, and strain lines in the grains. The fracture was primarily transgranular. Note the strain orientation variations within the original austenite grain.

Figure C-149 Stainless Steel A-286, Condition L: Optical Micrograph Showing 1,000X Magnification of Fracture Edge

METALLOGRAPHIC STUDY

Material Stainless Steel A-286 Neg.No. 105-10

Specimen LU 214 Neg.Mag. 7,500X

Etchant 10% Oxalic Acid (electrolytic) Photo Enlargement 2X

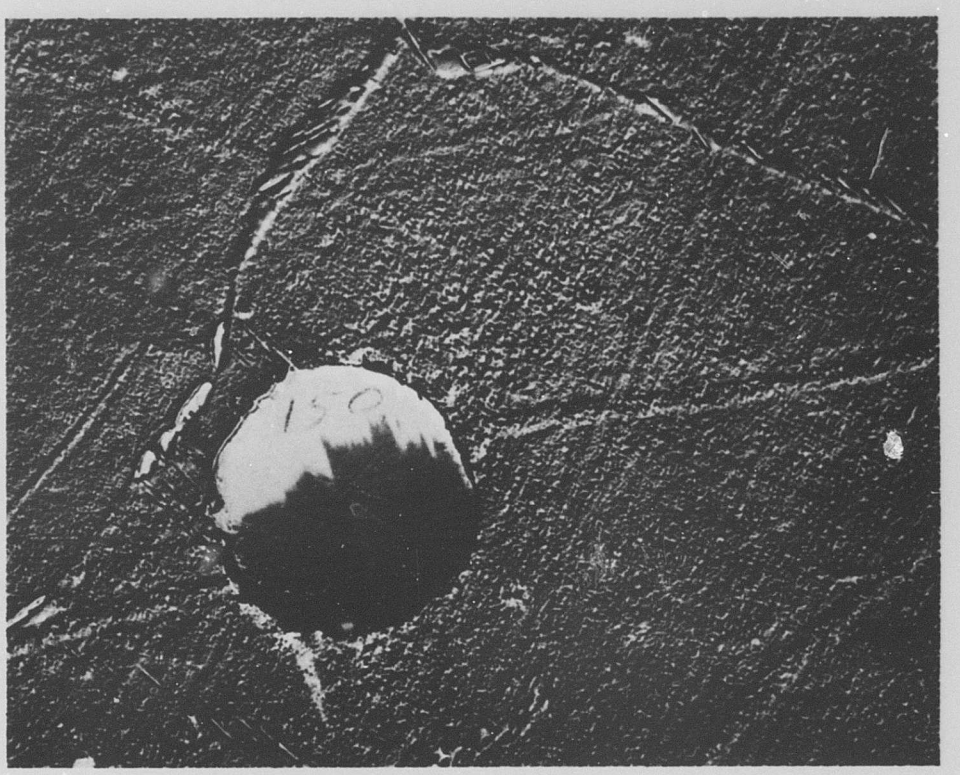

COMMENTS

The microstructure shows the austenite matrix with a large globular particle. The grain boundary shows a lamellar precipitate which, in some instances, extends into the grain. The larger precipitate in the grain boundary on the left appears to be a third type of precipitate.

Figure C-150 Stainless Steel A-286, Condition L: Electron Micrograph Showing 15,000X Magnification of Unstrained Area

METALLOGRAPHIC STUDY

Material Stainless Steel A-286 Neg.No. 106-8

Specimen LU 214 Neg.Mag. 7,500X

Etchant 10% Oxalic Acid (electrolytic) Photo Enlargement 2X

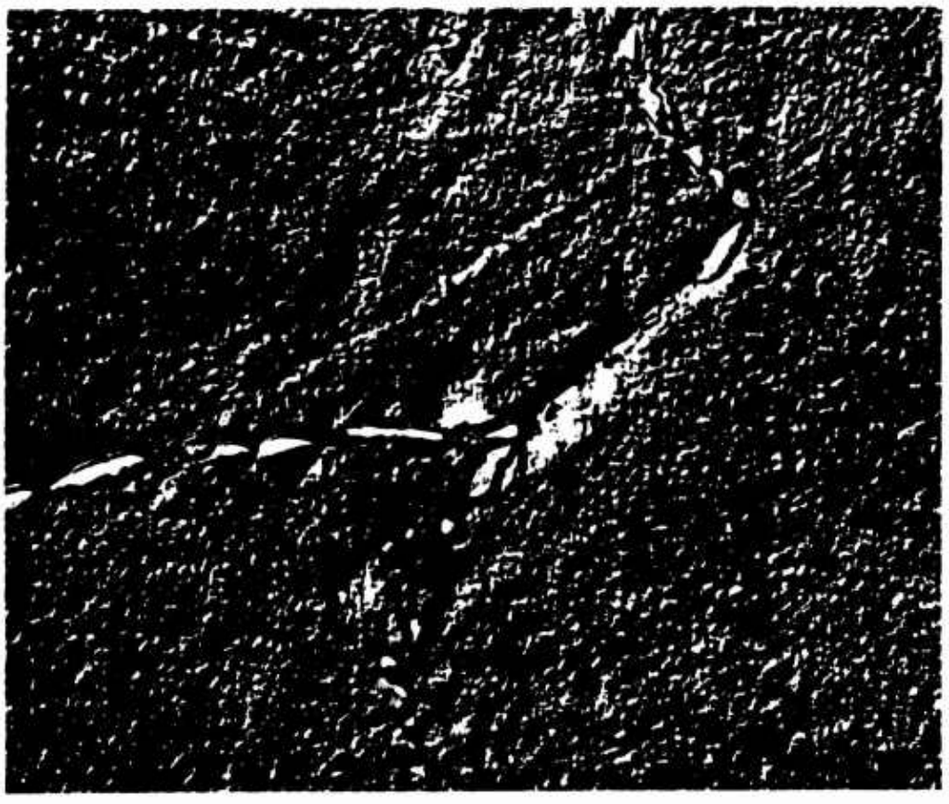

COMMENTS

The microstructure shows an austenite-matrix grain boundary and a precipitate along the boundary. Faint strain lines are visible.

Figure C-151 Stainless Steel A-286, Condition L: Electron Micrograph Showing 15,000X Magnification of Strained Area

METALLOGRAPHIC STUDY

Material Stainless Steel A-286 Neg.No. 111-5

Specimen LU 214 Neg.Mag. 2,100X

Etchant None Photo Enlargement 2X

COMMENTS

The fractograph of the center area shows a microvoid fracture mode, which is indicative of a ductile failure. Both small and large equiaxed dimples are present.

Figure C-152 Stainless Steel A-286, Condition L: Electron Fractograph Showing 4,200X Magnification at Center of Fracture

METALLOGRAPHIC STUDY

Material Stainless Steel A-286 Neg.No. 93-4

Specimen LU 214 Neg.Mag. 2,100X

Etchant None Photo Enlargement 2X

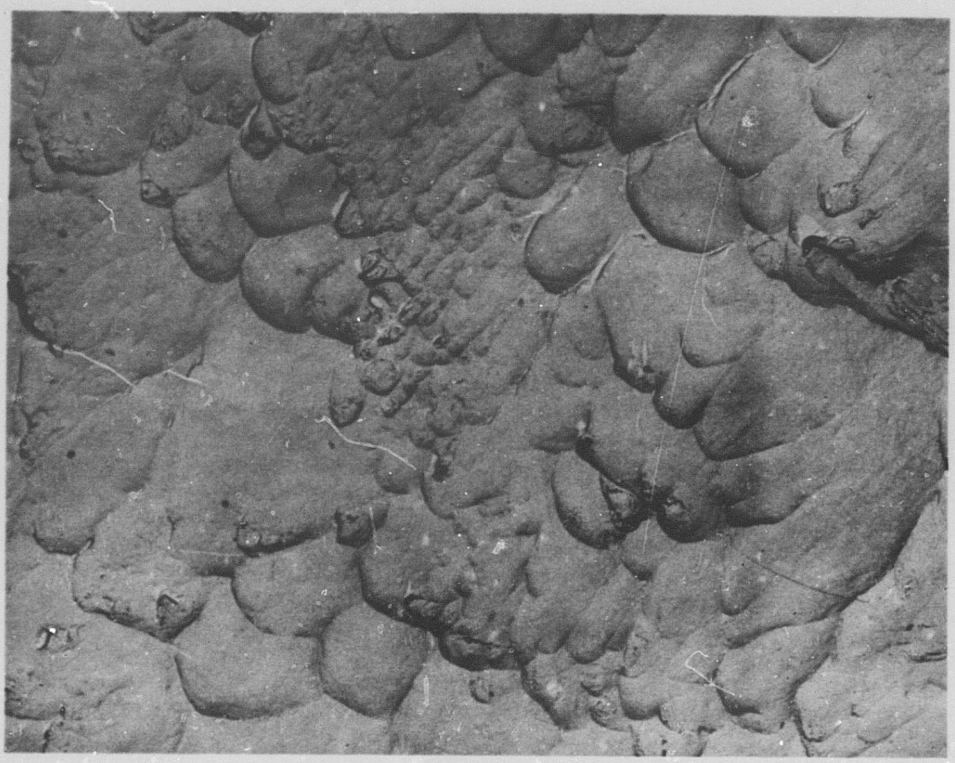

COMMENTS

The fracture at the edge shows oriented dimples, or a ductile shear failure. Some of the dimples have brittle particles at the tips.

Figure C-153 Stainless Steel A-286, Condition L: Electron Fractograph Showing 4,200X Magnification Near Edge of Fracture

METALLOGRAPHIC STUDY

Material Stainless Steel A-286 Neg.No. 100-2

Specimen LN 221 Neg.Mag. 2,100X

Etchant None Photo Enlargement 2X

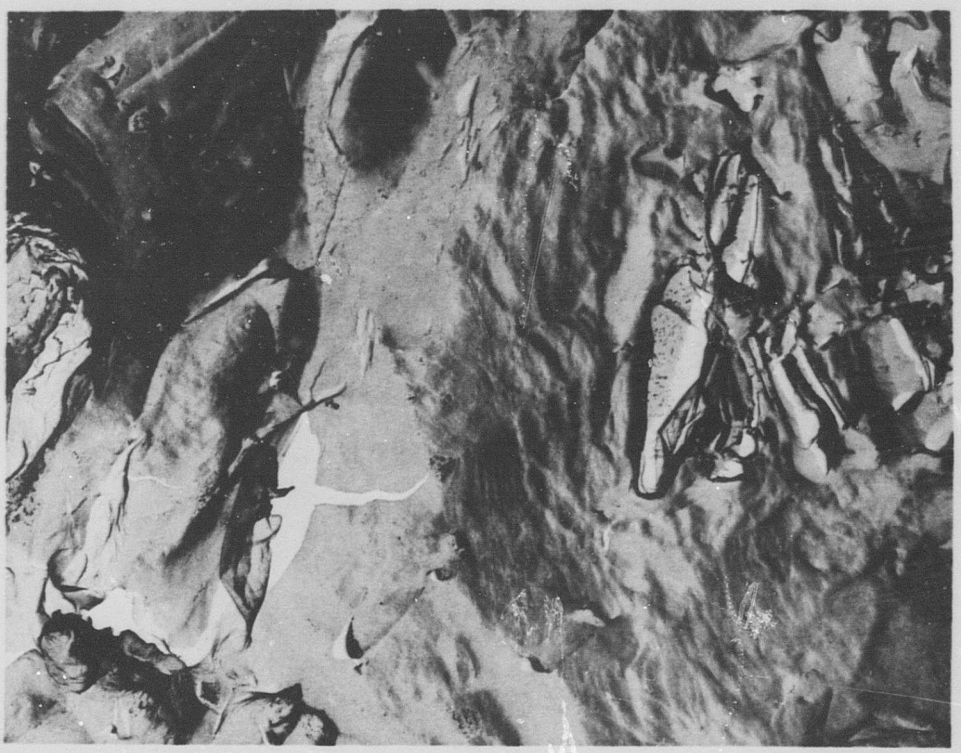

COMMENTS

The fracture surface is composed of large dimples and serpentine glide. The area on the right contains a large number of intermetallic compounds that have fractured in a brittle manner, possibly giving rise to a free surface distorted by serpentine glide.

Figure C-154a Stainless Steel A-286, Condition L: Electron Fractograph Showing 4,200X Magnification of Notched Fracture

METALLOGRAPHIC STUDY

Material	Stainless Steel A-286	Neg.No.	100-3
Specimen	LN 221	Neg.Mag.	2,100X
Etchant	None	Photo Enlargement	2X

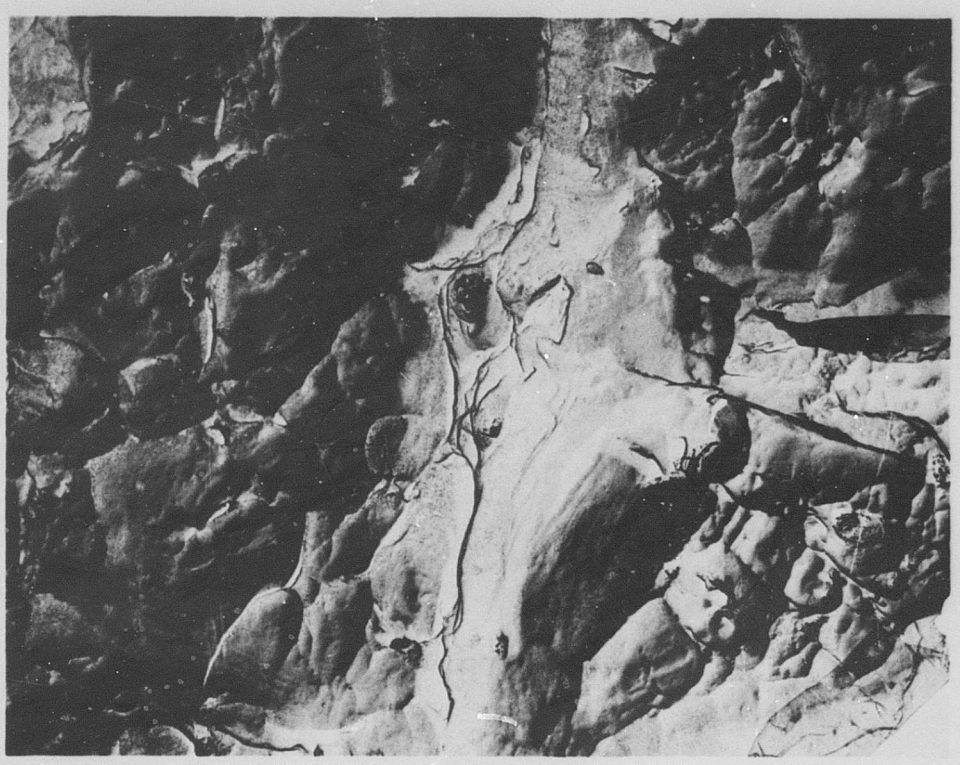

COMMENTS

The fracture surface is composed of dimples and ripples. A number of small, brittle, intermetallic compounds appear on the fracture surface.

Figure C-154b Stainless Steel A-286, Condition L: Electron Fractograph Showing 4,200X Magnification of Notched Fracture

Inconel X-750
Condition L

BLANK PAGE

Table C-24

Tensile and Shear Test Data

Material Inconel X-750 Specimen Condition L

Averaged Data (-423°F)		
Unnotched Specimens	Control	Irradiated
Ultimate Strength (ksi)	253.3	227.7
0.2% Yield Strength (ksi)	135.8	146.8
Elongation in Gage Length (%)	31.2	26.4
Reduction in Area (%)	27.1	26.6
Ultimate Shear Strength (ksi)	152.8	162.0
Notched Specimens		
Ultimate Strength (ksi)	191.6	197.2
Ratios		
Notched-Ult./Unnotched-Ult.	0.76	0.87
Notched-Ult./Unnotched-Yield	1.41	1.34

Unnotched Specimens				
Specimen Number	Ult. Tensile Strength (ksi)	Yield Strength 0.2% Offset (ksi)	Reduction in Area (%)	Elongation (%)
381	224.8	146.0	26.2	26.7
382	246.2	147.5	25.5	26.2
377	220.5	147.0	26.2	26.2
378	219.1	146.5	28.5	26.7

Notched Specimens		Shear Specimens	
Specimen Number	Ult. Tensile Strength (ksi)	Specimen Number	Ult. Shear Strength (ksi)
389	191.7	1	168.9
390	194.2	2	162.3
391	200.6	3	158.4
392	202.4	4	158.4

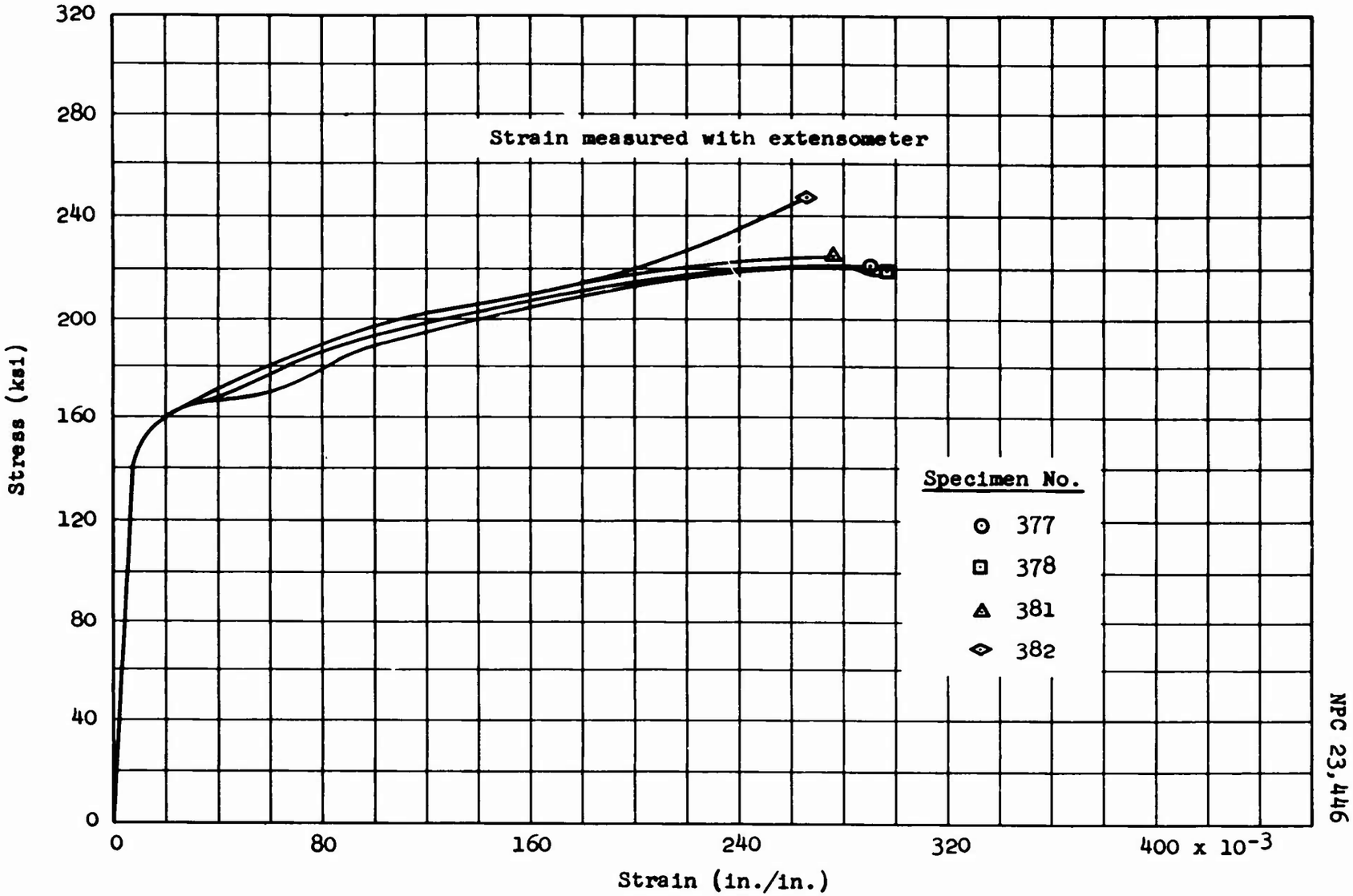

Figure C-155 Inconel X-750, Condition LU: Stress-Strain Curves

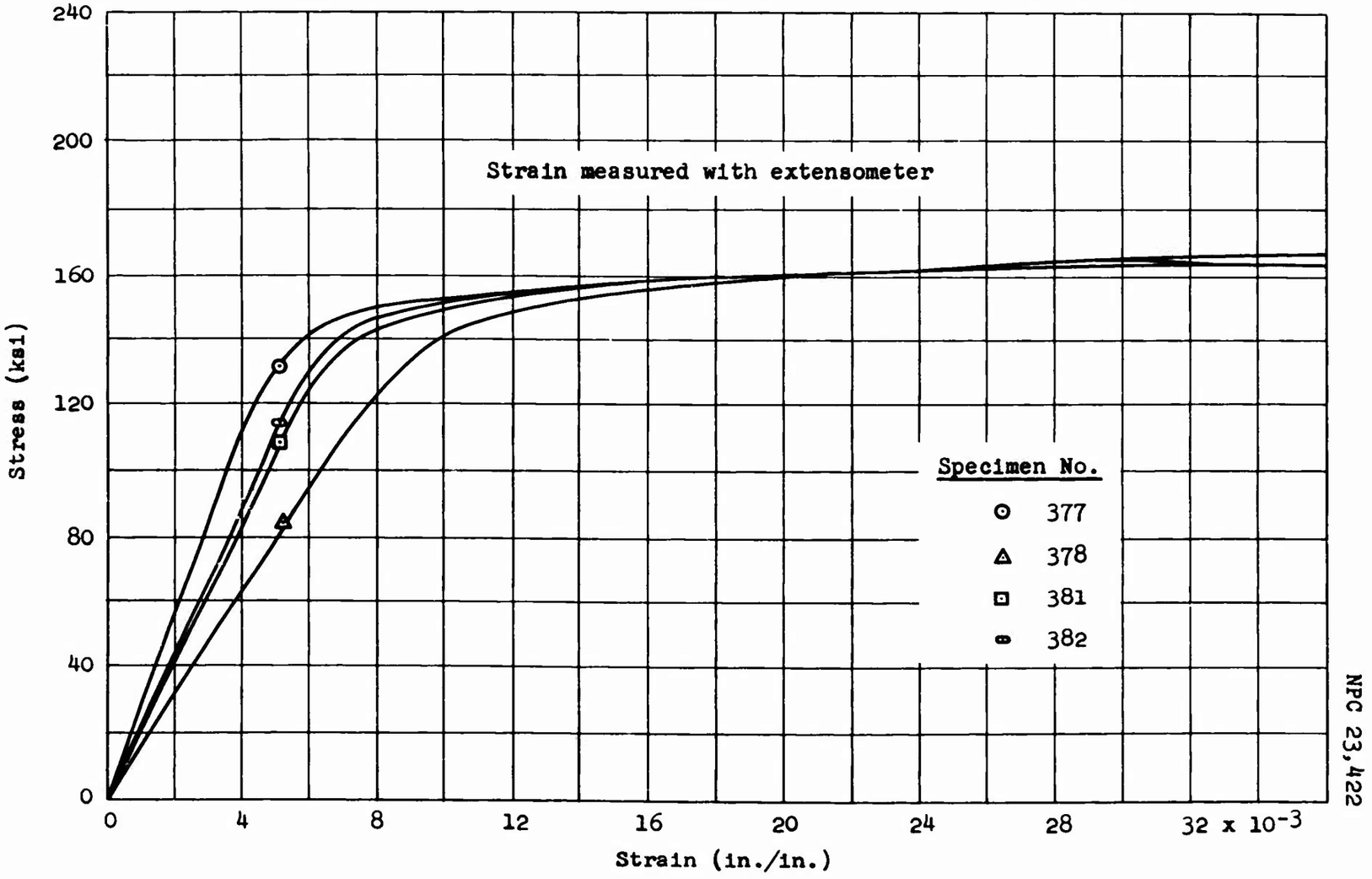

Figure C-156 Inconel X-750, Condition LU: Stress-Strain Curves (Expanded Scale)

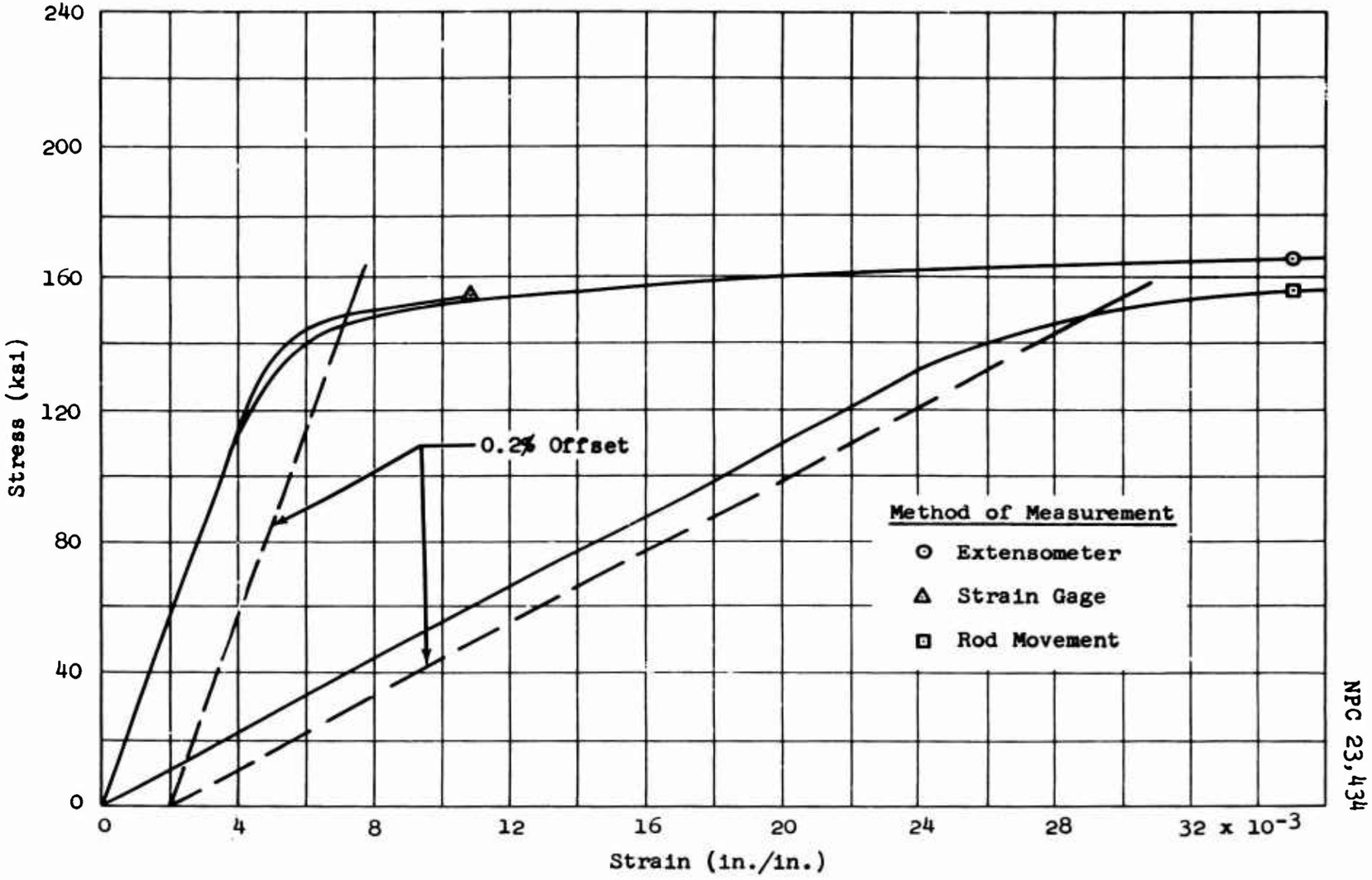

Figure C-157 Inconel X-750, Condition LU: Comparison of Strain-Measurement Methods

Table C-25
X-Ray Diffraction Data

Material Inconel X-750 Specimen LU 382

	STRAINED AREA		UNSTRAINED AREA	
DIFFRACTION PATTERN				
Miller Indices (hkl)	Interlattice Spacing, d (Å)	Relative Intensity (%)	Interlattice Spacing, d (Å)	Relative Intensity (%)
111	2.06	100	2.07	100
200	1.78	32	1.79	35
220	1.26	66	1.26	7
311	1.08	20	1.08	5

LATTICE PARAMETER (Å)		
111	3.57	3.58
200	3.56	3.58
220	3.56	3.56
311	3.58	3.58

MICROSTRESS, $\Delta\theta$	
0.21° (2θ = 43.8°)	0.15° (2θ = 43.8°)
No Peak (2θ = 130°)	No Peak (2θ = 130°)

METALLOGRAPHIC STUDY

Material Inconel X-750 Neg.No. None

Specimen LU 382 Neg.Mag. 3X

Etchant None Photo Enlargement None

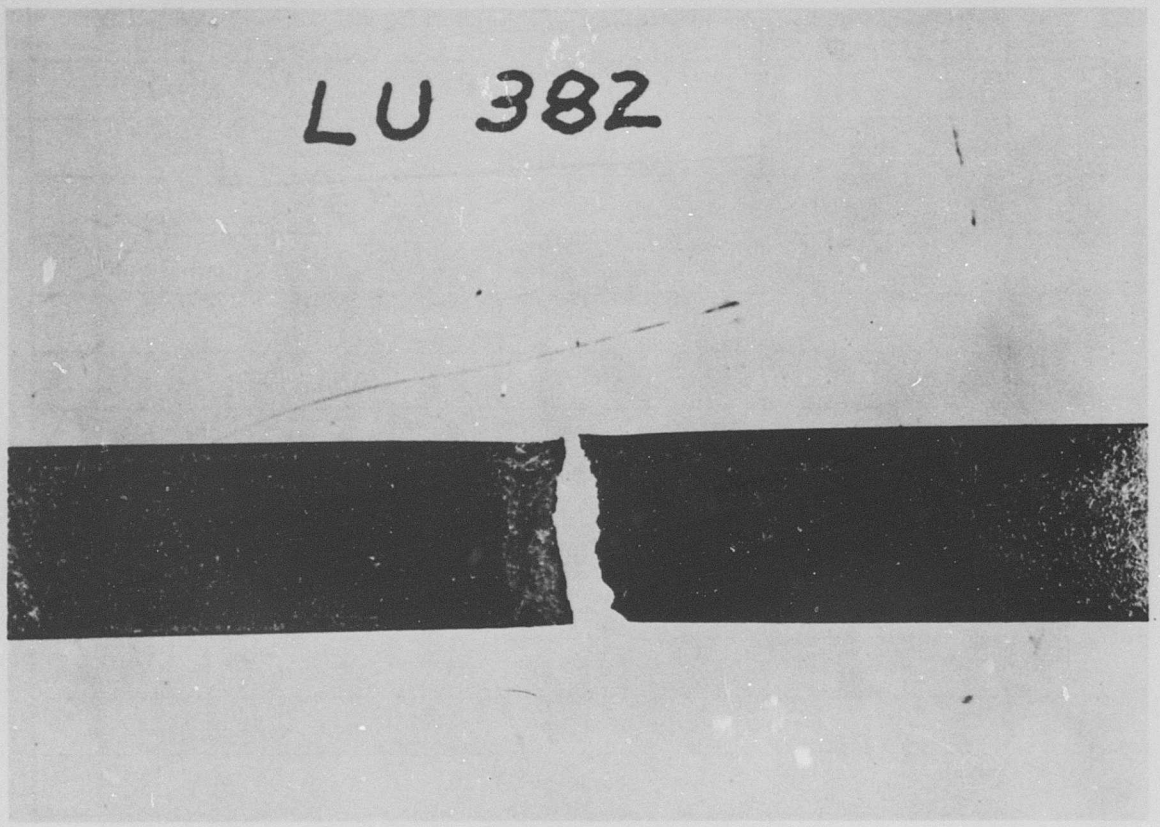

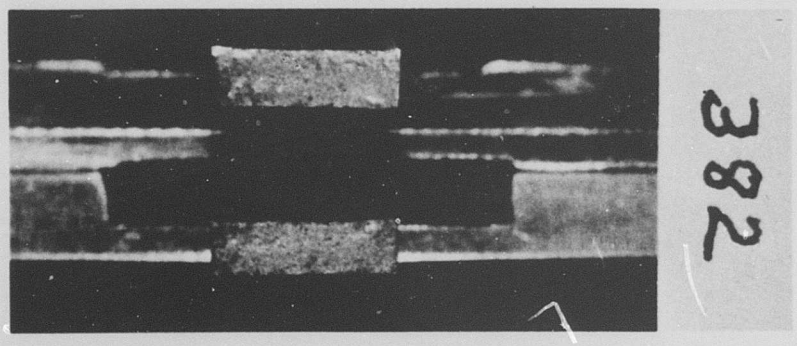

Figure C-158 Inconel X-750, Condition L: Macrophotograph Showing 3X Magnification of Specimen

METALLOGRAPHIC STUDY

Material Inconel X-750 Neg.No. W85

Specimen LU 382 Neg.Mag. 100X

Etchant 10% Oxalic Acid (electrolytic) Photo Enlargement None

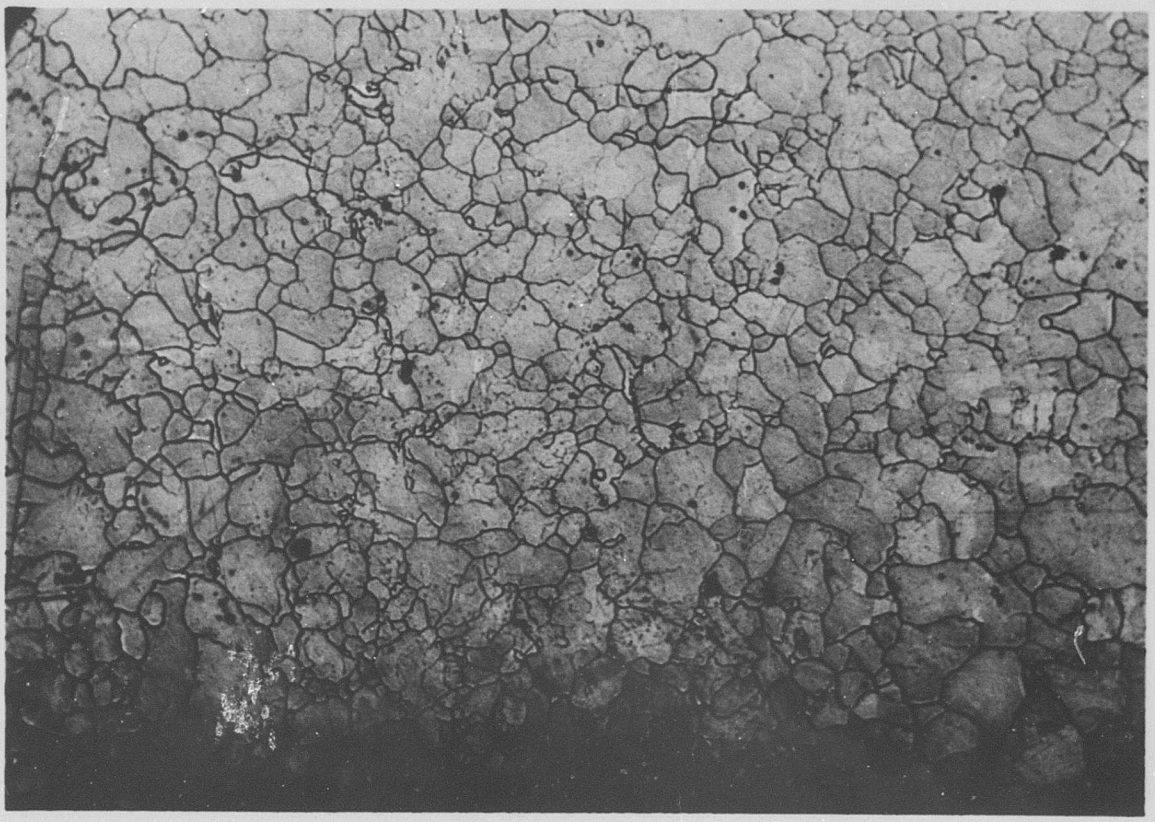

COMMENTS

The microstructure shows a typical austenitic matrix.

Figure C-159 Inconel X-750, Condition L: Optical Micrograph Showing 100X Magnification of Unstrained Area

METALLOGRAPHIC STUDY

Material Inconel X-750 Neg.No. W81

Specimen LU 382 Neg.Mag. 1,000X

Etchant 10% Oxalic Acid (electrolytic) Photo Enlargement None

COMMENTS

The microstructure shows an austenitic matrix with fine, dispersed carbides and a continuous precipitate at the grain boundaries.

Figure C-160 Inconel X-750, Condition L: Optical Micrograph Showing 1,000X Magnification of Unstrained Area

METALLOGRAPHIC STUDY

Material Inconel X-750 Neg.No. W83

Specimen LU 382 Neg.Mag. 100X

Etchant 10% Oxalic Acid (electrolytic) Photo Enlargement None

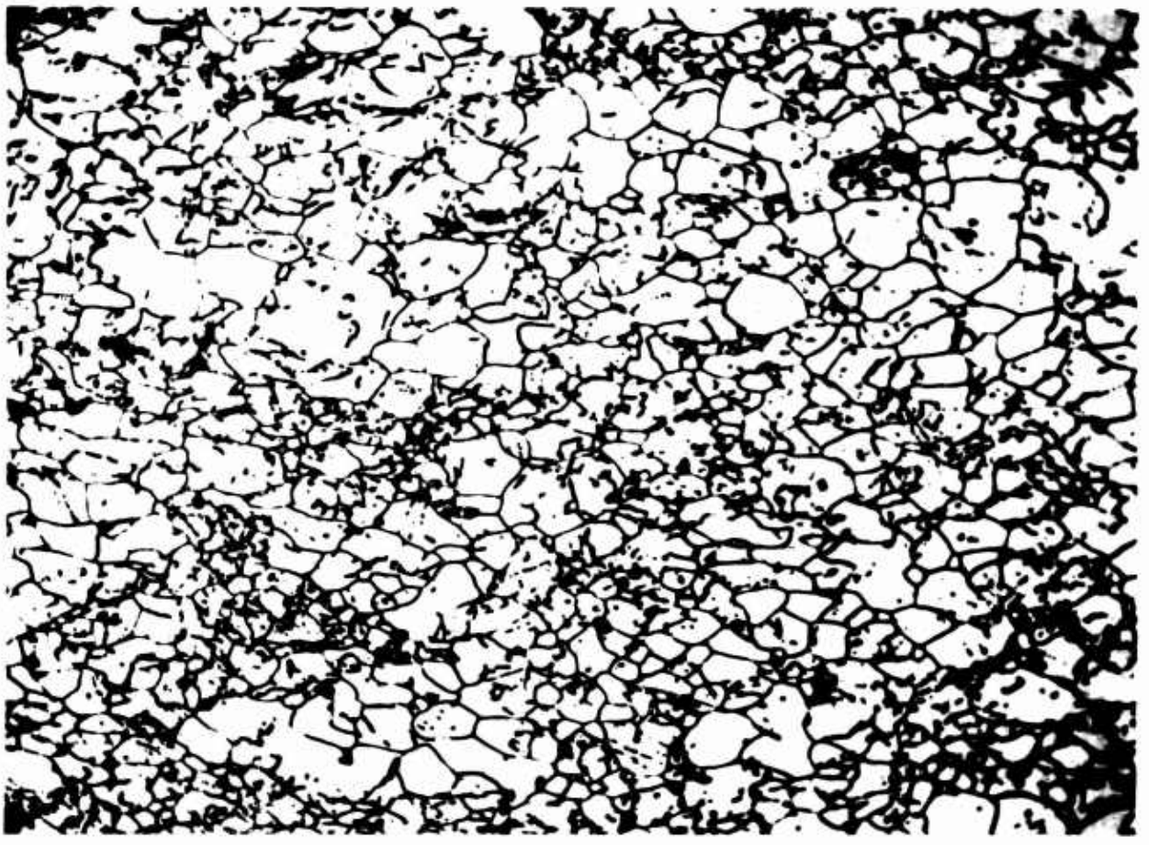

COMMENTS

The microstructure shows a deformed austenitic matrix.

Figure C-161 Inconel X-750, Condition L: Optical Micrograph Showing 100X Magnification of General Strained Area

METALLOGRAPHIC STUDY

Material Inconel X-750 Neg.No. W88

Specimen LU 382 Neg.Mag. 1,000X

Etchant 10% Oxalic Acid (electrolytic) Photo Enlargement None

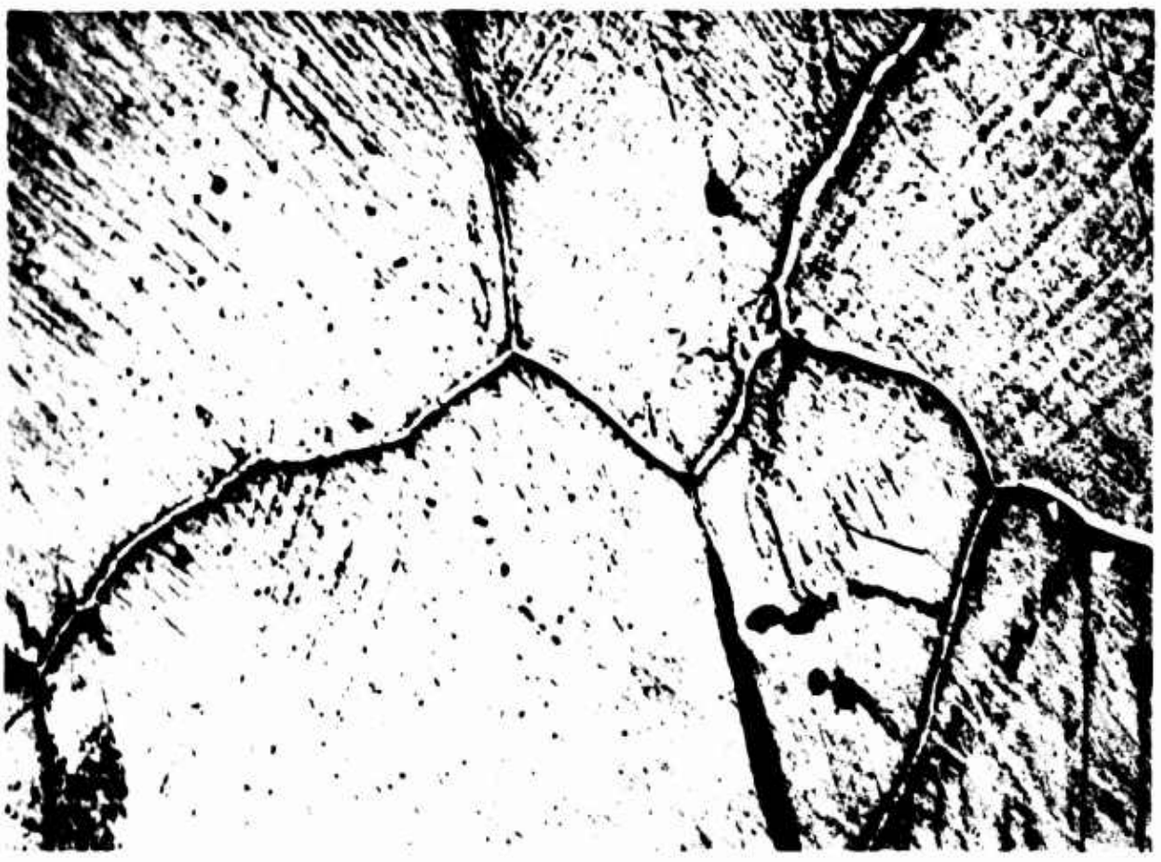

COMMENTS

The microstructure shows an austenitic matrix with a continuous precipitate at the grain boundaries and within the grain. Note the strain line orientation seen within the grains.

Figure C-162 Inconel X-750, Condition L: Optical Micrograph Showing 1,000X Magnification of General Strained Area

METALLOGRAPHIC STUDY

Material Inconel X-750 Neg.No. W84

Specimen LU 382 Neg.Mag. 100X

Etchant 10% Oxalic Acid (electrolytic) Photo Enlargement None

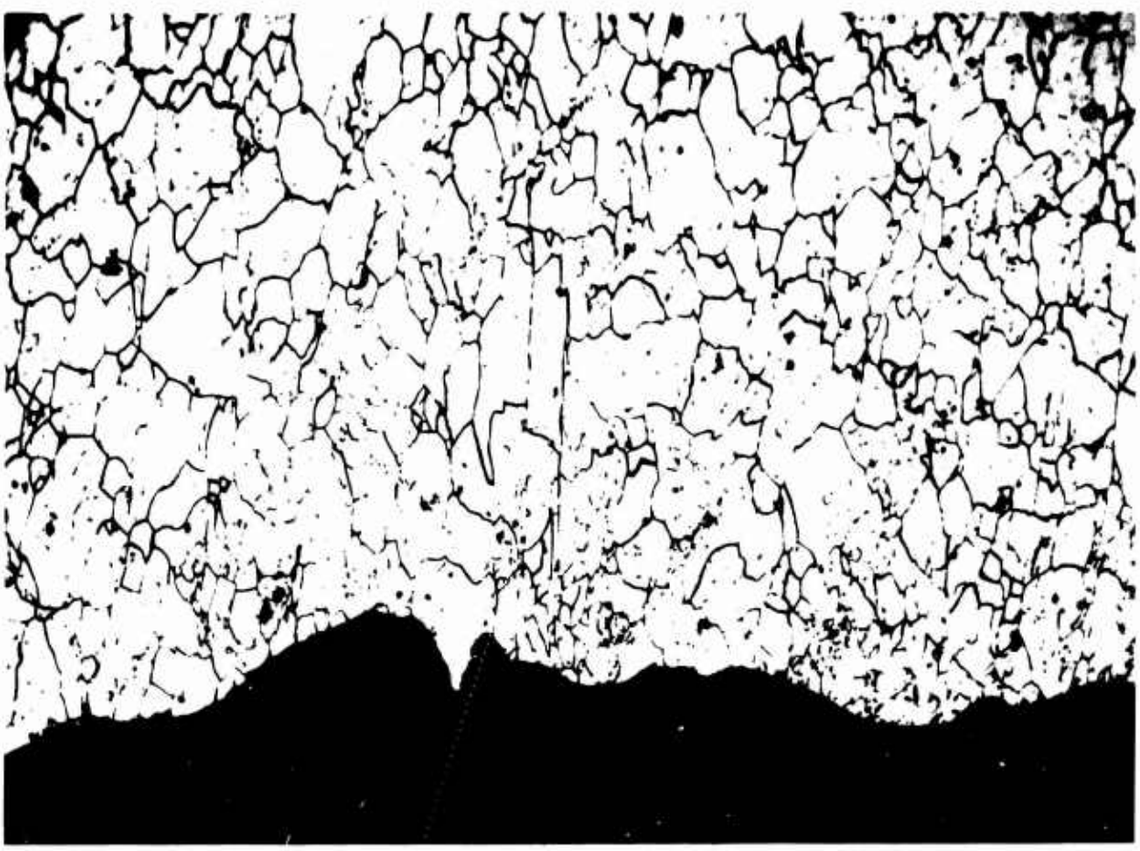

COMMENTS

The microstructure shows a transgranular fracture through the deformed austenitic matrix.

Figure C-163 Inconel X-750, Condition L: Optical Micrograph Showing 100X Magnification of Fracture Edge

METALLOGRAPHIC STUDY

Material Inconel X-750 Neg.No. W89

Specimen LU 382 Neg.Mag. 1,000X

Etchant 10% Oxalic Acid (electrolytic) Photo Enlargement None

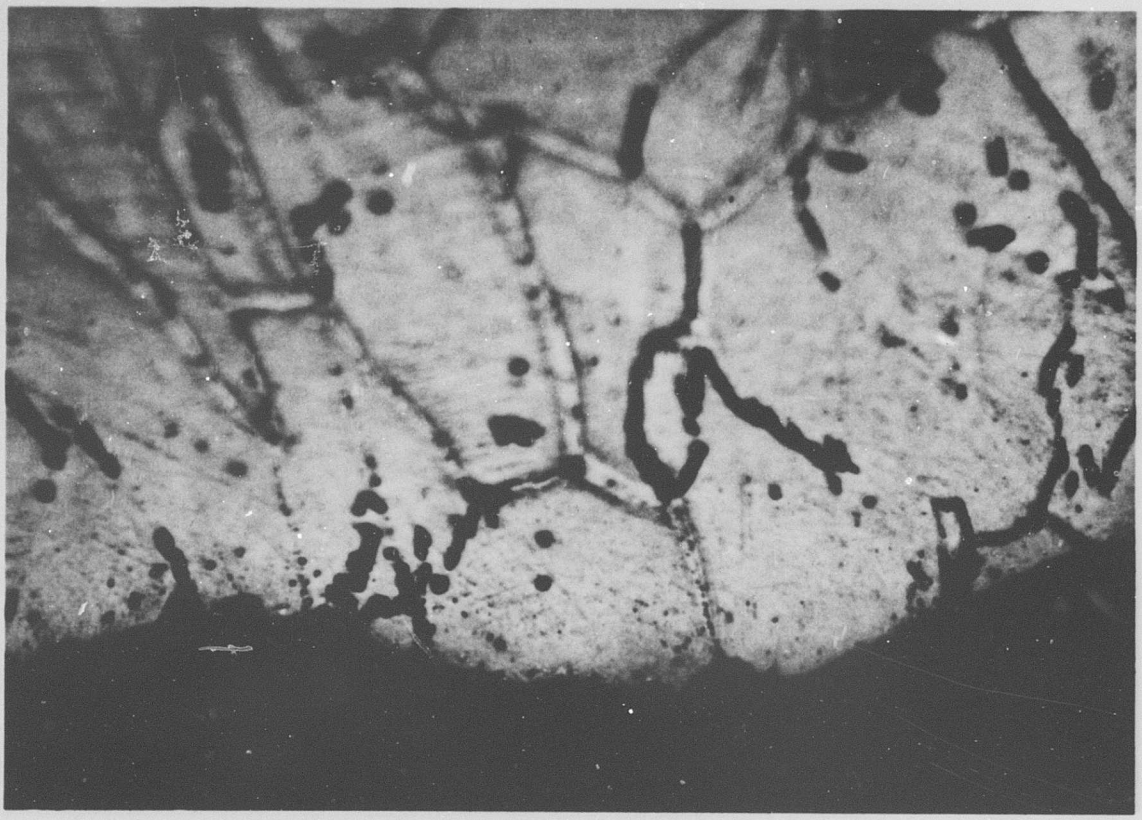

COMMENTS

The microstructure shows a transgranular fracture through the deformed austenitic matrix and a continuous precipitate at the grain boundary.

Figure C-164 Inconel X-750, Condition L: Optical Micrograph Showing 1,000X Magnification of Fracture Edge

METALLOGRAPHIC STUDY

Material Inconel X-750 Neg.No. 104-12

Specimen LU 382 Neg.Mag. 7,500X

Etchant 10% Oxalic Acid (electrolytic) Photo Enlargement 2X

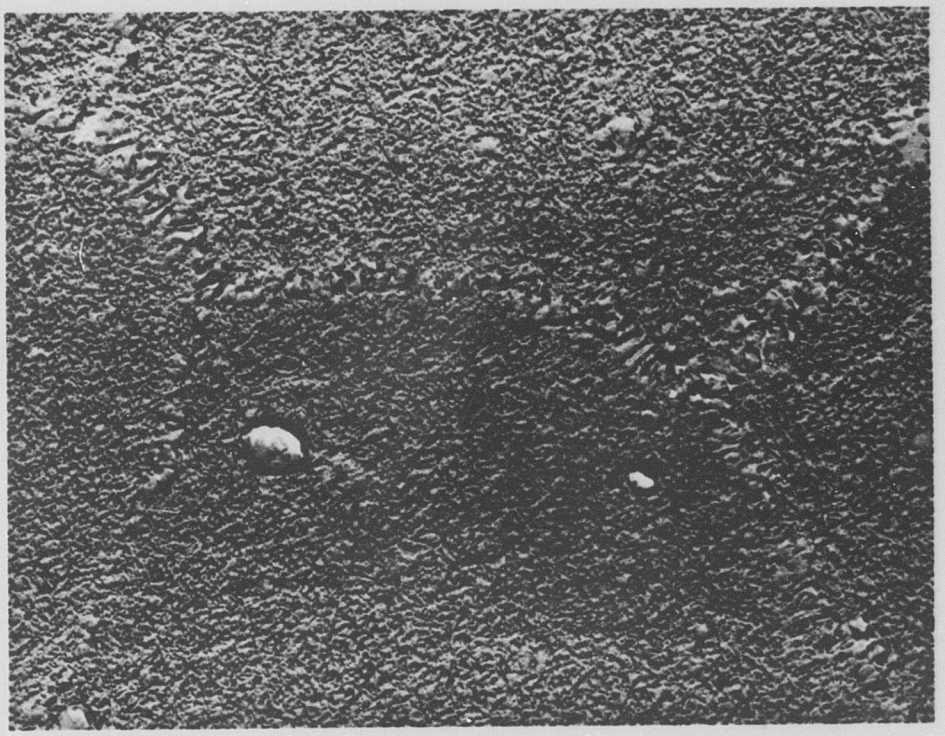

COMMENTS

The microstructure shows austenite with a continuous carbide precipitation taking place in the grain boundaries. Carbides can also be seen in the middle of the austenitic grain.

Figure C-165 Inconel X-750, Condition L: Electron Micrograph Showing 15,000X Magnification of Unstrained Area

METALLOGRAPHIC STUDY

Material Inconel X-750 Neg.No. 105-2

Specimen LU 382 Neg.Mag. 7,500X

Etchant 10% Oxalic Acid (electrolytic) Photo Enlargement 2X

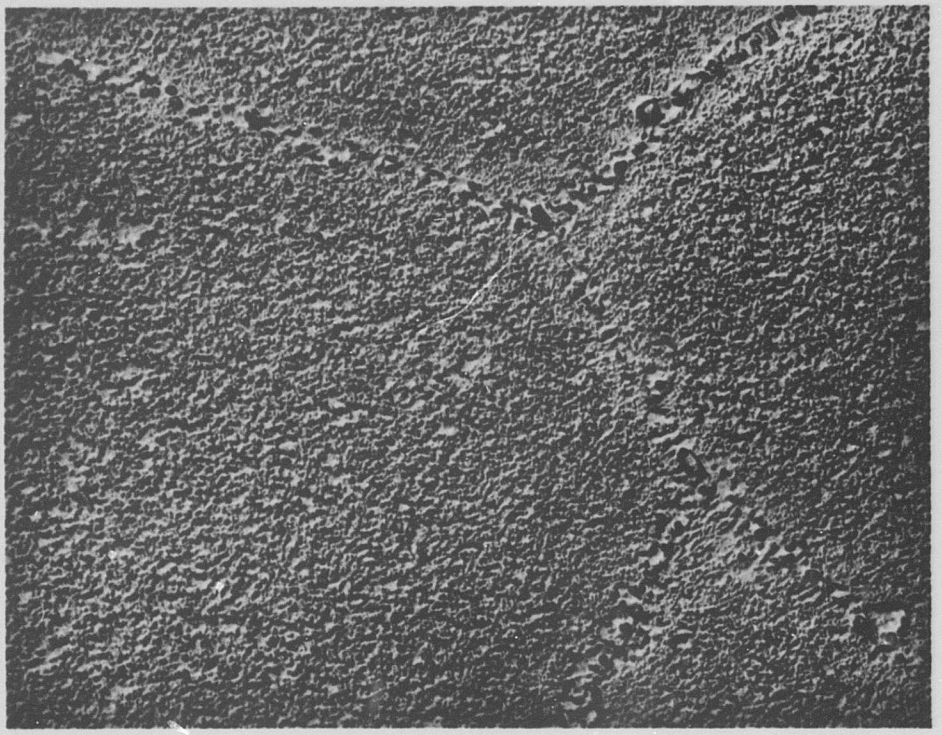

COMMENTS

The microstructure shows austenite with grain boundary precipitation. The strain lines present on the optical micrographs do not show in this photograph.

Figure C-166 Inconel X-750, Condition L: Electron Micrograph Showing 15,000X Magnification of Strained Area

METALLOGRAPHIC STUDY

Material Inconel X-750 Neg.No. 96-12

Specimen LU 382 Neg.Mag. 2,100X

Etchant None Photo Enlargement 2X

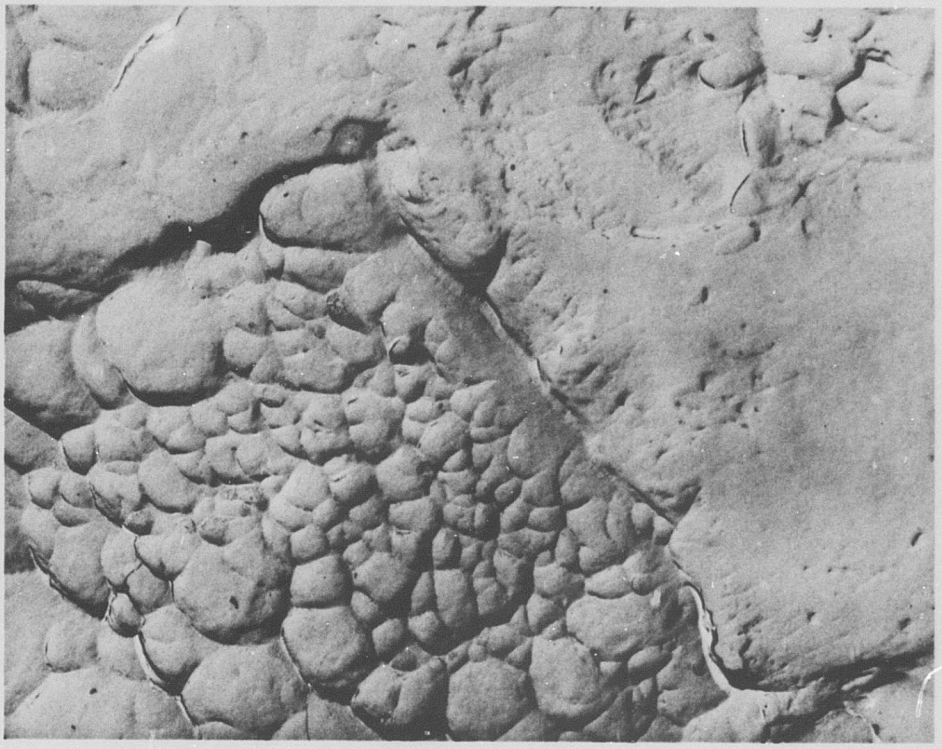

COMMENTS

The fracture at the central area of the specimen is made up of oriented dimples and glide-plane decohesion. The boundary in the center of the photograph is, in all probability, a grain boundary. In the grain on the right, a glide or slip plane is lined up with the shearing stresses and the failure is by glide-plane decohesion. In the area on the left, the plane of easy glide is not lined up and the failure is by microvoid formation and link-up. This type of fracture is associated with ductile failure.

Figure C-167 Inconel X-750, Condition L: Electron Fractograph Showing 4,200X Magnification at Center of Fracture

METALLOGRAPHIC STUDY

Material Inconel X-750 Neg.No. 97-3

Specimen LU 382 Neg.Mag. 2,100X

Etchant None Photo Enlargement 2X

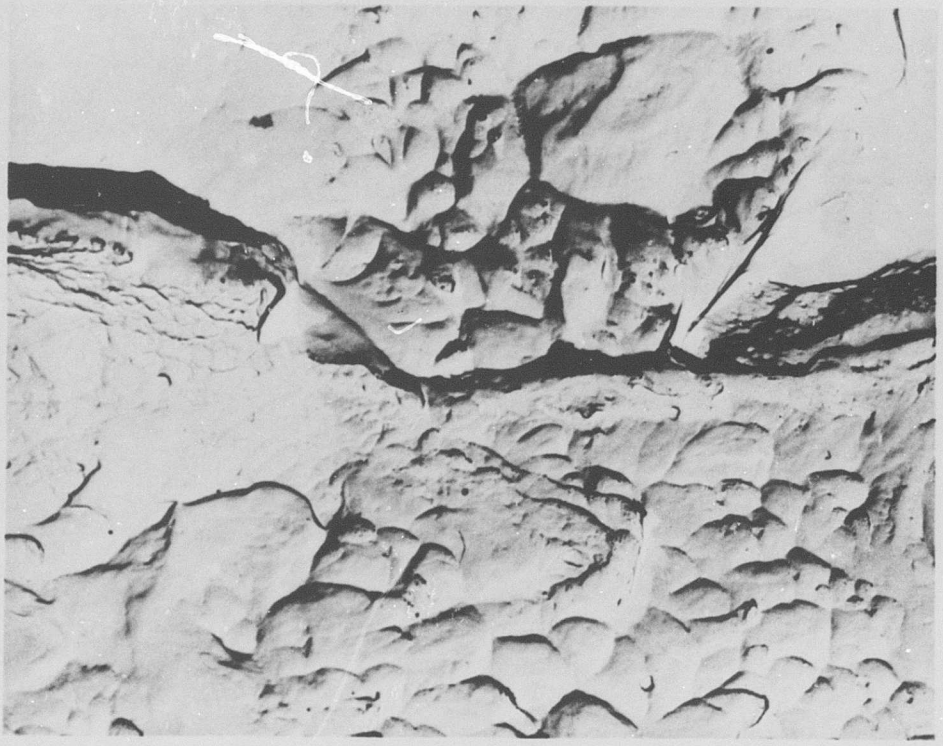

COMMENTS

The failure mode at the edge of the specimen is similar to that at the center and consists of microvoid formations and glide-plane decohesion.

Figure C-168 Inconel X-750, Condition L: Electron Fractograph Showing 4,200X Magnification Near Edge of Fracture

METALLOGRAPHIC STUDY

Material Inconel X-750 Neg.No. 97-10

Specimen LN 389 Neg.Mag. 2,100X

Etchant None Photo Enlargement 2X

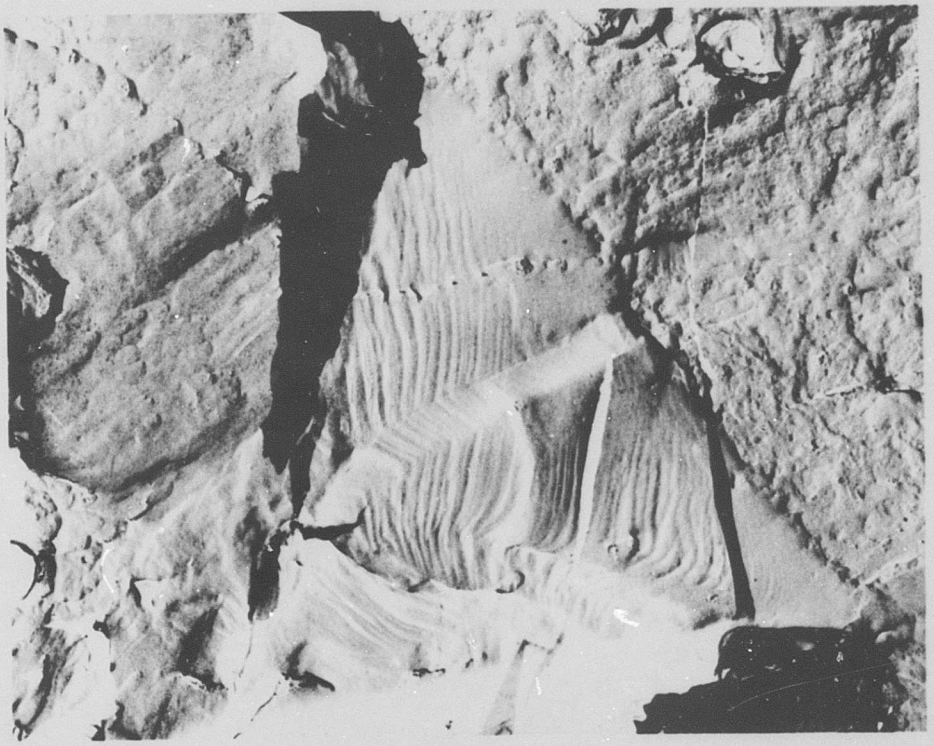

COMMENTS

The fracture is made up of an area of serpentine glide striations in the triangular area at the center of the photograph, a semi-ductile microvoid area on the left, and glide plane decohesion and shear microvoid on the right. The serpentine glide striations are a result of a local fracture giving a free surface ahead of the main crack. The material below this free surface is subsequently deformed as the main crack front advances, giving rise to slip-band striations or serpentine glide on the free surface. It is thought that the band across the middle of the serpentine glide zone represents a twin.

Figure C-169a Inconel X-750, Condition L: Electron Fractograph Showing 4,200X Magnification of Notched Fracture

METALLOGRAPHIC STUDY

Material Inconel X-750 Neg.No. 97-11

Specimen LN 389 Neg.Mag. 2,100X

Etchant None Photo Enlargement 2X

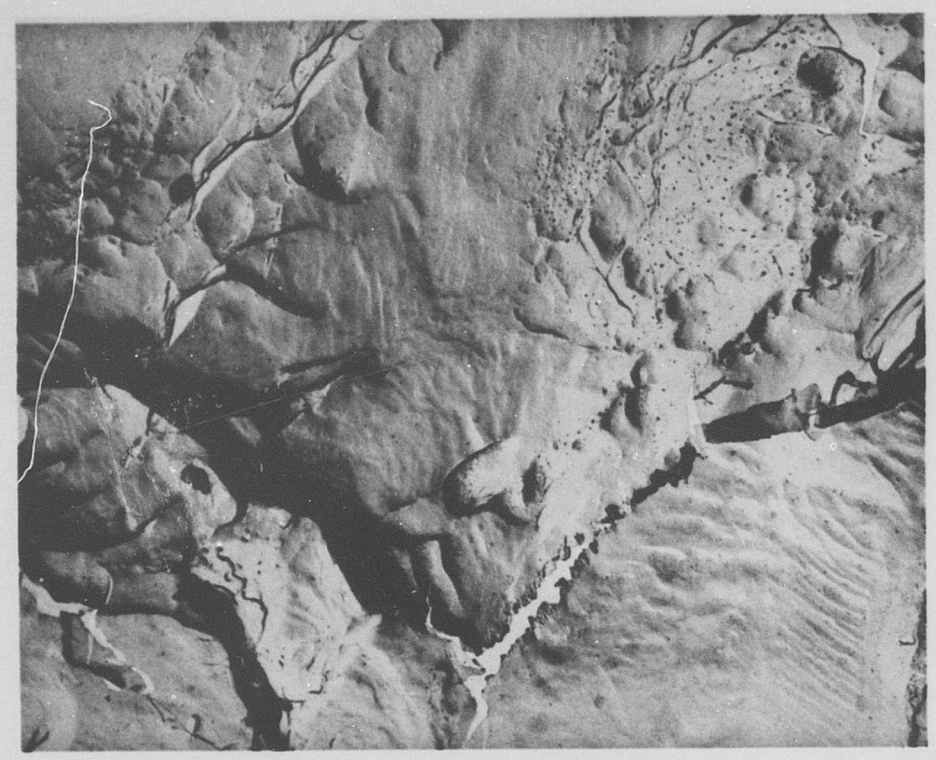

COMMENTS

This area of the fracture surface is composed of dimples and serpentine glide.

Figure C-169b Inconel X-750, Condition L: Electron Fractograph Showing 4,200X Magnification of Notched Fracture

Inconel 713C
Condition L

BLANK PAGE

Table C-26

Tensile and Shear Test Data

Material Inconel 713C Specimen Condition L

Averaged Data (-423°F)		
Unnotched Specimens	Control	Irradiated
Ultimate Strength (ksi)	111.6	133.4
0.2% Yield Strength (ksi)	108.0	133.2
Elongation in Gage Length (%)	3.0	1.75
Reduction in Area (%)	7.0	1.7
Ultimate Shear Strength (ksi)	144.5	c
Notched Specimens		
Ultimate Strength (ksi)	127.7	135.4
Ratios		
Notched-Ult./Unnotched-Ult.	1.14	1.01
Notched-Ult./Unnotched-Yield	1.18	1.02

Unnotched Specimens				
Specimen Number	Ult. Tensile Strength(ksi)	Yield Strength 0.2% Offset (ksi)	Reduction in Area (%)	Elongation (%)
401	130.5	130.0	1.7	2.1
402	137.5	132.0	2.5	1.9
405	126.2	[a]	2.6	0.88[b]
406	139.4	137.5	0.13	2.12

Notched Specimens		Shear Specimens*	
Specimen Number	Ult. Tensile Strength (ksi)	Specimen Number	Ult. Shear Strength (ksi)
413	127.1		
414	141.5		
417	146.5		
418	126.5		

[a]Broke before 0.2% offset
[b]Broke outside of gage length
[c]Not tested
*Not Applicable

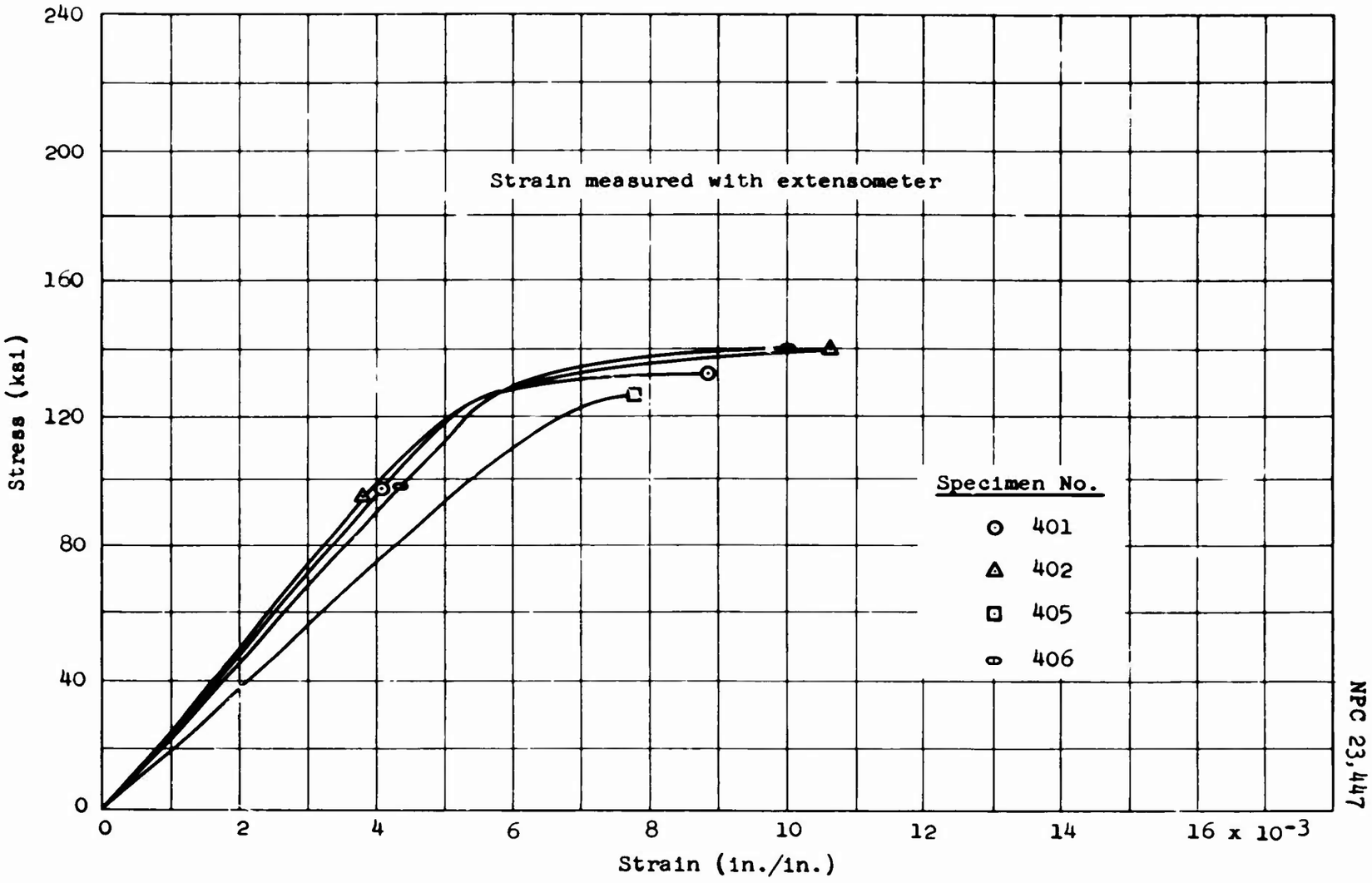

Figure C-170 Inconel 713C, Condition LU: Stress-Strain Curves

Table C-27
X-Ray Diffraction Data

Material Inconel 713C Specimen LU 401

	STRAINED AREA		UNSTRAINED AREA	
DIFFRACTION PATTERN				
Miller Indices (hkl)	Interlattice Spacing, d (Å)	Relative Intensity (%)	Interlattice Spacing, d (Å)	Relative Intensity (%)
111	No Peaks		2.07	100
200	Observable			
220				
311				
222				

LATTICE PARAMETER (Å)		
111		3.59

MICROSTRESS, Δθ	
No Peak ($2\theta = 69^\circ$)	0.22° ($2\theta = 43.6^\circ$)
No Peak ($2\theta = 129^\circ$)	No Peak ($2\theta = 69^\circ$)
	No Peak ($2\theta = 129^\circ$)

METALLOGRAPHIC STUDY

Material Inconel 713C Neg.No. None

Specimen LU 401 Neg.Mag. 3X

Etchant None Photo Enlargement None

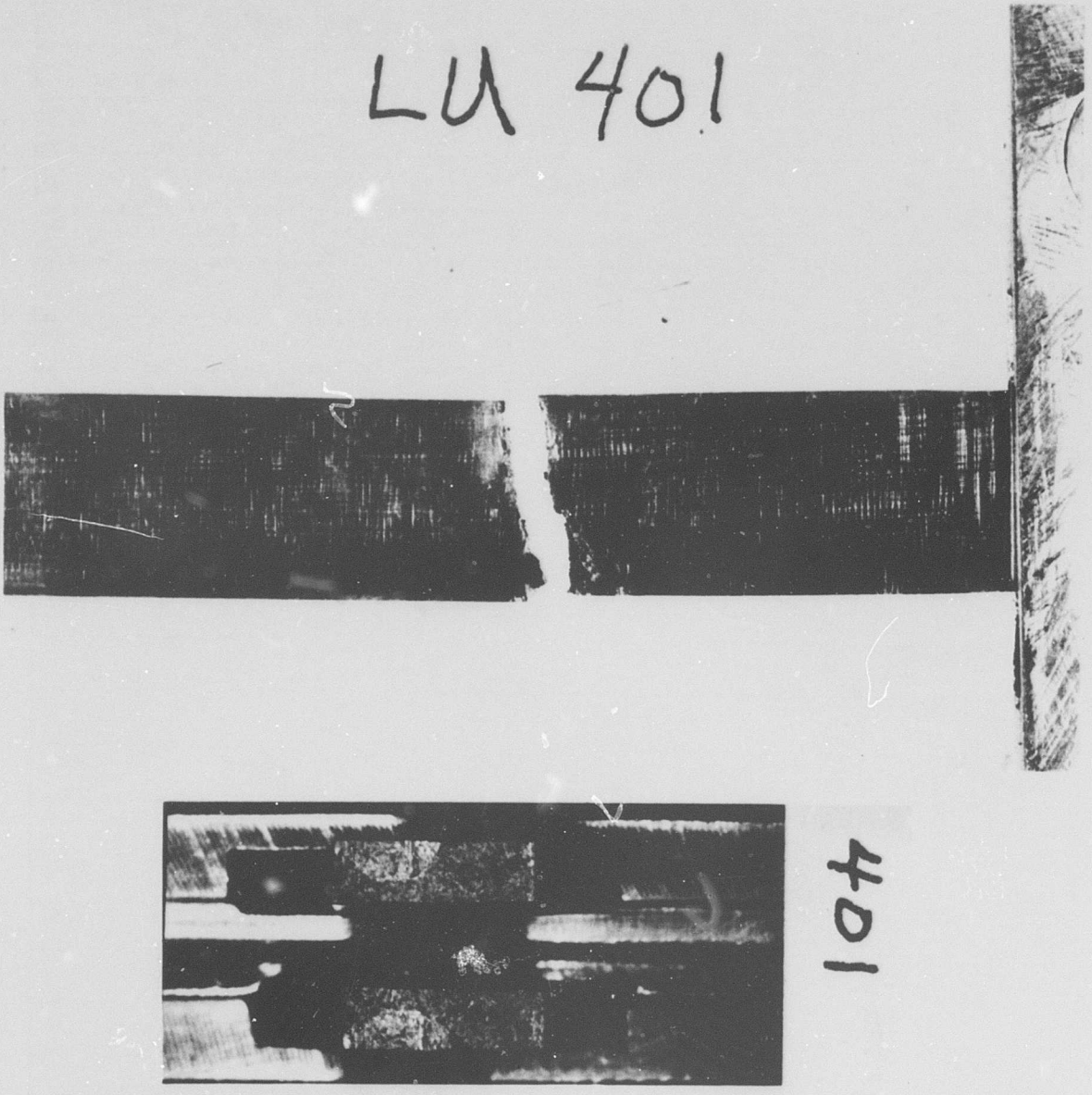

Figure C-171 Inconel 713C, Condition L: Macrophotograph Showing 3X Magnification of Specimen

METALLOGRAPHIC STUDY

Material Inconel 713C Neg.No. W86

Specimen LU 401 Neg.Mag. 100X

Etchant 10% Oxalic Acid (electrolytic) Photo Enlargement None

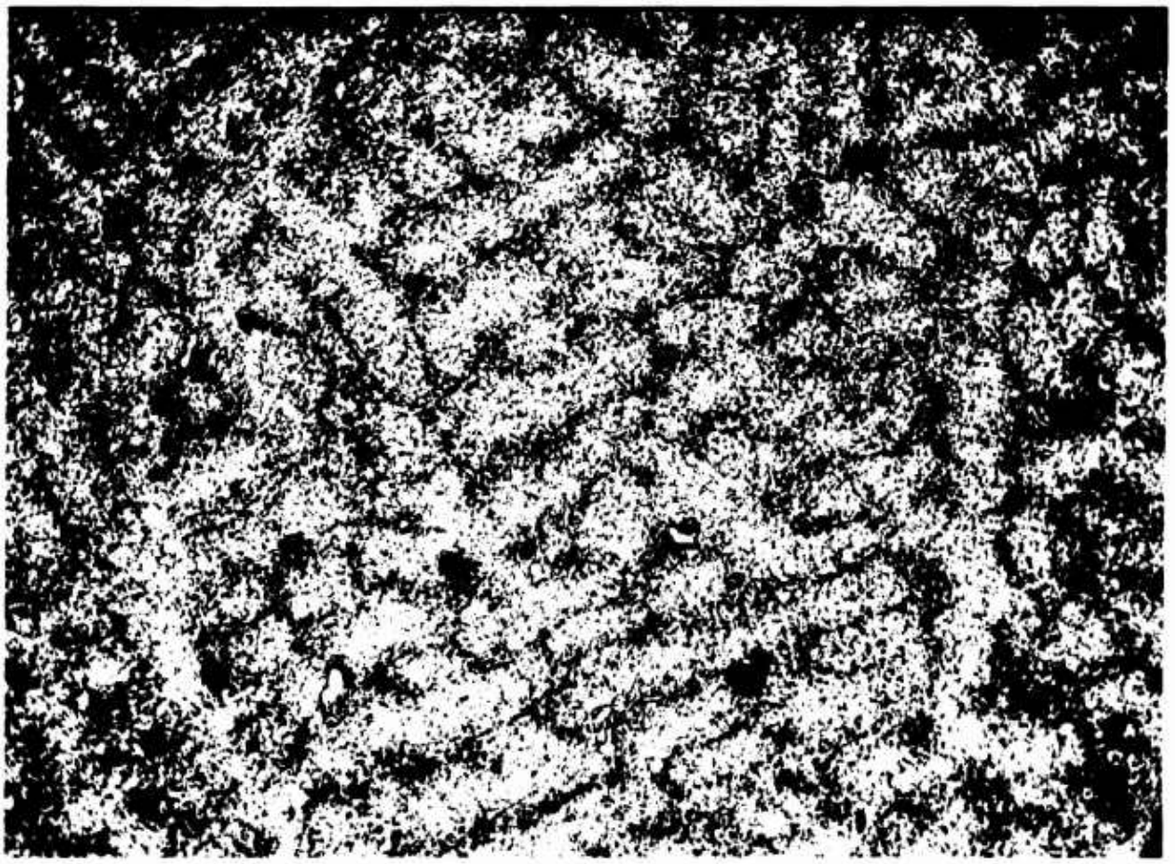

COMMENTS

The microstructure shows the typical dendritic structure characteristics of a casting (Ref. 13). A Ni-Cr phase constitutes the grain matrix, with the gamma prime precipitate as the primary strengthening mechanism. The grain boundary network contains Ti-C.

Figure C-172 Inconel 713C, Condition L: Optical Micrograph Showing 100X Magnification of Unstrained Area

METALLOGRAPHIC STUDY

Material Inconel 713C **Neg.No.** W87

Specimen LU 401 **Neg.Mag.** 1,000X

Etchant 10% Oxalic Acid (electrolytic) **Photo Enlargement** None

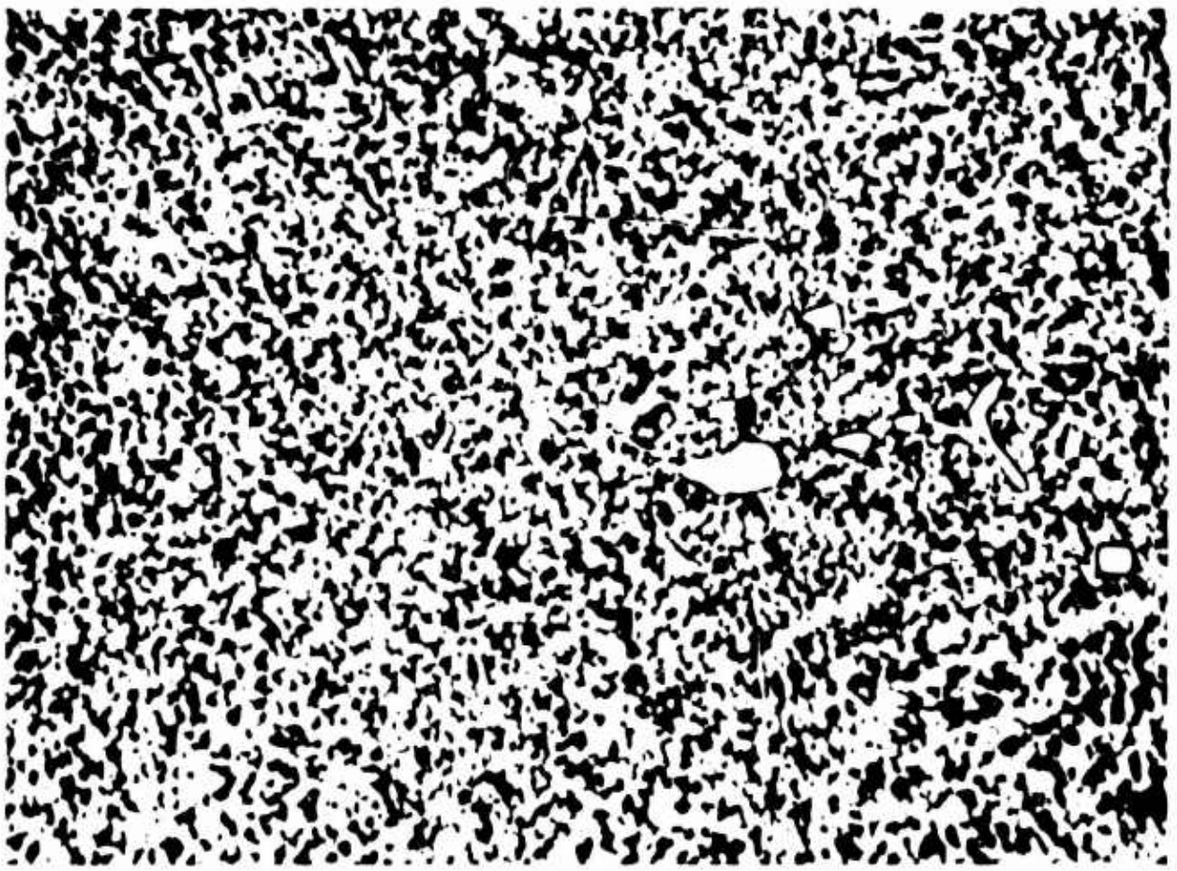

COMMENTS

The microstructure shows the typical structure characteristics of a casting. A Ni-Cr phase constitutes the grain matrix, with the gamma prime precipitate as the primary strengthening mechanism. The grain boundary network contains Ti-C.

Figure C-173 Inconel 713C, Condition L: Optical Micrograph Showing 1,000X Magnification of Unstrained Area

METALLOGRAPHIC STUDY

Material Inconel 713C Neg.No. W14

Specimen LU 401 Neg.Mag. 100X

Etchant 10% Oxalic Acid (electrolytic) Photo Enlargement None

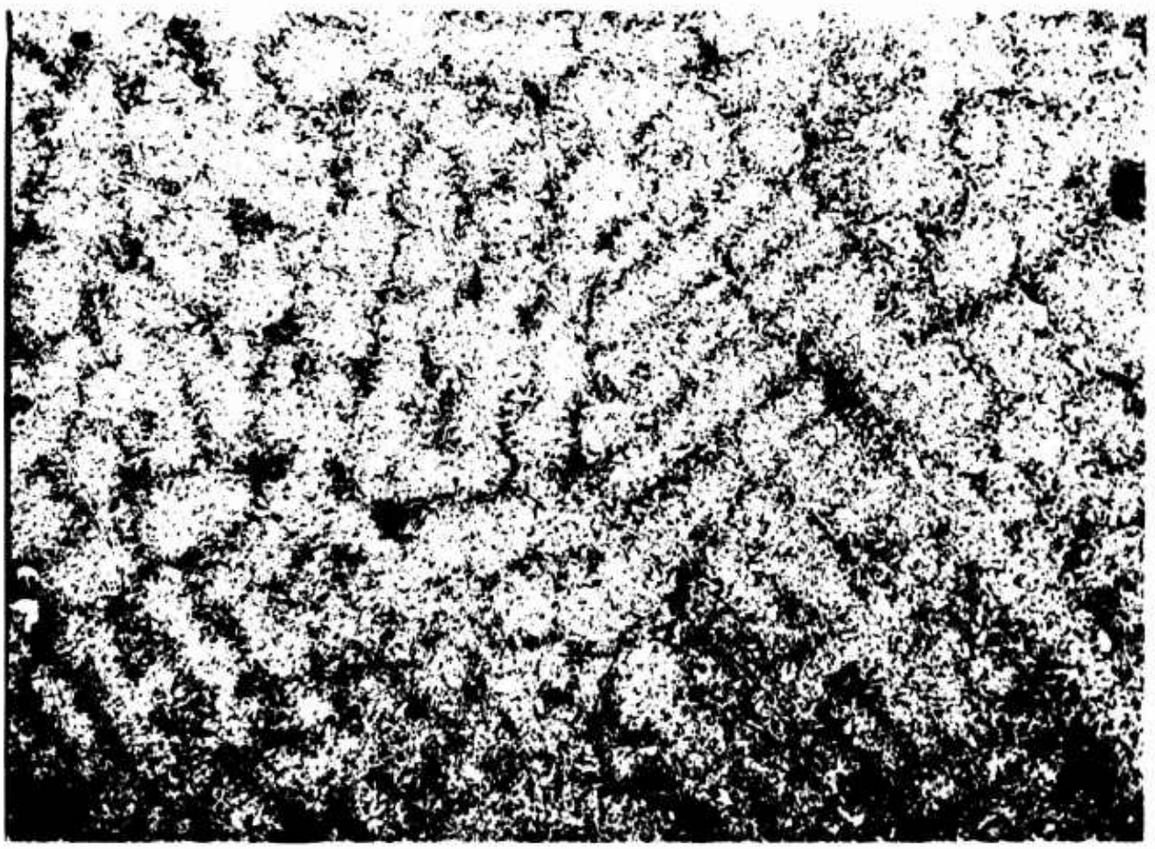

COMMENTS

The microstructure shows the typical dendritic structure characteristic of a casting. A Ni-Cr phase constitutes the grain matrix, with the gamma prime precipitate as the primary strengthening mechanism. The grain boundary network contains Ti-C.

Figure C-174 Inconel 713C, Condition L: Optical Micrograph Showing 100X Magnification of General Strained Area

METALLOGRAPHIC STUDY

Material Inconel 713C Neg.No. W13

Specimen LU 401 Neg.Mag. 1,000X

Etchant 10% Oxalic Acid (electrolytic) Photo Enlargement None

COMMENTS

The microstructure shows the Ni-Cr phase that constitutes the grain matrix. Gamma prime precipitate is the primary strengthening mechamism. The grain boundary network contains Ti-C.

Figure C-175 Inconel 713C, Condition L: Optical Micrograph Showing 1,000X Magnification of General Strained Area

METALLOGRAPHIC STUDY

Material Inconel 713C Neg.No. W15

Specimen LU 401 Neg.Mag. 100X

Etchant 10% Oxalic Acid (electrolytic) Photo Enlargement None

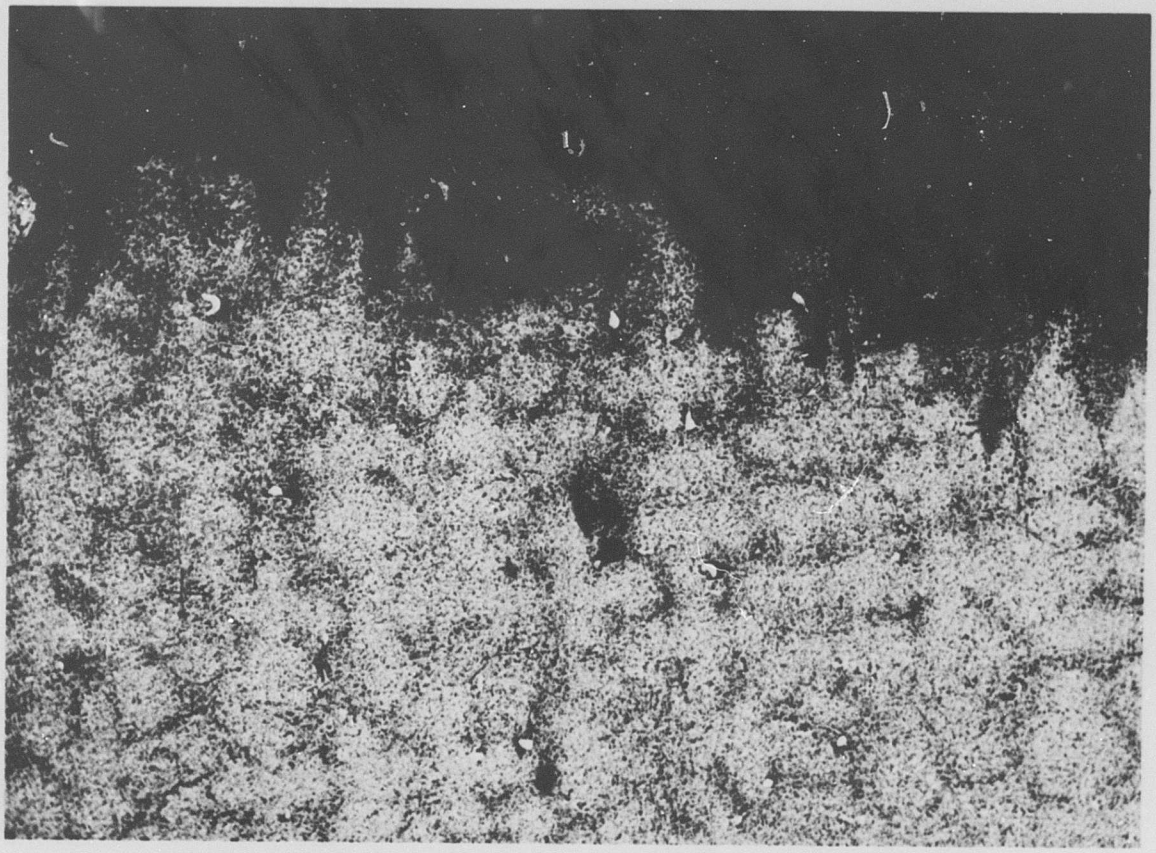

COMMENTS

The fracture is transgranular. The microstructure shows a Ni-Cr phase matrix with gamma prime precipitate and Ti-C grain boundary precipitate.

Figure C-176 Inconel 713C, Condition L: Optical Micrograph Showing 100X Magnification of Fracture Edge

METALLOGRAPHIC STUDY

Material Inconel 713C Neg.No. W12

Specimen LU 401 Neg.Mag. 1,000X

Etchant 10% Oxalic Acid (electrolytic) Photo Enlargement None

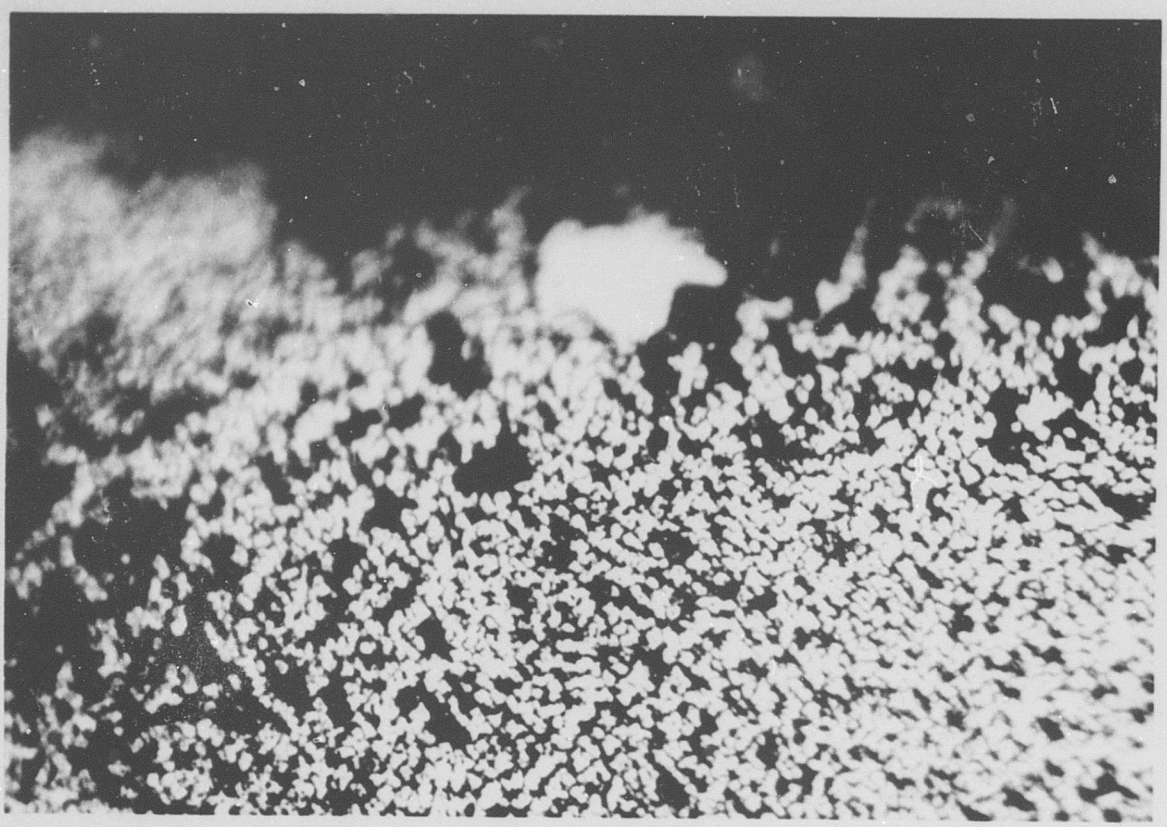

COMMENTS

The fracture is transgranular. The microstructure shows a Ni-Cr phase matrix with gamma prime precipitate and Ti-C grain boundary precipitate.

Figure C-177 Inconel 713C, Condition L: Optical Micrograph Showing 1,000X Magnification of General Strained Area

METALLOGRAPHIC STUDY

Material Inconel 713C Neg.No. 107-6

Specimen LU 401 Neg.Mag. 7,500X

Etchant 10% Oxalic Acid (electrolytic) Photo Enlargement 2X

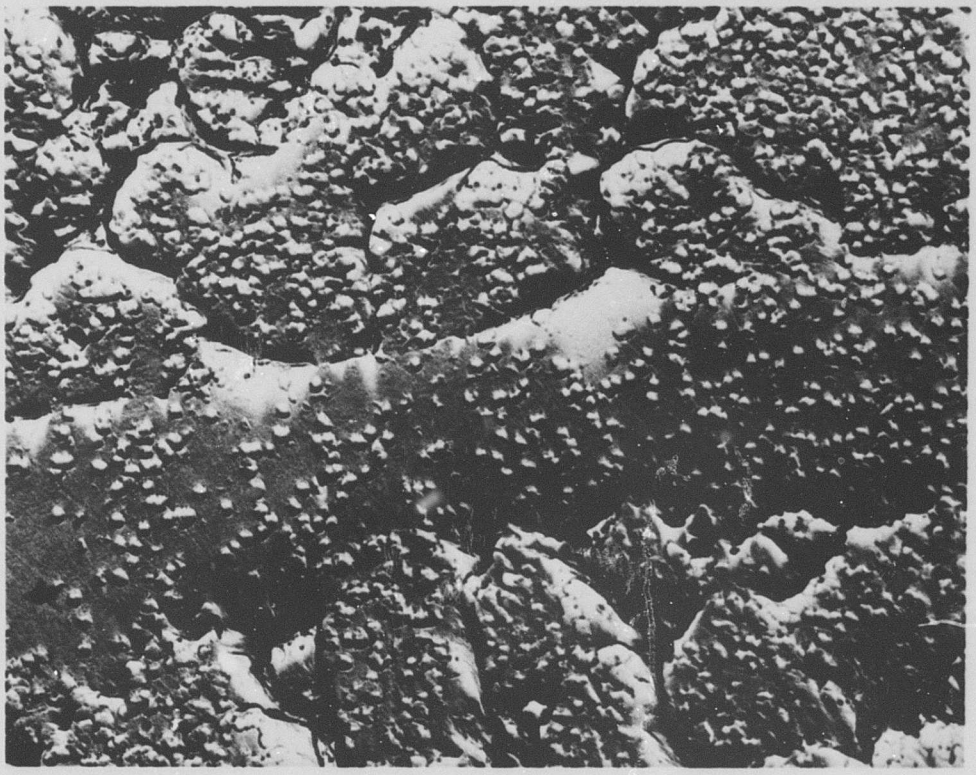

COMMENTS

The microstructure shows the Ni-Cr matrix with the gamma prime precipitate.

Figure C-178 Inconel 713C, Condition L: Electron Micrograph Showing 15,000X Magnification of Unstrained Area

METALLOGRAPHIC STUDY

Material Inconel 713C Neg.No. 107-8

Specimen LU 401 Neg.Mag. 7,500X

Etchant 10% Oxalic Acid (electrolytic) Photo Enlargement 2X

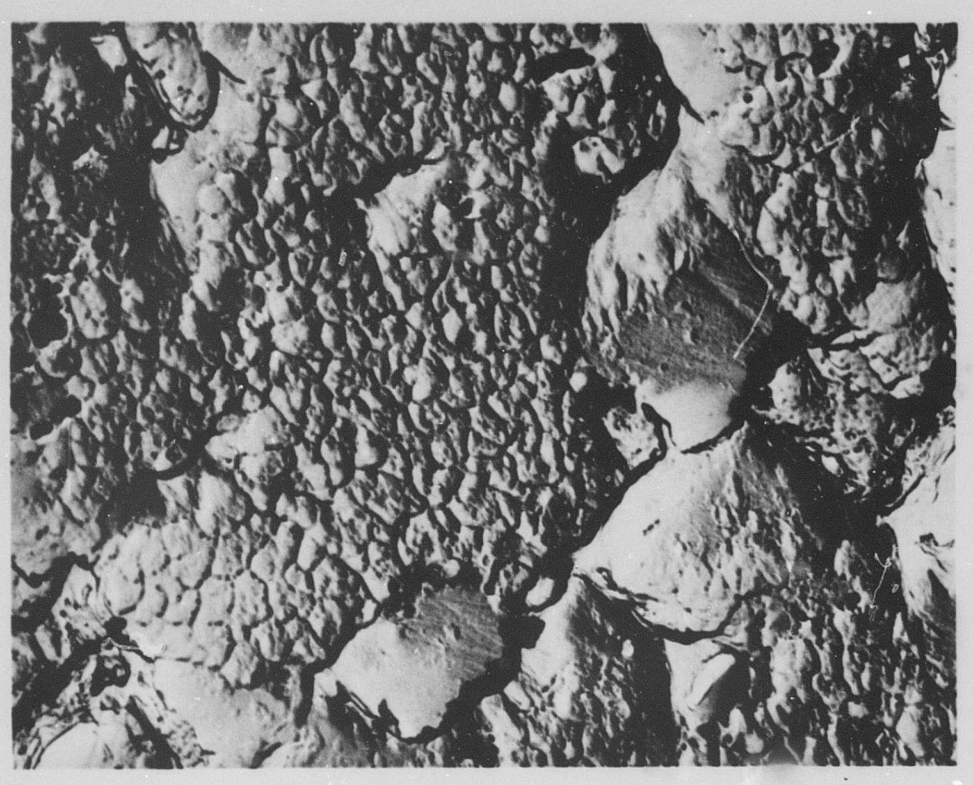

COMMENTS

The microstructure shows a Ni-Cr matrix and gamma prime precipitate.

Figure C-179 Inconel 713C, Condition L: Electron Micrograph Showing 15,000X Magnification of Strained Area

METALLOGRAPHIC STUDY

Material Inconel 713C Neg.No. 96-5

Specimen LU 401 Neg.Mag. 2,100X

Etchant None Photo Enlargement 2X

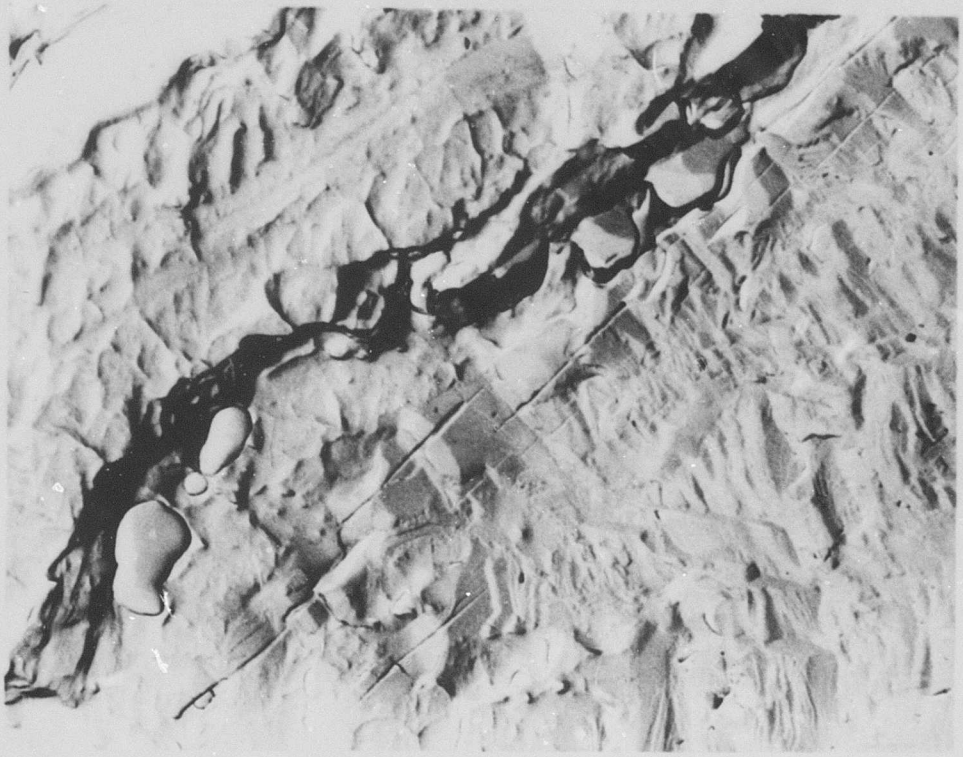

COMMENTS

The fracture surface shows a large area of brittle cleavage (lower right) and an area of shallow, partially formed microvoids (upper left). These shallow microvoids are often present on brittle failures.

Figure C-180 Inconel 713C, Condition L: Electron Fractograph Showing 4,200X Magnification at Center of Fracture

METALLOGRAPHIC STUDY

Material	Inconel 713C	**Neg.No.**	96-6
Specimen	LU 401	**Neg.Mag.**	2,100X
Etchant	None	**Photo Enlargement**	2X

COMMENTS

The fracture topography at the edge was the same as that found at the center (Fig. C-180).

Figure C-181 Inconel 713C, Condition L: Electron Fractograph Showing 4,200X Magnification Near Edge of Fracture

METALLOGRAPHIC STUDY

Material Inconel 713C Neg.No. 98-2

Specimen LN 413 Neg.Mag. 2,100X

Etchant None Photo Enlargement 2X

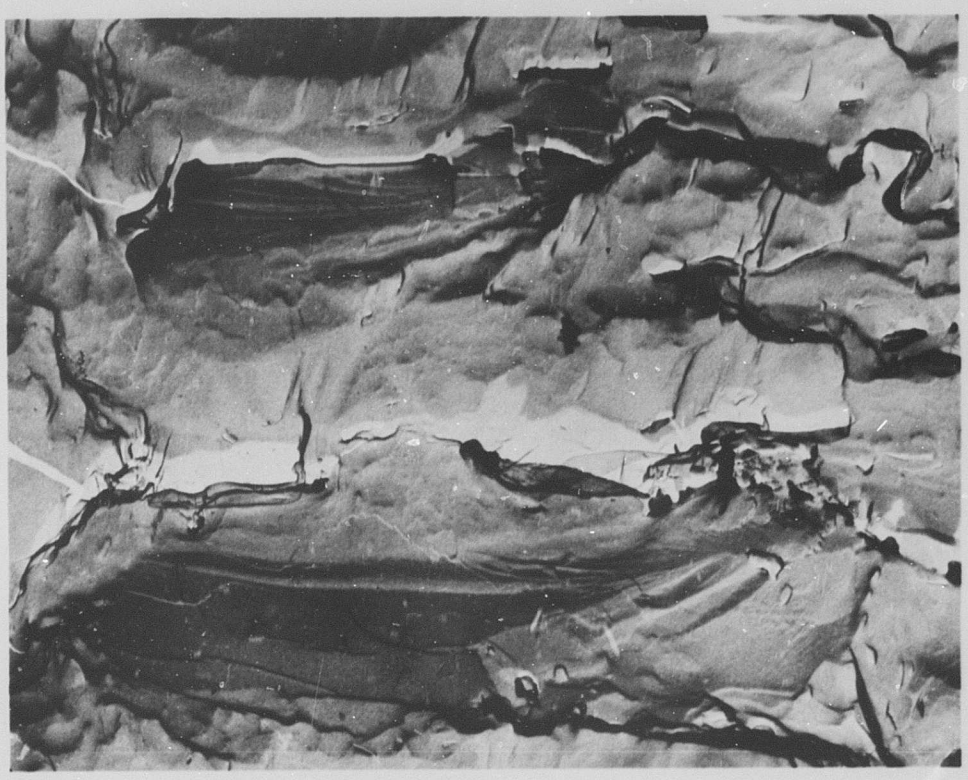

COMMENTS

The notched specimens displayed the same fracture characteristics as the unnotched specimens: large areas of brittle cleavage and shallow, partially formed dimples.

Figure C-182a Inconel 713C, Condition L: Electron Fractograph Showing 4,200X Magnification of Notched Fracture

METALLOGRAPHIC STUDY

Material	Inconel 713C	**Neg.No.**	98-3
Specimen	LN 413	**Neg.Mag.**	2,100X
Etchant	None	**Photo Enlargement**	2X

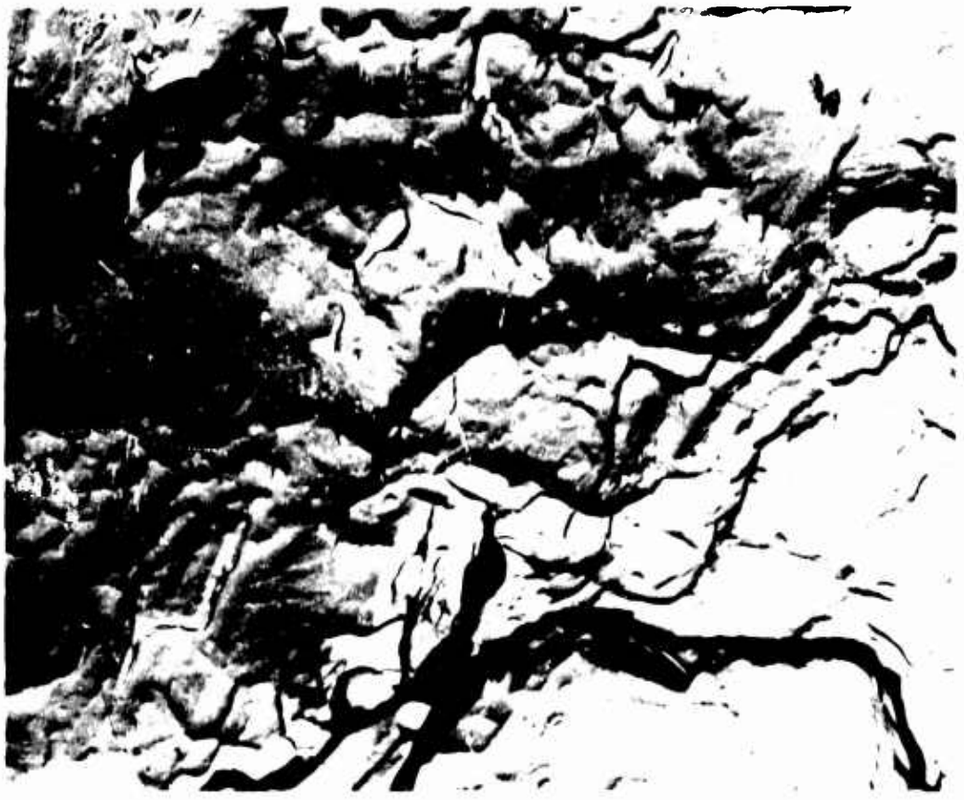

COMMENTS

This area of the notched specimen shows a large area of shallow, partially formed dimples.

Figure C-182b Inconel 713C, Condition L: Electron Fractograph Showing 4,200X Magnification of Notched Fracture

Hastelloy C
Condition L

BLANK PAGE

Table C-28
Tensile and Shear Test Data

Material Hastelloy C Specimen Condition L

Averaged Data (-423°F)		
Unnotched Specimens	Control	Irradiated
Ultimate Strength (ksi)	185.7	185.4
0.2% Yield Strength (ksi)	111.0	111.5
Elongation in Gage Length (%)	29.2	35.1
Reduction in Area (%)	32.6	31.6
Ultimate Shear Strength (ksi)	170.8	139.2
Notched Specimens		
Ultimate Strength (ksi)	No Data	156.3
Ratios		
Notched-Ult./Unnotched-Ult.		0.84
Notched-Ult./Unnotched-Yield		1.40

Unnotched Specimens				
Specimen Number	Ult. Tensile Strength (ksi)	Yield Strength 0.2% Offset (ksi)	Reduction in Area (%)	Elongation (%)
353	183.0	112.0	28.6	30.9
354	185.9	112.0	38.4	41.0
357	192.0	108.0	36.8	46.3[a]
358	188.2	114.0	27.2	33.3

Notched Specimens		Shear Specimens	
Specimen Number	Ult. Tensile Strength (ksi)	Specimen Number	Ult. Shear Strength (ksi)
365	158.8	1	140.6
366	Broke on rebound	2	140.6
369	Broke on rebound	3	137.7
370	153.8	4	137.7

[a]Picked up next specimen

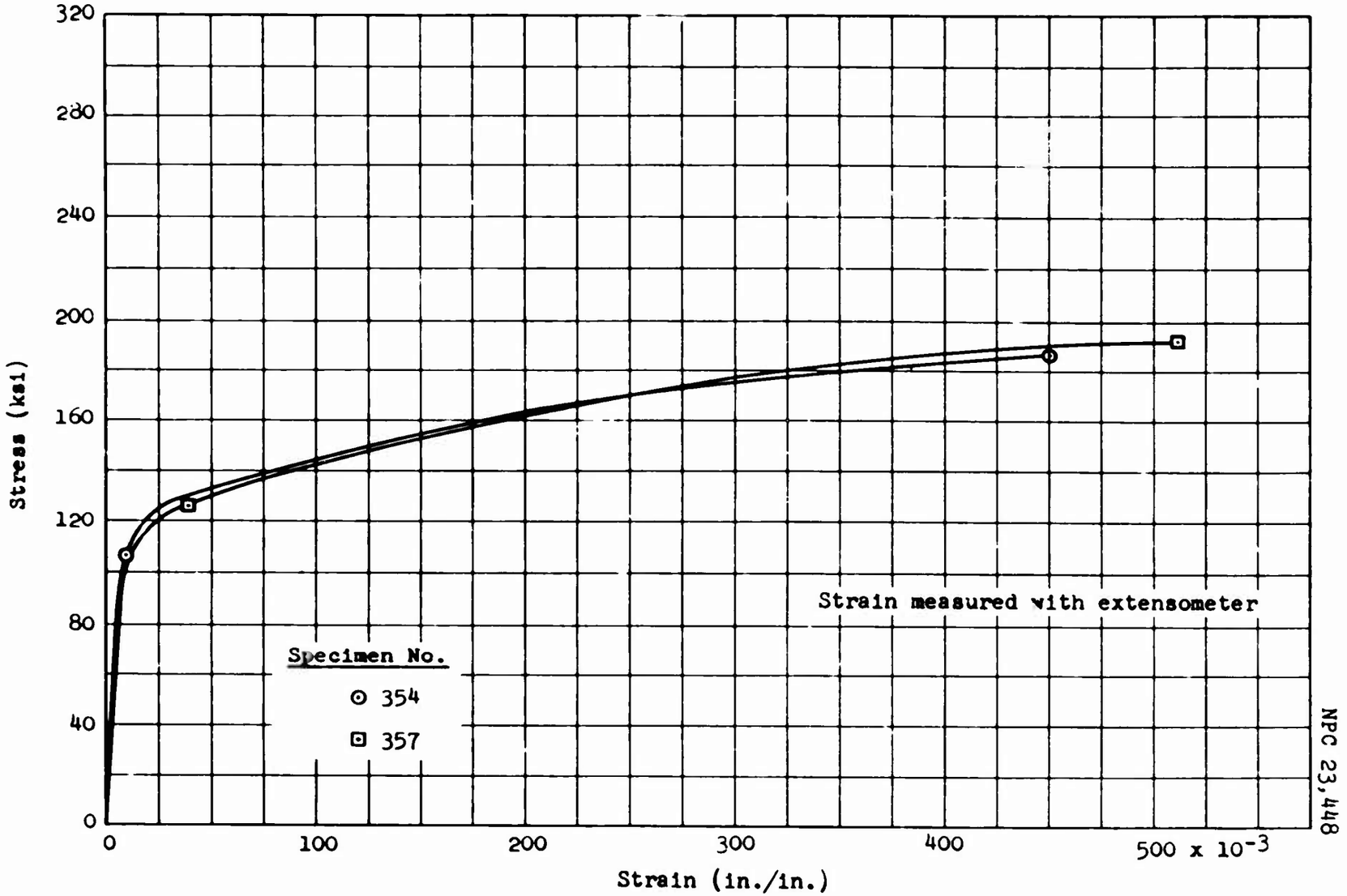

Figure C-183 Hastelloy C, Condition LU: Stress-Strain Curves

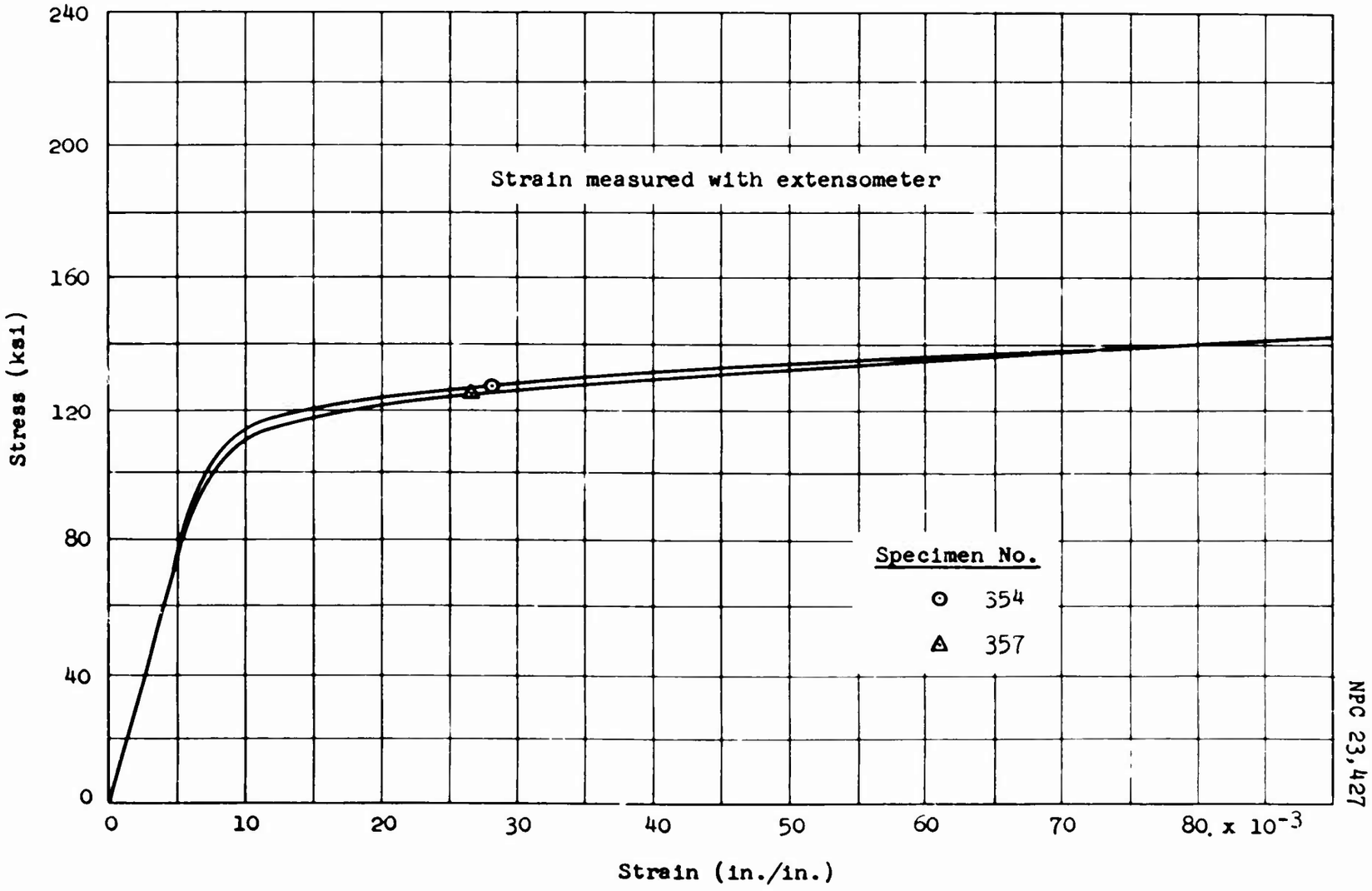

Figure C-184 Hastelloy C, Condition LU: Stress-Strain Curves (Expanded Scale)

Table 2-2

X-Ray Diffraction Data

Material Hastelloy C Specimen LW 354

	STRAINED AREA		UNSTRAINED AREA	
DIFFRACTION PATTERN				
Miller Indices (hkl)	Interlattice Spacing, d (Å)	Relative Intensity (%)	Interlattice Spacing, d (Å)	Relative Intensity (%)
111	2.09	75	2.09	100
200	1.81	55	1.81	69
220	1.28	100	1.28	55
311	1.09	35	1.09	25
LATTICE PARAMETER (Å)				
111	3.62		3.62	
200	3.62		3.62	
220	3.62		3.62	
311	3.62		3.62	
MICROSTRESS, $\Delta\theta$				
0.32^{o} ($2\theta = 74.20$)			0.22^{o} ($2\theta = 74.00$)	
No Peak ($2\theta = 129^{o}$)			No Peak ($2\theta = 129^{o}$)	

METALLOGRAPHIC STUDY

Material Hastelloy C Neg.No. None

Specimen LU 354 Neg.Mag. 3X

Etchant None Photo Enlargement None

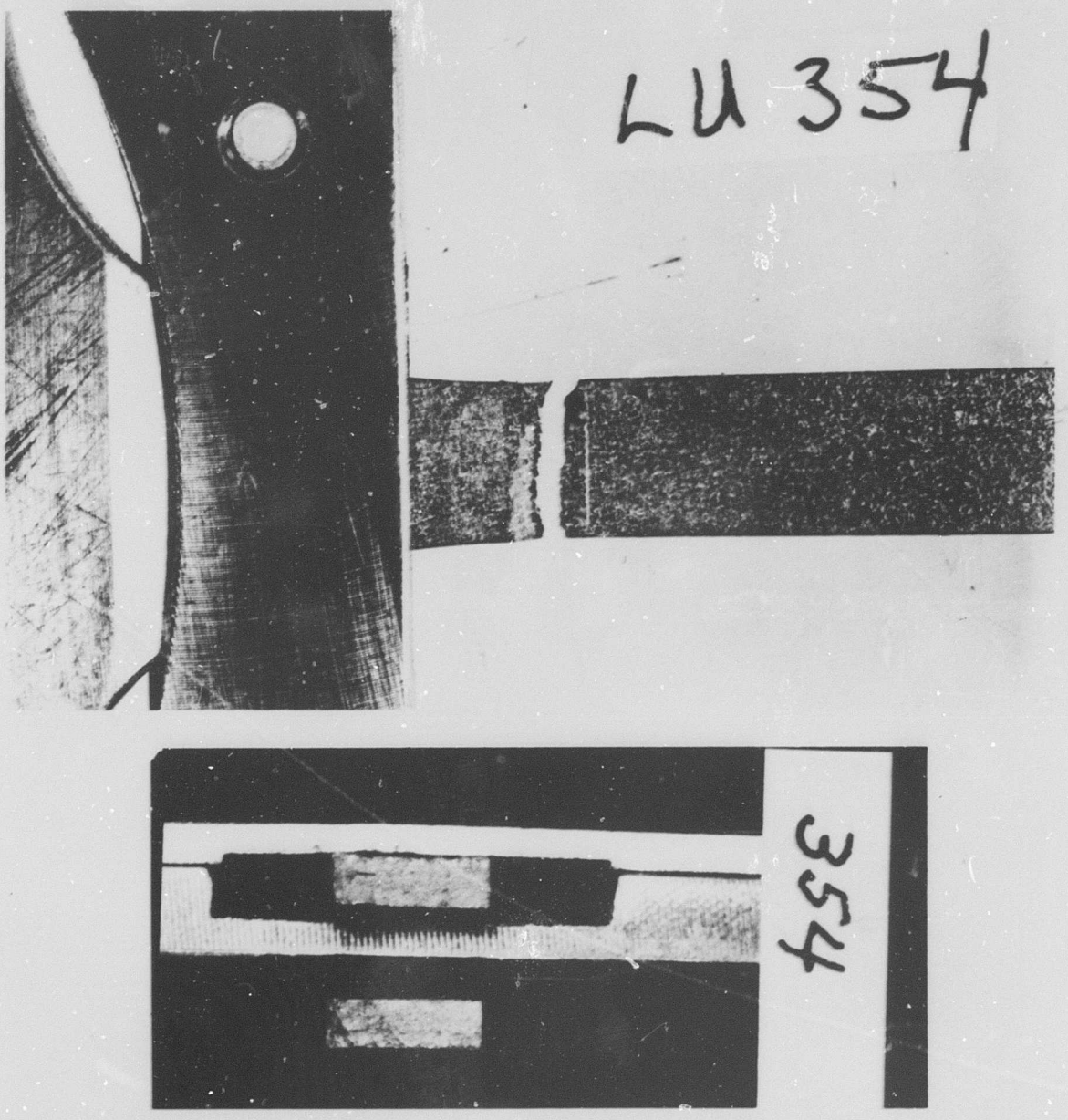

Figure C-185 Hastelloy C, Condition L: Macrophotograph Showing 3X Magnification of Specimen

METALLOGRAPHIC STUDY

Material Hastelloy C **Neg.No.** W68

Specimen LU 354 **Neg.Mag.** 100X

Etchant $HCl+H_2O_2$ **Photo Enlargement** None

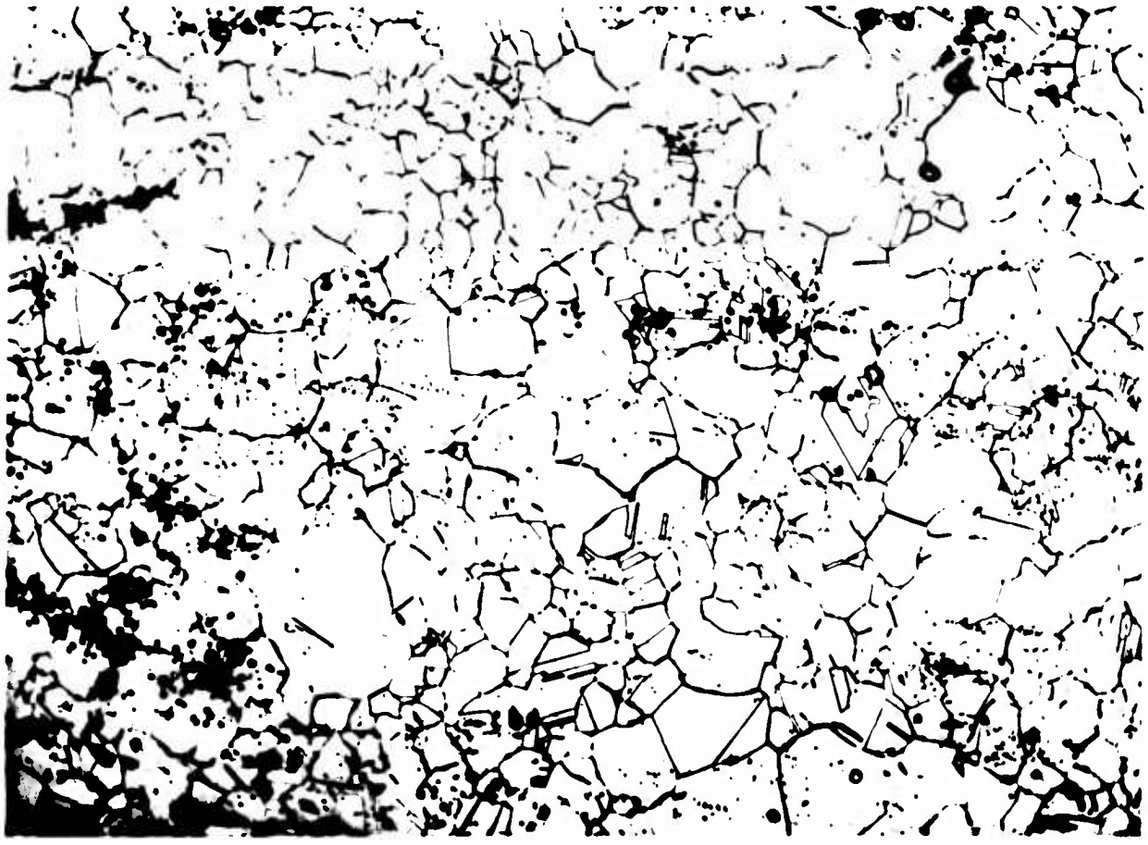

COMMENTS

The microstructure consists of an equiaxed, Ni-rich, austenitic matrix with a semi-banded carbide distribution. Annealing twins are visible.

Figure C-186 Hastelloy C, Condition L: Optical Micrograph Showing 100X Magnification of Unstrained Area

METALLOGRAPHIC STUDY

Material Hastelloy C Neg.No. W66

Specimen LU 354 Neg.Mag. 1,000X

Etchant $HCl+H_2O_2$ Photo Enlargement None

COMMENTS

The microstructure consists of an equiaxed, Ni-rich, austenitic matrix with a semi-banded carbide distribution. Annealing twins are visible.

Figure C-187 Hastelloy C, Condition L: Optical Micrograph Showing 1,000X Magnification of Unstrained Area

METALLOGRAPHIC STUDY

Material Hastelloy C **Neg.No.** W73

Specimen LU 354 **Neg.Mag.** 100X

Etchant $HCl+H_2O_2$ **Photo Enlargement** None

COMMENTS

The microstructure of the strained area shows a severely deformed, Ni-rich, austenitic matrix. Note the strain orientation direction within each grain and on the annealing twins.

Figure C-188 Hastelloy C, Condition L: Optical Micrograph Showing 100X Magnification of General Strained Area

METALLOGRAPHIC STUDY

Material Hastelloy C — Neg.No. W76

Specimen LU 354 — Neg.Mag. 1,000X

Etchant $HCl+H_2O_2$ — Photo Enlargement None

COMMENTS

The microstructure shows the severely deformed, Ni-rich, austenitic matrix and the strain orientation direction within each grain and on the annealing twins. Note that the large carbide has ruptured perpendicular to the load direction.

Figure C-189 Hastelloy C, Condition L: Optical Micrograph Showing 1,000X Magnification of General Strained Area

METALLOGRAPHIC STUDY

Material	Hastelloy C	**Neg.No.**	W64
Specimen	LU 354	**Neg.Mag.**	100X
Etchant	$HCl+H_2O_2$	**Photo Enlargement**	None

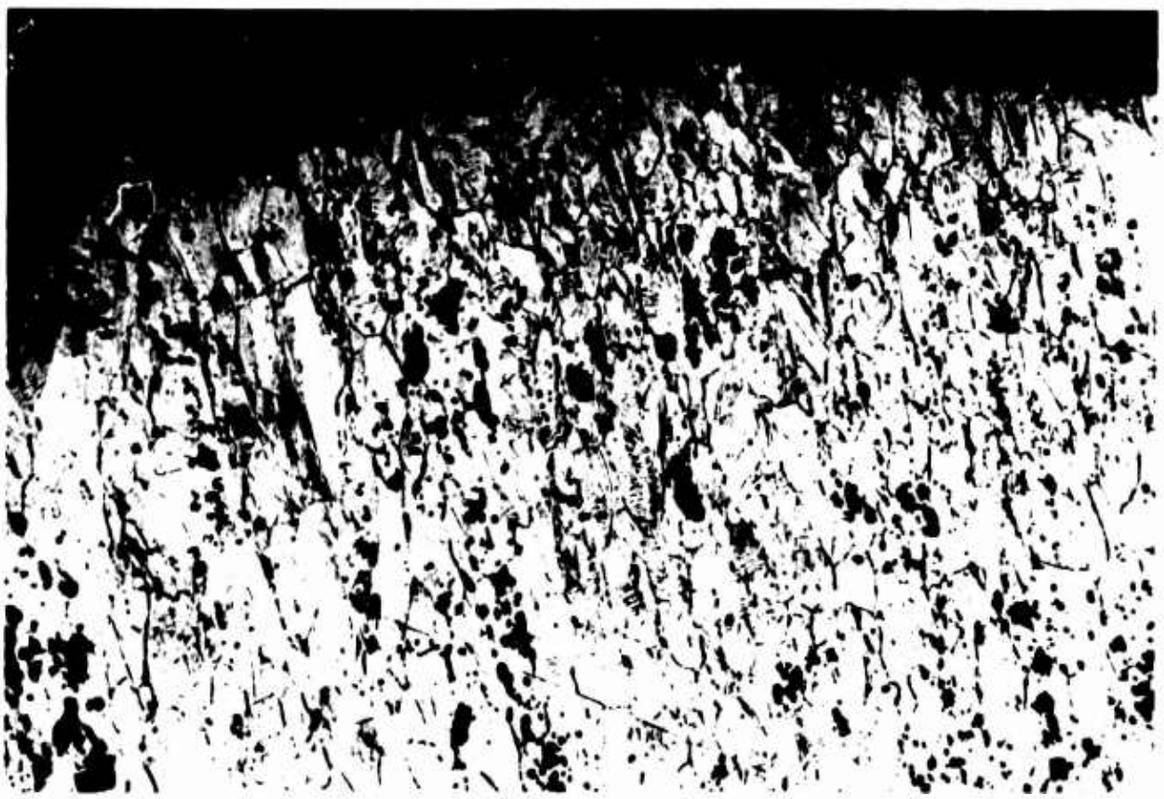

COMMENTS

The microstructure shows the fracture to be transgranular. Note the strain orientation direction within each grain and on the annealing twins.

Figure C-190 Hastelloy C, Condition L: Optical Micrograph Showing 100X Magnification of Fracture Edge

METALLOGRAPHIC STUDY

Material	Hastelloy C	Neg.No.	W77
Specimen	LU 354	Neg.Mag.	1,000X
Etchant	$HCl+H_2O_2$	Photo Enlargement	None

COMMENTS

The microstructure shows a transgranular fracture through the severely deformed, Ni-rich austenitic matrix. Note the strain orientation direction within each grain and on the annealing twins.

Figure C-191 Hastelloy C, Condition L: Optical Micrograph Showing 1,000X Magnification of Fracture Edge

METALLOGRAPHIC STUDY

Material Hastelloy C — Neg.No. 110-5

Specimen LU 354 — Neg.Mag. 7,500X

Etchant $HCl+H_2O_2$ — Photo Enlargement 2X

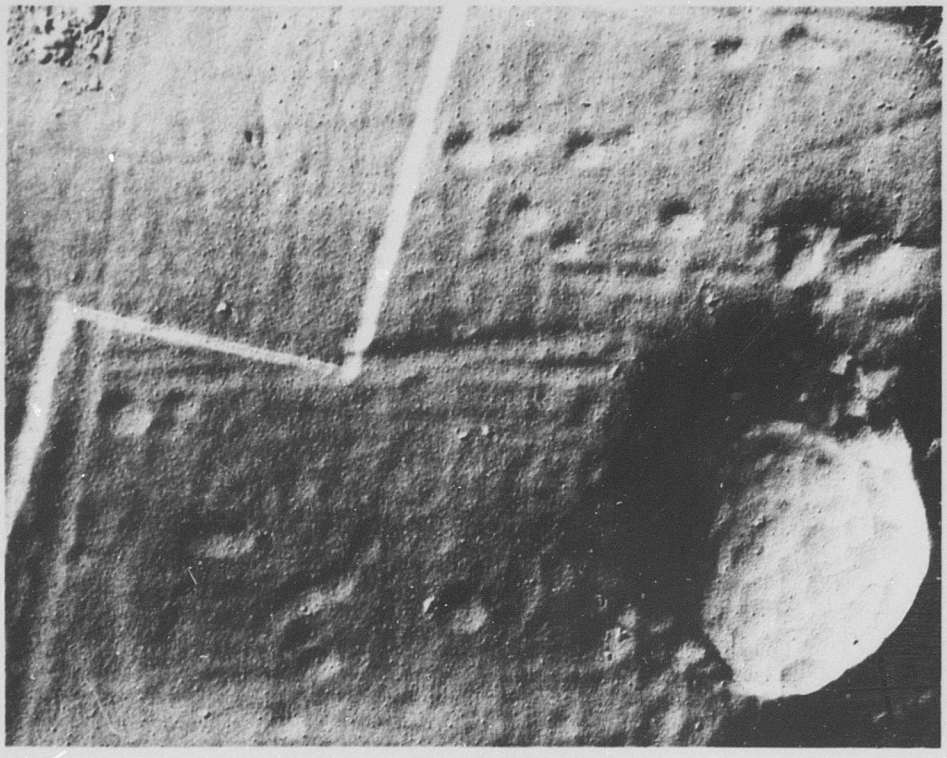

COMMENTS

The microstructure shows a twin, the austenitic matrix, and a large carbide site.

Figure C-192 Hastelloy C, Condition L: Electron Micrograph Showing 15,000X Magnification of Unstrained Area

METALLOGRAPHIC STUDY

Material Hastelloy C Neg.No. 104-11

Specimen LU 354 Neg.Mag. 7,500X

Etchant $HCl+H_2O_2$ Photo Enlargement 2X

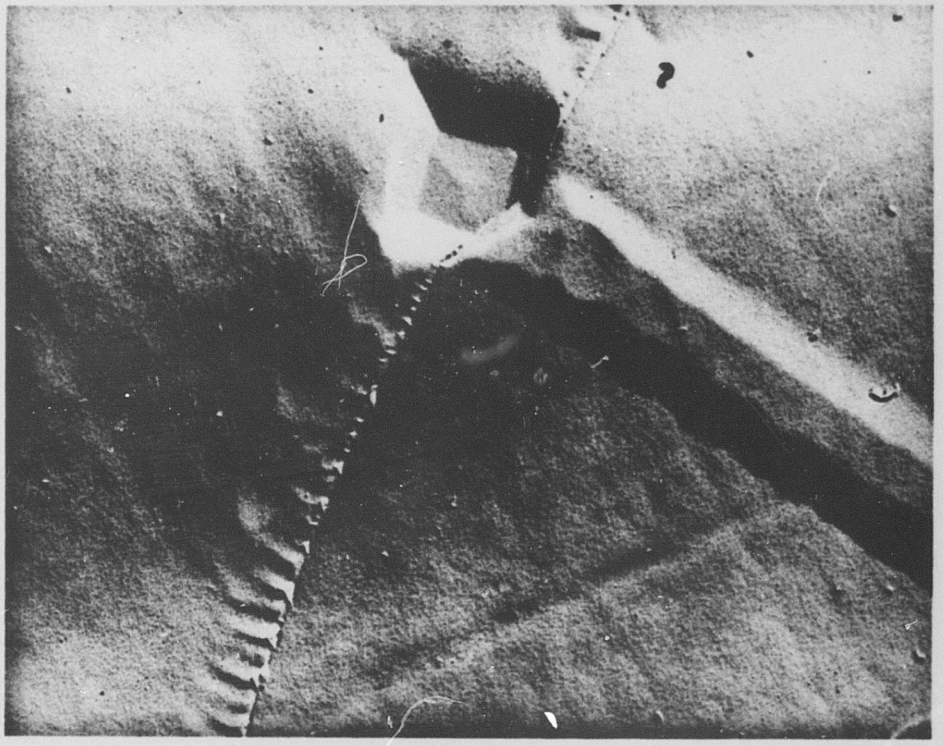

COMMENTS

The microstructure shows an annealing twin, a grain boundary with fine precipitate, and the austenitic matrix. The strain lines present in the optical photographs show up as shallow troughs in this photograph. The rectangular precipitate site is unusual for a carbide.

Figure C-193 Hastelloy C, Condition L: Electron Micrograph Showing 15,000X Magnification of Strained Area

METALLOGRAPHIC STUDY

Material Hastelloy C — Neg.No. 91-5

Specimen LU 354 — Neg.Mag. 2,100X

Etchant None — Photo Enlargement 2X

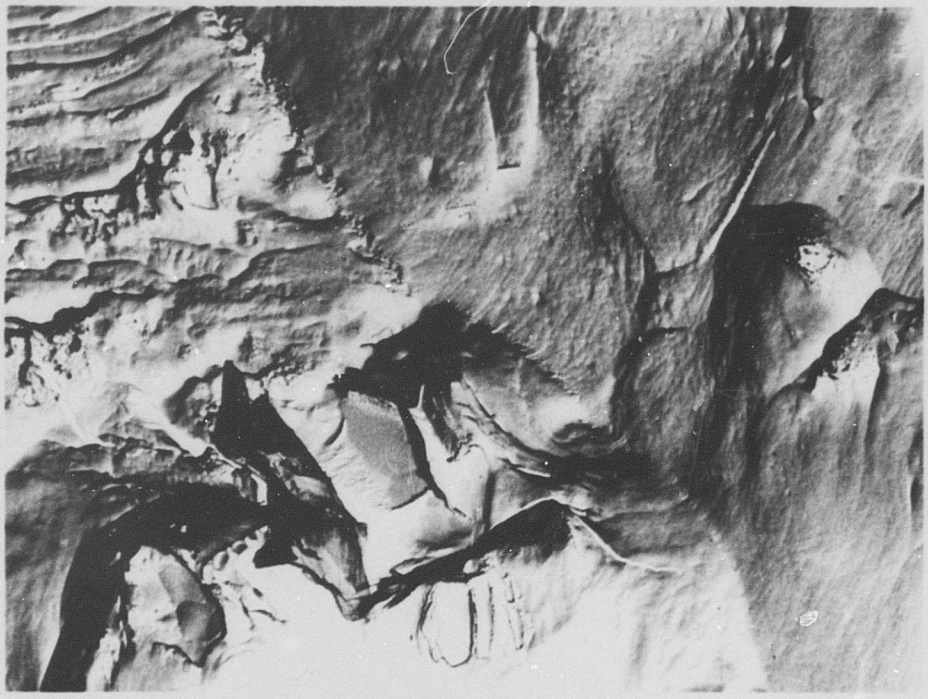

COMMENTS

A grain boundary runs diagonally across the photograph. There appears to be a fine carbide network on the boundary similar to that of Fig. C-193. The structure on the right is decohesion glide with large microvoids. The structure across the boundary is probably a type of serpentine glide. In the lower center of the photo are large carbides that have fractured in a brittle manner, probably ahead of the main crack front initiating the free surface necessary for serpentine glide.

Figure C-194 Hastelloy C, Condition L: Electron Fractograph Showing 4,200X Magnification at Center of Fracture

METALLOGRAPHIC STUDY

Material Hastelloy C Neg.No. 91-7

Specimen LU 354 Neg.Mag. 2,100X

Etchant None Photo Enlargement 2X

COMMENTS

This area taken near the edge exhibits a ductile failure mode, as evidenced by the large microvoids and decohesion glide markings.

Figure C-195 Hastelloy C, Condition L: Electron Fractograph Showing 4,200X Magnification Near Edge of Fracture

METALLOGRAPHIC STUDY

Material	Hastelloy C	**Neg.No.**	97-12
Specimen	LN 365	**Neg.Mag.**	2,100X
Etchant	None	**Photo Enlargement**	2X

COMMENTS

The fracture is made up of large, oriented microvoids and decohesion glide markings indicative of a ductile failure. The striations that lie across the large microvoid in the upper center of the photograph have been classified as ripples or a type of serpentine glide.

Figure C-196 Hastelloy C, Condition L: Electron Fractograph Showing 4,200X Magnification Near Edge of Fracture

Titanium A-110-AT
Condition T

BLANK PAGE

Table C-30

Tensile and Shear Test Data

Material Titanium A-110-AT Specimen Condition T

Averaged Data (-423°F)		
Unnotched Specimens	Control	Irradiated
Ultimate Strength (ksi)	216.4	226.5
0.2% Yield Strength (ksi)	199.5	205.1
Elongation in Gage Length (%)	17.1	12.8
Reduction in Area (%)	17.8	16.8
Ultimate Shear Strength (ksi)	130.6	142.5
Notched Specimens		
Ultimate Strength (ksi)	171.0	153.7
Ratios		
Notched- Ult./Unnotched-Ult.	0.79	0.68
Notched-Ult./Unnotched-Yield	0.86	0.75

Unnotched Specimens				
Specimen Number	Ult. Tensile Strength(ksi)	Yield Strength 0.2% Offset (ksi)	Reduction in Area (%)	Elongation (%)
281	220.1	202.0	17.9	11.5
282	230.9	208.0	16.8	13.3
285	227.4	205.0	17.5	13.9
286	227.7	205.5	15.0	13.0

Notched Specimens		Shear Specimens	
Specimen Number	Ult. Tensile Strength (ksi)	Specimen Number	Ult. Shear Strength (ksi)
329	146.1	1	133.1
330	170.9	2	154.4
333	139.5	3	140.0
334	158.1	4	142.6

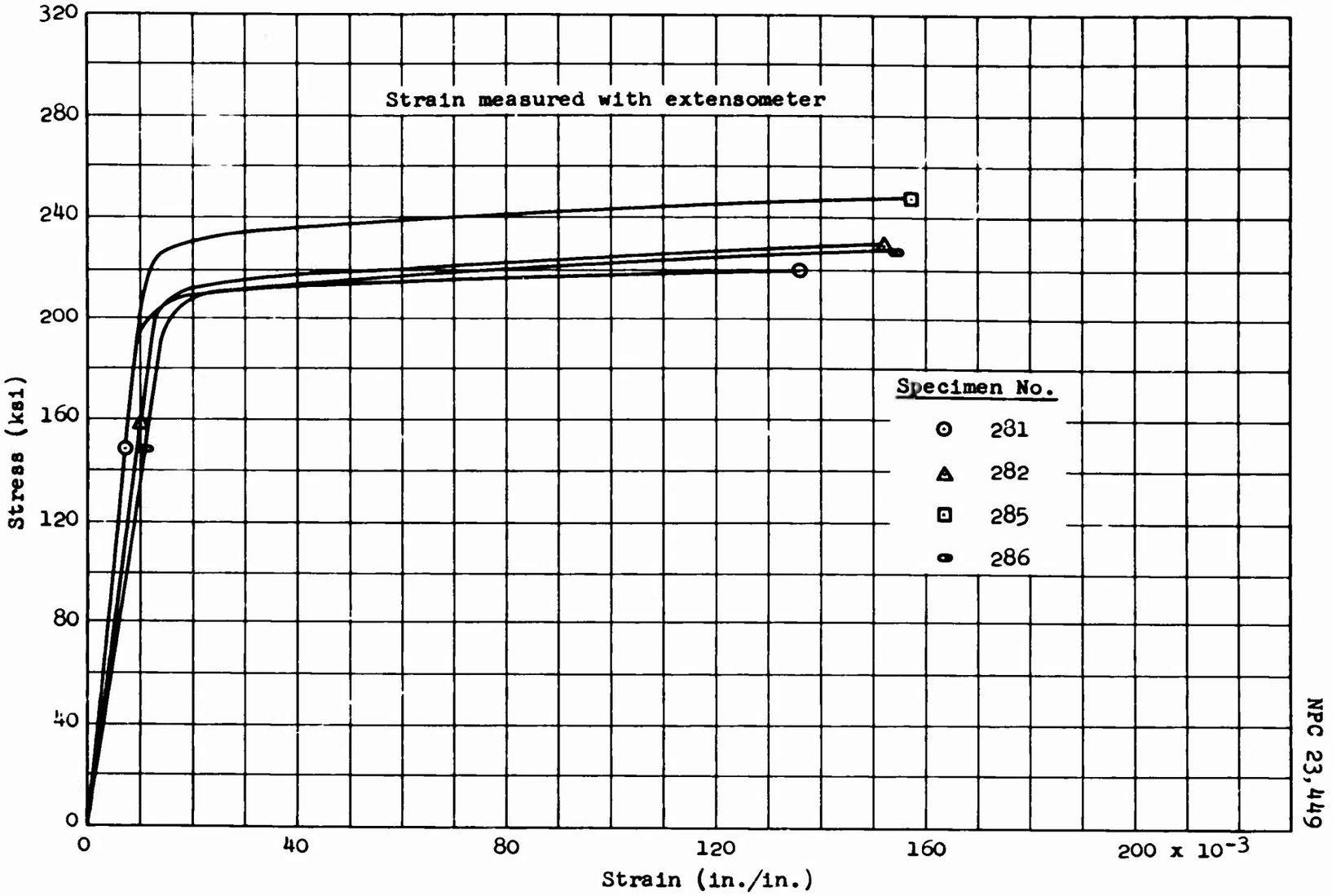

Figure C-197 Titanium A-110-AT, Condition TU: Stress-Strain Curves

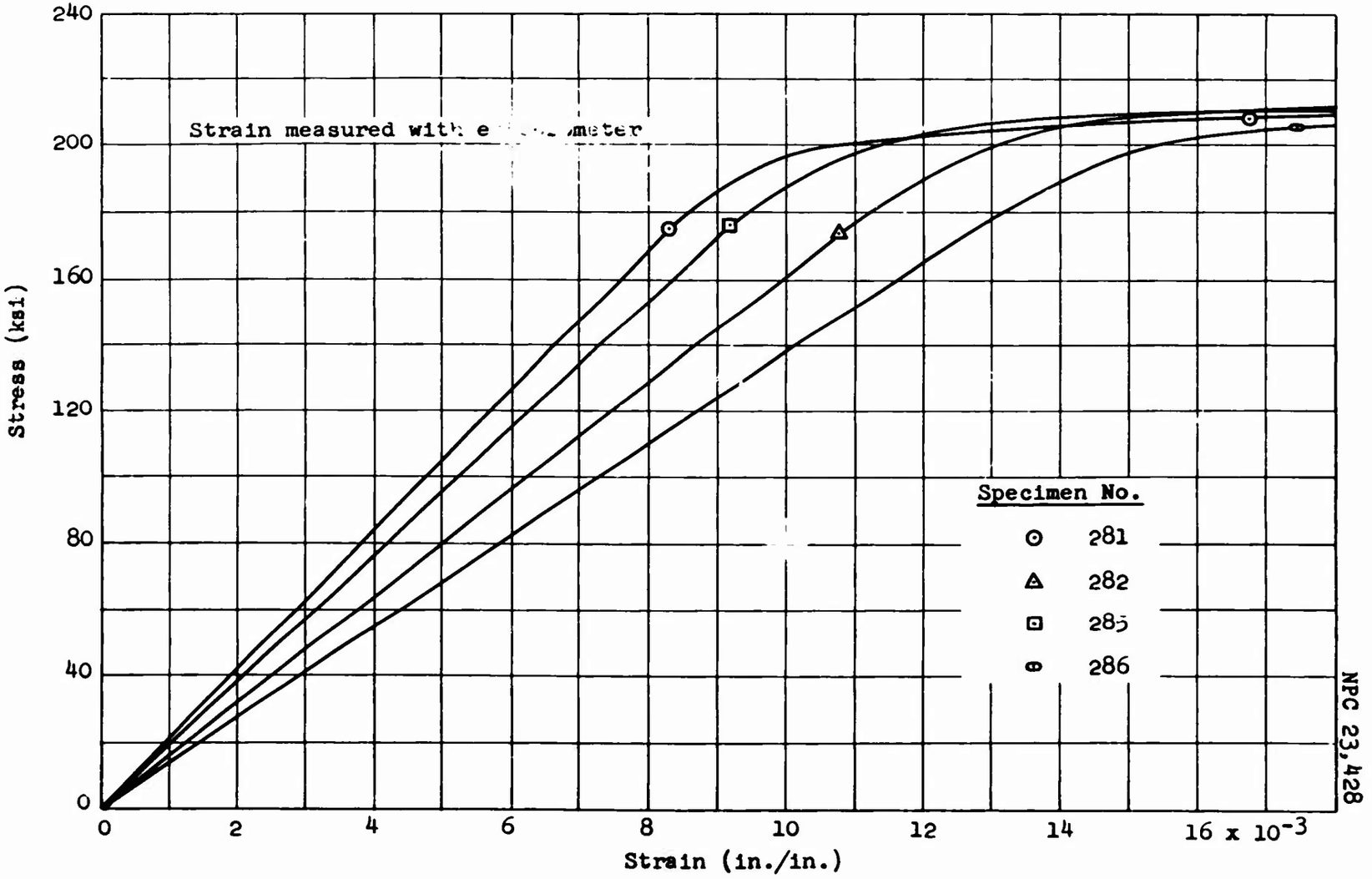

Figure C-198 Titanium A-110-AT, Condition TU: Stress-Strain Curves (Expanded Scale)

Table C-31
X-Ray Diffraction Data

Material Titanium A-110-AT Specimen TU 285

	STRAINED AREA		UNSTRAINED AREA	
DIFFRACTION PATTERN				
Miller Indices (hkl)	Interlattice Spacing, d (Å)	Relative Intensity (%)	Interlattice Spacing, d (Å)	Relative Intensity (%)
002	2.35	100	2.35	100
011	2.24	28	2.24	35
012	1.73	15	1.92 1.73	10 40
110			1.47	8
103	1.33	25	1.33	80
112			1.24	8
004	1.17	7		
014	1.06	7	1.06	8

LATTICE PARAMETER (Å)

Axis a	2.95	2.95
Axis c	4.68	4.68

MICROSTRESS, $\Delta\theta$

0.17° ($2\theta = 82.2^{\circ}$)	No Peak ($2\theta = 82^{\circ}$)
0.13° ($2\theta = 38.25^{\circ}$)	0.15° ($2\theta = 38.35^{\circ}$)

METALLOGRAPHIC STUDY

Material Titanium A-110-AT Neg.No. None

Specimen TU 285 Neg.Mag. 3X

Etchant None Photo Enlargement None

TU 285

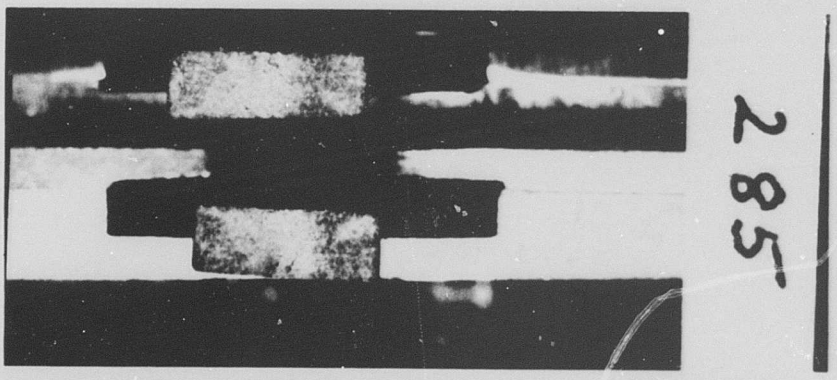

Figure C-199 Titanium A-110-AT, Condition T: Macrophotograph Showing 3X Magnification of Specimen

METALLOGRAPHIC STUDY

Material Titanium A-110-AT **Neg.No.** W35

Specimen TU 285 **Neg.Mag.** 100X

Etchant Kroll's Reagent, then HG-NYU **Photo Enlargement** None

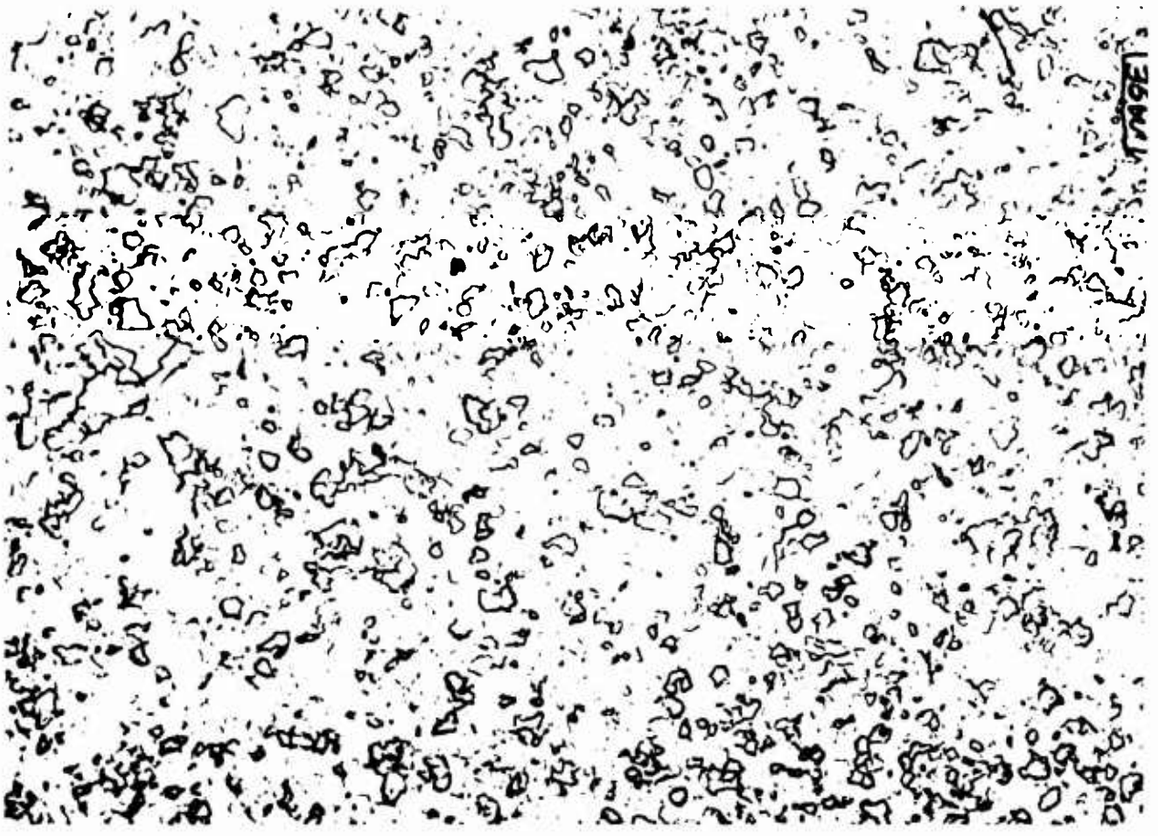

COMMENTS

The microstructure shows the typical alpha-Ti matrix.

Figure C-200 Titanium A-110-AT, Condition T: Optical Micrograph Showing 100X Magnification of Unstrained Area

METALLOGRAPHIC STUDY

Material Titanium A-110-AT Neg.No. W32

Specimen TU 285 Neg.Mag. 1,000X

Etchant Kroll's Reagent, then HG-NYU Photo Enlargement None

COMMENTS

The microstructure shows the typical alpha-Ti matrix. Note the alpha-grain orientation as depicted by the etchant attack.

Figure C-201 Titanium A-110-AT, Condition T: Optical Micrograph Showing 1,000X Magnification of Unstrained Area

METALLOGRAPHIC STUDY

Material Titanium A-110-AT **Neg.No.** W92

Specimen TU 285 **Neg.Mag.** 100X

Etchant Kroll's Reagent, then HG-NYU **Photo Enlargement** None

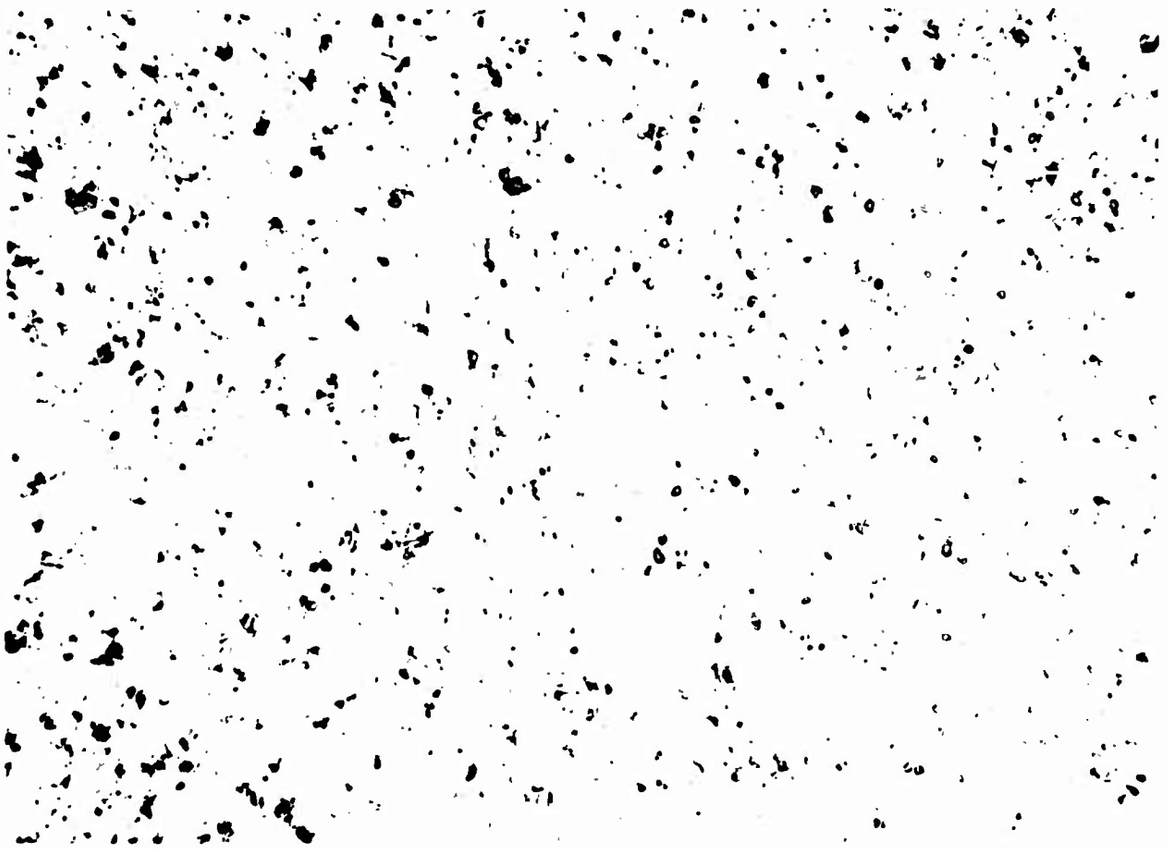

COMMENTS

The optical micrograph shows the structure to be the alpha-Ti matrix.

Figure C-202 Titanium A-110-AT, Condition T: Optical Micrograph Showing 100X Magnification of General Strained Area

METALLOGRAPHIC STUDY

Material Titanium A-110-AT Neg.No. W90

Specimen TU 285 Neg.Mag. 1,000X

Etchant Kroll's Reagent, then HG-NYU Photo Enlargement None

COMMENTS

The microstructure shows the structure to be the alpha-Ti matrix. The high strain has altered the ends of the annealing twins within the alpha-Ti matrix. Note also the strain lines in the twins.

Figure C-203 Titanium A-110-AT, Condition T: Optical Micrograph Showing 1,000X Magnification of General Strained Area

METALLOGRAPHIC STUDY

Material Titanium A-110-AT **Neg.No.** W93

Specimen TU 285 **Neg.Mag.** 100X

Etchant Kroll's Reagent, then HG-NYU **Photo Enlargement** None

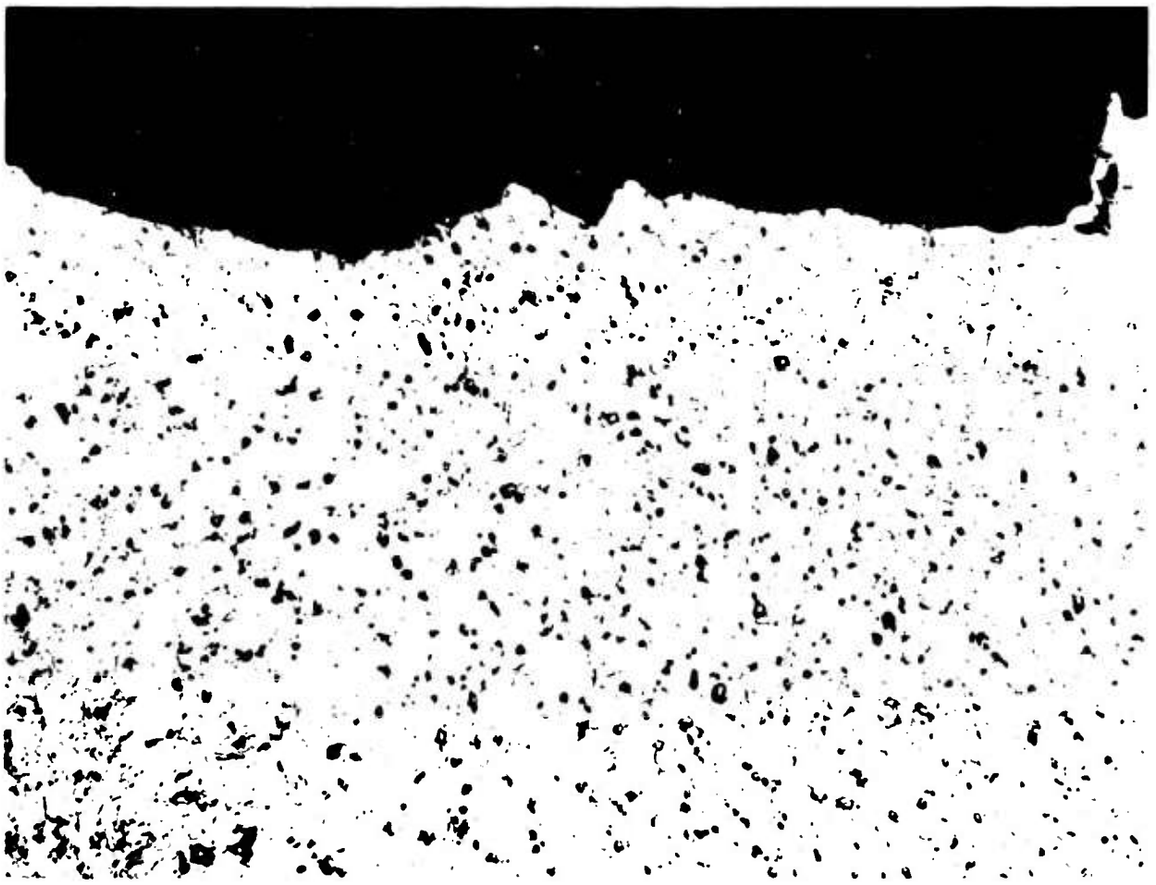

COMMENTS

The microstructure shows the fracture to be transgranular through the alpha-Ti matrix. Note the strain lines.

Figure C-204 Titanium A-110-AT, Condition T: Optical Micrograph Showing 100X Magnification of Fracture Edge

METALLOGRAPHIC STUDY

Material Titanium A-110-AT Neg.No. W91

Specimen TU 285 Neg.Mag. 1,000X

Etchant Kroll's Reagent, then HG-NYU Photo Enlargement None

COMMENTS

The microstructure shows the fracture to be transgranular through the alpha-Ti matrix. The high strain has altered the ends of the annealing twins within the alpha-Ti matrix. Note also the strain lines in the twins.

Figure C-205 Titanium A-110-AT, Condition T: Optical Micrograph Showing 1,000X Magnification of Fracture Edge

METALLOGRAPHIC STUDY

Material Titanium A-110-AT Neg.No. 108-1

Specimen TU 285 Neg.Mag. 7,500X

Etchant Kroll's Reagent Photo Enlargement 2X

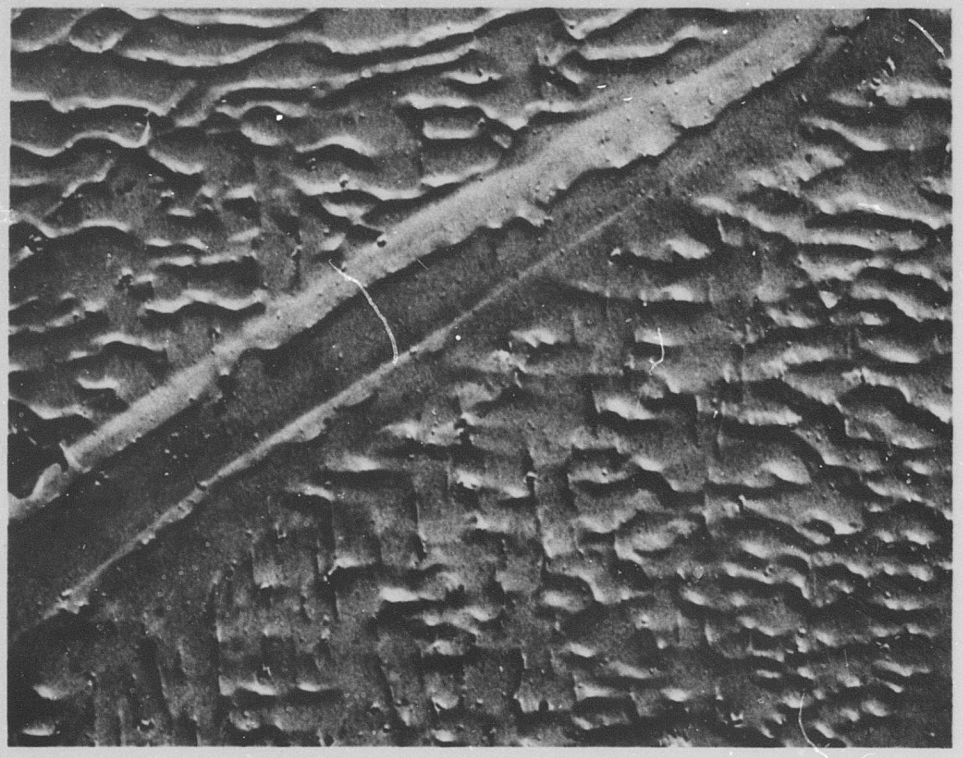

COMMENTS

The microstructure shows the alpha-Ti grains with different orientations.

Figure C-206 Titanium A-110-AT, Condition T: Electron Micrograph Showing 15,000X Magnification of Unstrained Area

METALLOGRAPHIC STUDY

Material	Titanium A-110-AT	Neg.No.	104-9
Specimen	TU 285	Neg.Mag.	7,500X
Etchant	Kroll's Reagent	Photo Enlargement	2X

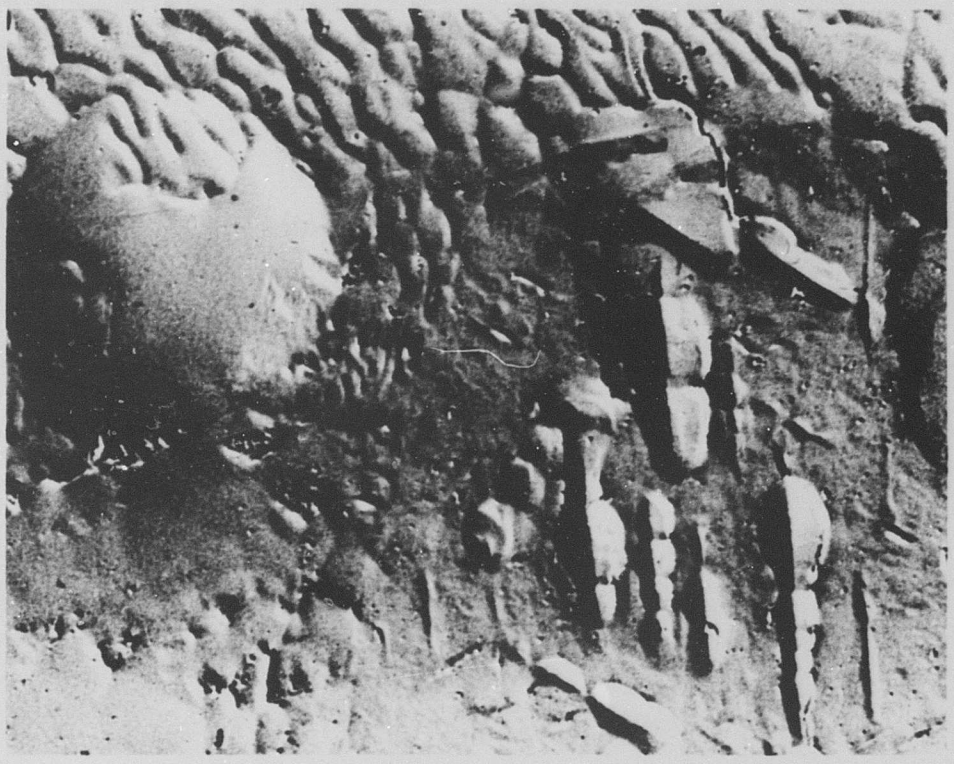

COMMENTS

The microstructure shows two alpha-Ti grains with different orientations. Note the circular former inclusion site.

Figure C-207 Titanium A-110-AT, Condition T: Electron Micrograph Showing 15,000X Magnification of Strained Area

METALLOGRAPHIC STUDY

Material Titanium A-110-AT Neg.No. 91-9

Specimen TU 285 Neg.Mag. 2,100X

Etchant None Photo Enlargement 2X

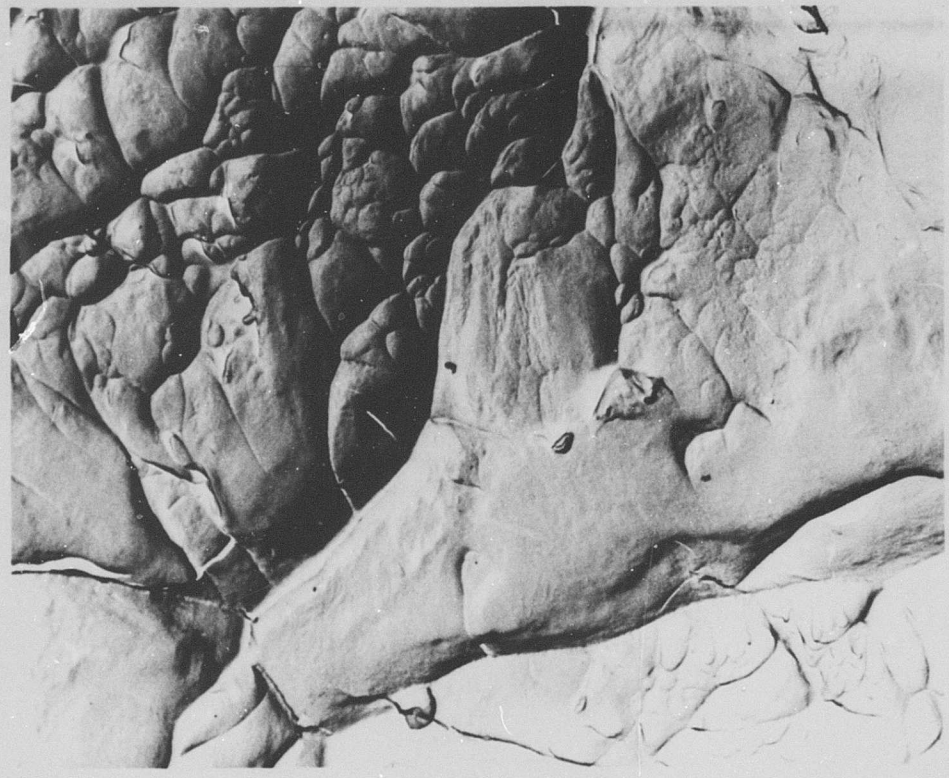

COMMENTS

The fracture consists mainly of ductile microvoid; however, the shallow dimple pattern on the right is possibly the result of cleavage cracking.

Figure C-208 Titanium A-110-AT, Condition T: Electron Fractograph Showing 4,200X Magnification At Center of Fracture

METALLOGRAPHIC STUDY

Material	Titanium A-110-AT	Neg.No.	91-11
Specimen	TU 285	Neg.Mag.	2,100X
Etchant	None	Photo Enlargement	2X

COMMENTS

The fracture at the edge consists of low-angle shear microvoids (dimples).

Figure C-209 Titanium A-110-AT, Condition T: Electron Fractograph Showing 4,200X Magnification Near Edge of Fracture

METALLOGRAPHIC STUDY

Material Titanium A-110-AT Neg.No. 98-10

Specimen TN 330 Neg.Mag. 2,100X

Etchant None Photo Enlargement 2X

COMMENTS

The fracture topography consists of ductile microvoid.

Figure C-210 Titanium A-110-AT, Condition T: Electron Fractograph Showing 4,200X Magnification of Notched Fracture

Titanium A-110-AT
Condition TW

BLANK PAGE

Table C-32

Tensile and Shear Test Data

Material Titanium A-110-AT Specimen Condition TW

Averaged Data (-423°F)		
Unnotched Specimens	Control	Irradiated
Ultimate Strength (ksi)	214.6	217.1
0.2% Yield Strength (ksi)	198.6	204.2
Elongation in Gage Length (%)	5.9	4.8
Reduction in Area (%)	9.4	11.4
Ultimate Shear Strength (ksi)		
Notched Specimens		
Ultimate Strength (ksi)	118.1	121.2
Ratios		
Notched-Ult./Unnotched-Ult.	0.55	0.56
Notched-Ult./Unnotched-Yield	0.59	0.59

Unnotched Specimens				
Specimen Number	Ult. Tensile Strength(ksi)	Yield Strength 0.2% Offset (ksi)	Reduction in Area (%)	Elongation (%)
293	No Data	No Data	15.00	6.5
294	210.7	198.5	7.4	3.7
297	226.9	214.0	11.1	3.5
298	213.8	200.0	12.2	5.3

Notched Specimens		Shear Specimens*	
Specimen Number	Ult. Tensile Strength (ksi)	Specimen Number	Ult. Shear Strength (ksi)
341	108.2		
342	136.0		
345	125.3		
346	115.2		

*Not Applicable

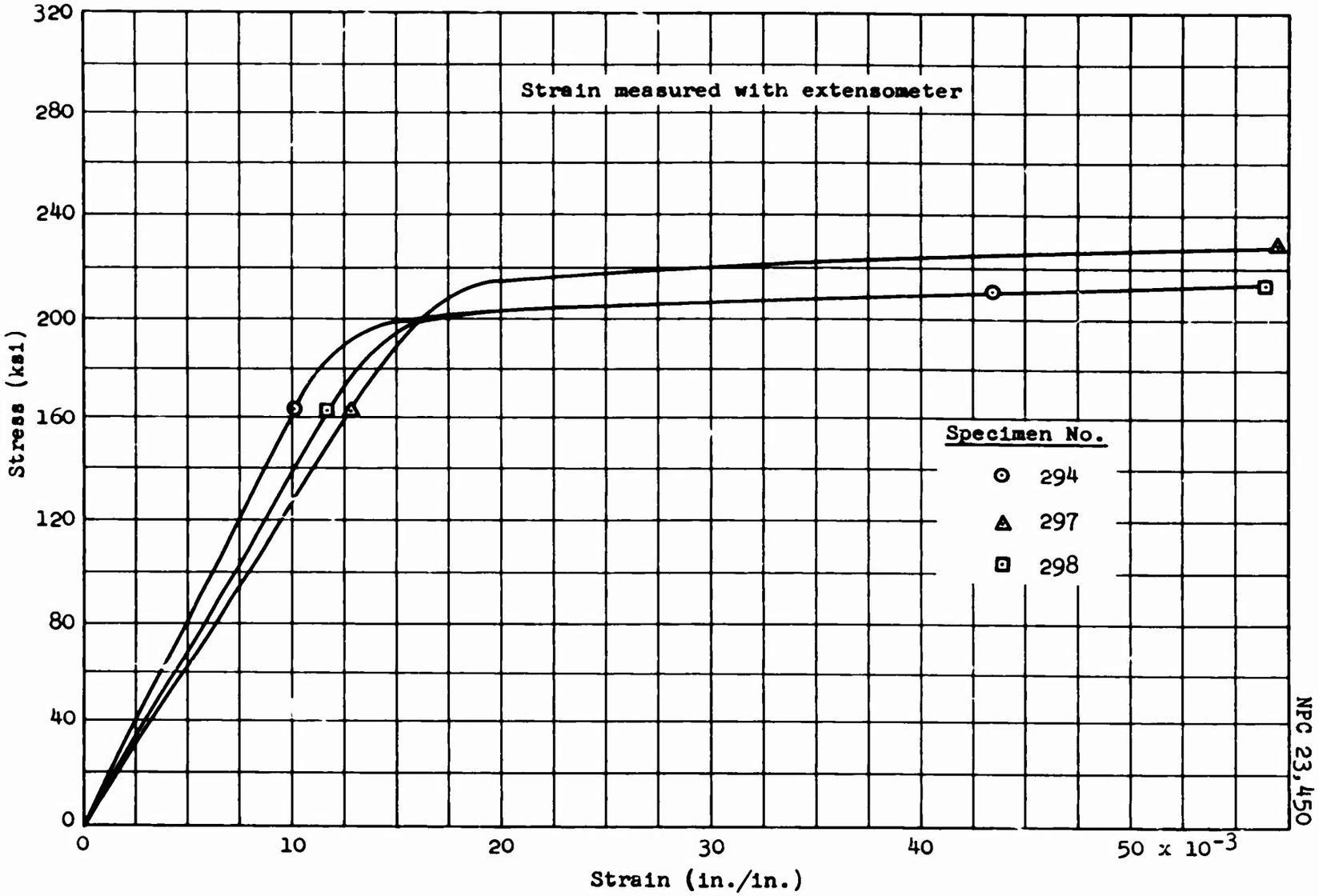

Figure C-211 Titanium A-110-AT, Condition TWU: Stress-Strain Curves

Table C-33

X-Ray Diffraction Data

Material Titanium A-110-AT Specimen TWU 298

	STRAINED AREA		UNSTRAINED AREA	
DIFFRACTION PATTERN				
Miller Indices (hkl)	Interlattice Spacing, d (Å)	Relative Intensity (%)	Interlattice Spacing, d (Å)	Relative Intensity (%)
002	2.35	100	2.34	15
011	2.24	24	2.23	100
012	1.73	10	1.72	8
110			1.47	5
103	1.33	20	1.33	11
112	1.25	4	1.24	7
004	1.17	5	1.23	6
014	1.06	2		

LATTICE PARAMETER (Å)

Axis a	2.95	2.95
Axis c	4.68	4.68

MICROSTRESS, $\Delta\theta$

0.23° ($2\theta = 82.2^\circ$)	No Peak ($2\theta = 82^\circ$)
0.12° ($2\theta = 38.3^\circ$)	0.12° ($2\theta = 38.4^\circ$)

METALLOGRAPHIC STUDY

Material Titanium A-110-AT Neg.No. None

Specimen TWU 298 Neg.Mag. 3X

Etchant None Photo Enlargement None

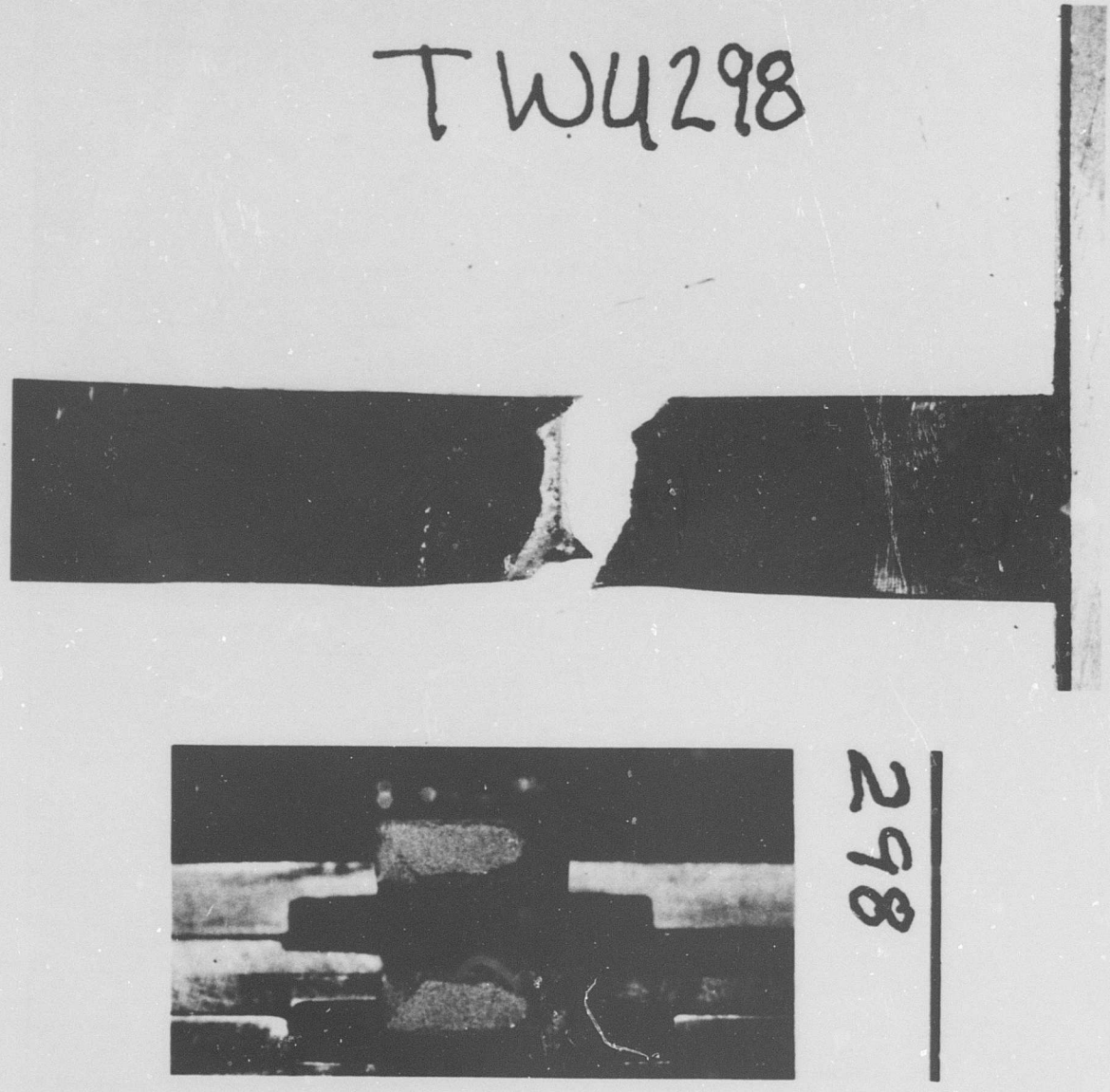

Figure C-212 Titanium A-110-AT, Condition TW: Macrophotograph Showing 3X Magnification of Specimen

METALLOGRAPHIC STUDY

Material Titanium A-110-AT Neg.No. W34

Specimen TWU 298 Neg.Mag. 100X

Etchant Kroll's Reagent, then HG-NYU Photo Enlargement None

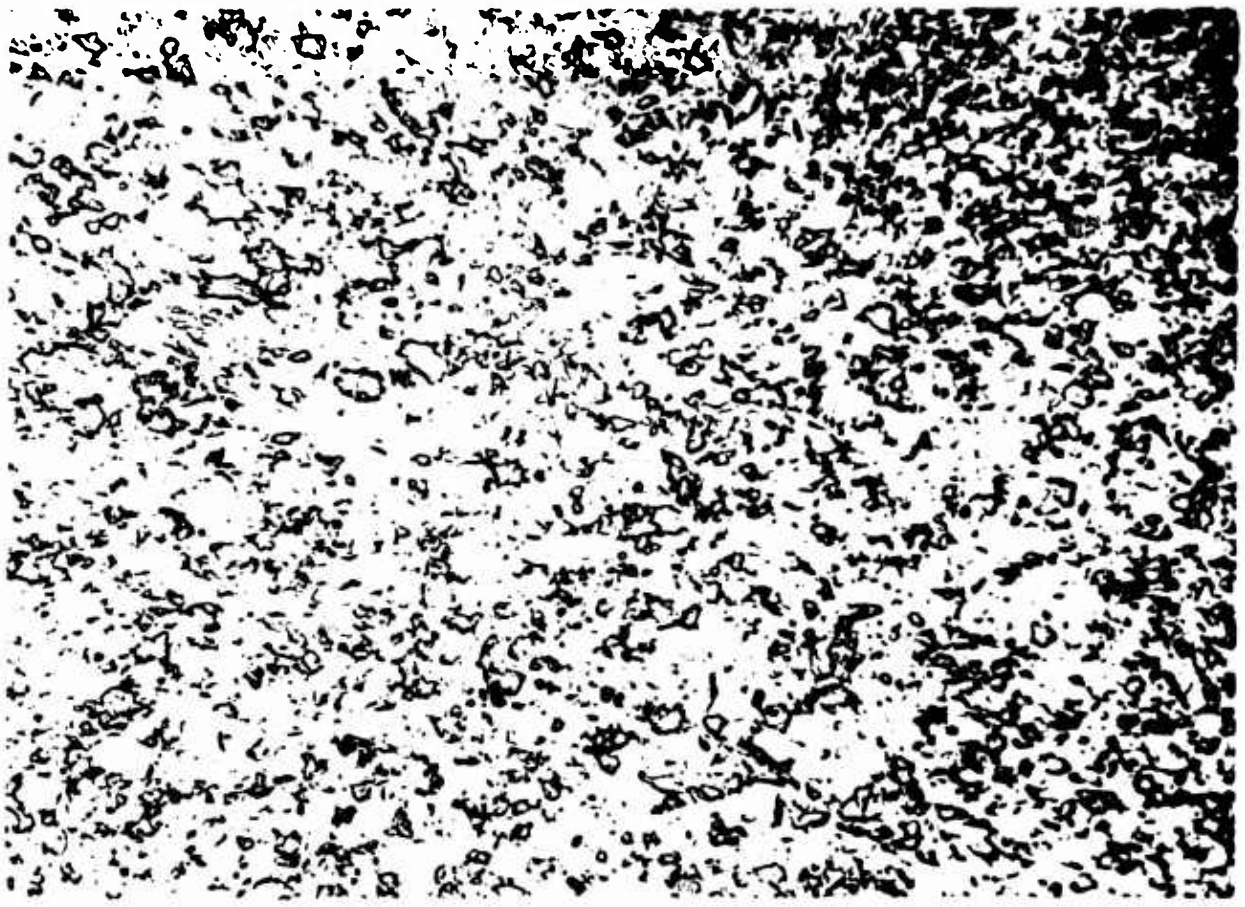

COMMENTS

The microstructure shows the typical alpha-Ti matrix.

Figure C-213 Titanium A-110-AT, Condition TW: Optical Micrograph Showing 100X Magnification of Unstrained Area

METALLOGRAPHIC STUDY

Material Titanium A-110-AT Neg.No. W33

Specimen TWU 298 Neg.Mag. 1,000X

Etchant Kroll's Reagent, then HG-NYU Photo Enlargement None

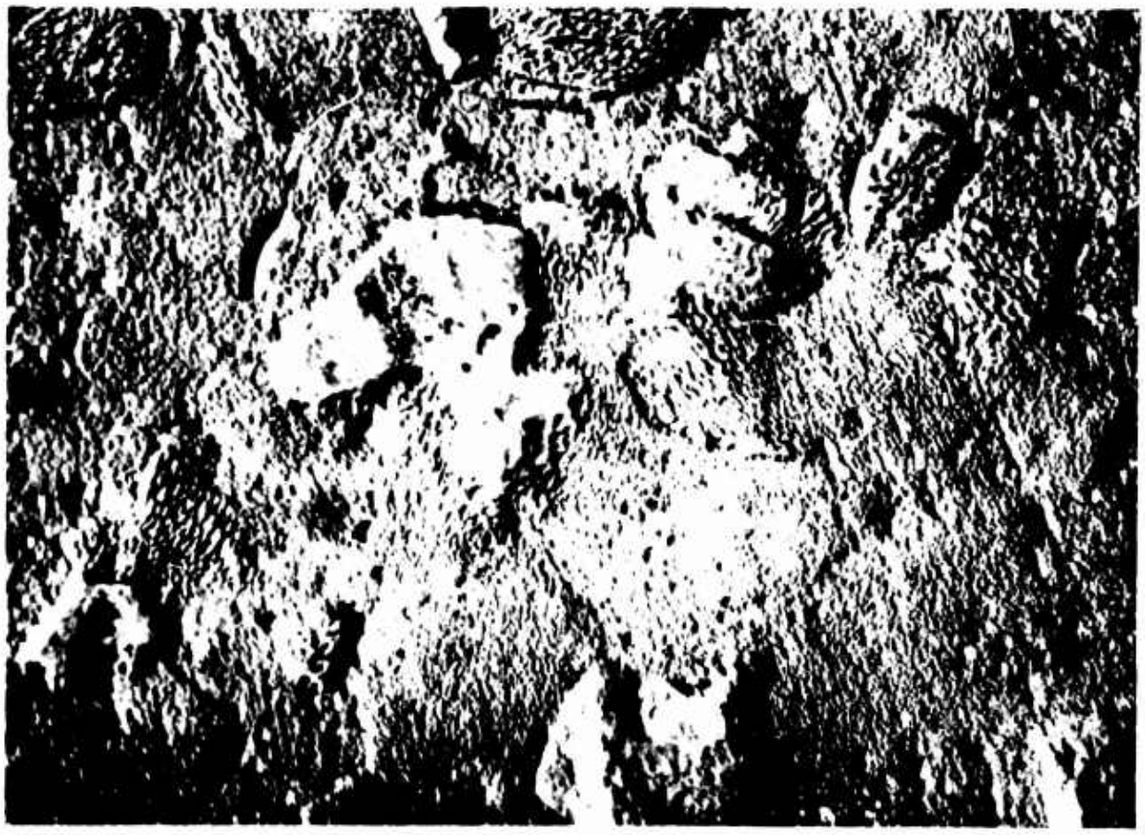

COMMENTS

The microstructure shows the typical alpha-Ti matrix. Note the alpha-Ti grain orientation as depicted by the etchant.

Figure C-214 Titanium A-110-AT, Condition TW: Optical Micrograph Showing 1,000X Magnification of Unstrained Area

METALLOGRAPHIC STUDY

Material Titanium A-110-AT Neg.No. W95

Specimen TWU 298 Neg.Mag. 100X

Etchant Kroll's Reagent, then HG-NYU Photo Enlargement None

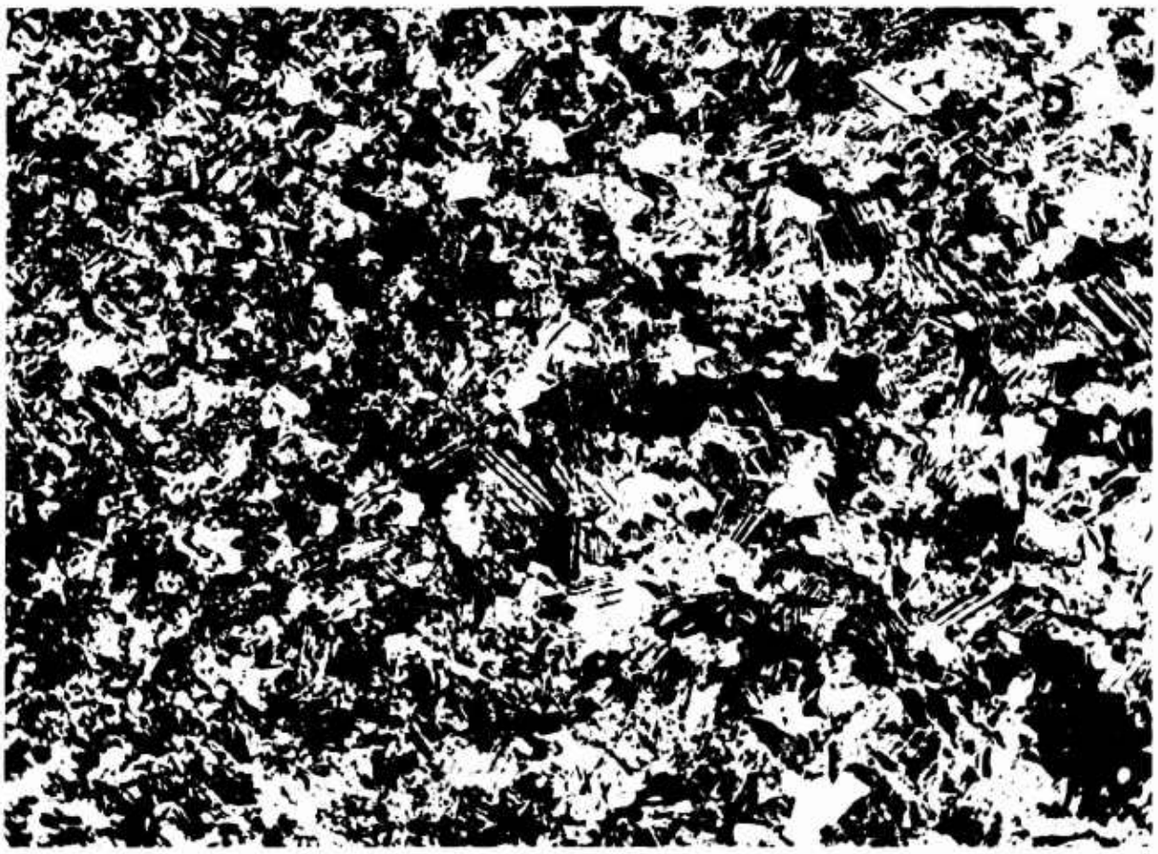

COMMENTS

The microstructure shows an acicular alpha-Ti in the weld metal (right) which has a larger grain size than the parent metal alpha-Ti (left).

Figure C-215 Titanium A-110-AT, Condition TW: Optical Micrograph Showing 100X Magnification of Parent Metal and Weld Interface

METALLOGRAPHIC STUDY

Material	Titanium A-110-AT	Neg.No.	W100 (left) and W99 (right)
Specimen	TWU 298	Neg.Mag.	1,000X
Etchant	Kroll's Reagent, then HG-NYU	Photo Enlargement	None

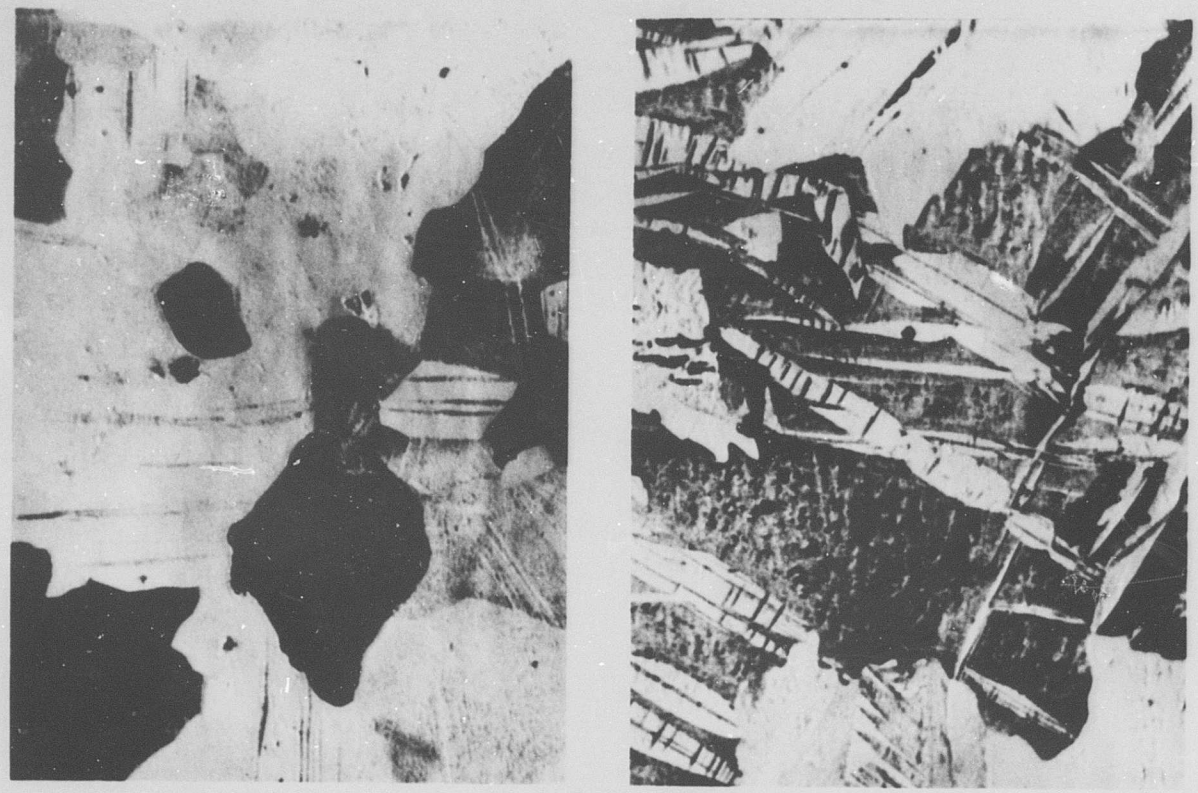

COMMENTS

The demarcation interface of this material was not pronounced enough to give a clear presentation at a magnification of 1,000X. The parent metal and weld metal microstructures are therefore presented individually for comparison. The parent material microstructure shows the alpha-Ti matrix (left). Note the deformation of the annealing twins and the formation of mechanical twins. The weld metal microstructure shows the typical acicular alpha-Ti. Note the strain lines within the alpha-Ti needles.

Figure C-216 Titanium A-110-AT, Condition TW: Optical Micrograph Showing 1,000X Magnification of Parent Metal and Weld Interface

METALLOGRAPHIC STUDY

Material Titanium A-110-AT Neg.No. W94

Specimen TWU 298 Neg.Mag. 100X

Etchant Kroll's Reagent, then HG-NYU Photo Enlargement None

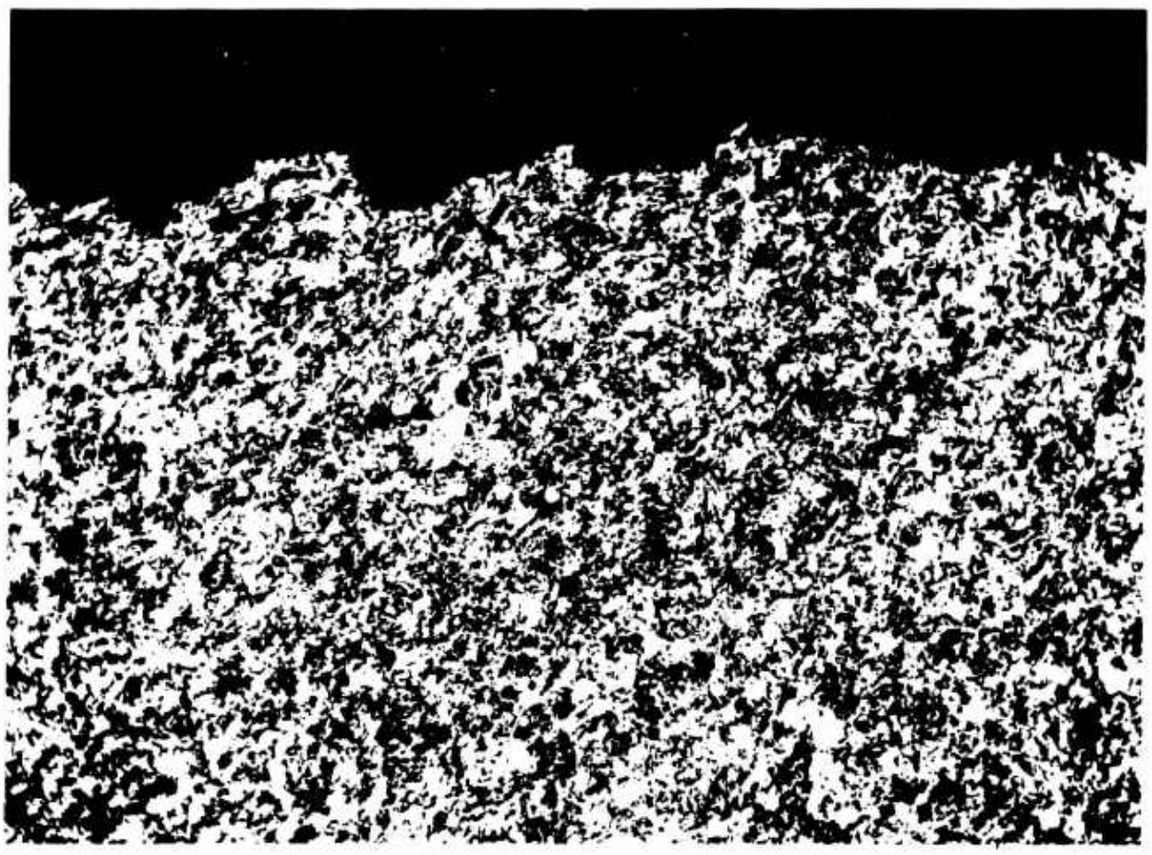

COMMENTS

The microstructure shows the fracture to be transgranular through the alpha-Ti matrix and not through the weld or heat-affected area.

Figure C-217 Titanium A-110-AT, Condition TW: Optical Micrograph Showing 100X Magnification of Fracture Edge

METALLOGRAPHIC STUDY

Material Titanium A-110-AT Neg.No. W98

Specimen TWU 298 Neg.Mag. 1,000X

Etchant Kroll's Reagent, then HG-NYU Photo Enlargement None

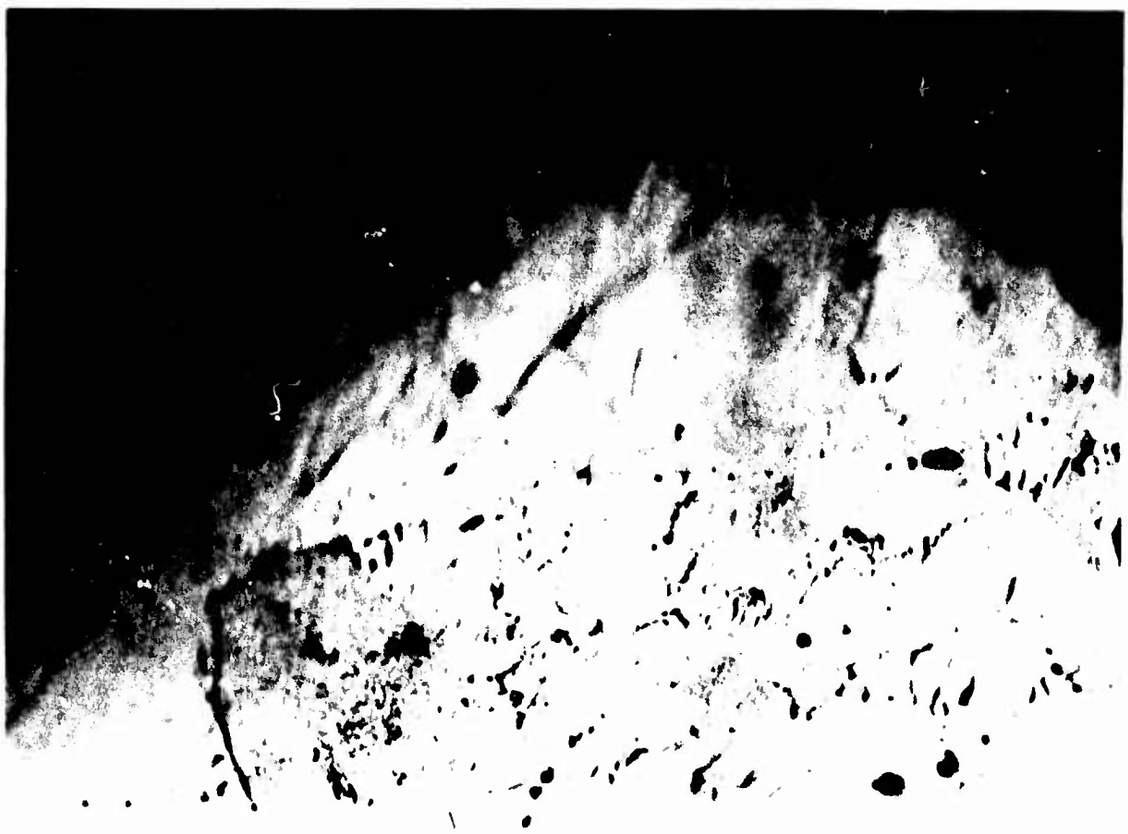

COMMENTS

The microstructure shows the fracture to be trans-granular through the alpha-Ti matrix and not through the weld or heat-affected area.

Figure C-218 Titanium A-110-AT, Condition TW: Optical Micrograph Showing 1,000X Magnification of Fracture Edge

METALLOGRAPHIC STUDY

Material Titanium A-110-AT Neg.No. 106-3

Specimen TWU 298 Neg.Mag. 7,500X

Etchant Kroll's Reagent Photo Enlargement 2X

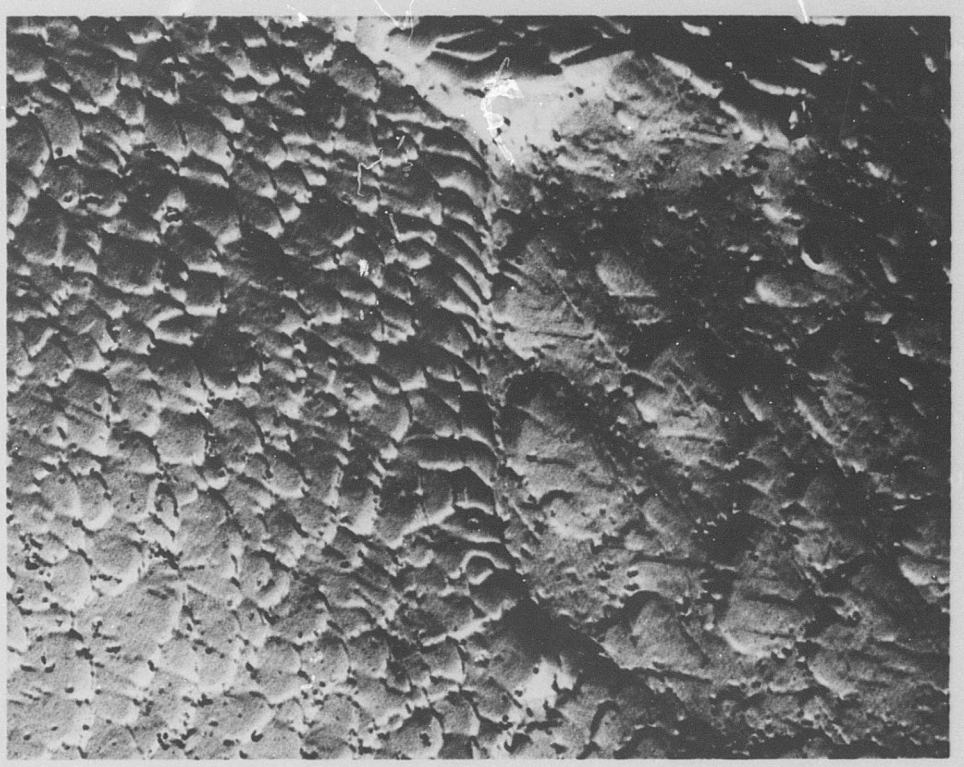

COMMENTS

The photo shows two alpha-Ti grains of different orientation by displaying a variation in texture.

Figure C-219 Titanium A-110-AT, Condition TW: Electron Micrograph Showing 15,000X Magnification of Unstrained Area

METALLOGRAPHIC STUDY

Material	Titanium A-110-AT	**Neg.No.**	106-11
Specimen	TWU 298	**Neg.Mag.**	7,500X
Etchant	Kroll's Reagent	**Photo Enlargement**	2X

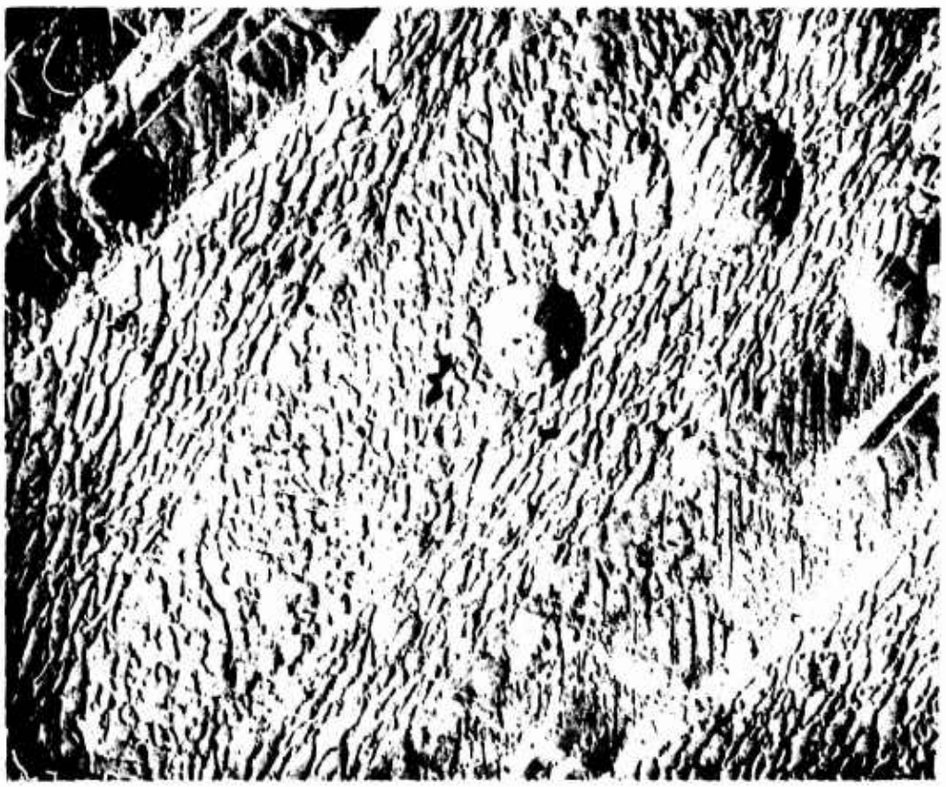

COMMENTS

The microstructure is an acicular alpha-Ti weld structure. Note the various orientations present and what appear to be mechanical twins in the acicular alpha-Ti grains. The large globular areas represent inclusions removed during polishing.

Figure C-220a Titanium A-110-AT, Condition TW: Electron Micrograph Showing 15,000X Magnification of Strained Area

METALLOGRAPHIC STUDY

Material	Titanium A-110-AT	Neg.No.	107-1
Specimen	TWU 298	Neg.Mag.	7,500X
Etchant	Kroll's Reagent	Photo Enlargement	2X

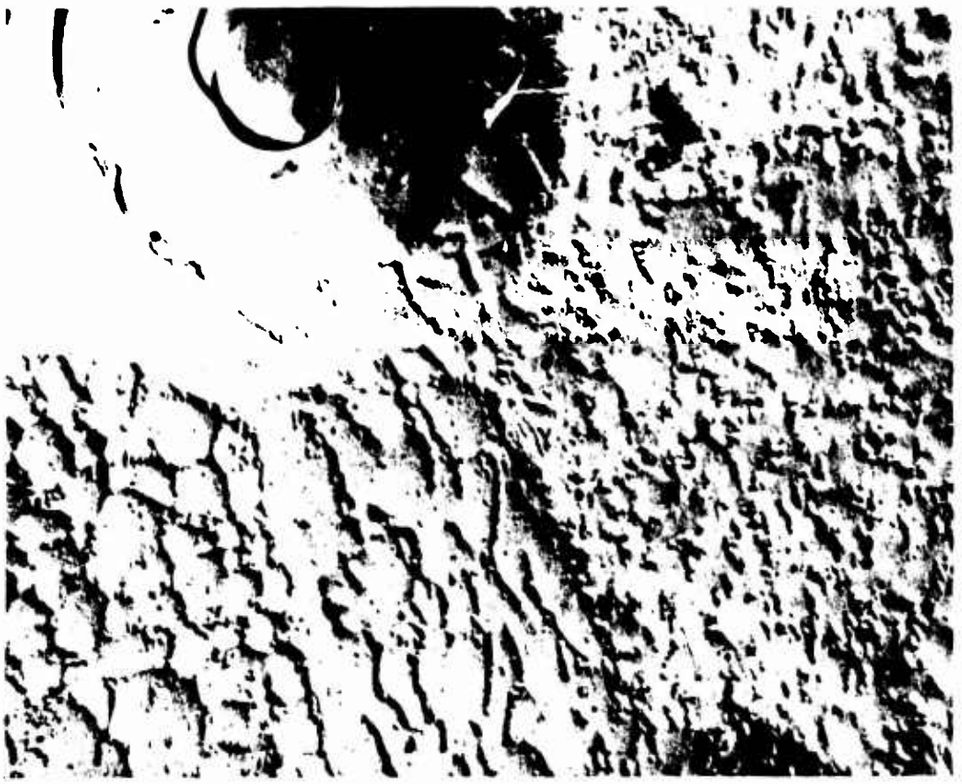

COMMENTS

This microstructure shows three alpha-Ti grains with different orientations. The large particle site in the upper left-hand corner is probably a carbide site.

Figure C-220b Titanium A-110-AT, Condition TW: Electron Micrograph Showing 15,000X Magnification of Strained Area

METALLOGRAPHIC STUDY

Material	Titanium A-110-AT	Neg.No.	92-7
Specimen	TWU 298	Neg.Mag.	2,100X
Etchant	None	Photo Enlargement	2X

COMMENTS

The fracture at the center is made up of large areas of shallow dimples connected by large dimples, indicating a discontinuous ductile fracture. The shallow dimples follow a cleavage pattern, indicating that cleavage cracks initiated the failure.

Figure C-221 Titanium A-110-AT, Condition TW: Electron Fractograph Showing 4,200X Magnification at Center of Fracture

METALLOGRAPHIC STUDY

Material Titanium A-110-AT Neg.No. 92-8

Specimen TWU 298 Neg.Mag. 2,100X

Etchant None Photo Enlargement 2X

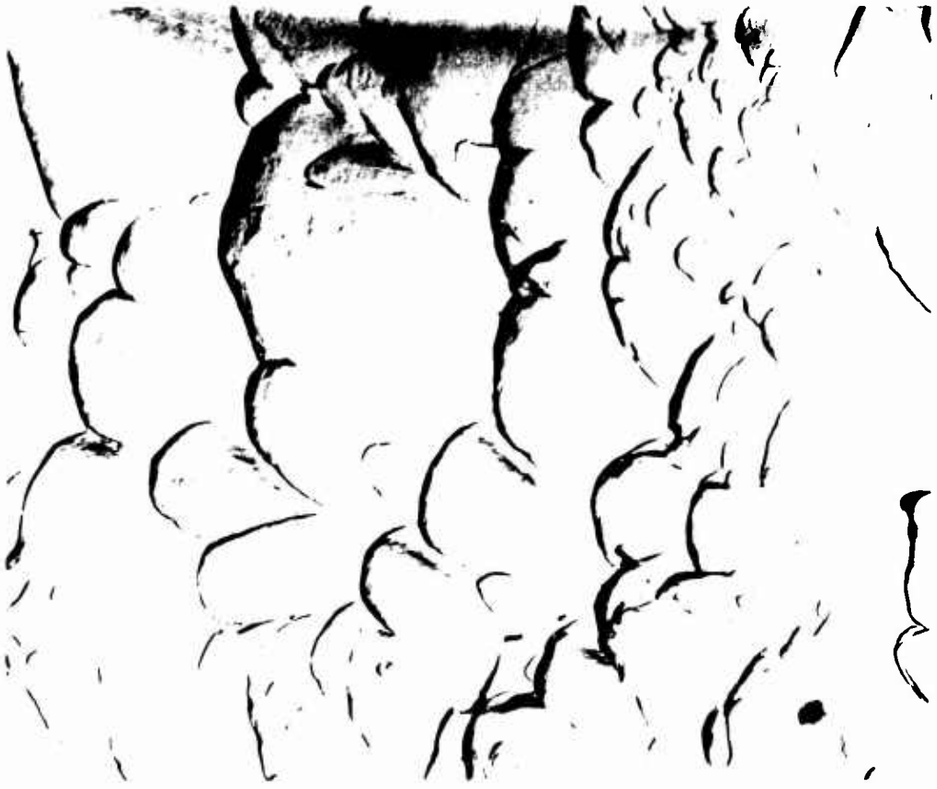

COMMENTS

The fracture at the edge is composed of large oriented dimples of the ductile shear type.

Figure C-222 Titanium A-110-AT, Condition TW: Electron Fractograph Showing 4,200X Magnification Near Edge of Fracture

METALLOGRAPHIC STUDY

Material	Titanium A-110-AT	**Neg.No.**	99-4
Specimen	TWN 342	**Neg.Mag.**	2,100X
Etchant	None	**Photo Enlargement**	2X

COMMENTS

The fracture of this notched specimen was through the weld zone and the acicular microstructure is reflected in the fracture topography. What is probably a grain boundary begins in the lower left-hand corner and passes through the center of the photograph. The flat facet in the center of the photograph above the grain boundary has a cleavage-type pattern indicating the effect of orientation on the fracture, which is primarily microvoid.

Figure C-223 Titanium A-110-AT, Condition TW: Electron Fractograph Showing 4,200X Magnification of Notched Fracture

Nickel Base Alloy D-979
Shear Specimens

Table C-34

Shear Test Data

Material D-979

Specimen Number	INSTRON				RAM			
	Total Load (lb)	Tare Load (lb)	1/2 Net Load (lb)	Ult. Shear Strength* (ksi)	Total Load (lb)	Tare Load (lb)	1/2 Net Load (lb)	Ult. Shear Strength* (ksi)
Room Temperature - Nonirradiated								
2B	5438	540	2449	130.3	4500	80	2210	117.6
4B	5175	540	2318	123.3	4400	80	2160	114.9
6B	5175	540	2318	123.3	4400	80	2160	114.9
8B	5043	540	2252	119.8	4300	80	2110	112.2
LH_2 Temperature - Nonirradiated								
10B	7275	450	3412	180.9	6100	110	2995	158.8
1C	6637	450	3093	164.0	5610	110	2750	145.8
3C	6825	450	3187	168.5	5760	110	2825	149.4
7C	7162	450	3356	177.7	6000	110	2945	156.0
LH_2 Temperature - Irradiated								
9A	7935	450	3743	198.5	7451	80	3686	195.4
1A	6773	450	3162	167.6	6316	80	3118	165.3
3A	6495	450	3023	160.3	6069	80	2995	158.8
5A	6338	450	2944	156.1	5970	80	2945	156.1

*Cross-sectional area of specimen = 0.01886 in^2.

REFERENCES

1. NERVA Components Irradiation Program, General Dynamics/Fort Worth Reports FZK-170-1 (19 July 1963) through FZK-170-8 (30 December 1963).

2. NERVA Components Irradiation Program, General Dynamics/Fort Worth Reports FZK-184-1 (15 March 1964) through FZK-184-6 (19 March 1965).

3. Palmer, E. E., NERVA Materials Irradiation Program, Vol. 2, GTR Test 16 - WANL Materials Test, General Dynamics/Fort Worth Report FZK-263-2, October 1965.

4. Final Test Specifications for GTR Test No. 16, REON Report RN-S-0184, December 1964.

5. NARF Facilities Handbook, General Dynamics/Fort Worth Report FZK-185A, March 1964.

6. Equipment Specification, Pressure Vessel, Cryogenic, Vacuum-Jacketed, REON Report AGC-10272A, 19 November [illegible]

7. Structural Analysis of Cylindrical Pressure Vessel, REON Report 746-18, March 1964.

8. Bradford, E. W., and Thornton, H. G., Investigation of the Effects of Radiation and Cryotemperature on Engineering Materials - Test No. 2 Control Data, General Dynamics/Fort Worth Report FZK-181, 31 March 1964.

9. Trigger, K. J., Heat Treatment of Metals, Champaign, Ill., Campus Book Store, 1954.

10. Kerlins, V., et al., Electron Fractography Handbook, Douglas Aircraft Company Report SM-44630, Vol. V, August 1964.

11. Strengthening Iron-Base Alloys by Shock Waves, Quarterly Progress Report for Period 16 January - 15 April 1964, North American Aviation Report (Rocketdyne Division) R-5413-3.

REFERENCES (Cont'd)

12. Reed, R. P., and Guntner, C. J., "Stress-Induced Martensitic Transformation in 18-Cr-8-Ni Steel," Trans. Am. Inst. Met. Engrs., 230 (December 1964), 1713.

13. Greenewald, H., Jr., and Riley, T. J., Development of a Nickel Base Alloy Sheet for High Temperature Application, AF Aeronautical Systems Division Report ASD-TDR-62-869 (Chance Vought Corp., Dallas, Texas), April 1963.